

*Dr Madhumita Roy* PhD

Ex-Head & Senior Scientific Officer (Assistant Director)

Dept Environmental Carcinogenesis & Toxicology

Chittaranjan National Cancer Institute

37, S. P. Mukherjee Road, Kolkata – 700 026, INDIA

mitacnci@yahoo.co.in; mitacnci@gmail.com

Dial: 9831018691; 8017723092

### CERTIFICATE FROM THE SUPERVISOR

This is to certify that the thesis entitled “**Black Tea in Prevention of Arsenic Induced Skin Carcinogenesis: A Mechanistic Study**” Submitted by Sri. **Archismaan Ghosh** who got his name registered on **18.09.2018** for the award of Ph. D. (Science) Degree of Jadavpur University [**Index No.: 183/18/Life Sc./26**], is absolutely based upon his own work under the supervision of **Dr. Madhumita Roy** and that neither this thesis nor any part of it has been submitted for either any degree / diploma or any other academic award anywhere before.

*Madhumita Roy*

**MADHUMITA ROY**

12.07.2023

Ex - **Dr. Madhumita Roy (Pal), Ph.D.**  
Head & Senior Scientific Officer (Asst. Director Grade)  
Dept. of Environmental Carcinogenesis & Toxicology  
Chittaranjan National Cancer Institute  
37, S. P. Mukherjee Road, Kolkata-700026

# Black Tea in Prevention of Arsenic Induced Skin Carcinogenesis: A Mechanistic Study

By

**Archismaan Ghosh**

Department of Environmental Carcinogenesis  
and Toxicology  
Chittaranjan National Cancer Institute, Kolkata



**Index No.- 183/18/Life Sc./26**

**Thesis Submitted For The Degree Of  
Doctor of Philosophy (Science)  
Department of Life Science and Biotechnology,  
Jadavpur University.  
2023.**





Dedicated to my lovely mother  
Smt. Chitra Ghosh, the reason of  
my existence and my constant  
source of motivation. She has been  
my guardian angel, nourishing me  
with her love and compassion, and  
guiding me through my highs and  
lows in life. Her dedication, hard  
work, honesty, tenacity and will  
power continues to amaze me.

Hope, one day I will be able to  
inculcate all these qualities. May  
she always remain by my side  
protecting me and guiding me.

# Table of Contents

<b>Acknowledgement</b>	<b>i</b>
<b>Abbreviations</b>	<b>iv</b>
<b>1. Introduction</b>	<b>1</b>
<b>1.1. History of Arsenic</b>	<b>2</b>
<b>1.2. Sources of Arsenic</b>	<b>5</b>
<b>1.2.1. Natural sources of Arsenic</b>	<b>5</b>
<b>1.2.2. Anthropogenic sources of Arsenic</b>	<b>6</b>
<b>1.3. Global scenario of inorganic Arsenic contamination</b>	<b>8</b>
<b>1.4. Stages of carcinogenesis and hallmarks of cancer</b>	<b>11</b>
<b>1.5. Skin problems due to chronic iAs exposure</b>	<b>16</b>
<b>1.6. Arsenic metabolism</b>	<b>19</b>
<b>1.7. Effect of chronic iAs exposure on ROS generation and beyond</b>	<b>21</b>
<b>1.8. Effect of iAs on DNA repair enzymes</b>	<b>23</b>
<b>1.9. Arsenic and inflammation</b>	<b>26</b>
<b>1.10. Arsenic and epigenetic modulations</b>	<b>32</b>
<b>1.10.1. Arsenic induced Post translational histone modifications</b>	<b>33</b>
<b>1.10.2. Arsenic induced DNA methylations</b>	<b>36</b>
<b>1.11. iAs induced modulation of TGF-<math>\beta</math> and induction of EMT</b>	<b>38</b>
<b>1.12. Chemoprevention</b>	<b>41</b>
<b>1.13. Tea as a chemopreventive agent against iAs induced toxicity</b>	<b>44</b>



<b>2. Aims and Objectives</b>	<b>49</b>
<b>3. Materials and Methods</b>	<b>52</b>
<b>3.1. Model of the study</b>	<b>53</b>
<b>3.2. Materials</b>	<b>53</b>
<b>3.3. Kits used</b>	<b>55</b>
<b>3.4. Equipment's used</b>	<b>56</b>
<b>3.5. Methods</b>	<b>57</b>
<b>4. Results</b>	<b>83</b>
<b>A. Preliminary results</b>	<b>84</b>
<b>B. <i>in vivo</i> Results</b>	<b>88</b>
<b>C. <i>in vitro</i> Results</b>	<b>103</b>
<b>5. Discussion</b>	<b>113</b>
<b>6. Conclusion</b>	<b>131</b>
<b>7. References</b>	<b>136</b>
<b>8. List of Publications</b>	<b>177</b>
<b>9. Conferences attended</b>	<b>180</b>
<b>10. Achievements/Awards</b>	<b>183</b>

# Acknowledgement

The journey of a PhD student requires a lot of dedication, discipline, and hard work. Standing at this fag end of my PhD career, I do realise that it would have been impossible for me to reach this far, without the generous help of few people whom I would like to acknowledge here. First of all, I would like to express my gratitude to my PhD supervisor, guide and mentor Dr. Madhumita Roy, ex- Head and Assistant Director Grade Scientist, Department of Environmental Carcinogenesis and Toxicology (ECT), Chittaranjan National Cancer Institute (CNCI), Kolkata. Her self-discipline and hard work helped reinstating these values in me. Her patience, zeal for perfection, constructive criticism and practicality are admirable. Her valuable advices and constant motivation acted as guiding lights for my PhD path. Apart from professional field, her impeccable hospitality and warmth are praiseworthy. She has taught me many life lessons which will act as shining stars guiding my future path. It is difficult to sum up her contribution in my PhD journey within few words, sentences, or paragraphs and all I want to say is that, I will remain indebted to her throughout my life. I hope, I will be able to relay the virtues I learnt from her to my juniors and fellow colleagues in future.

Secondly, I would like to heartily thank Prof. Amitava Datta, Department of Computer Science and Software Engineering, University of Western Australia, Perth. Though belonging to the department of Computer science, his passion, enthusiasm, and knowledge in biology is awe striking. Without his colossal contribution in the in-silico field, my research work would have remained incomplete. Apart from that, he has also thanklessly fact checked and proofread some of my manuscripts, making valuable inputs

and improving their quality. His meticulous, firm, and logical approach to problems is praiseworthy. I will remain grateful to this wonderful person for his inspiring words and immense help in my PhD journey.

I would also like to thank Dr. Sutapa Mukherjee, Senior Scientific Officer, ECT, CNCI. She has always been kind, cooperative and helpful. Her amicable nature is commendable. I am grateful to her for motivation and guidance. I would also like to thank Prof. Arghya Taraphder, Centre for theoretical studies, IIT Kharagpur and Prof. Ansuman Lahiri, Department of Bio-Physics, Molecular biology and bioinformatics, University of Calcutta, for their help, and contribution in certain avenues of my research work.

I would like to express my gratitude towards Dr Jayanta Chakrabarti, Director, Chittaranjan National Cancer Institute, Kolkata, for providing me the infrastructure, resources, and fellowship to carry out my research in the esteemed institute. I would also like to thank Central Instrument Research Facility team and CNCI support staff for their cooperation and help.

I would take the privilege to express my gratitude towards my lab seniors Dr. Ruma Sarkar, Dr. Apurba Mukherjee and Mr. Souvick Biswas for their cooperation and help. They were kind enough to help me whenever I sought for it. I would also like to extend my gratitude towards Dr. Debomita Sengupta, CSIR-Senior Research Associate (Scientists' Pool), for extensively helping me out in my RT-PCR work. Her scientific discussions on various topics would often enlighten and encourage me to further pursue my research work. Next, I would like to warmly express my gratitude towards my friend, classmate, and lab mate Elizabeth Mahapatra. Without her constant support, help and motivation it would have been very difficult for me to complete my research. I am happy to have known this gem of a person for past 11 years and her sincerity, hard work and enthusiasm in research has



constantly encouraged me. I will always cherish our friendship and hope the best for her future. Lastly, I would also like to extend my thanks to junior lab members Salini Das and Debanjan Thakur as well as lab attendant Sunit Roy for their cooperation and help.

Last, but not the least, I would like to acknowledge my mother, Chitra Ghosh, without whom, it would be impossible for me to achieve this feat. She had always advised and encouraged me to pursue higher education without worrying about finances. She has always been my role model and superhero since childhood. I would like to heartily thank her for all she has done for me and for the uncountable sacrifices she has happily made, so that I am able to do better. I will always remain indebted to her for everything.

**Archismaan Ghosh**

## Abbreviations

- 8-oxo-G: 8-oxoguanine
- AAS-VGA: Atomic Absorption Spectrophotometry with Vapour  
Generation Assembly
- AKT: Protein kinase B
- ANOVA: Analysis of Variance
- AP: apurinic/aprimidinic
- APE1: AP endonuclease I
- AS3MT: arsenic methyltransferase
- BCC: Basal cell carcinoma
- BCIP-NBT: 5-bromo-4-chloro-3-indolyl phosphate- nitro blue  
tetrazolium
- BER: Base Excision Repair
- BMI1: B lymphoma Mo-MLV insertion region 1 homolog
- BSA: Bovine serum albumin
- BTE: Black tea extract
- CCA: Chromated copper arsenate
- CD4+: Clusters of differentiation 4
- CD8+: Clusters of differentiation 8
- CDKN1A: Cyclin dependent kinase inhibitor 1A
- CDNB: Chloro-2,4-Dinitrobenzene
- COX2: Cyclooxygenase 2

- CPCSEA: Committee for the Purpose of Control and Supervision of Experiments on Animals
- CRP: C-reactive proteins
- CSIF: Cytokine synthesis inhibitory factor
- DAB: Diaminobenzidine
- DAPI: 4',6-diamidino-2-phenylindole
- DAPK: Death-associated protein kinase
- DCFDA: 2',7'-dichlorofluorescein diacetate
- DDB2: DNA damage-binding protein 2
- DMA<sup>III</sup>: Dimethylarsinous acid
- DMA<sup>V</sup>: Dimethylarsinic acid
- DMBA: 7,12-Dimethylbenz[a]anthracene
- DMEM/F-12: Dulbecco's Modified Eagle Medium: Ham's Nutrient Mixture F12
- DMPS: 2-3-dimercapto-1-propanesulfonate
- DMSA: meso 2, 3-dimer-captosuccinic acid
- DMSO: Dimethyl sulfoxide
- DNA Pol $\beta$ : DNA polymerase
- DNA-PKcs: DNA dependent protein kinase
- DNMT: DNA cytosine-5-methyltransferases
- DNMT 3A: DNA cytosine-5-methyltransferases 3A
- DNMT 3B: DNA cytosine-5-methyltransferases 3B
- DNPH: 2,4-Dinitrophenylhydrazine
- DPX: Dibutylphthalate Polystyrene Xylene
- EC: Epicatechin



- ECG: Epicatechin Gallate
- ECM: Extracellular matrix
- EGC: Epigallocatechin
- EGCG: Epigallocatechin gallate
- EGFR: Epidermal growth factor receptor
- ELISA: Enzyme-linked immunosorbent assay
- EMT: Epithelial to Mesenchymal Transition
- ER: Endoplasmic Reticulum
- ERCC1: Excision repair cross complementation group 1
- ESR1: Estrogen Receptor 1
- EtBr: Ethidium bromide
- EZH2: Enhancer of zeste homolog 2
- FBS: Fetal Bovine Serum
- FITC: Fluorescein isothiocyanate
- FL1: Fluorescence channel 1
- GAPDH: Glyceraldehyde phosphate dehydrogenate
- GM-CSF: Granulocyte-macrophage colony stimulating factor
- GPx: Glutathione Peroxidase
- GR: Glutathione Reductase
- GSH: Glutathione
- GST: Glutathione -S- Transferase
- HaCaT: High sensitivity of human epidermal keratinocytes cells
- HBS: HEPES buffered saline.
- HEPES: Hydroxyethyl piperazine ethane sulfonic acid
- HNSCC: Head and Neck Squamous Cell Carcinoma

- Hoechst 33342: 2'-[4-ethoxyphenyl]-5-[4-methyl-1-piperazinyl]-2,5'-bi-1H benzimidazole trihydrochloride trihydrate
- HOXB7: Homeobox B7
- HPLC: High Performance Liquid Chromatography
- HRP: Horse radish peroxidase
- HuCCT-1: Human liver bile duct carcinoma cells
- IAEC: Institutional Animal Ethics Committee
- IARC: International Agency for Research on Cancer
- iAs: Inorganic Arsenic.
- IFN- $\gamma$ : Interferon-gamma
- IHC: Immunohistochemistry
- IL1: Interleukin-1
- IL10: Interleukin-10
- IL13: Interleukin-13
- IL15: Interleukin-15
- IL17a: Interleukin-17a
- IL18: Interleukin-18
- IL2: Interleukin-2
- IL22: Interleukin-22
- IL2R $\alpha$ : Interleukin-2 Receptor  $\alpha$  subunit
- IL2R $\beta$ : Interleukin-2 Receptor  $\beta$  subunit
- IL2R $\gamma$ : Interleukin-2 Receptor  $\gamma$  subunit
- IL4: Interleukin-4
- IL6: Interleukin-6
- IL7: Interleukin-7

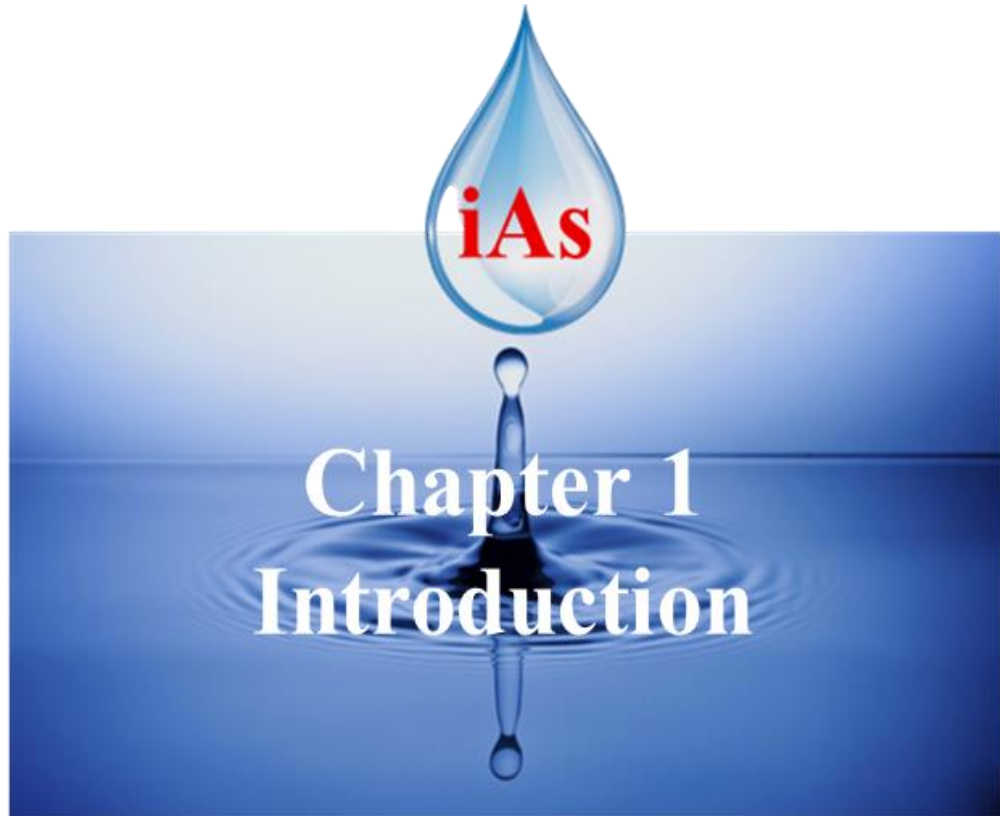
- IL8: Interleukin-8
- IκBα: Inhibitor of nuclear factor kappa B
- JAK: Janus Kinase
- JARID1B/KDM5B: Lysine-specific demethylase 5B
- JNK: Jun N-terminal kinase
- KDM6A: Lysine demethylase 6A
- LMA: Low melting agarose
- LSD1: Lysine-specific demethylase 1
- MAPK: Mitogen-activated protein kinase
- MAPKKK: MAP kinase kinase kinase
- MC: Mast cells
- MDA: Malondialdehyde
- MLL1: Mixed lineage leukemia protein-1
- MLL3: Mixed lineage leukemia protein-3
- MM/PBSA: Molecular mechanics Poisson Boltzmann surface area
- MMA<sup>III</sup>: Monomethylarsonous acid
- MMA<sup>V</sup>: Monomethylarsonic acid
- MMP2: Matrix metalloproteinase 2
- MMP9: Matrix metalloproteinase 9
- MNNG: N-methyl-N'-nitro-N-nitrosoguanidine
- MT-1: Metallothionein-1
- mTOR: Mammalian target of rapamycin
- MTT: 3-(4,5-Dimethylthiazol-2-yl)-2,5-Diphenyltetrazolium  
Bromide
- MYST1/KAT8: Lysine acetyltransferase 8



- NAD(P)H: Nicotinamide adenine dinucleotide phosphate
- NBF: Neutral Buffered Formalin
- NCPH: Non-cirrhotic portal vein hypertension
- NER: Nucleotide Excision Repair
- NF- $\kappa$ B: Nuclear factor kappa B
- NHEJ: Non-homologous end joining
- NK: Natural Killer cells
- NMA: Normal melting agarose
- NMSC: Non-melanoma skin cancers
- NOX: Nicotinamide adenine dinucleotide phosphate oxidase
- OD: Optical density
- OGG1: 8-Oxoguanine glycosylase
- OSCC: Oral Squamous Cell Carcinoma
- p14ARF: ARF tumour suppressor
- p16INK4a: Cyclin-dependent kinase inhibitor 2A
- p38: Mitogen-activated protein kinases
- PAH: Polycyclic aromatic hydrocarbons
- PARP1: Poly (ADP-ribose) polymerase 1
- PBMC: Peripheral blood mononuclear cells
- PBS: Phosphate buffered saline.
- PCNA: Proliferating cell nuclear antigen
- PE: Phycoerythrin
- PET: Polyethelyene terephthalate
- PHA: Phytohaemagglutinin
- PI3K: Phosphoinositide-3-kinase

- PMSF: Phenylmethylsulfonyl fluoride
- PRC2: Polycomb repressive complex 2
- PTEN: Tensin homolog deleted on chromosome 10
- PTM: Post translational histone modifications
- RFC: Replication factor C
- RHOA: Ras Homolog Family Member A
- RIPA: Radioimmunoprecipitation Assay Buffer
- RNS: Reactive nitrogen species
- ROS: Reactive Oxygen Species
- RT-PCR: Reverse transcription-polymerase chain reaction
- S6K: Ribosomal S6 kinase
- SAH: S-adenosylhomocysteine
- SAM: S-adenosylmethionine
- SCC: Squamous cell carcinoma
- SCGE: Single cell gel electrophoresis
- SDS: Sodium dodecyl sulfate
- Smad: Suppressor of mothers against decapentaplegic
- SOD: Superoxide dismutase
- SOES: School of Environmental Studies
- STAT: Signal transducers and activators of transcription
- TAK1: TGF- $\beta$ -associated kinase 1
- TBA: Thiobarbituric acid
- TBS: Tris buffered saline
- Tet: Ten-eleven translocation
- TF: Theaflavin

- TGF- $\beta$ : Transforming growth factor beta
- Th1: T-helper1 cells
- Th2: T-helper2 cells
- TMA<sup>III</sup>: Trimethyl arsine.
- TMAO<sup>V</sup>: Trimethylarsine oxide
- TME: Tumour microenvironment
- TNF- $\alpha$ : Tumor necrosis factor alpha
- TPA: 12-O-tetradecanoyl phorbol-13-acetate
- Tregs: Regulatory T cells
- TRIzol: Guanidine thiocyanate and phenol
- VEGF: Vascular endothelial growth factor
- WHO: World Health Organization
- XPA: Human xeroderma pigmentosum group A
- XPB: Human xeroderma pigmentosum group B
- XPC: Human xeroderma pigmentosum group C
- XPD: Human xeroderma pigmentosum group D
- XRCC1: X-Ray Repair Cross Complementing 1
- XRCC4: X-Ray Repair Cross Complementing 4



## **1. Introduction**

Arsenic (As), a colourless, tasteless, odourless, metalloid, is the 33<sup>rd</sup> element in the periodic table and the 20<sup>th</sup> abundant element in the earth's crust. It is found ubiquitously in the environment and its presence can be detected in air, water, soil and biosphere [Rahaman et al., 2021]. Arsenic appears to be readily soluble in water and is obtained in both organic and inorganic forms. Inorganic arsenic is generally found in trivalent (arsenite) and pentavalent (arsenate) states but it can also exist in elemental form as As<sup>0</sup> [Garland, 2018].

### **1.1. History of Arsenic**

The name 'arsenic' evokes a fear in most individuals as the metalloid has been intricately associated with both intentional and un-intentional poisoning in humans. The use of arsenic as a homicidal and suicidal agent was quite frequent in the Middle Ages. The notoriety of arsenic as a murder weapon peaked when it was involved in many high-profile murders. It is often designated as "King of poisons" and "poison of Kings" due to its usage in instances involving assassination of members of the aristocracy and ruling class during the Middle age and Renaissance [Vahidnia et al., 2007], for example the famous Borgia and Medici families of Europe. According to certain conspiracy theorists, death of Napoleon Bonaparte in 1851 was also due to arsenic poisoning [Cullen, 2008].

Exposure to any toxicant can be either acute or chronic. High dose of exposure for short period of time is commonly known as acute exposure, while exposure to small quantities of toxicant for prolonged period is called chronic exposure. Acute lethal dose of inorganic arsenic in humans is estimated to be 0.6 mg/kg/day [Ratnaike, 2013]. The

popularity of arsenic as poison of choice soared until the mid-1850's, the reasons behind this was its colourless, odourless, tasteless and highly soluble nature which makes it undetectable in food and beverages. Acute arsenic poisoning symptoms like nausea, vomiting, diarrhoea, and abdominal pain could easily be confused with symptoms of other common diseases like cholera etc. Absence of proper analytical techniques for detection and measurement of arsenic in cells, tissues and food products was a major factor of concern since ancient times. Detection of arsenic was revolutionised when John Marsh devised an analytical method to detect arsenic. His analytical method was first used as conclusive evidence, to detect arsenic, in the famous trial of Marie LaFarge, in France, in 1840 [Cullen, 2008]. Madame LaFarge was accused of killing her husband by feeding him arsenic laden cake. The samples obtained from the crime site were mixed with zinc and acid, followed by heating in a glass vessel; accumulation of silvery substance on the inner body of the vessel suggested presence of arsenic, as low as 0.02mg of Arsenic could be detected using this method [Marsh, 1837]. Establishment of Marsh test as an effective detecting test, reduced the number of homicides using Arsenic. A detailed study of the cases of deliberate arsenic poisoning, gives us important information regarding, the symptoms and target organs of acute arsenic exposure [Hughes et al., 2011].

Though arsenic is a potential poison, yet historically it has also been used as a medicine. Hippocrates, Father of medicine, is known to use arsenic pastes to treat ulcers and wounds as early as 2000 BCE [Waxman and Anderson, 2001]. Other famous physicians like Aristotle and Paracelsus have also used arsenic medically. Fowler's reagent or 1% potassium arsenite solution was used extensively in the late 18<sup>th</sup> century to treat various disorders like malaria, eczema, psoriasis, asthma etc [Scheindlin, 2005]. Salvarsan, an arsenic-based drug, developed by Paul Ehrlich in 1910, was considered a 'magic bullet' for the treatment of syphilis. The use of Salvarsan for treating syphilis, was quite

widespread until penicillin was discovered in 1940's [Riethmiller, 2005]. Pharmacological records from 1880's state that arsenic pastes were also used as chemotherapeutic agents to treat skin and breast cancers. According to certain reports, Fowlers' reagent was also used to treat Leukaemia but later was stopped due to high toxicity. Arsenic trioxide ( $As_2O_3$ ) has been found to be effective against Promyelocytic Leukaemia and the chemotherapeutic role of arsenic trioxide in other cancers is being investigated [Antman, 2001; Sekeres, 2007].

Historically arsenic has also been used in many fields apart from medicine and poison. Paris green or copper acetoarsenite had been used as a popular pigment for many consumer products like toys, candles, etc. but its extensive use in wallpaper was found to be associated with widespread illness and death. Under damp conditions, molds would grow on the walls pasted with Paris green coated wall papers. It was suggested that these molds bio transformed the arsenic present in the pigment into a toxic gas, trimethylarsine, this phenomenon was first explained by Bartolomeo Gosio, hence it was popularly called as 'Gosio gas' [Cullen and Bentley, 2005]. Apart from colouring pigment, Paris green was also used extensively as an insecticide against Colorado potato beetles and mosquitoes [Cullen, 2008]. Another arsenic compound, lead arsenate, was also used extensively as a pesticide in the apple and cherry orchards in the early 1900s. Later the use of lead arsenate was banned, as its use was found to be correlated with many health problems, in the orchard workers. The presence of lead arsenate residues on the fruits was also a potential health concern. Till early 20<sup>th</sup> century, studies regarding the toxicity of arsenic focused on its acute exposure, but studies on the orchard workers revealed that, low doses of arsenic exposure over prolonged periods of time can lead to severe health problems including cancer [Nelson et al., 1973]. Though the use of lead arsenate and other arsenic containing pesticides has been banned for over 50 years, yet its presence can be found in acres of contaminated lands [Peryea, 1973]. In modern times, few compounds of arsenic are still

being used in industries. One such compound is Chromated copper arsenate (CCA), which is used as wood preservative against insects and microbes. In 2003, the residential use of CCA was prohibited and CCA treated woods were only permitted to be used for marine industry, highway construction etc [EPA, 2008]. Arsenic compounds have also been used in copper smelting, workers exposed to it have been reported to suffer from lung cancer, establishing a link between occupational exposure to arsenic and development of lung cancer [Hughes et al., 2011].

## **1.2. Sources of Arsenic**

### **1.2.1. Natural sources of arsenic**

Human exposure to arsenic can be both due to natural and anthropogenic causes. Naturally, varying proportions of arsenic can be found in sedimentary rocks, volcanic rocks and in the ores of various metals. Studies have reported presence of arsenic in over 200 different types of mineral ores, where, it may exist as elemental arsenic, arsenide, sulphide, oxide, arsenite and arsenate [Beck et al., 2017]. Highest concentrations of inorganic arsenic in mineral ores have been reported in Iron pyrites ( $\text{FeS}_2$ ) followed by chalcopyrite, galena and marcasite, where the amount of arsenic can be more than 10% of the total weight of the ore. Under certain geochemical conditions like modulation of the pH and presence of reducing or aerobic environment, arsenic may be released from these mineral ores into the surroundings, resulting in contamination of soil and water [Pal et al., 2009]. Groundwater, which lies in close vicinity of these arsenic containing ores have much higher chance of getting contaminated by it. Number of theories have been proposed which explain the leaching of arsenic from the sediments and ores into groundwater and some of them are:

- i. Oxidation of Pyrite: Lowering of the water table naturally or due to anthropogenic causes (excess pumping of water due to irrigation) leads to aeration of the



anoxic sediments and oxidation of arsenic containing pyrite ores, resulting in release of arsenic in groundwater.

- ii. **Competitive Ion Exchange:** The process of, competitive replacement of arsenic oxyanions of the mineral ores, by phosphate ions present in the underground water, is generally referred to as competitive ion exchange mechanism. The organic matter provides the abundance of phosphate ions in the aquifers which are exchanged for arsenic containing anions, thus increasing the concentration of arsenic in the groundwater.
- iii. **Reductive Dissolution of Iron Oxyhydroxides:** The liberation of arsenic by reductive dissolution of metal oxides and hydroxides have been frequently observed and can contribute to increase in concentration of arsenic in groundwater. The redox potential of arsenic contaminated water of Gangetic plains is quite low, supporting this hypothesis of arsenic accumulation in groundwater [Bhattacharya et al., 2011].

Varying degrees of oxidation and reduction of mineral ores, fluctuation of the groundwater table during dry and wet season, presence of organic matter (peat) in the sedimentary rocks, as well as presence of few strains of microorganisms can influence the mobilization and concentration of inorganic arsenic in groundwater [Bhattacharya et al., 2011]. Volcanic and geothermal activities are other natural phenomena which can lead to arsenic contamination of air, water and soil [Shaji et al., 2021].

### **1.2.2. Anthropogenic sources of Arsenic**

Major anthropogenic sources of inorganic arsenic in the environment range from mining, smelting, burning of fossil fuels to use of arsenic containing pesticides, herbicides, fertilizers, wood preservatives etc. [Chung et al., 2014]. Arsenic is also used in

pharmaceutical, cosmetic, metallurgy, glassmaking and semiconductor industries, which can also be potential source of anthropogenic arsenic contamination. Inorganic forms of arsenic are found to be more toxic to human beings than the organic forms [Rahaman et al., 2021]. Amongst inorganic arsenicals, trivalent oxidation state is more toxic than pentavalent oxidation state. Some organic forms of arsenic like arsenobetaine, arsenocholine etc. are frequently found in marine organisms. Consumption of these marine organisms are potential source of arsenic exposure but most of these compounds are readily passed out of the body via urine almost unchanged, thus causing no damage to the system due to their organic nature [Taylor et al., 2017].

Arsenic is a toxic, global environmental pollutant as well as an established carcinogen. It is listed as a class I carcinogen by International Agency for Research on Cancer (IARC) [Martinez et al., 2011]. Exposure to inorganic arsenic (iAs) can result in detrimental health hazards both in acute and chronic doses. Acute exposure can result in stomach ache, vomiting, diarrhoea, muscle pain, muscle cramping, fatigue, skin rashes, lethargy, delirium, convulsions and dehydration which may eventually lead to death [Rahaman et al., 2021]. Chronic exposure to iAs may lead to development of dermatological, cardiovascular, respiratory, gastrointestinal, reproductive, developmental and neurological disorders. Induction of diabetes mellitus, peripheral arterial disease, as well as cancer of various organs like skin, lungs, liver, urinary tract, urinary bladder and kidney have also been linked to chronic iAs exposure [Chakraborti et al., 2018]. Acute iAs poisoning results in development of immediate symptoms (vomiting, diarrhoea etc.) which can be treated by administration of chelating agents like Dimercaprol (2, 3-dimercaptopropanol, also known as British anti Lewisite or BAL), 2-3-dimercapto-1-propanesulfonate (DMPS) and meso 2, 3-dimer-captosuccinic acid (DMSA) [Flora et al., 2007], unlike chronic iAs exposure, which remains symptomless for long periods (5-10

years) and then shows the development of numerous non-communicable diseases as well as cancer of various organs.

### **1.3. Global scenario of groundwater iAs contamination**

Humans can be exposed to iAs by inhalation of contaminated air, ingestion of contaminated water and food, as well as by direct dermal contact [Rahaman et al., 2021]. Groundwater is one of the most reliable sources of drinking water and near about 2.5 billion people worldwide depend on it [Shaji et al., 2021]. It was considered a relatively safe source of drinking water but, of late, contamination of arsenic and other heavy metals has rendered it to be hazardous. Groundwater iAs contamination has now emerged to be the most effective route of iAs exposure, it is a worldwide phenomenon, with the South Asian and South American regions being the worst affected areas. According to Shaji et al., nearly 107 countries around the globe have groundwater contaminated with iAs beyond the permissible limit (higher than 10 µg/L as recommended by WHO). Continent wise, 32 countries in Asia, 31 in Europe, 11 in North America, 9 in South America and 4 in Australia appear to suffer from groundwater iAs contamination. Regions with heavy groundwater pollution are usually found near the sedimentary basins located close to young mountains and deltas. Countries lying in the tropical zone appear to be more vulnerable to iAs contamination, as the temperature favours release of iAs from the rocks into the water [Ranjan, 2019]. South and South-east Asian countries like Bangladesh, India, Nepal, China, Vietnam, Myanmar, Laos, Indonesia are few of the worst affected countries [McArthur, 2019]. Countries like Argentina, Chile, Hungary, Canada, Pakistan, Mexico, South Africa, and USA also appear to be highly affected due to iAs contamination. Volcanic and geothermal activities appear to be the main culprit behind the arsenic contamination of groundwater in Latin American countries. 8.81 million people in Mexico

are exposed to iAs in groundwater above the level of 25  $\mu\text{g/L}$  [Alarcón-Herrera et al.,2020]. Central American countries like El Salvador and Guatemala too suffer from high iAs in groundwater due to volcanic activities [Libbey et al., 2015]. Developed countries like USA and Canada also suffer from widespread contamination of iAs in groundwater but the concentration of iAs is much lower than those found in south Asian countries [Sorg et al., 2019].

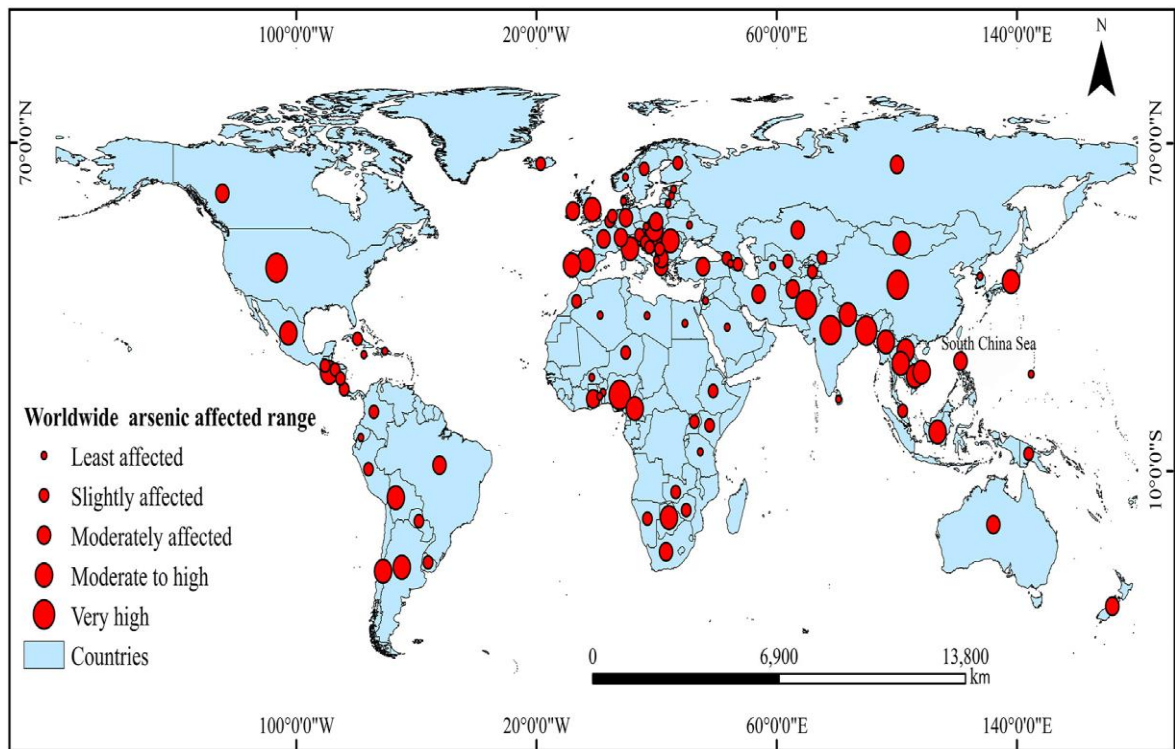


**Figure 1.1 Global scenario of arsenic contamination Shaji et al., 2021.**

Groundwater appears to be the most reliable source of water for industry, agriculture and household purposes in India [Saha and Ray, 2019]. Ganga-Brahmaputra plains account for the richest source of groundwater in the country, accounting for 26% of the Indian landmass and supporting a population of over 500 million. It is the most fertile and densely populated region of the world [Khan et al., 2016; Chakraborty et al., 2018]. Recent reports have indicated Ganga to be one of the most polluted rivers in the world.

Studies have reported presence of numerous toxins, heavy metals like chromium, arsenic, cadmium, lead, copper, mercury, pesticides and pathogenic microbes in Ganga almost 3000 times above the safe level [Tandon and Sinha, 2018]. Arsenic contamination of groundwater in India was first reported from Chandigarh in 1976. The patients from these regions suffered from non-cirrhotic portal vein hypertension (NCPH) due to concentration of arsenic in the liver. Presence of high amount of arsenic in drinking water was identified as the main culprit. The second case of arsenic poisoning was reported from West Bengal in 1983 which was brought into limelight by School of Environmental Studies (SOES), Jadavpur, Kolkata [Chakraborty et al., 2018]. Investigations following these early reports led to identification of numerous states where the groundwater iAs contamination was very high. At present, nearly 20 states like West Bengal, Jharkhand, Bihar, Uttar Pradesh, Assam, Gujarat, Haryana, Madhya Pradesh, Punjab, Arunachal Pradesh, Karnataka, Tamil Nadu, Himachal Pradesh, Telangana, Andhra Pradesh, Orissa, Nagaland, Tripura, Manipur, Chhattisgarh and 4 Union territories Delhi, Daman and Diu, Puducherry, Jammu and Kashmir are affected due to groundwater iAs contamination [Shaji et al., 2021]. West Bengal appears to be one of the worst affected states where, in the districts like Bardhaman, Hooghly, Howrah, Cooch Behar, Malda, Murshidabad, Nadia, North 24 Parganas and South 24 Parganas, the groundwater iAs contamination is many folds higher than the safe limit [Chakraborty et al., 2018]. iAs contamination of groundwater in India occurs in two types of soil, (i) fertile alluvial soil and (ii) hard rocky soil. 90% of arsenic contamination is found in aquifers located in the alluvial regions while the rocky landmass accounts only for 10% of iAs contaminated regions (aquifers found in the states of Karnataka and Chattisgarh). Arsenic is mainly released from arsenopyrites found in the gold mining areas of Raichur and Yadgiri districts, in Karnataka. Acid volcanic eruptions in the Kotri regions in Chattisgarh account for the arsenic depositions in groundwater [Shaji et al., 2021].

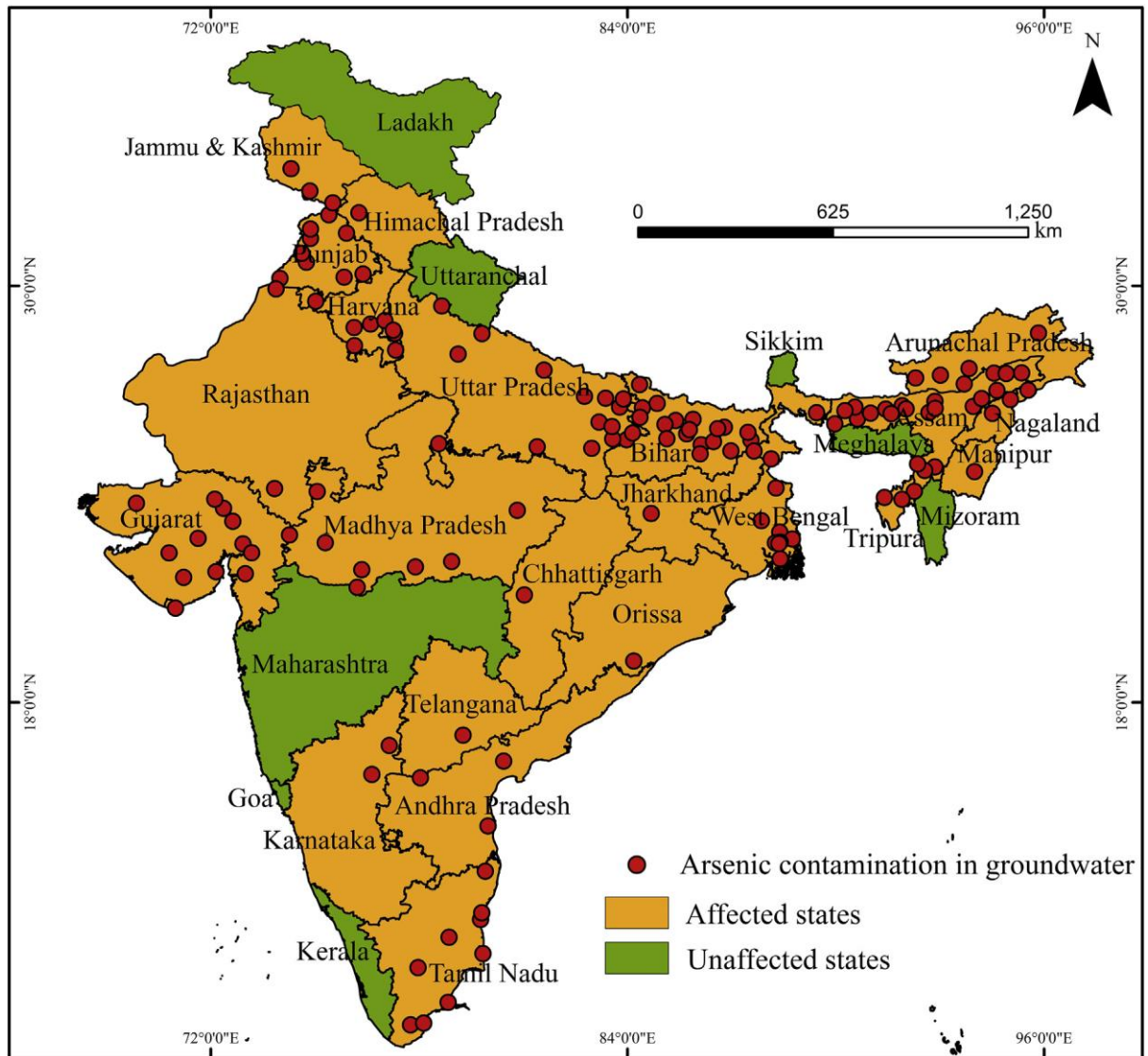


**Figure 1.2 Indian scenario of arsenic contamination Shaji et al., 2021.**

#### **1.4. Stages of carcinogenesis and hallmarks of cancer**

Theoretically, carcinogenesis can be divided into four major events like tumour initiation, tumour promotion, malignant transformation, and tumour progression [Weston and Harris, 2003]. During carcinogenesis benign hyperplastic cells are transformed into malignant forms which proceed further to become invasive and metastatic in nature. Tumour initiation refers to formation of DNA

adducts, due to carcinogen exposure, that leads to activation of protooncogenes or suppression of tumour suppressor genes, triggering cancer. These DNA adducts give rise to mutations. A positive correlation has been found between development of tumours and DNA-carcinogen adducts in animal models. Tissues devoid of DNA-carcinogen adducts rarely form tumours. Therefore, it appears that formation of DNA-carcinogen adduct is important for tumorigenesis but may not be a necessity. Tumour promotion deals with clonal selection of carcinogen initiated/mutated cells. The rate of cell division is proportional to the rate of aggregation of mutations; therefore, clonal expansion of the initiated/mutated cells result in formation of a larger population of cells where further genetic damage may accumulate, resulting in malignant conversion. The transformation of preneoplastic cells into cells displaying malignant features, is referred to as malignant conversion [Weston and Harris, 2003].

During tumour promotion, initiated/mutated cells are increased in number and during malignant conversion, a proportion of these cells are converted into malignant cells by further accumulation of genetic damage and alteration of the rate of cell division. Exposure to DNA damaging agents, increases the rate of malignant conversion of preneoplastic cells. Tumour progression refers to expression of malignant traits and aggressive features within the cells, over time. Genetic instability and uncontrolled proliferation of cells are the prominent malignant traits observed. This phenomenon also includes accumulation of invasive characteristics by the cells which may lead to metastasis beyond the primary location of the tumour [Weston and Harris, 2003]. This stage marks the final stage of carcinogenesis which is very often fatal for the victims. The biological changes which are commonly acquired by the cells during these stages of carcinogenesis are

generally referred to as hallmarks of cancer. These changes contribute to increase the complexity of the disease [Fouad and Aanei, 2017]. These hallmarks of cancer can be classified in the following categories [Hanahan and Weinberg, 2000; Hanahan and Weinberg 2011]:

- i. Sustenance of proliferation – Malignant cells are endowed with the property of sustaining chronic proliferation. Different signalling pathways effectively maintain the balance between cell proliferation and cell death in normal cells, which appear to be disrupted in malignant cells. This loss of balance results in uncontrolled proliferation of cancer cells [Hanahan and Weinberg, 2000].
- ii. Avoiding signals of growth suppressors – Tumour suppressors are known to inhibit tumour formation by suppressing the signalling pathways which control cell growth and proliferation. Tumour suppressor genes are inhibited or their activity is suppressed in cancer cells, due to which cell divisions are not controlled. Malignant cells also lack contact inhibition which promotes their uncontrolled proliferation [Hanahan and Weinberg, 2000].
- iii. Evading apoptosis (programmed cell death) – Cellular damage or infection leads to triggering of programmed cell death or Apoptosis in normal cells. Cancer cells are able to escape programmed cell death by circumventing the signalling pathways and downregulating the signalling intermediates which induce apoptosis [Hanahan and Weinberg, 2000].
- iv. Replicative immortality – The number of cells divisions for a normal mammalian cell is limited, beyond which they undergo senescence or death. This is due to the presence of telomeres, which gets shortened after every



cell division. In cancer cells, telomeres are not shortened due to hyperactivation of telomerases (enzyme which maintains the length of the telomere), resulting in indefinite replication without induction of senescence. Hence, cancer cells achieve replicative immortality [Hanahan and Weinberg, 2000].

- v. Induction of angiogenesis – Cells require a constant supply of oxygen and nutrients from blood vessels for their survival. In tumours where cells are constantly proliferating, the need for oxygen and nutrients is very high. Under such circumstances cancer cells perform angiogenesis which gives rise to new blood vessels, to supply nutrients to the tumour cells. Angiogenesis is important for tumour growth and maintenance. Cancer cells are able to induce the secretion of pro-angiogenic factors for their survival and proliferation [Hanahan and Weinberg, 2000].
- vi. Promotion of tissue invasion and metastasis – Cancer cells undertake aggressive proliferation which is followed by invasion. EMT, epithelial to mesenchymal transition, is a phenomenon during which epithelial cells are transformed into mesenchymal cells, which helps in their invasion of the surrounding tissues. Cancer cells are known to invade the layers of the underlying tissue, following which they migrate away from its site of origin and colonize tissues of another organ or lymph node, which is known as metastasis [Hanahan and Weinberg, 2000].
- vii. Genomic instability – Though the genomic modifications observed in different cancer cells vary dramatically, yet most of them appear to be associated with genome maintenance, repair defects, destabilization of gene

copy number and nucleotide sequences, indicating a prominent role of genomic instability in tumorigenesis. Therefore, genome instability appears to be a key factor strongly influencing other hallmarks of cancer [Hanahan and Weinberg, 2011].

- viii. Inflammation – Inflammation influences numerous hallmarks of cancer like maintenance of tumour microenvironment; induction of growth factors which sustain proliferation; promotion of signalling pathways inducing cell survival and inhibit cell death; elevation of angiogenic factors and matrix metalloproteases facilitating angiogenesis, invasion, migration and metastasis. Therefore, inflammation can be considered a primary hallmark which strongly influences other hallmarks of cancer [Hanahan and Weinberg 2011].
- ix. Modulation of energy metabolism – The energy metabolic pathways are deregulated in cancer cells. Cancer cells switch to glycolysis even in the presence of oxygen. This leads to switching on of intermediary pathways and production of precursor compounds which play important role in maintenance of carcinogenic conditions. Higher rate of oxidative phosphorylation accompanied with glycolysis are required to meet the high anabolic demands of cancer cells and thus energy metabolism is an essential hallmark of cancer [Pavlova and Thompson, 2016].
- x. Modulation of the immune system – Evading immune surveillance is important for the survival of cancer cells. Cancer cells undergo genetic and epigenetic modifications and perform immune-editing, in order to escape the immune cells. These malignant cells may also enter into latent phases and

remain dormant for long periods of time to evade immune cells [Dunn et al.,2002; Malladi et al., 2016]. Evasion of immune surveillance is an essential hall mark of cancer [Hanahan and Weinberg 2011].

### **1.5. Skin problems due to chronic iAs exposure**

One of the preliminary effects of chronic iAs exposure appears in the form of dermatological manifestations like hyperpigmentation and hyperkeratosis. Hyperpigmentation results in darkening of the skin, palms and soles of the hands and feet [Hunt et al., 2014]. It may also take the form of spotted melanosis, where dark spots may appear on the chest, back and limbs of the victim. In certain cases, spotted melanosis may also occur in the mucous membrane of the victims' mouth, resulting in spotted pigmentation of the gums, lips and the tongue [Chakraborti et al., 2018]. Hyperkeratosis results in the formation of diffused, nodular and sometimes palpable keratosis on the palms, soles of the feet as well as on the dorsal side of the hands and limbs [Chakraborti et al., 2017]. iAs exposed individuals having dermal manifestations like hyperkeratosis, hyperpigmentation or Bowen's disease have also been reported to develop internal cancers like lung cancer and urothelial cancers. A cohort study in Taiwanese population had reported significant relationship between hyperkeratosis and lung cancer [Hsu et al 2013]. Many of these preliminary dermal manifestations may further develop into Bowen's disease, Squamous cell carcinoma (SCC) and Basal cell carcinoma (BCC) of the skin.



**Figure 1.3 Preliminary cutaneous manifestation of chronic iAs exposure (a) spotted melanosis (b) leucomelanosis (c) tongue melanosis (d) spotted keratosis present on the soles of the feet (e) keratosis present on the palms of the hands (f) black foot disease.**

Bowen’s disease, also referred to as *in situ* SCC is multifocal. Histopathological studies indicate development of full-layered epidermal dysplasia, enhanced thickness of the epidermis, dyskeratosis and dermal infiltrations. It may also lead to thickening of the rete ridges and appearance of atypical keratinocytes, spanning the entire breadth of the epidermis. These keratinocytes appear to have increased mitotic activity as indicated by pleomorphic and enlarged nuclei. The presence of these atypical keratinocytes provides a “windblown” appearance to the epidermis. Multinucleated giant cells, dyskeratotic cells and highly vacuolized cells are also found scattered throughout the epidermis in Bowen’s disease [Yanofsky et al 2011]. Invasive Squamous Cell Carcinoma (SCCI) is demarcated by the presence of infiltrating cells which cross the basement membrane and reach the

dermis forming large nests. SCCI can be both well differentiated as well as poorly differentiated. Presence of enlarged hyperchromatic nuclei as well as large keratin depositions, giving rise to huge keratin pearls are hallmarks of well differentiated SCCI. Well differentiated SCCI show lesser aggressive and malignant traits than poorly differentiated SCCI. Poorly differentiated SCCI display pleomorphic nuclei and reduced keratin deposits, which are highly aggressive, metastatic and have high rates of recurrence [Yanofsky et al 2011]. Development of both differentiated and poorly differentiated SCCI have been reported from chronic iAs exposure.

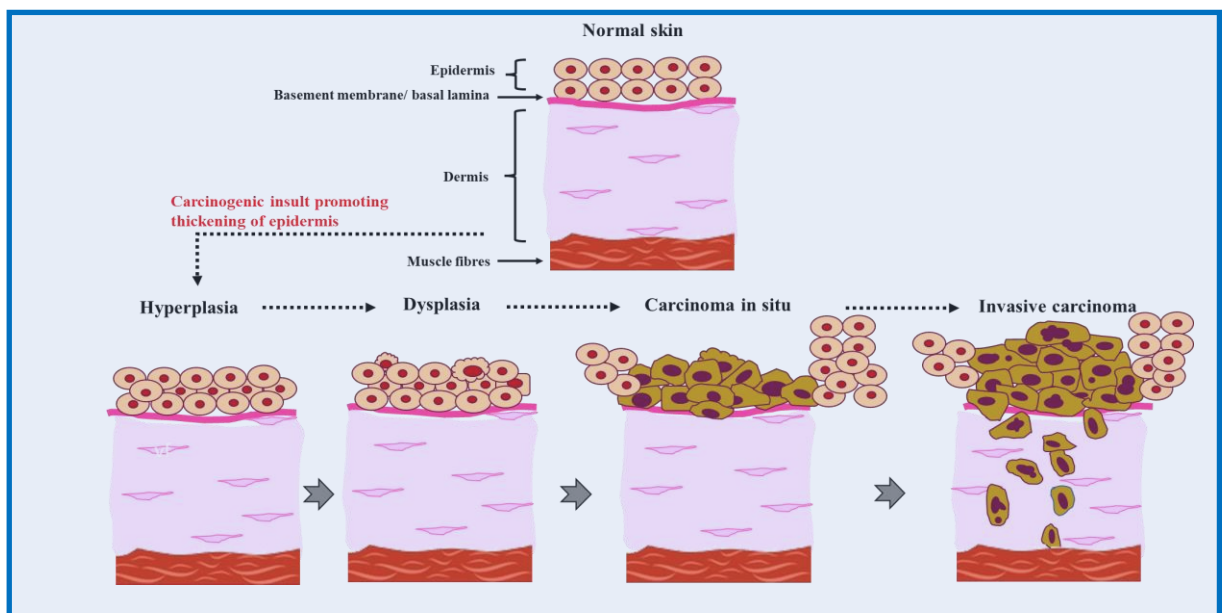


**Figure 1.4. Schematic representation of the development of squamous cell carcinoma of the skin. Carcinogen insult results in thickening of the epidermis and increase in the number of cells, leading to hyperplasia, which may be the initial sign of abnormal or precancerous changes. Hyperplasia may develop into dysplasia, where a number of abnormal cells are seen. These may further promote to localised squamous cell carcinoma (SCC) of the skin, called in situ carcinoma. With passage of time, progression may occur and invasive carcinoma results, where the cancer cells breach the adjacent tissue structure, penetrating and infiltrating it which promotes metastasis and secondary tumour formation.**

## 1.6. Arsenic metabolism

Biotransformation is a metabolic pathway which transforms the exogenous or endogenous substances chemically into a form which can be easily excreted. This phenomenon mainly occurs in the liver but may also take place in other organs [Watanabe and Hirano, 2013]. A series of chemical reactions increases the polarity of the exogenous/endogenous substance, makes it more soluble in water and facilitates its excretion. Biotransformation of iAs mainly involves reduction, methylation and oxidation. The rate and extent of iAs methylation seems to vary from person to person and has been linked to development of iAs induced diseases. The metabolism of iAs and its biotransformation occurs primarily in the liver. Methylation of iAs occurs in the presence of a methyl donor, S-adenosylmethionine (SAM), a cofactor, glutathione (GSH) and a catalyst, arsenic methyltransferase (AS3MT) which catalyses the transfer of methyl group from SAM to iAs [Khairul et al., 2017]. Methylation of iAs results in the formation of two monomethylated species namely monomethylarsonous acid ( $\text{MMA}^{\text{III}}$ ) and monomethylarsonic acid ( $\text{MMA}^{\text{V}}$ ) and two dimethylated species dimethylarsinous acid ( $\text{DMA}^{\text{III}}$ ), dimethylarsinic acid ( $\text{DMA}^{\text{V}}$ ). Apart from liver, *in-vitro* studies have also shown that, high rates of iAs methylation also takes place in testes, kidney and lungs [Healy et al., 1998]. The metabolism of iAs was first reported by Frederick Challenger in microorganisms which was called the reductive/oxidative methylation pathway. In this pathway of metabolism,  $\text{iAs}^{\text{V}}$  is reduced to  $\text{iAs}^{\text{III}}$ , methylated to  $\text{MMA}^{\text{V}}$ , which is then reduced to  $\text{MMA}^{\text{III}}$ . In the next step oxidative methylation occurs and  $\text{MMA}^{\text{III}}$  is converted to  $\text{DMA}^{\text{V}}$  which is again reduced to  $\text{DMA}^{\text{III}}$  and ultimately passes out via the urinary tract [Rehman and Naranmandura, 2012]. In certain species,  $\text{DMA}^{\text{V}}$  can also be converted to trimethylarsine oxide ( $\text{TMAO}^{\text{V}}$ ), but this event does not occur in humans. The existence of

methylated intermediates of the iAs metabolism pathway as described by Challenger, was experimentally proved by Cullen in fungal and algal cultures [Cullen, 2014]. Apart from the one put forward by Challenger, other alternative iAs methylation pathways have also been reported where glutathione or protein conjugated intermediates are formed. According to Hayakawa et al., conversion of  $iAs^{III}$  to pentavalent arsenical compound occurs after methylation where the arsenic bound glutathione acts as the major substrate for AS3MT. The  $iAs^{III}$  conjugated glutathione species undergo methylation giving rise to monomethylarsonic<sup>III</sup> diglutathione and dimethylarsinic<sup>III</sup> diglutathione, in the presence of SAM and GSH [Hayakawa et al., 2005]. The conjugated glutathiones or other exogenous bound proteins provided thiol groups to the arsonium centre, which would nullify the charges on the arsenic molecule thus making it possible for the C-3 group to leave the positive centre of the molecule and making the reaction feasible [Khairul et al., 2017]. Reductive methylation appears to be the most important part of arsenic metabolism.  $iAs^{III}$  gets metabolised to the respective methylated products, while remaining bound to thiol containing proteins (GSH) due to reductive methylation by AS3MT, in the presence of SAM which is then oxidized to its pentavalent forms. The schematic representation of metabolism of iAs has been given in Figure 1.5.  $iAs^{III}$  and its methylated products  $MMA^{III}$  and  $DMA^{III}$  have been found to be more toxic to the cells than its pentavalent counterpart suggesting that under certain circumstances biotransformation of iAs may lead to its bioactivation rather than its detoxification, for example, in case of chronic iAs exposure, metabolism results in bioactivation whereas for acute exposures, the methylation of iAs results in its detoxification [Mass et al., 2001]. Certain reports have also suggested the methylated trivalent arsenical species are more toxic than trivalent iAs. Recent investigations have observed a correlation between, high concentration of methylated arsenicals in the urine and development of bladder and skin cancer [Steinmaus et al., 2003].

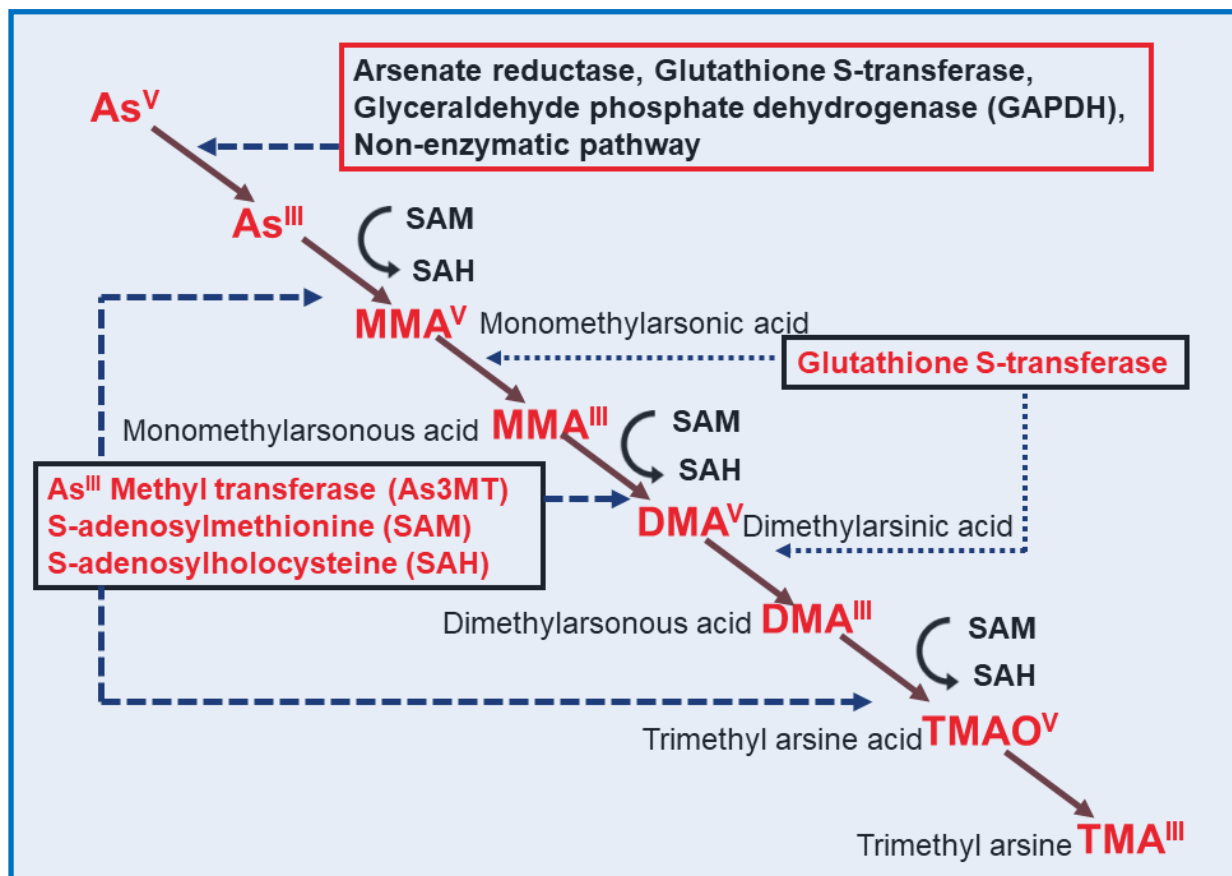


**Figure 1.5. Schematic representation of arsenic metabolism.**

### 1.7. Effect of chronic iAs exposure on ROS generation and beyond.

One of the primary mechanisms through which iAs mediates its carcinogenicity is by the excess generation of Reactive Oxygen Species (ROS). Reduction of molecular oxygen during metabolism of iAs results in the formation of superoxide radical anion, hydrogen peroxide, peroxy radical, hydroxyl radical and singlet oxygen, all of which fall under the ROS family [Shi et al., 2004]. The superoxide radical anion is produced by the mitochondrial complexes I and II in the electron transport chain as a by-product. iAs induces mitochondrial toxicity and suppresses the activity of succinic dehydrogenase resulting in disruption of oxidative phosphorylation and gives rise to superoxide anion, as



well as other forms of ROS [Hu et al., 2020]. iAs also induces ROS generation by modulating the activity of Nicotinamide adenine dinucleotide phosphate [NAD(P)H] oxidase (NOX), which is a membrane associated enzyme. Study on endothelial cells has confirmed this phenomenon [Ellinsworth, 2015]. Metabolism of arsenic may also lead to generation of ROS for example, biotransformation of DMA<sup>V</sup> results in peroxy radical formation. Oxidation of arsenite to arsenate also leads to excess ROS generation [Hu et al., 2020]. DMA<sup>III</sup> has been reported to induce Endoplasmic Reticulum (ER) and promote generation of ROS [Naranmandura et al., 2012]. iAs has been reported to suppress the activity of antioxidant enzymes like Catalase, Superoxide dismutase (SOD), Glutathione Peroxidase (GPx), Glutathione Reductase (GR) and Glutathione -S- Transferase (GST) which indirectly promotes accumulation of ROS [Ghosh et al., 2021]. iAs induced excess ROS generation has been reported to inflict severe damage to DNA, lipids and proteins. ROS interacts with the DNA bases giving rise to 8-oxoguanine (8-oxo-G) DNA adducts and promotes strand breaks, thus inducing DNA damage [Srinivas et al., 2019]. ROS damages lipids by promoting lipid peroxidation of polyunsaturated fatty acids, which results in formation of malondialdehyde (MDA). Accumulation of higher amounts of MDA has cytotoxic effects on the cell. Peroxidation of the unsaturated fatty acids promote fragmentation of the lipid-chains resulting in enhanced fluidity of the cell membrane and increased permeability [Yusupov et al., 2010]. ROS can also induce oxidation of amino acids in the proteins resulting in formation of carbonyl compounds and inducing protein damage [Sinha et al., 2010]. Agglomeration of these cellular damages over the period of chronic iAs exposure promotes carcinogenesis. Reactive oxygen species (ROS) can modulate several molecules implicated in tumorigenesis. Some of these include pro- and anti-inflammatory cytokines like Tumour necrosis factor alpha (TNF- $\alpha$ ), interleukins, nuclear factor kappa B (NF $\kappa$ B). ROS can also alter the signalling cascade of Transforming

growth factor beta (TGF- $\beta$ ), mitogen-activated protein kinase (MAPK) etc. resulting in epithelial to mesenchymal transition (EMT), ultimately promoting tumour growth and cancer progression. [Yu and Kim, 2014].

### **1.8. Effect of iAs on DNA repair enzymes**

DNA damage is one of the major causative factors for carcinogenesis. Impairment of DNA repair enzymes lead to accumulation of damaged DNA giving rise to mutations and chromosomal aberrations. These modifications in the DNA may alter the activity of tumour suppressor genes and activate oncogenes, which promote malignant transformation of the cancer cells [Torgovnick and Schumacher, 2015]. One of the pathways by which iAs promotes cancer is by suppressing the activity of DNA repair enzymes. iAs has been reported to alter the expression as well as inhibit the activity of several enzymes involved in base excision repair (BER) and nucleotide excision repair (NER) pathways [Tam et al., 2020]. BER is an important repair pathway which deals with removal of alkylated nucleobase lesions produced due to oxidation, apurinic/apyrimidinic (AP) bases and breaks in DNA strands. Repair of 8-oxo-G by DNA glycosylase I (OGG1) is a BER pathway [Ba and Boldogh, 2018]. According to a study, iAs reduced the mRNA content as well as the enzymatic activity of OGG1 in A549 human lung epithelial cells [Ebert et al., 2011]. AP endonuclease I (APE1) is a major endonuclease which recognizes the AP sites and removes them in eukaryotic cells. Exposure to iAs has been reported to suppress the expression of APE1 both at the mRNA level and at the protein level [Sykora and Snow, 2008]. iAs exposure greater than  $\geq 5 \mu\text{M}$  has also been reported to inhibit the expression of DNA polymerase  $\beta$ , which is an important enzyme involved in DNA repair synthesis [Idriss et al., 2002]. Another study on neonate BALB/c mice revealed that sub chronic iAs exposure via drinking water resulted in prominent reduction in the mRNA's of BER enzymes like

APE1, DNA ligase I, OGG1, Poly (ADP-ribose) polymerase 1 (PARP1), and DNA polymerase (DNA Pol $\beta$ ) [Osmond et al., 2010]. Therefore, iAs seems to effectively downregulate the expression and activity of BER enzymes.

Bulky DNA adducts and helix distorting lesions, formed by carcinogens like UV radiation, polycyclic aromatic hydrocarbons (PAH) etc. are often repaired by the nucleotide excision repair (NER) pathway [Scharer, 2013]. Exposure to iAs has also been reported to hinder the expression and activity of many important enzymes involved in NER pathway. excision repair cross complementation group 1 (ERCC1), human xeroderma pigmentosum group B (XPB) and XPF are important NER enzymes which were found to be suppressed upon exposure to iAs in drinking water [Andrew et al., 2003a]. ERCC1 showed a dose dependent decline in mRNA, when exposed to iAs for 72 hours, in cardiomyocytes [Mo et al., 2011]. A DNA microarray study on human epidermal keratinocytes showed prominent suppression of DNA repair genes like human xeroderma pigmentosum group C (XPC), DNA damage-binding protein 2 (DDB2) and tumour protein 53 (TP53) upon exposure to iAs [Hamadeh et al., 2002]. Another microarray study on human lung epithelial cells showed almost 1.5-fold decrease in the mRNAs of the human xeroderma pigmentosum group D (XPD), XPC, proliferating cell nuclear antigen (PCNA), DNA ligase I, APE1 and Replication factor C (RFC) genes, upon a 4-hour exposure to 5  $\mu$ M of iAs [Andrew AS., 2003b]. iAs along with its methylated product MMA<sup>III</sup> inhibited the expression of XPC at both the mRNA and protein level, in a dose dependent manner, in human skin fibroblasts [Nollen et al., 2009]. A recent study on human lung fibroblast IMR-90 cells, showed downregulation of XPC along with other DNA repair genes like human xeroderma pigmentosum group A (XPA) and DDB2 upon iAs exposure [Holcomb et al., 2017]. A study on xenograft mice model prepared by intraperitoneal injection of human ovarian cancer cells, reported that iAs administration was able to inhibit the activity of NER

enzyme XPC in resistant ovarian cancer cell line and thus enhanced the activity of chemotherapeutic drug cisplatin [Helm and States, 2011]. DNA repair enzymes have several zinc finger domains in their active site, iAs substitutes the zinc ions in the zinc finger domain thus disrupting the activity of the DNA repair enzymes. NER enzymes like XPA and PARP1 have been found to be preferable targets of Zinc ion substitution by  $iAs^{3+}$  and MMA<sup>III</sup> [Tam et al., 2020]. iAs can also induce NO-mediated nitrosylation of DNA repair enzymes belonging to NER pathway which ultimately results in their deactivation and suppression [Bau et al., 2001; Zhou et al., 2016]. These findings indicate that, iAs and its methylated metabolites employ several mechanisms to downregulate DNA repair enzymes of NER pathway both at the mRNA and protein level.

NHEJ pathway is a double strand break repair pathway. The main players of this repair pathway include DNA dependent protein kinase (DNA-PKcs), X-Ray Repair Cross Complementing 4 (XRCC4) and DNA ligase IV. XRCC4 and DNA ligase IV complex completes the final ligation step. A field study from our lab had reported that, in chronically iAs exposed population, the expression of DNA-PKc, XRCC4 and DNA ligase IV was effectively downregulated both at the protein and at the mRNA level [Roy et al., 2011]. This indicates that iAs also inhibits the activity of the repair enzymes belonging to the NHEJ pathway. DNA ligases play very prominent role in DNA repair and replication. iAs had been reported to significantly inhibit the expression and activity of DNA ligase I and III, in mammalian cells. iAs interacts with the vicinal cysteines present in DNA ligase III and retards its ligation activity [Tam et al., 2020]. X-Ray Repair Cross Complementing 1 (XRCC1) plays an important role in recruiting and stabilizing DNA ligase III, iAs has been found to downregulate XRCC1 thus inhibiting the recruitment and activity of DNA ligase III [Cannan et al., 2017]. Inhibition of ligating activity leads to accumulation of

single or double stranded breaks in the DNA, which ultimately results in genomic instability, mutations and carcinogenesis.

### **1.9. Arsenic and inflammation**

Inflammation is a hallmark of cancer and excess ROS generation has been intricately linked to induction of inflammatory conditions within the system [Hanahan and Weinberg, 2011]. Inflammation can be acute or chronic. The cytokine signalling is different for acute and chronic inflammation. Acute inflammation acts as a defensive mechanism for the system while chronic inflammation sustains tumour, promotes migration of tumour cells and metastasis [Neagu et al., 2019]. Acute inflammatory reaction involves T-helper (Th)1 cells stimulating the secretion of cytokines like interleukin (IL)-2 and interferon (IFN)- $\gamma$ . Chronic inflammatory reaction involves regulatory T cells (Tregs) and Th2 cells, along with secretion of an array of pro-inflammatory cytokines like IL4, IL6, IL13 and transforming growth factor (TGF)- $\beta$  [DeNardo and Coussens, 2007]. There are many factors that enhance the secretion and activity of many pro-inflammatory cytokines and suppress anti-inflammatory cytokines [Rea et al., 2018]; ROS is one such inflammation inducing factor. Accumulation of inflammatory factors like cytokines and chemokines for prolonged period in the skin tissue leads to immunosuppression, ultimately resulting in tumorigenesis. Keratinocytes, Langerhans's cells, melanocytes, mast cells (MCs) and macrophages found in the layers of the skin, play important role in induction of pro-inflammatory cytokines and tumour microenvironment. In chronic inflammatory condition, the cytokine production is upregulated and the auto-regulatory loop is broken which results in constant elevation of pro-inflammatory factors [Neagu et al., 2010]. Keratinocytes can play a major role in inducing a microenvironment which promotes chronic inflammation. Keratinocytes are known to secrete pro-inflammatory cytokines like IL1, granulocyte-

macrophage colony stimulating factor (GM-CSF), tumour necrosis factor (TNF)- $\alpha$  , IL6, IL7, IL22, IL15 as well as IL18. The T cells may interact with keratinocytes by secreting other cytokines like IFN- $\alpha$ , IL17 and IL4 and this interaction promotes tumorigenesis [Neagu et al., 2009]. Some of the pro-inflammatory factors which play important role in induction of cancer have been discussed here.

TNF- $\alpha$  is a proinflammatory cytokine, produced by innate immune cells like macrophages and Antigen Presenting Cells (APC) which chemotactically acts along various interleukins like IL1 $\alpha$ , IL1 $\beta$ , IL6 and IL8 resulting in linking up of the innate and adaptive immunity [Zehnder et al., 2003; Alam and Gorska, 2003]. TNF- $\alpha$  is secreted along with IL1 during bacterial infections. TNF- $\alpha$  controls the pro-inflammatory signalling, induces vascular and cellular changes, recruits neutrophils and initiates the primary immune response in the hosts [Silva et al., 2019]. T and B Leukocytes are potentiated by TNF- $\alpha$  which further affects chemotaxis, macrophages and natural killer cells by feedback loop. These events are followed by other cascading events which eventually leads to activation of adaptive immune response. TNF- $\alpha$  has also been found to induce prostaglandins, fever, C-reactive proteins (CRP), activation of endothelial cells, as well as bone reabsorption [Prso et al., 2007; Boyce et al., 2005]. Upregulation of TNF- $\alpha$  has been recorded in cases of breast cancer and its recurrences [Aggarwal et al., 2006]. Moreover, upregulation of TNF- $\alpha$  has also been observed in serous ovarian tumours [Liu et al., 2020]. TNF- $\alpha$  knocked out mice showed reduced susceptibility towards skin tumour formation even after application of 7,12-Dimethylbenz[a]anthracene (DMBA) and 12-O-tetradecanoyl phorbol-13-acetate (TPA) [Moore et al., 1999]. TNF- $\alpha$  can also activate NF $\kappa$ B through canonical as well as non-canonical pathways along with Jun N-terminal kinase (JNK), MAPK and Protein kinase B (AKT). It has been reported that TNF- $\alpha$  can up-regulate over 400 inflammatory

genes which includes cell-adhesion molecules, anti-apoptotic proteins, cytokines and chemokines [Liu et al., 2020].

IL2 is another cytokine which plays important role in immune response. It is one of the most studied cytokines and is mainly produced by clusters of differentiation 4 (CD4+) T cells. It can also be produced by clusters of differentiation 8 (CD8+) T cells, Natural Killer cells and activated dendritic cells [Jiang et al., 2016]. IL2 induces differentiation of CD4+ T cells as well as promotes differentiation of naive CD4+ T cells into T helper (Th1) and T helper 2 (Th2) cells. It can also promote cytotoxic activity of CD 8+ T cell and natural killer (NK) cells [Paul and Zhu, 2010; Littman and Rudensky, 2010]. IL2 receptor is made up of three subunits namely IL2R $\alpha$ , IL2R $\beta$  and IL2R $\gamma$ . IL2R $\alpha$  is a specific receptor of only IL2 and is expressed on T regulatory (Treg) cells, activated CD4+ and CD8+T cells, B cells, mature dendritic cells as well as in endothelial cells [Rudensky, 2011; Krieg et al., 2010]. The  $\alpha$  chain is known to bind with IL2 and redirects it to the cell surface, increases its concentration, induces conformational change in IL2 and then binds with the  $\beta\gamma$  chain. The trimeric receptor  $\alpha\beta\gamma$  has the highest affinity for the cytokine IL2. Binding of IL2 to the IL2R $\alpha\beta\gamma$  and IL2R $\beta\gamma$  receptors result in activation of various intracellular signalling cascades like the Janus kinase-signal transducers and activators of transcription (JAK-STAT) pathway, phosphoinositide-3-kinase–protein kinase B (PI3K-AKT) pathway and MAPK pathway 2. Activation of these pathways result in survival, proliferation, differentiation, activation and cytokine production in various immune cells [Malek, 2008; Sim and Radvanyi, 2014]. Therefore, IL2 plays an important role in differentiation of immune cells in the presence of antigens but it also helps in the proliferation and maintenance of Treg cells. The role of Treg cells is to suppress the immune response, thus, it plays a prominent role in development and maintenance of Tumour microenvironment. Infiltration of Treg cells has been reported in various cancers, including breast and

pancreas, and is associated with poor prognosis and survival rate. Therefore, downregulation of IL2 would result in reduction of the Treg cells resulting in proper immune functioning and suppression of tumorigenesis [ Ha, 2009].

IL6 is an important pro-inflammatory cytokine secreted by T cells, macrophages as well as B cells. It is known to play important role in inducing acute phase inflammation during infection within the body and also performs haematopoietic functions [Hunter and Jones, 2015]. Upregulation of IL6 has been observed in conditions like tumorigenesis, graft rejection etc. [Feng et al., 2018]. Reports have also suggested IL6 to be a prognostic marker in pancreatic, renal and ovarian cancer [Ebrahimi et al., 2004; Kallio et al., 2017; Kawabata et al., 2017]. Elevated levels of IL6 were found to be correlated to reduced survival rate and bad prognosis [Mitsunaga et al., 2013]. IL8 is another important cytokine which is known to play important role during infection as well as tumour inhibition. This cytokine is a strong chemotactic agent and is known to activate neutrophils, lymphocytes and basophils [Russo et al., 2012]. High levels of IL8 have been observed in the regions surrounding the inflammatory zone and, in the serum, in cases of infection or certain autoimmune disorders. It has also been reported in the proliferation of tumour cells. IL8 has been implicated in the development and proliferation of pancreatic, nasopharyngeal, colorectal and lung cancer [Ning and Lenz, 2012; Lo et al., 2013; Chen et al., 2014]. IL8 has also been reported to an important prognostic marker in various cancers; individuals with high IL8 showed lower survival rate [Feng et al., 2018].

IL13 is a cytokine which modulates inflammation and immune response. Expression of IL13 mainly induces type 2 immune response and they have been found to be linked to numerous atopic diseases like asthma and atopic dermatitis [Gandhi et al., 2017]. IL13 has been reported to be secreted by immune cells such as CD4-T cells, basophils,



neutrophils and natural killer T cells [Junttila, 2018]. IL13 transmits its signalling via three different receptors namely Type I, II and III. Type I and II IL13 receptors are expressed in non-haematopoietic cells, whereas Type III receptor are expressed on the surface of the haemocytes [Suzuki et al., 2015]. IL13 and its receptors have been found to be intricately linked to apoptosis, chemosensitivity and prognosis of different cancers [Song et al., 2021]. It has also been reported to be involved in signalling cross talk with the tumour microenvironment (TME) and have been found to activate tumour associated macrophages and myeloid derived suppressor cells, which display tumour promoting activities [Lin et al., 2016]. IL13 has been reported to negatively regulate immune surveillance in metastatic breast cancer, in mice [Sinha et al., 2005]. This interleukin also seems to play important role in cancer cell proliferation as well as in migration and invasion of aggressive metastatic cells [Bartolome et al., 2015]. Over expression of IL13 receptors have been reported in pancreatic cancer cells lines like PANC-1, MIAPaCa-2 and CAPAN-1 [Song et al., 2021]. A study on human samples also reported to have very high expression of IL13 in the plasma of 46 pancreatic cancer patients, 25 gastric cancer patients and 60 oesophageal cancer patients compared to the healthy individuals. Therefore, IL13 is another proinflammatory cytokine which promotes tumour growth and carcinogenesis [Gabitass et al., 2015].

In non-melanoma skin cancers (NMSC) like SCC and BCC, the secretion of specific cytokines IL17 and IL22 by T cells were found to be very high. In-vitro studies had shown that upregulation of IL17 and IL22 resulted in prominent increase in the proliferative and migratory abilities of the cells. It was also observed that, IL17 was able to stimulate the production of pro-inflammatory cytokines like IL6 and IL8. In-vivo studies also showed that IL17 and IL22 helped to create and maintain tumour microenvironment as well as induce tumorigenesis [Nardinocchi et al., 2015].

IL10 is an anti-inflammatory cytokine secreted by the Th2 cells, activated B cells, monocytes and macrophages [Sabat et al., 2010]. IL10 hinders the pro-inflammatory role of antigen presenting cells (APC's) by upregulating antagonistic co-stimulatory molecules [Acuner-Ozbabacan et al., 2014]. Low activity and expression of IL10 has strong correlation with poor survival in cases of breast cancer [Li et al., 2010]. IL10 exhibits both immunosuppressive and anti-angiogenic role. IL10 is involved in regulation of inflammation, progression of infection, autoimmune responses, transplantation tolerance and carcinogenesis [Sheikhpour et al., 2018]. IL10 has been found to suppress the expression of IL1 $\alpha$ , IL1 $\beta$ , IL6, IL8, IL12, IL18, TNF- $\alpha$ , and granulocyte-macrophage colony-stimulating factor (GM-CSF) in T cells and macrophages [Khan et al., 2012], so it is often regarded as cytokine synthesis inhibitory factor (CSIF). Apart from these it also inhibits the expression of IFN- $\gamma$  in activated Th cells, peripheral blood mononuclear cells (PBMC's) as well as induces the differentiation of mast cells. Inhibition of IL10 results in production of pro-inflammatory cytokines in mice which promote tumour growth [Acuner-Ozbabacan et al., 2014]. IL10 also appears to have a dual role and elevated levels of it have been considered as a prognostic marker in multiple myeloma and thyroid cancer [Wang et al., 2016; Cunha et al., 2017].

NF $\kappa$ B is an important transcriptional regulator which acts as the downstream effector molecule of different inflammatory cytokines. It can modulate the expression of different genes and alter cell growth and proliferation [Lingappan, 2018]. ROS are persistently elevated in many types of cancers, which phosphorylates the tyrosine residue of I $\kappa$ B $\alpha$  (a regulatory protein which inhibits the activation of NF $\kappa$ B) resulting in its degradation. Degradation of I $\kappa$ B $\alpha$  activates NF $\kappa$ B and promotes its translocation to the nucleus, thus ROS modulates proliferation and growth of cells by promoting NF $\kappa$ B

activation and its translocation to the nucleus [Hoesel and Schmid, 2013; Maru et al., 2014].

Chronic iAs exposure can induce inflammatory conditions by impairing the function of immune cells and modulating the expression of cytokines like TNF- $\alpha$ , IL6, IL10 etc. A meta-study reported significant upregulation of IL6, IL8, IL12 and subsequent downregulation of IL10 upon chronic iAs exposure [Zhang et al., 2022]. According to a study, low dose of arsenic has been found to induce pulmonary and systemic inflammation [Das et al., 2014]. Another study reported severe upregulation of TNF- $\alpha$ , IL8 and TGF- $\beta$  in the urothelial cells of arsenic exposed individuals [Liu et al., 2014]. iAs exposed individuals suffering from atherosclerosis showed upregulation of CD14 and other pro-inflammatory cytokines in their lymphocytes [Wu et al., 2003]. Chronic low dose iAs exposure led to increase in the plasma levels of pro-inflammatory cytokines likes TNF- $\alpha$ , IL6, IL8 and IL12 with simultaneous downregulation of anti-inflammatory cytokine IL10 in women population. These women also showed high activity of MMP2 (matrix metalloproteinase 2) and MMP9 (matrix metalloproteinase 9) with a prominent upregulation of NF $\kappa$ B [Dutta et al., 2015]. Therefore, chronic iAs exposure results in upregulation of a number of pro-inflammatory cytokines, and NF $\kappa$ B with subsequent downregulation of anti-inflammatory cytokines, resulting in development of prolonged inflammatory conditions. Prolonged inflammatory conditions due to iAs promote induction and maintenance of tumour microenvironment, ultimately leading to cancer and metastasis.

### **1.10. Arsenic and epigenetic modulations**

Epigenetic modifications refer to those heritable changes which occur without the alteration of the DNA sequence. Epigenetic alterations can occur by DNA methylation, post translational histone modifications (PTM), regulation of non-coding RNA's etc. Variations

in epigenetic marks result in aberrant expression of genes ultimately leading to development of innumerable pathological conditions including cancer [Liu et al., 2015]. Arsenic has been reported to promote epigenetic changes by inducing PTMs and alteration of DNA methylation patterns. iAs induced epigenetic modifications, which suppress expression of tumour suppressor genes and activate oncogenes, may induce cancer [Eckstein et al., 2017].

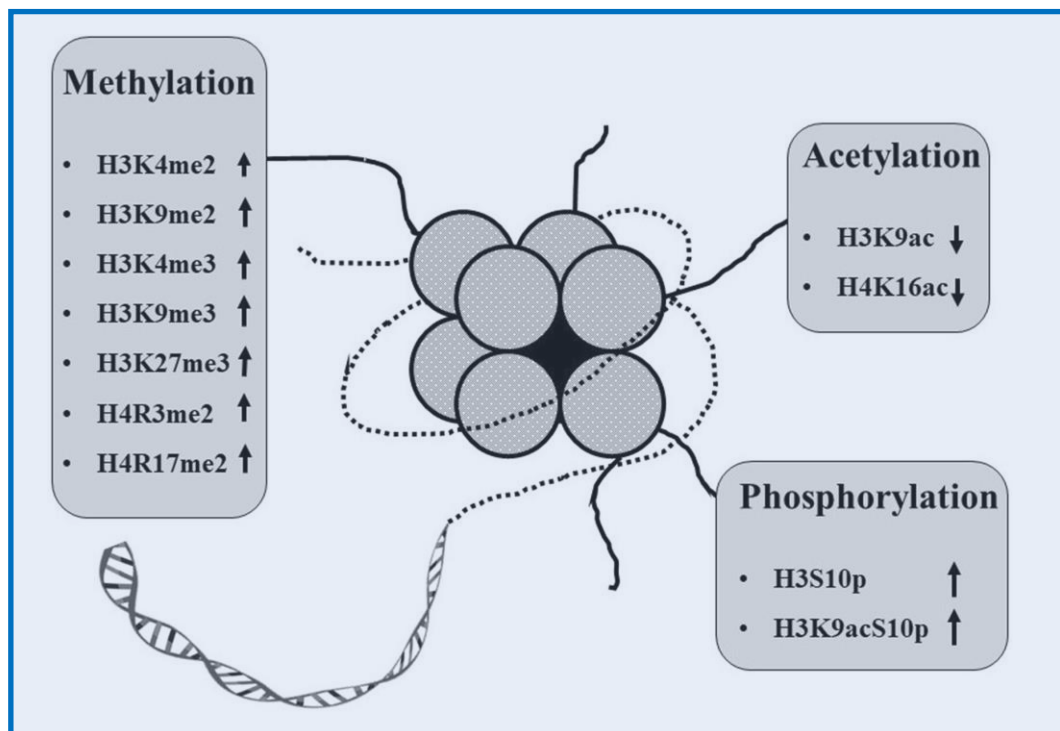


**Figure 1.6. Post-translational histone modifications induced by chronic iAs exposure.**

### 1.10.1. Arsenic induced Post translational histone modifications

According to the nucleosome model of DNA wrapping, the thread like negatively charged DNA remains wrapped around a positively charged histone core in the chromatin. This histone core is an octamer made up of two sets four histone proteins namely H2A, H2B, H3 and H4. The N-terminal ends of these histones remain extended from the

nucleosomes which are the sites for PTMs like methylation, acetylation, phosphorylation, ubiquitination, SUMOylation etc. All these modifications change the condensation and structure of the chromatin resulting in modulation of gene expression [Tam et al., 2020]. H2AX phosphorylation, H2AX ubiquitination, H2B ubiquitination, H3 methylation and H4K16 acetylation are the most commonly reported PTM induced by iAs [Eckstein et al, 2017; Howe and Gamble, 2016; Ren et al., 2011]. A study on dose dependent administration of iAs resulted in reduction of H4K16 acetylation in human bladder epithelial cells [Ren et al., 2011]. Another study reported reduction of H4K16 acetylation upon administration of MMA<sup>III</sup> and As<sup>III</sup> resulting in development of carcinoma in the bladder epithelial cells [Zhou and Xi, 2018]. A previous study had reported that, knock down of MYST1, the acetyltransferase of H4K16, resulted in increased toxicity of the bladder epithelial cells upon iAs exposure, indicating that H4K16Ac plays important role in imparting resistance against iAs induced toxicity [Jo et al., 2009]. A recent report stated that, arsenite can bind to the zinc finger motifs of MYST family of histone acetyltransferases TIP60 and hMOF resulting in inhibition of H4K16 acetylation. Loss of this acetylation prevents the unwinding of the chromatin, which further inhibits the repair activities of double strand break repair enzymes. [Tam et al., 2020; Liu D et al., 2015]. Loss of H4K16ac has also been reported in different cancers like renal cell carcinoma, colorectal cancer, medulloblastoma, breast cancer [Wu et al., 2020] as well as ovarian cancer [Liu et al., 2013]. Contrarily, gain of H4K16ac has been observed in non-small cell lung carcinoma [Wu et al., 2020] and elevation of H4K16 acetyltransferase MYST1 has been reported in glioblastoma [Dong et al., 2019].

In an *in-vitro* study, conducted on human lung carcinoma cell line, downregulation of H3K4me1 with simultaneous upregulation of H3K4me2 and H3K4me3 was observed, after 24 hours of exposure to 1 $\mu$ M of iAs. H3K4me3 remains upregulated till one week

after withdrawal of iAs [Zhou et al., 2009]. Population working in steel plants, exposed to particulate matter containing arsenic had increased expression of histone marks H3K9ac and H3K4me2 in their blood leukocytes [Cantone et al., 2011]. A prominent global upregulation of histone repressive marks H3K9me2 and H3K27me3 have been reported in A549 cells which were exposed to iAs for 24 hours [Zhou et al., 2008].

Increased expression of H3K9me2 due to elevation of its methyltransferase G9a, leads to transcriptional repression of tumour suppressor genes in cells. H3K27me3 is a repressive histone mark which results in silencing of the genes and inactivation of their promoters. In another study conducted on BALB/c 3T3 cells, exposure to 0.5  $\mu$ M of arsenic trioxide (ATO) resulted in elevated expression of polycomb repressive complex 2 (PRC2) protein complex enzymes like SUZ12, Enhancer of zeste homolog 2 (EZH2) and B lymphoma Mo-MLV insertion region 1 homolog (BMI1), ultimately leading to upregulation of H3K27me3. This upregulation of H3K27me3 leads to suppression of tumour suppressor genes like cyclin-dependent kinase inhibitor 2A (p16INK4a) and ARF tumour suppressor (p14ARF) [Kim et al., 2012]. iAs induced upregulation of H3K27me3 can also result in suppression of tumour suppressor genes like HOXB7 and CDKN2A, which play prominent role in DNA repair [Rubin et al., 2007; Li et al., 2011]. H3K27me3, a transcriptional repressor, has been found to be elevated in different cancers. It is also considered as a prognostic marker in certain cancers and negatively correlates with patient survival rates [Tzao et al., 2009]. In gastric cancer, H3K27me3 modulates the expression of oncogenes, tumour suppressor genes, cell-cycle regulatory and cell adhesion genes [Zhang et al., 2009]. EZH2 helps in tri-methylation of H3K27me3 via the PRC2 complex. Prominent upregulation of EZH2 was observed in prostate cancer, breast cancer and ovarian cancer, with concomitant upregulation of H3K27me3 [Varambally et al., 2002; Ngollo et al., 2017; Gan et al., 2018]. The histone marks like H4K16ac,

H3K4me1/me2/me3 and H3K27me3 are important PTMs which appear to be associated with numerous cancers. These epigenetic marks also show significant modulations upon iAs exposure; therefore, in order to understand the carcinogenic PTM induced by chronic iAs exposure, expression of these epigenetic marks needs investigation.

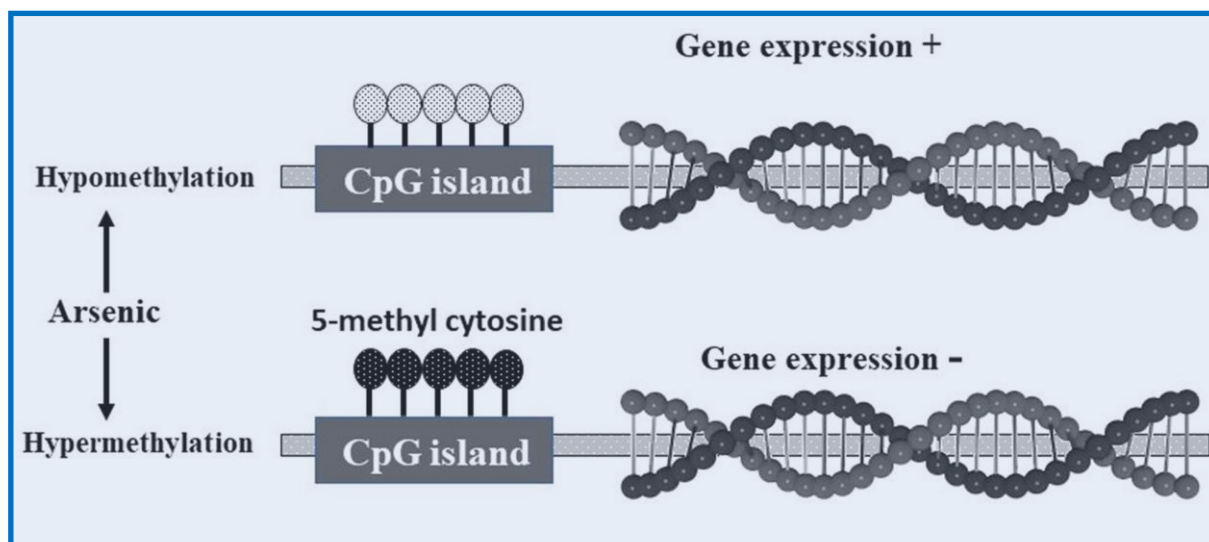


**Figure 1.7. Modulation of DNA methylation due to chronic iAs exposure.**

### 1.10.2. Arsenic induced DNA methylations

Another important mechanism of epigenetic modulations is DNA methylation. Methylation of the DNA in the promoter region leads to repression while methylation in the gene body results in gene activation [Jjingo et al., 2012]. Modifications in these methylation patterns lead to tumorigenesis by inactivation of tumour suppressor genes and activation of oncogenes [Tam et al., 2020]. The different mechanisms by which iAs induces alterations in DNA methylation patterns are S-adenosyl Methionine (SAM) deficiency, suppression of DNA cytosine-5-methyltransferases (DNMTs), downregulation of ten-eleven translocation (Tet) etc. Biotransformation of iAs requires SAM and chronic exposure to iAs depletes it. SAM is essential for DNMT to carry out the DNA methylations, thus, depletion of SAM hinders DNA methylation patterns. Chronic iAs exposure was also found to downregulate the expression and activity of DNMT1,

DNMT3A and DNMT3B which again results in loss of DNA methylations [Reichard et al., 2007]. Exposure to iAs has been reported to cause global hypomethylation [Chen et al., 2004; Coppin et al., 2008]. Global hypomethylation has been implicated in numerous human cancers [Pfeifer, 2018; Hon et al., 2012]. Rat liver cells when exposed to 0.5 $\mu$ M of sodium arsenite, it led to global DNA hypomethylation [Zhao et al., 1997]. Global hypomethylation was observed in the leukocytes of the people who were exposed to iAs chronically and had also developed skin cancer [Pilsner et al., 2009]. Mice chronically exposed to 45 $\mu$ M of arsenic for 48 weeks, developed hepatic global DNA hypomethylation. The promoter region of the ESR1 (codes for estrogen receptor) gene was also hypomethylated. This hypomethylation of the ESR1 gene leads to its activation which can promote cell cycle dependent Double strand breaks and initiate breast cancer [Williamson and Lees-Miller, 2011; Caldon, 2014].

Though iAs exposure has been linked to DNA hypomethylation, yet there are also reports where it led to hypermethylation of the promoters, resulting in repression of tumour suppressor genes. In humans chronically exposed to iAs, the promoter of the DNA repair gene MLH1 was found to be hypermethylated [Hossain et al., 2012]. Prominent promoter hypermethylation of NER genes like ERCC2, POLE2 etc. was found in the hepatocytes of humans who were exposed to 0.5 $\mu$ M of arsenic trioxide for a period of three months [Miao et al., 2015]. Another study reported promoter hypermethylation of NER genes like ERCC1 and ERCC2, in human cells upon chronic iAs exposure [Zhang A, et al., 2017]. Promoter methylation of Death-associated protein kinase (DAPK) was observed in a study conducted on the arsenic endemic people of Taiwan suffering from bladder cancer. The results of this study indicate that there is a strong correlation between arsenic exposure and promoter methylation [Chen et al., 2007]. Another study, conducted on iAs exposed individuals in West Bengal, India, reported a strong correlation between iAs exposure and promoter



hypermethylation of tumour suppressor genes like DAPK and p16 [Banerjee et al., 2013]. Promoter hypermethylation of tumour suppressor genes p21/CDKN1A (cyclin dependent kinase inhibitor 1A) and Metallothionein-1 (MT-1) were also observed upon chronic iAs exposure [Liu et al., 2006]. Therefore, the above studies clearly indicate that chronic exposure to iAs promotes alterations in DNA methylation pattern by inducing both DNA hypomethylation and hypermethylation, which ultimately lead to cancer progression.

### **1.11. iAs induced modulation of TGF- $\beta$ and induction of EMT**

It has already been discussed that chronic exposure to iAs leads to excess ROS generation and this ROS can act as secondary messenger in various signalling pathways including those which control cell proliferation and survival. One such pathway which has been reported to be modulated by iAs induced ROS generation is the TGF- $\beta$  pathway [Glasauer and Chandel, 2014]. Modulation of the TGF- $\beta$  pathway has been implicated in different cancers including squamous cell carcinoma of the skin [Glick, 2012]. TGF- $\beta$  is a cytokine which is known to play important role in cell proliferation, differentiation, apoptosis, migration etc. TGF- $\beta$  ligand binds with the constitutively activated TGF- $\beta$  receptor type II (T $\beta$ RII) which then interacts and activates T $\beta$ RI and forms a heterotetrameric complex [Pang et al., 2018]. This activated T $\beta$ RI can transmit the signalling via canonical as well as non-canonical pathways. Canonically T $\beta$ RI transduces its signalling via the suppressor of mothers against decapentaplegic (Smad) pathway, whereas noncanonically it can act by the phosphoinositide-3-kinase (PI3K)-protein kinase B (AKT), as well as mitogen-activated protein kinase (MAPK) signalling [Pang et al., 2018]. In canonical pathway, activated T $\beta$ RI phosphorylates Smad2 or Smad3 (Regulatory Smads) which again phosphorylates Smad4 (Common mediator Smads) and forms a heteromeric complex with it. This heteromeric complex of Smad4 and Smad2/3 translocates to the

nucleus where they bind with Smad responsive elements and transcribe genes associated with cell proliferation, differentiation, apoptosis etc. [Tzavlaki and Moustakas, 2020]. Smad 6 and Smad 7 are known as inhibitory Smads and they negatively regulate the Smad pathway. Smad6/7 competes with the regulatory Smads and bind with the activated T $\beta$ RI, upon which they recruit ubiquitin ligases which degrade the T $\beta$ RI as well as the regulatory Smads, thus ceasing Smad mediated signalling [Tzavlaki and Moustakas, 2020]. In the non-canonical pathways, activated T $\beta$ RI and T $\beta$ RII receptor complex phosphorylates PI3K which is followed by activation of AKT. Activated AKT can phosphorylate and activate mammalian target of rapamycin (mTOR) which is followed by cascade of events leading to formation of mTOR complex1 (mTORC1), mTOR complex2 (mTORC2), activation of ribosomal S6 kinase (S6K), NF $\kappa$ B etc. The activated TGF- $\beta$  receptor complex can also act by the Ras homolog gene family member A and MAPK pathways. TGF- $\beta$  signalling via the MAPK pathway occurs by the activation of TGF- $\beta$ -associated kinase 1 (TAK1) which is a MAP kinase kinase kinase (MAPKKK), followed by subsequent activation of MAP kinase kinases 3/4 (MAPKK3/4) which further activates JNK and p38. JNK and p38 are known to modulate important cellular events like inflammation, cell differentiation, cell growth and death [Zhang YE, 2017].

TGF- $\beta$ , the most potent cytokine, increases production of ROS with a concomitant suppression of antioxidant machinery [Ishikawa et al., 2014]. ROS on the other hand may activate or induce TGF- $\beta$ . This can initiate a cascade of events including induction of apoptosis and epithelial to mesenchymal transition (EMT). ROS and TGF- $\beta$  therefore appear to be interdependent. TGF- $\beta$  has been seen to exhibit a dual role in carcinogenesis i.e., in normal cells and early stages of carcinogenesis, it acts as a tumour and growth suppressor, whereas at later stages it promotes tumour growth, induces EMT, stimulates invasion and metastasis of cancer cells [Baba et al., 2022]. Epithelial to mesenchymal

transition is a phenomenon during which the epithelial cells lose their epithelial characteristics and adopt a mesenchymal phenotype. EMT occurs during embryogenesis, wound healing, and cancer progression. In tumorigenesis, EMT leads to invasion of the aggressive cancer cells within the tissue destroying its architecture and ultimately promoting metastasis. During EMT, the epithelial cells lose cell to cell contacts due to depletion of junctional proteins (claudins, zonula occludens, and E-cadherin) and downregulation of desmosomal proteins (desmoplakin, desmoglein, etc.) [Lamouille et al., 2014; Huang et al., 2022]. Along with these modifications, loss of apical-basal polarity, rearrangement of actin filaments and elevation of intermediate mesenchymal filamentous proteins like Vimentin also take place within the epithelial cells [Datta et al., 2021]. Along with loss of junctional and desmosomal proteins, gain of mesenchymal proteins like N-cadherin and transcription factors like Snail, Slug, Twist, Zeb etc. are also upregulated during EMT. These transcription factors further promote upregulation of mesenchymal traits within the cells to promote their invasive and metastatic properties. TGF- $\beta$  has been reported to play an important role in induction of EMT. A study revealed that TGF- $\beta$  induces EMT by the activation of Smad3 and Smad4, following the canonical pathway [Vincent et al., 2009]. While another study presented a contrasting report stating that Smad2 and Smad3 are inhibitors of EMT and loss of Smad2 initiates EMT and skin carcinogenesis [Rose et al., 2018]. Smad4 is considered to be a gatekeeper gene in Head and Neck Squamous Cell Carcinoma (HNSCC) and loss of function of Smad4 has been documented to support TGF- $\beta$  mediated tumour growth [Korc, 2009]. These reports suggest that inhibition of the canonical pathway of TGF- $\beta$  signalling may promote cancer.

The signalling intermediates of the non-canonical pathway of TGF- $\beta$  have also been frequently reported to be inducers of EMT for example, activated PI3K has been reported to induce EMT by rearranging the actin filaments and increasing migratory capacity of the

invasive cells [Lamouille et al., 2014]. Phosphorylated AKT induced the formation of mTORC1, which along with S6K enhanced protein synthesis, motility and invasion in breast epithelial cells and keratinocytes [Lamouille and Derynck, 2007]. Activation of mTORC2 by TGF- $\beta$  leads to alteration of actin cytoskeletal arrangement, activation of Ras Homolog Family Member A (RHOA) and cell migration which ultimately results in EMT. mTORC2 can form a positive feedback loop, where upregulated mTORC2 can further phosphorylate AKT and induce its own activation [Lamouille et al., 2012]. Following the non-canonical pathway, TGF- $\beta$  can induce the activation and translocation of NF $\kappa$ B into the nucleus via the phosphorylation of TAK1. This activated NF $\kappa$ B induces different pro-survival signalling which helps the cancer cells to escape apoptosis and become invasive [Hamidi et al., 2012]. TGF- $\beta$  can also activate JNK and p38 which have also been reported to induce EMT by altering cytoskeletal rearrangement [Zhang Y, 2017]. In Oral Squamous Cell Carcinoma (OSCC), TGF- $\beta$  has been found to promote EMT by upregulation of Snail and Matrix Metalloprotease9 (MMP9) [Qiao et al., 2010]. MMP9 helps in the invasion of the aggressive cancer cells within the tissue by destroying the extracellular matrix and the basement membrane. In HNSCC TGF- $\beta$  was found to elevate levels of Snail via upregulation of ERK1/2 [Smith et al., 2013]. Another study reported upregulation of Slug and MMP9 by TGF- $\beta$  [Joseph et al., 2009]. Therefore, it is evident that TGF- $\beta$  along with its signalling intermediates can promote EMT within the tissue. It may be inferred that, the ROS generated due to chronic iAs exposure leads to modulation of the TGF- $\beta$  signalling, ultimately promoting EMT and metastasis.

### **1.12. Chemoprevention**

Epidemiological studies have indicated that people endemic to iAs contaminated groundwater zones have higher chances of developing cancer due to the evils of chronic

As exposure [Chakraborty et al., 2017]. Cancer is not a single disease and the treatment is also not same for all types of cancer. For various types of cancer, different combinations of treatment regimen are followed, depending on the stage, grade, and general health condition of the cancer patient. Treatment modalities that are followed to cure cancer are surgery, radiotherapy, chemotherapy; besides immunotherapy, targeted therapy, hormone therapy, stem cell transplant and precision medicine are also employed by the oncologist. Treatment of cancer is a painful and costly affair. The chemotherapeutic drugs used in cancer can be broadly classified into antimetabolites like methotrexate, cytarabine etc.; DNA interacting agents like cisplatin, doxorubicin etc.; tubulin inhibitors like paclitaxel, docetaxel etc. antihormonal drugs like Tamoxifen, etc. and molecular targeting chemotherapeutic drugs like lapatinib, crizotinib etc. Drawbacks of these chemotherapeutic agents include cancer recurrence, drug resistance as well as unwanted toxicity on non-target tissues and cells. These undesirable side effects hamper the patient's quality of life. Therefore, the need of the hour is to look for alternative remedy, which display effective anticancer property with minimum or no side effects [Choudhari et al., 2020]. Prevention of cancer induction might be a better approach of cancer control. The process of preventing, inhibiting, or reversing carcinogenesis before it clinically manifests itself, by using naturally available chemicals or extracted pharmacological compounds, is known as chemoprevention [Steward and Brown, 2013]. Many dietary phytochemicals (plant derived chemicals) have shown promising chemopreventive potential both experimentally as well as epidemiologically [Pop et al., 2019]. Phytochemicals have exhibited anti-cancer ability both *in vitro* and *in vivo* models. They own the ability to slow down carcinogenesis by quenching free radicals [Lee et al., 2013], killing and inhibiting the proliferation of malignant cells [Yan et al., 2018], as well as suppressing invasion and angiogenesis of tumours [Lu et al., 2020]. Phytochemicals are also known to alter the activity of few target molecules; modulate the signalling pathways,

including the expression of surface receptors, downstream oncoproteins and tumour suppressors, kinases, transcriptional regulators, miRNAs, cyclins and caspases [Deng et al., 2017; Dou et al., 2018; Adams et al., 2010; Zhang W, et al., 2017; Cojocneanu et al., 2015].

Anticancer properties of few of the commonly available phytochemicals, which are being investigated both at the pre-clinical and clinical levels have been discussed. Allicin, extracted from garlic (*Allium sativum*), is an organic allyl sulphur compound, which has been reported to exhibit anticancer effects on cholangiocarcinoma [Chen et al., 2018]. Allicin has been found to suppress MMP2 and MMP9 by downregulating the activity of STAT3 as well as inhibit invasion, migration and EMT in human liver bile duct carcinoma cells (HuCCT-1). It has also been reported to induce caspase activity, apoptosis and suppress PI3K-AKT signalling [Chen et al., 2018; Hunag et al., 2017]. Curcumin, a yellowish polyphenol, extracted from turmeric (*Curcuma longa*) is a well-established chemopreventive agent. It known to modulate numerous signalling cascades and gene regulatory pathways [Kunnumakkara et al., 2017]. It has been reported to exhibit cancer inhibitory roles in blood, breast, liver, head and neck, ovary, prostate and skin cancers. [Taverna et al., 2015; Mock et al., 2015; Darvesh et al., 2012; Choudhari et al., 2020]. Curcumin can suppress melanoma by downregulating the signalling intermediates of the PI3K-AKT pathway and inducing cell cycle arrest and autophagy in them [ Zhao et al., 2016]. Epigallocatechin (EGCG), one of the major catechins of green tea has been reported to exhibit anticancer activity in vivo and in vitro models [Wang and Bachrach, 2002; Fujiki et al., 2015]. Clinical trials have found EGCG to be effective in suppressing the progression of prostate cancer [Kumar et al., 2016]. In bladder cancer EGCG was found to be accumulated in the cancer tissues and inhibit proliferation markers [Gee et al., 2017]. It was also found to inhibit the proliferation of breast cancer cell MDA-MB-231 and induce apoptosis in them [Thangapazham et al., 2007]. A dietary isothiocyanate, Sulforaphane

(SFN), found primarily in cruciferous plants like broccoli (*Brassica oleracea*), has shown promising anticancer properties like modulation of signalling pathways, induction of apoptosis, inhibition of cell cycle progression as well as enhancement of the antiproliferative activity of chemotherapeutic drugs like paclitaxel [Qazi et al., 2010; Su et al., 2018]. It has shown promising anticancer properties in prostate cancer patients [Cipolla et al., 2015]. Moreover, its role in lung cancer is being investigated in clinical trials. Resveratrol, a polyphenolic stilbenoid found mainly in the skin of red grapes (*Polygonum cuspidatum*), has displayed its antiproliferative role in breast, colon, prostate, liver and lung cancer [Banerjee et al., 2002]. It has been reported to inhibit tumour growth and metastasis by inhibiting vascularization, and angiogenesis, in Lewis lung carcinoma [Kimura and Okuda, 2001]. It has also been reported to reduce the number of tumours by suppressing NF $\kappa$ B, Cyclooxygenase-2 (COX-2) and MMP9 in 7,12-dimethylbenz(a)-anthracene (DMBA)-induced mammary cancer mouse model [Banerjee et al., 2002]. In another report, resveratrol was found to induce apoptosis in metastatic colorectal cancer cells [Howells et al., 2011]. Moreover, in a pilot study, it was also found to reduce the methylation and increase the expression of tumour suppressor gene Ras Association Domain Family Member 1 (RASSF1) in women, highlighting its anticancer capabilities [Zhu et al., 2012]. Other than these Apigenin (*Petroselinum crispum*), Genistein (*Glycine max*), Gingerol (*Zingiber officinale*), Nimbolide (*Azadirachta indica*) and many other dietary phytochemicals have exhibited excellent anticancer abilities [Choudhari et al., 2020].

### **1.13. Tea as a chemopreventive agent against iAs induced toxicity.**

In the present scenario of iAs induced carcinogenesis, use of phytochemicals as a chemopreventive agent to mitigate the deleterious effects of iAs may be an excellent

strategy. One of the primary pathways by which iAs induces its carcinogenic effect is by the excess generation of ROS. iAs induced excess ROS generation has been linked to DNA, protein and lipid damage, inflammation, epigenetic modulations, alteration of TGF- $\beta$  signalling, induction of EMT, which ultimately leads to cancer and metastasis. Therefore, quenching of iAs induced excess ROS, by antioxidative phytochemicals, might be a good strategy to counter its carcinogenicity. The list of dietary phytochemicals showing promising antioxidative capacity is unending, but out of these, exploring the antioxidative and chemopreventive properties of widely consumed and commonly available phytochemicals is desirable, so that the remedy remains within the reach of the common people [Zhang et al., 2015; Guan et al., 2021].

Tea is the most popular beverage worldwide. Tea gardens are a serene and peaceful escapes from the hustle and bustle of daily life. Tea is not just a beverage; it is an experience. Apart from the picturesque view of a tea garden, in times of stress nothing is more comforting than savouring a cup of tea due to its relaxing and calming effect, bringing a feeling of tranquillity.





Tea is prepared as an infusion of the leaves of *Camelia sinensis* in water. The three most common varieties of tea are green tea, black tea and oolong tea. Tea prepared from less fermented leaves are commonly known as green tea whereas completely fermented leaves are used to produce black tea [Qiao et al., 2014]. Black tea is the most globally preferred variety accounting for about 78% of consumption worldwide whereas green tea is mainly preferred in China and Japan, it accounts for 20% of consumption. Oolong tea is consumed by only 2% of people worldwide [Oba et al., 2010]. One of the most active constituents of tea is polyphenols which include variety of active flavonoids. Catechins like Epigallocatechin gallate (EGCG), Epigallocatechin (EGC), Epicatechin Gallate (ECG), and Epicatechin (EC) are the primary active constituents of green tea. EGCG accounts for 50–80% of the total catechins in green tea (TF). Oxidation and polymerisation of these catechins give rise to Theaflavins and Thearubigins, the primary polyphenols present in black tea. Theaflavin's structure is made up of seven membered benzotropolone rings which is formed due to epimerisation of the catechins [Qiao et al., 2014].

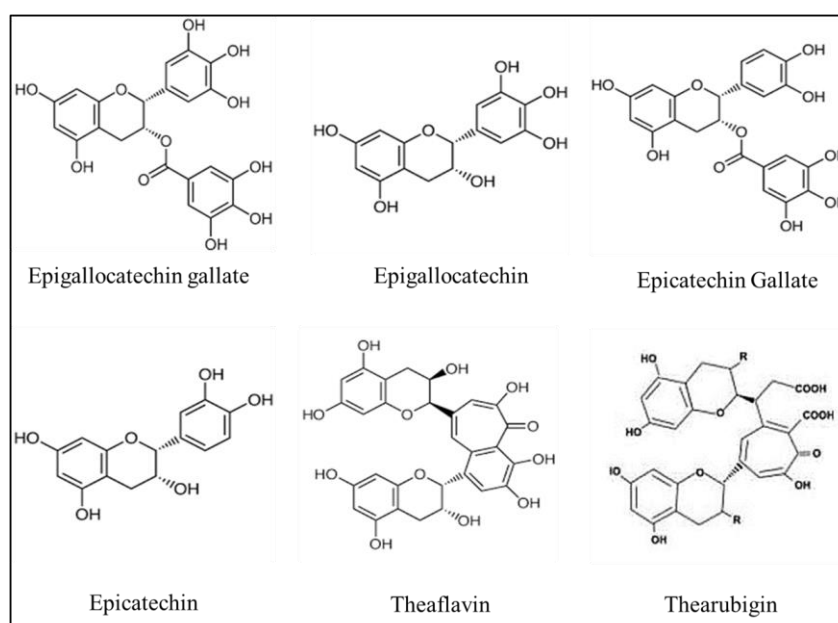


**Figure 1.8. Chemical structure of tea polyphenols**

Tea polyphenols have shown effective antioxidative, antigenotoxic and anticancer properties. Numerous reports have established the anticlastogenic, antigenotoxic and anticancer properties of green tea and its polyphenols, but reports on black tea polyphenols are sporadic and scanty [Roy et al., 2003; Khan and Mukhtar, 2008; Miyata et al., 2019; Hayakawa et al., 2020]. Therefore, in the present study, we have investigated the role of black tea in alleviating the detrimental effects of chronic iAs exposure. Dept. of Environmental Carcinogenesis & Toxicology, CNCI had reported that black tea polyphenols are no less potent than green tea polyphenols in their antioxidative, anticytotoxic and DNA repair properties [Sinha et al., 2003; Sinha et al., 2010]. Theaflavin is capable of chelating transition metals and countering free radicle generation. Benzotropolone moieties show resonance which allows them to donate an electron and quench the oxidation states of compounds [Wu et al., 2011]. This phenomenon reveals the antioxidative nature of black tea and makes it an excellent choice to be explored for its chemopreventive properties. Black tea polyphenols were found to downregulate some pro-inflammatory cytokines and inhibit inflammation both in cell line and in C57BL/6J mice [Gosslau et al., 2011; Heber et al., 2014]. A study in human tongue squamous cell carcinoma cell line (SCC4) had reported that, black tea polyphenols were able to reverse EMT, inhibit invasion of cells as well as downregulate the secretion of proteolytic enzymes [Chang et al., 2012]. Out of the different derivatives of theaflavin, the most stable derivatives are theaflavin-3-gallate, theaflavin-3'-gallate, and theaflavin-3-3'-digallate. Theaflavin-3-3'-digallate has shown the propensity to enter the nucleus and bind with the histone proteins and double stranded DNA suggesting that, it can play important role in regulating the transcription and translation of genes [Mikutis et al., 2013]. This trait can make black tea an effective candidate to mitigate the epigenetic alterations brought about by chronic iAs exposure. Black tea polyphenols were also found to regulate epigenetic

modulations by inhibiting the activity of mammalian DNA methyltransferase 3a (Dnmt3a) [Bag and Bag, 2018]. Therefore, investigating the ameliorative and anticancer properties of Black tea extract against the malignant effects of chronic iAs exposure might be a productive chemopreventive strategy.



# Chapter 2

## Aims and Objectives




The work is to be carried out both *in vivo* and *in vitro* model. For *in vitro* model, normal human keratinocyte cell line, **HaCaT** cells will be used and for *in vivo* model male **Swiss albino mice** will be used. Skin carcinoma will be developed in Swiss albino mice by the topical application and oral administration of iAs. Co-carcinogenicity of iAs in Swiss albino mice will also be studied where 7,12-dimethylbenzanthracene (DMBA), a polycyclic aromatic hydrocarbon (PAH) will be used as an initiator. HaCaT cells will be continuously maintained in culture medium containing non-toxic dose of sodium arsenite to illicit the effect of chronic iAs exposure on epithelial keratinocytes. The cells would be observed regularly for alterations in morphology and doubling time in order to record carcinogenic transformations.

Aim of the study is to elucidate the effect of chronic exposure to iAs and its amelioration by Black tea extract (BTE). The objectives of the study are:

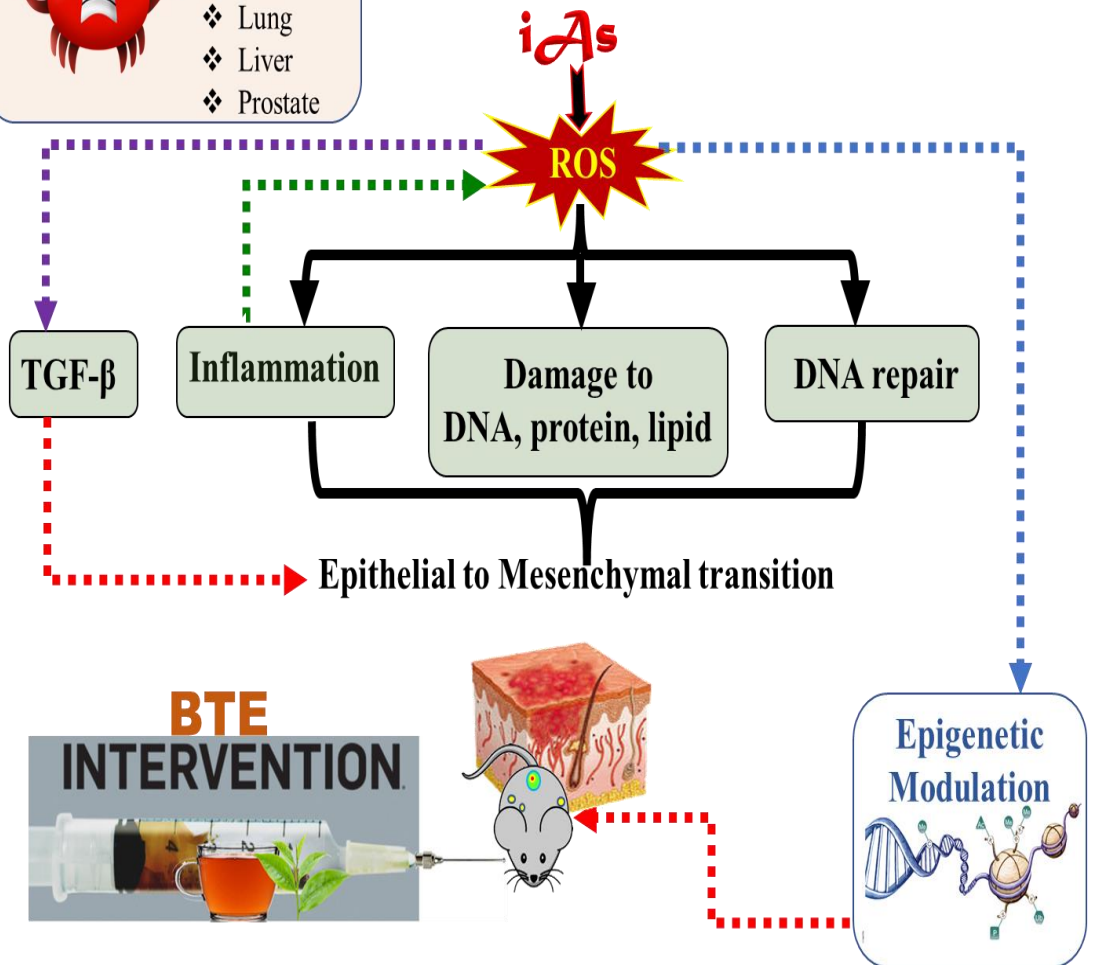
1. To investigate generation of free radicals (ROS) upon chronic iAs exposure and its effect on
  - a. DNA damage, protein damage and lipid damage.
  - b. Repair potential [i.e. proteins involved in Base Excision Repair (OGG1, PARP1, XRCC1 and DNA ligase I), Nucleotide Excision Repair (ERCC 1, ERCC 2 and XPA) and Non-Homologous End Joining Repair (DNA PKcs, Ku70 and DNA Ligase IV)].
  - c. Total Antioxidant capacity (Trolox equivalent) and antioxidant enzymes (Catalase, Sodium Oxide Dismutase, Glutathione S-Transferase, Glutathione Reductase and Glutathione Peroxidase).

- d. Inflammation (TNF- $\alpha$ , IL2, IL6, IL8, IL10, IL13, IL17a, IL22 and NF $\kappa$ B expression and activity).
2. To investigate epigenetic alterations (Histone modifications) promoting skin carcinogenesis.
3. To investigate the induction of EMT via the modulation of the TGF- $\beta$  pathway.
4. To investigate regulation of metastatic events by targeting VEGF, EGFR, MMP2 & MMP9.
5. To assess the chemopreventive potential of black tea in the above-mentioned events, in the light of skin carcinogenesis.



- ❖ Skin
- ❖ Bladder
- ❖ Kidney
- ❖ Lung
- ❖ Liver
- ❖ Prostate

## Work plan





# Chapter 3

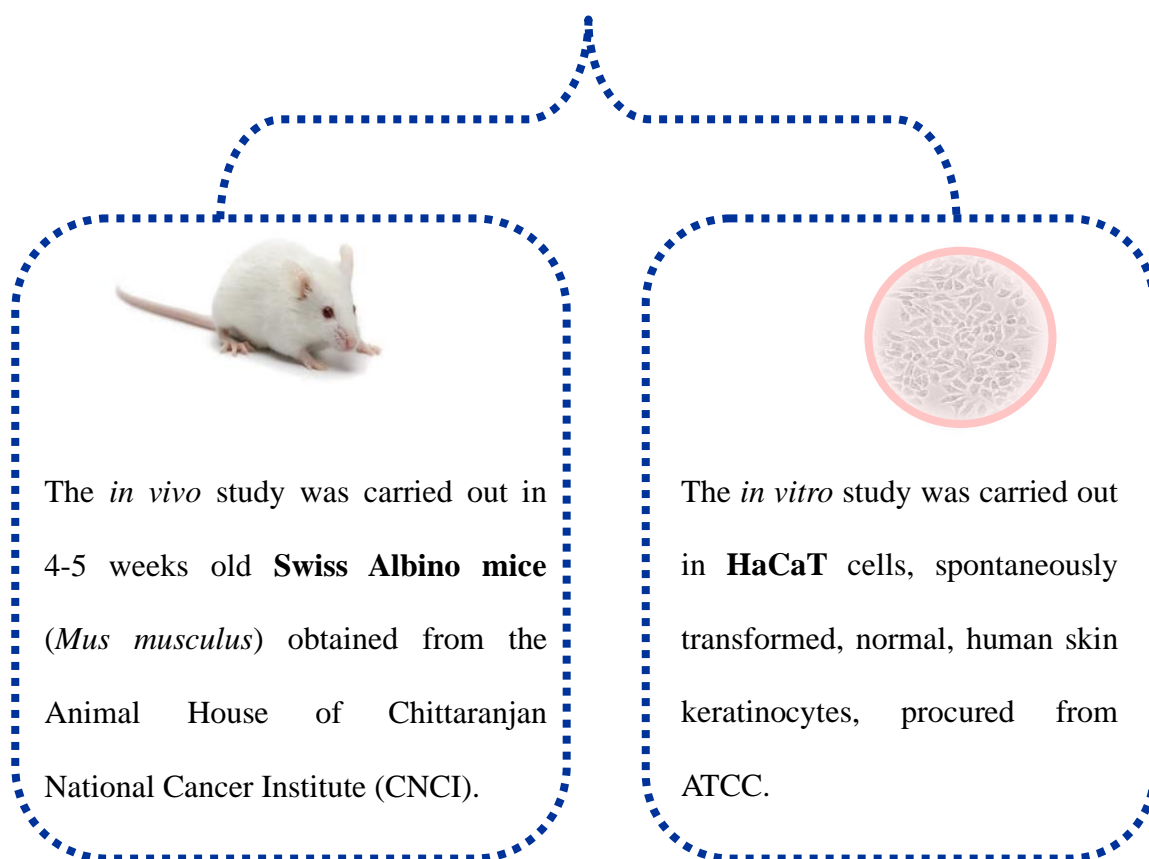
## Materials and Methods





### 3.1.

### Model of the study



### 3.2. Materials

Fetal bovine serum (FBS), Dulbecco's Modified Eagle Medium: Ham's Nutrient Mixture F-12 (DMEM/F-12), RPMI-1640, Acrylamide, N-, N'-methylenebis-acrylamide and TRIzol were procured from Invitrogen BioServices India Pvt. Ltd. Taq-polymerase was procured from HiMedia. 7,12-Dimethylbenz[a]anthracene (DMBA), 12 O tetradecanoyl phorbol 13 acetate (TPA), Ethidium bromide (EtBr), Low melting agarose, high melting agarose, Cytochalasin-B, sulphanilamide, n-(1-naphthyl)ethylenediamine dihydrochloride, Histopaque 1077, sodium arsenite

(NaAsO<sub>2</sub>), Thiobarbituric acid (TBA), Phytohaemagglutinin (PHA), phenylmethylsulfonyl fluoride (PMSF), Sodium Deoxycholate, paraformaldehyde, sodium nitroprusside, diaminobenzidine (DAB), Giemsa, Crystal violet, bisBenzimide H 33342 trihydrochloride, Coomassie blue R-250, 2',7'-dichlorofluorescein diacetate (DCFDA), gelatin, extracellular matrix (ECM) gel, DAPI (4',6-diamidino-2-phenylindole), MTT (3-(4,5-Dimethylthiazol-2-yl)-2,5-Diphenyltetrazolium Bromide), versine, saponin and bovine serum albumin, were obtained from Sigma-Aldrich. Nitric Acid, Hydrochloric Acid, Sodium Hydroxide, Sodium Chloride, Sodium Borohydride, Potassium Iodide, Ammonium Chloride, Magnesium Chloride, Calcium Chloride, Potassium dihydrogen phosphate, Sodium dihydrogen phosphate, Sodium Citrate, Ethyl Alcohol, Methanol, Ammonium aluminium sulphate, Dimethyl sulfoxide, HEPES, Potassium Chloride, Tetrapotassium ethylenediaminetetraacetate, Hydrogen peroxide, Sodium Azide, Paraffin wax, Xylene, TRIS-HCl, Eosin, Haematoxylin, Tween-20, TritonX-100, Ethylenediamine tetra acetic acid, EGTA, Dextrose and Mesoinositol were obtained from Sisco Research Laboratories Pvt. Ltd. (SRL) India. Goat Immunoglobulin G anti-rabbit and anti-mouse (FITC, alkaline phosphatase conjugated and horseradish peroxidase conjugated) were purchased from Genetex, 5-bromo-4-chloro-3-indolyl phosphate/nitro blue tetrazolium (BCIP-NBT) was bought from Santa Cruz Biotechnology; nitrocellulose membrane was purchased from GE Health-Care; Glycine, Tris and sodium dodecyl sulphate (SDS) were purchased from Amresco. Primary antibodies anti-E-Cadherin [67A4] (FITC), anti-Vimentin [VI-RE/1] (PEs), anti-JARID1B, anti- JARID2, anti-EZH2, anti-LSD-1, anti-H3K4me1, anti-H3K4me3, anti-MLL1, anti-MLL3, anti-KDM6A, anti-MYST1, anti-H4K16ac, anti-H3K27me3, anti-Ki67, anti-MMP2, anti-MMP9, anti-VEGF, anti-EGFR, anti-

TGF- $\beta$ , anti-Smad2 (phospho [p] Ser467), anti-Smad3 (pSer423/425), anti-phosphatase and tensin homolog deleted on chromosome 10 (PTEN), anti-PI3Kp110 $\alpha$ , anti-AKT (pSer473), anti-mTOR, anti-S6Kp70, anti-NF- $\kappa$ Bp65, anti-TAK1(pThr184), anti-MAPKK3 (pSer189), anti-p38 MAPK, anti-MAPKK4 (pThr 261), anti-JNK, anti-E-cadherin, anti-desmoplakin, anti-vimentin, anti-N-cadherin, anti-Snail, anti-Slug, anti-Twist, anti- $\beta$ -actin, and anti-Zeb1 were purchased from Genetex. Anti-Smad4 (pThr277) was purchased from Thermo Fisher Scientific.

### **3.3. Kits used**

- i. Protein Carbonyl Colorimetric Assay Kit manufactured by Cayman Chemicals (10005020)
- ii. Antioxidant Assay Kit, manufactured by Cayman chemicals (709001).
- iii. Catalase enzyme assay kit (707002) manufactured by Cayman chemicals.
- iv. SOD enzyme assay kit manufactured by Cayman chemicals (706002).
- v. GST assay kit manufactured by Cayman chemicals (703302).
- vi. Glutathione Reductase Assay Kit manufactured by Cayman chemicals (703202).
- vii. Glutathione Peroxidase assay kit manufactured by Cayman chemicals (703302).
- viii. TNF alpha ELISA kit manufactured by Abcam (ab208348).
- ix. IL-2 ELISA kit manufactured by Abcam (ab223588).
- x. IL-6 ELISA kit manufactured by Abcam (ab100712).
- xi. IL-8 ELISA kit manufactured by Abcam (ab213859).
- xii. IL-13 ELISA kit manufactured by Abcam (ab219634).
- xiii. IL-17A ELISA kit manufactured by Abcam (ab199081).
- xiv. IL-22 ELISA kit manufactured by Abcam (ab223857).

- xv. IL-10 ELISA kit manufactured by Abcam (ab255729).
- xvi. NF- $\kappa$ B p50 Transcription Factor Assay ELISA Kit (ab207217) manufactured by Abcam.
- xvii. NF- $\kappa$ B p65 Transcription Factor Assay ELISA Kit (ab176648) manufactured by Abcam.
- xviii. EpiQuik TMGlobal Histone H3K4 methylation Assay Kit (P-3017-96) manufactured by Epigentek Group Inc.
- xix. RETROscript (reverse transcriptase [RT]-PCR kit; Ambion; Thermo Fisher Scientific) (AM1710).

### **3.4. Equipment's used**

- i. Laminar Airflow Cabinet (Klenzaid).
- ii. Carbon dioxide incubator (Thermo Fisher Scientific).
- iii. Inverted Microscope (Nikon, Olympus)
- iv. Fluorescence microscope (Leica).
- v. Bright field microscope (Zeiss).
- vi. Top pan balance (Sartorius).
- vii. Milligram balance (Millipore).
- viii. Gel documentation apparatus (BioRad, Thermo Fisher Scientific).
- ix. ELISA plate reader (Tecan).
- x. Cold centrifuge (SIGMA, Sartorius).
- xi. Dry bath (GENEI).
- xii. Thermal Cycler for Polymerase Chain Reaction (Bio Rad).
- xiii. Magnetic stirrer (SPINOT).
- xiv. Spectrophotometer (Varian).
- xv. Horizontal gel apparatus (Biotech).

- xvi. Vertical gel apparatus (Bio Rad).
- xvii. Microtome (Leica)
- xviii. Flowcytometer (Becton Dickinson, Beckman Coulter Life Sciences)
- xix. Nanodrop-spectrophotometer (Nabi Microdigital)
- xx. Spectrofluorometer (Varian Eclipse)
- xxi. Hot Air oven (Thermo Fisher Scientific)
- xxii. Lyophilizer (SCANVAC)
- xxiii. Mechanised homogenizers (Remi)
- xxiv. Dounce homogenizer
- xxv. High Performance Liquid Chromatography system (Waters, USA)
- xxvi. MARS 6 microwave digestion system (CEM Corporation).
- xxvii. Atomic absorption spectrophotometer (Varian)

### **3.5. Methods**

#### **3.5.1. Preparation of Black tea extract (BTE)**

2.5 g of black tea (leaf) was boiled in 100 ml of Milli-Q water to prepare 2.5 % infusion. It was lyophilized using a SCANVAC lyophilizer and was kept in an air-sealed vessel at 4°C. The lyophilized product was weighed, reconstituted in water and administered to the mice by gavage. The dose administered to the mice was 0.33 mg/gm body weight at an interval of 8 hours. For *in vitro* administration, a grand stock solution of 100 µM of lyophilized BTE was prepared in Milli-Q water which was administered to the cells so that the final concentration administered to the cells is 1 µM.

#### **3.5.2. Quantification of BTE**

The constituents of the BTE were determined by HPLC (Waters, USA) following the standard laboratory protocol [Sinha et al., 2003]. HPLC

was carried out using a 515 lb dual pump with a control, a Rheodyne injector, a RP C-18 column by Nova-Pak which was attached to the guard column regulated at 30°C and a 996 PDA detector (Waters, USA) adjusted to 278 nm. Separation of catechins were achieved using gradient of 5–25 % of acetonitrile in 0.025 M KH<sub>2</sub>PO<sub>4</sub> at pH 2.4 while theaflavins were separated in an isocratic mode which constituted a mobile phase made up of acetic acid: acetone: water in the ratio of 1: 60: 39 and detected at 365 nm. Integration and calibration of mixture containing catechins and theaflavins were done using the software Millennium 32. Catechins and Theaflavins were quantified by plotting against a standard.

### **3.5.3. Mice treatment protocol**

4-5 weeks old, male, Swiss albino mice (*Mus musculus*) were obtained from the animal house of Chittaranjan National Cancer Institute (CNCI), with approval from the Institutional Animal Ethics Committee (IAEC 1774/MR- 3/2017/9). Mice were handled according to the protocols and standard guidelines laid down by the IAEC, certified by CPCSEA (Committee for the Purpose of Control and Supervision of Experiments on Animals), New Delhi. Mice were fed with synthetic pellets and maintained in alternate 12 h of light and darkness at a temperature of 22°- 24°C. All the mice were kept at the same level of the rack, to maintain identical housing condition. Mice were euthanized by an overdose of thiopentone sodium (100 mg/kg body wt). The animals were divided into four groups, each group consisting of 25 mice, kept in separate cages, each cage harbouring 5 mice. To remove the hair, mice were shaved in their hind leg region with the help

of a razor. The treatment regime of the different groups of mice were as follows:

- i. Group 1: Control group, where the mice were given normal food pellets and tap water.
- ii. Group 2: DMBA group, mice belonging to this group were painted topically with 10 % DMBA solution in acetone, twice only, at an interval of one week. 2% TPA solution in acetone was given twice weekly till development of carcinogenesis.
- iii. Group 3: iAs treated group, where the mice were given sodium arsenite (500 µg/L) dissolved in water, as the only source of drinking water. Mice were painted in the shaved hind leg region with the same concentration of iAs.
- iv. Group 4: DMBA+BTE treated mice group. The mice belonging to this group received the DMBA treatment and were also administered lyophilized BTE at a concentration of 0.33 mg/g body weight via gavage, thrice daily (an interval of 8 hours).
- v. Group 5: iAs + BTE treated mice group. The mice belonging to this group received the iAs treatment (drinking water and topical application) as well as the BTE treatment by gavage.
- vi. Group 6: BTE group, where the mice were provided with normal food pellets and tap water, along with BTE (0.33 mg/ g body weight). BTE was administered thrice daily, at an interval of 8 hours daily. Previous studies had shown that BTE elicited no effect; therefore, results have not been provided.

Treatment of the mice continued until 330 days. Mice were sacrificed at regular intervals to harvest tissue, organs and blood for analysis.

#### **3.5.4. Performance of MTT assay to determine the dose of iAs and BTE for HaCaT cells**

Cytotoxicity of the different doses of iAs and BTE were assessed by MTT [3-(4,5-dimethylthiazol-2-yl)-2,5-diphenyl tetrazolium bromide] assay and it confirmed the non-toxicity of iAs and BTE doses used in our experiments. This assay is based on the reduction of MTT by the mitochondrial dehydrogenase enzyme of living cells to form a purple formazan derivative which can be measured spectrophotometrically. Logarithmic doses of iAs and BTE were given to exponentially growing HaCaT cells, grown in the 96 well plates and incubated for 48 h. The cytotoxicity of iAs and BTE were recorded and safe doses were chosen to be administered to the cells. MTT assay was also performed periodically at different time intervals (0, 30, 90, 150, 210, 240 days) throughout the treatment period to assess the toxicity of the selected iAs (100 nM), BTE (1  $\mu$ M) and iAs + BTE (100 nM+ 1  $\mu$ M) doses on the exposed cells. Cells were seeded in triplicate for each treatment dose. Then MTT solution (1.2 mg/ml in water) was added to each well and incubated for 5 h in dark. The 96 plate well was centrifuged and MTT-formazan product formed was dissolved in DMSO. Absorbance at 570 nm was recorded using ELISA plate reader (TECAN infinite2000)

#### **3.5.5. Cell culture and treatment**

HaCaT cells were maintained in 1:1 mixture of Dulbecco's Modified Eagle Medium: Ham's Nutrient Mixture F-12 (DMEM/F-12) and



supplemented with 10 % Fetal Bovine Serum (FBS) and antibiotics (gentamycin 40 µg, penicillin 100 units, streptomycin 10 µg/ml) and maintained at 37°C in a humidified CO<sub>2</sub> (5%) incubator. The cells were seeded in sterile tissue culture petri dishes and were divided into the following groups based upon the different treatment regime

- i. Group 1: control group, cells of this group did not receive any other treatment other than medium, serum and the antibiotics
- ii. Group 2: iAs group, cells of this group were treated with 100 nM of sodium arsenite (NaAsO<sub>2</sub>) in the culture medium, along with serum and antibiotics. The cells were continuously maintained in iAs contaminated medium for a period of 240 days to mimic the conditions of chronic iAs exposure.
- iii. Group 3: BTE+iAs group, cells of this group were continuously maintained in 100 nM of sodium arsenite and 1 µM of BTE for a period of 240 days, to assess the effect of BTE on chronic iAs exposure.
- iv. Group 4: BTE group, cells of these groups were continuously maintained in 1 µM of BTE for a period of 240 days.

The cells were passaged at regular intervals to maintain healthy population of cells. Doubling time was studied for each cell treatment groups, by calculating the number of cells present after 28 h (Doubling time of HaCaT cells) of seeding. This was done to identify induction of malignant transformation induced in the cells.

HaCaT cells are spontaneously transformed keratinocytes which are immortal even after 140 passages, and are nontumorigenic [Boukamp et al.,

1988]. These cells represent normal keratinocytes and form structured and differentiated epithelium when transplanted into a xenograft mouse model. Primary keratinocytes cannot be used to study the effect of chronic iAs exposure because these cells cannot be maintained after 16–20 passages. Therefore, immortalized normal keratinocytes, HaCaT cells, are an excellent *in vitro* model to study the effect of chronic iAs exposure on human skin.

### **3.5.6. Tumour assessment**

The mice were carefully observed for development of skin lesions. Tumours appearing on the skin, greater than 1 mm in diameter were measured periodically using Vernier callipers in all the groups of mice and the mean tumour diameter was calculated. The diameter was then used to obtain the tumour area using the formula ( $\text{area} = \pi r^2$ ), where  $r$  is the radius, i.e., half the diameter. The invasiveness of the cutaneous tumours appearing on the mice skin were confirmed by histological studies.

### **3.5.7. Estimation of iAs accumulation in the hair and nails of mice using AAS**

The amount of iAs in the hair and nails of the mice were quantified using atomic absorption spectrophotometry with vapour generation assembly (AAS-VGA). For correct estimation, all the arsenic present in the samples were required to be reduced to  $\text{As}^{\text{III}}$ , which were then converted to arsenic hydride ( $\text{AsH}_3$ ) vapours. These vapours in turn released free arsenic atoms which were detected using AAS. Hair and nail samples from the mice were first digested in nitric acid and hydrogen peroxide in a microwave digestion system MARS-6. The acid channel of the AAS was filled with 10M HCl, while the reduction channel was filled with 0.6% Sodium Borohydride and 0.5% Sodium Hydroxide. The digested samples were

mixed with 6M HCl. 10% Potassium Iodide was directed added in the reduction channel and HCl added samples were aspirated into the VGA reduction channel. The resulting free arsenic atoms released, were detected by the AAS at a wavelength lower than 200 nm (193.7 nm). A standard curve was drawn by recording the absorbance of iAs at known concentrations which was then used to determine the concentration of iAs in the samples.

### **3.5.8. Confirmation of skin cancer by histology**

The skin tissues collected after sacrificing the mice, were fixed in 10% Neutral Buffered Formalin (NBF). They were then treated with increasing grades of alcohol (50%, 70%, 90% and 100%) and xylene to remove water and fat content respectively. The tissues were then embedded in paraffin and cut into 4 µm thick sections using a microtome (Leica). These tissue sections were stretched on glass slides, stained with Delafield's haematoxylin (0.6%, using ammonium aluminium sulphate as a mordant) and eosin (1% dissolved in 70% ethanol), mounted with DPX and observed under light microscope (Zeiss). The nucleus appeared blue due to haematoxylin staining on a pink background of the cytoplasm, due to counter-staining by eosin. The development of squamous cell carcinoma in the mice skin was confirmed by histology.

### **3.5.9. Isolation of Leukocytes from the blood of the mice**

Leukocytes were isolated from the uncoagulated mice blood, according to the lab protocol of [Roy et al., 2011]. Blood was mixed with Solution A (10 mmol/l of Tris-HCl and 0.87% of NH<sub>4</sub>Cl; pH 7.2) in the ratio 1:3 and incubated at 4°C for 30 min, followed by centrifugation at 1200 rpm

for 30 min. Pellets thus obtained were suspended in solution A and centrifuged for 10 min. To the resultant pellet, 500 µl of solution B (0.25 mol/l mesoinositol, 10mmol/l NaH<sub>2</sub>PO<sub>4</sub> and 1 mmol/l MgCl<sub>2</sub>; pH 7.2) was added and centrifuged at 1200–1400 rpm for 10 min. The pellet obtained consisted of isolated leukocytes which were again suspended in solution B and stored at 4°C for further investigation.

### **3.5.10. Estimation of ROS generation**

- i. **Using Spectrofluorometer:** Leukocytes isolated from the blood of the mice were pelleted down and suspended in hydroxyethyl piperazine ethane sulfonic acid (HEPES) buffered saline (HBS; consisting of 140 mM HCl, 5 mM KCl, 10 mM HEPES, 1 mM CaCl<sub>2</sub>, 1 mM MgCl<sub>2</sub>, 10 mM glucose). To wash away remnants of previously used buffers, the leukocyte suspension was again pelleted down in HBS by centrifugating at 1500 rpm for 5 minutes. The pellets were resuspended in HBS and 10mM of 2',7'-dichlorodihydrofluorescein diacetate (DCFDA), dissolved in DMSO, was added to the cell suspension. It was then incubated in dark for 45 minutes. After 45 minutes, fluorescence was measured using a Varian Cary Eclipse spectrofluorometer. The excitation and emission ranges were 485 nm and 530 nm respectively.
- ii. **Using Flowcytometer:** ROS was estimated using flowcytometer in isolated leukocytes as well as in HaCaT cells. The cells were washed in HBS and incubated in dark for 45 minutes after the addition of DCFDA. After incubation, the cells were once again washed in HBS to remove excess staining and were subjected to flowcytometry.

Special care was taken so that the cell suspension was not exposed to direct light after staining and incubation with DCFDA. Flowcytometry was performed using both FACSCalibur (Becton Dickinson) and DxFLEX (Beckman Coulter Life Sciences) flowcytometers and 10,000 events were recorded for each sample. The fluorescence generated due to DCFDA staining was analysed in fluorescence channel 1 (FL1).

DCFHDA is a small non-polar, cell membrane permeable oxidation-sensitive probe. Upon entry into the cells, it gets converted into a non-fluorescent compound DCFH by the deacetylation of intracellular esterases. Upon further oxidation of DCFH by ROS, a fluorescent compound 2,7-dichlorofluorescein (DCF) is produced which is detected by spectrofluorometer as well as flowcytometer.

#### **3.5.11. Estimation of Reactive Nitrogen Species (RNS) generation**

RNS generation was measured in the isolated leukocytes using Griess reagent (1% sulphanilamide, 0.1% naphthylethylenediamine-dihydrochloride and 5% orthophosphoric acid) following the standard protocol [Green et al., 1982]. The density of cells in each sample were counted and equalized, 1 ml of the cell suspension was incubated with equal volume of Griess reagent and incubated at room temperature for 30 minutes in a humid chamber. Absorbance was measured at 550 nm using a spectrophotometer. Amount of RNS generated was estimated against a standard curve of sodium nitroprusside.

### **3.5.12. Single Cell Gel Electrophoresis (SCGE)/ Comet Assay.**

DNA damage in the isolated leukocytes and HaCaT cells was estimated by SCGE/Comet Assay. 20 µl of cell suspension was mixed with 120 µl of 0.6% Low melting agarose (LMA). It was then layered over half-frosted slides pre-coated with 0.75% Normal melting agarose (NMA) and kept at 4°C until it had solidified into a thin layer with cells embedded in it. Slides were then immersed in lysis buffer (2.5M NaCl, 0.1M Na<sub>2</sub>EDTA, 10mM TRIS, 0.3M NaOH, 10% DMSO and 1% TritonX-100; pH-10) and kept overnight at 4°C. Next day, the slides were taken out and pre-soaked in highly alkaline electrophoresis buffer (10mM NaOH, 0.2 m Na<sub>2</sub>EDTA; pH>13) for 20 minutes, which was followed by electrophoresis for 25 minutes at 15V, 220mA. After electrophoresis, the slides were taken out of the electrophoretic chamber and soaked in neutralising buffer (0.4M TRIS, pH-7.5) to adjust the pH. Next the slides were stained with ethidium bromide (EtBr) in complete darkness and observed under a fluorescent microscope (Leica).

### **3.5.13. Micronuclei Assay**

Micronuclei assay was also employed to assess DNA damage in both mice and HaCaT cells. The mice were injected with cytochalasin B (3 mg/Kg body weight two doses at an interval of 24 hours) intraperitoneally and 48 hours after the last dose, the mice were sacrificed and their femur bones were removed. These femur bones were flushed with 0.9% normal saline to collect rapidly dividing, binucleated, hematopoietic stem cells. These cells were washed in saline solution by centrifugating at 1500 rpm for 5 minutes and the pellet obtained was resuspended in the saline solution.

For estimation of micronuclei in *in vitro*, 5µg/ml of cytochalasin B was added in culture plates. After 48 hours of cytochalasin B treatment, HaCaT cells were harvested, washed and resuspended in saline solution for further processing. Addition of cytochalasin B halts actin polymerisation and results in the formation of binucleate cells, which is used to study micronuclei formation. Cytochalasin treated cells were then fixed using a fixative (methanol: glacial acetic acid in the ratio 3:1). Fixative treatment was repeated thrice. Finally, cells in fixative were dropped onto chilled, grease free, clean glass slides. Next the slides were dried and kept at room temperature. These dried and fixed slides were then stained with 5 % Giemsa, observed under light microscope and calculated as number of micronuclei generated per 1000 binucleate cells. Hoechst 33342 nuclear stain was also used to visualize micronuclei formation in cytochalasin treated cells. A 10mg/ml stock solution of Hoechst 33342 was prepared in deionized water which was diluted in the ratio 1:1000, in PBS. This PBS was used to stain the cytochalasin treated cells which were then incubated in the dark for 20 minutes at 37°C. The stained cells were washed with PBS once to remove excess stain and were then mounted on slides and observed under a fluorescent microscope.

#### **3.5.14. Lipid peroxidation assay**

ROS induced damage to cell membrane was measured using the lipid peroxidation and experiment was performed according to the standard protocol [Okhawa et.al.1979]. The assay was performed on mice tissue and HaCaT cell homogenates. 10% Sodium dodecyl sulfate (SDS), 20% acetic acid and 0.8% Thiobarbituric acid (TBA) was added to the homogenates,

which was then placed in boiling water bath for 1 hour and immediately transferred to ice for 10 minutes. The samples were then centrifuged at 2500 rpm for 10 minutes. The supernatant was collected and absorbance was measured at 535 nm. Lipid peroxidation was calculated as the number of moles of Malondialdehyde (MDA) generated.

#### **3.5.15. Protein carbonyl assay**

The protein carbonyl content was estimated in the mice tissue and HaCaT cell homogenates following the protocol as mentioned in Protein Carbonyl Colorimetric Assay Kit manufactured by Cayman Chemicals (10005020). According to the assay, protein carbonyls present in the homogenates would form Schiff's base in the presence of 2,4-Dinitrophenylhydrazine (DNPH), which can be detected spectrophotometrically at 360-385 nm of wavelength. The amount of protein carbonyl formed could be obtained by plotting against a standard.

#### **3.5.16. Estimation of the activity of antioxidant enzymes**

##### **i. Estimation of total antioxidant capacity**

The overall antioxidant capacity of mice tissue and HaCaT cell lysates were analysed using the Antioxidant Assay Kit, manufactured by Cayman chemicals (709001). This assay determines the antioxidant capacity of the sample by measuring its ability to prevent the oxidation of ABTS [2,2'-Azino-di-(3-ethylbenzthiazoline sulphate)]. Presence of antioxidants in the sample suppresses the absorbance at 750 nm and 405 nm which has been measured using a 96-well plate reader. This ability of the antioxidants to prevent the oxidation of ABTS is compared with that of Trolox (Tocopherol



analogue), which is used a standard. The antioxidant capacity is quantified as Trolox equivalent.

**ii. Estimation of Catalase activity**

Catalase activity in the mice tissues and HaCaT cells were estimated using the Catalase enzyme assay kit (707002) manufactured by Cayman chemicals. The peroxidative capacity of Catalase has been assayed here. In the presence of methanol and  $H_2O_2$ , catalase produces formaldehyde, the presence of which is measured by the chromogen, 4-amino-3-hydrazino-5-mercapto-1,2,4-triazole (Purpald). Upon reaction with aldehydes, the chromogen changes its colour from colourless to purple. The OD is recorded at 540 nm and the activity is determined by plotting against a standard curve.

**iii. Estimation of the activity of Superoxide Dismutase (SOD)**

Activity of SOD has been measured in the mice tissues and HaCaT cells using the SOD enzyme assay kit manufactured by Cayman chemicals (706002). SOD performs dismutation of the superoxide radical generated by Xanthine Oxidase and this radical is detected by the tetrazolium salt provided in the assay kit. The absorbance is measured at 440-460 nm using an ELISA plate reader. Active SOD dismutates larger number of radicals thus reducing the OD of the mixture. Bovine erythrocyte SOD was provided as the standard which was diluted to various concentrations to obtain the standard curve.

**iv. Estimation of the activity of Glutathione-S-Transferase (GST)**

Activity of GST has been measured in the mice tissue and HaCaT cell homogenates using the GST assay kit manufactured by Cayman chemicals (703302). GST is an enzyme which conjugates xenobiotic (toxic) compounds with glutathione. The total activity of GST is measured by the conjugation of glutathione with 1-Chloro-2,4-Dinitrobenzene (CDNB) which shows increase in absorbance at 340 nm. Addition of CDNB to the homogenates produces the identifying conjugate which is measured using the ELISA plate reader at 340 nm. The rate of increase of the absorbance is directly proportional to GST activity present in the sample.

**v. Estimation of the activity of Glutathione Reductase (GR)**

Activity of GR was estimated in the mice tissue and HaCaT cell homogenates using Glutathione Reductase Assay Kit manufactured by Cayman chemicals (703202). Activity of GR is measured by measuring the rate of oxidation of NADPH. The rate of oxidation of NADPH to NADP<sup>+</sup> results in decrease of absorbance at 340nm, which is again proportional to the activity of GR. Therefore, by measuring the decrease in absorbance using a microplate reader, at 340 nm, the activity of GR has been estimated.

**vi. Estimation of the activity of Glutathione Peroxidase (GPx)**

Activity of GPx was measured in the mice and HaCaT cell homogenates by Glutathione Peroxidase assay kit manufactured by Cayman chemicals (703302). This assay involves an indirect method of measuring the activity of GPx where reduction of oxidised

Glutathione results in oxidation of NADPH and leads to reduction of absorbance at 340 nm. This reduction of absorbance is directly proportional to the activity of GPx and was measured using a microplate reader.

### **3.5.17. Isolation of mice lymphocytes**

Uncoagulated mice blood (5mg of Tetrapotassium ethylenediaminetetraacetate was added in each 5 ml blood collecting glass vial to prevent blood coagulation) was pooled from different treatment groups, layered on top of Histopaque and centrifuged to obtain a buffy coat rich in lymphocytes. The isolated lymphocytes were seeded in RPMI-1640 media supplemented with 10% FBS, antibiotics and 20µg/ml Phytohaemagglutinin (PHA). The cells were cultured at 37°C in a humidified atmosphere of 5% CO<sub>2</sub>/95% air.

### **3.5.18. Determination of DNA repair potential**

Isolated mice lymphocytes were treated with MNNG (N-methyl-N'-nitro-N-nitrosoguanidine), a DNA damaging agent, for 1 hour. After removal of MNNG, cells were allowed a repair time of 3 hours in fresh medium, then harvested and DNA damage was estimated by SCGE (Comet assay). The reduction in tail length of DNA in comparison to the unrepaired DNA lymphocytes provided the repair percentage of the lymphocytes.

### **3.5.19. Estimation of the activity of cytokines**

Activity of pro and anti-inflammatory cytokines in mice serum and spent medium of HaCaT cells were assayed using respective ELISA kits like; TNF alpha (ab208348), IL2 (ab223588), IL6 (ab100712), IL8

(ab213859, IL13 (ab219634), IL17A (ab199081), IL22 (ab223857) and IL10 (ab255729) manufactured by Abcam. These assay kits employed quantitative sandwich ELISA technique, using tagged monoclonal antibodies, to measure the activity of respective cytokines, using colorimetric analysis. The results were obtained at 450nm using a microplate reader.

#### **3.5.20. Estimation of the activity of NF- $\kappa$ B subunits.**

The activity of p50 and p65 subunits of NF $\kappa$ B were assessed by NF $\kappa$ B p50 Transcription Factor Assay Kit (ab207217) and NF $\kappa$ B p65 ELISA Kit (ab176648) respectively. The assay was performed according to the manufacturer's protocol employing the sandwich ELISA technique. The results were obtained at 450nm using a microplate reader.

#### **3.5.21. Histone extraction from mice tissues.**

Histone proteins were isolated by acid extraction [Shechter et al., 2007] method. Mice skin tissues were homogenised in Dounce homogeniser utilising the Triton-X Extraction Buffer (0.5% Triton-X, 2 mM PMSF, 0.02% NaN<sub>3</sub>). Following which, the mixture was centrifuged at 10,000 rpm for 1 min at 4°C. The obtained pellet was suspended in extraction buffer (0.5N HCl and 10% glycerol). After centrifugation at 12,000 rpm for 5 min at 4°C, the supernatant was collected and kept overnight with 600 $\mu$ l of acetone at -20°C. The supernatant mixed with acetone was thawed at room temperature and was subjected to centrifugation at 12,000 rpm for 10 minutes. Finally, the pellet was dissolved in deionized water and stored at -80°C.

### 3.5.22. Estimation of global H3K4 methylation

Global histone methylation was assessed spectrophotometrically from the isolated histone extracts using EpiQuik TMGlobal Histone H3K4 methylation Assay Kit (P-3017-96) manufactured by Epigentek Group Inc. This method employs high affinity antibody and HRP tagged secondary antibody with the ability to produce colour. The methylation of H3K4 is proportional to the intensity of colour development. The absorbance OD was measured using a microplate reader, at 450 nm and the methylation (%) was calculated according to the formula:

$$[\text{Methylation\%} = \{ \text{OD (Sample-blank)} / \text{OD (untreated control-blank)} \} \times 100].$$

### 3.5.23. Immunohistochemistry (IHC) Assay

IHC was performed on formalin-fixed and paraffin-embedded mice tissues. The tissue embedded paraffin blocks were cut using a microtome machine to 4- $\mu\text{m}$  thickness, which were then stretched and mounted on poly-l-lysine coated slides. The slides were then deparaffinization in xylene, hydrated by lowering alcohol grades and then immersed in deionized water. For antigen retrieval, the slides were immersed in 10mM citrate buffer, pH 6.0 and was placed in hot-air oven at 80°C for 40 minutes. To prevent nonspecific binding, the slides were covered with 1% Bovine Serum Albumin (BSA) dissolved in Phosphate Buffered Saline (PBS) (137 mM NaCl, 2.7 mM KCl, 8 mM Na<sub>2</sub>HPO<sub>4</sub>, and 2 mM KH<sub>2</sub>PO<sub>4</sub>) and kept in humid chamber for 30 minutes at room temperature. After blocking, the slides were washed with PBS, primary antibody was added in the ratio 1:500 and incubated in a humid chamber over night at 4°C. Next day, the slides were

again washed with PBS to remove excess antibody, followed by addition of Horse Radish peroxidase (HRP) tagged secondary antibody (1:1000 ratio) and incubation at room temperature in a humid chamber for one hour. After incubation, excess antibody was washed away, stained with diaminobenzidine (DAB) while the nucleus was counterstained with haematoxylin, dehydrated with increasing grades of alcohol and finally mounted in Dibutylphthalate Polystyrene Xylene (DPX).

The slides were observed under a bright field microscope, images were captured at 400x and minimum of 50 fields were analysed for each point. The expressions of various proteins in IHC were analysed using the scoring system as formulated by [Allred et al. 1998]. The scoring system classifies the percentage of stained cells into 6 proportion scores (PS) and the intensity of staining into 4 intensity scores (IS). The final Allred score is calculated as the sum of PS and IS. The six categories of PS and four categories of IS are as follows:

<b>Percentage of stained cells</b>	<b>Percentage Score (PS)</b>
0	0
<1	1
1-10	2
11-33	3
34-66	4
≥67	5

<b>Intensity of Staining</b>	<b>Intensity Score (IS)</b>
None	0
Weak	1
Intermediate	2
Strong	3

The final Allred Score (AS) is calculated as: PS + IS =AS. The Allred score can be categorized into 9 categories (0–8), the highest score being 8. Each section was scored 5 times and the highest AS was reported

#### **3.5.24. Immunoblot Assay.**

Radioimmunoprecipitation Assay Buffer (RIPA) (10mM Tris-HCl, pH 8.0, 1mM EDTA, 0.5mM EGTA, 1% Triton X-100, 0.1% Sodium Deoxycholate, 0.1% SDS, 140mM NaCl and 1mM PMSF added immediately before use) was used to extract whole tissue and cell proteins from the mice tissues and HaCaT cells. 300µl of RIPA was added to 5mg of tissue and homogenised, which was followed by sonication and centrifugation at 13,000g for 20 minutes at 4°C, the resultant supernatant was collected. The HaCaT cells were harvested, washed in PBS and incubated with RIPA buffer at 4°C for 30 minutes (500µl of RIPA was added for 10<sup>7</sup> cells). It was followed by sonication and centrifugation at 13,000g for 20 minutes at 4°C. The resultant supernatant contained the whole tissue and cell proteins respectively, the concentration of the proteins was estimated using Bradford's reagent.

80 µg of protein was loaded into each well and then electrophoresed on SDS-Polyacrylamide gels respectively, using the electrophoresis buffer (250 mM TRIS, 192 mM glycine, 10% SDS). The separated proteins were electro-transferred to nitrocellulose membranes using transfer buffer (250 mM TRIS, 192 mM glycine, 10% Methanol). After blocking with BSA, membranes were incubated with primary antibodies overnight at 4°C with constant shaking. The blots were washed 4 times with TBST (TBS and 0.5% Tween 20) followed by treatment with either alkaline phosphatase conjugate

anti-mouse or anti-rabbit IgG (1:2000 dilutions in TBS) at 4°C. Membrane was then washed 4 times with TBST and incubated with substrate 5-bromo-4-chloro-3-indolyl phosphate (BCIP)/nitro blue tetrazolium (NBT) to visualize the proteins. The Western blot bands were scanned and quantified by using IMAGE MASTER Software (Amersham Pharmacia biosciences, USA).

### **3.5.25. Semi-quantitative RT-PCR analysis**

TRIzol reagent (guanidine thiocyanate and phenol) was used to isolate RNA from the animal tissues. Two micrograms of extracted RNA were converted to cDNA using a RETROscript kit manufactured by Ambion, ThermoFischer Scientific. The cDNA's were then subjected to amplification by PCR using respective forward and reverse primers. The primer sequences used for the amplification are as follows:

#### **E-cadherin**

Forward primer = 5'-GGCTTCAGTTCCGAGGTCT-3'

Reverse primer = 5'-GAAAAGAAGGCTGTCCTTGG-3'

#### **Desmoplakin**

Forward primer = 5'- TCAACGACCAGAACTCCGAC-3'

Reverse primer = 5'-TTTGCAGCATTTCTTGGATGG-3'

#### **Vimentin**

Forward primer = 5'-AAAGCACCCCTGCAGTCATTC-3'

Reverse primer = 5'-AGCCACGCTTTCATACTGCT-3'

#### **N-cadherin**

Forward primer = 5'-AAGGACAGCCCCCTTCTCAAT-3'

Reverse primer = 5'-CTGGCTCGCTGCTTTCATAC-3'



### **Snail**

Forward primer = 5'-CACCTCATCTGGGACTCTC -3'

Reverse primer = 5'-AGGTGGACGAGAAGGACGAC-3'

### **Slug**

Forward primer = 5'-AACATTTCAACGCCTCCAAG-3'

Reverse primer = 5'-TGAACCACTGTGATCCTTGG-3'

### **Twist**

Forward primer = 5'-CGGACAAGCTGAGCAAGATT-3'

Reverse primer = 5'-CCAGACGGAGAAGGCGTAG-3'

### **Zeb1**

Forward primer = 5'-CCAAGAAGCTGCTGGCAAGA-3'

Reverse primer = 5'-GATAAATGACGGCGGTGTCT-3'

The PCR products were subjected to electrophoresis in 2% agarose gel, stained with EtBr. After electrophoresis, the gel was viewed in ChemiDoc XRS and Imaging system (BioRad) and the band intensities were documented.

#### **3.5.26. Immunofluorescence assay**

The presence and location of EMT markers in the HaCaT cells were detected using the Immunofluorescence assay. Sterile cover slips were placed on 6 well plates and cells were seeded and grown into confluence. After attaining 80% confluence, the cells growing on the coverslips were washed with PBS and fixed in 2% paraformaldehyde solution. Permeabilization of the cells was done via 0.1% Triton X-100, it was then kept at room temperature for 20 min. Blocking was performed by 2% BSA solution for 2 hours at room temperature. Primary antibodies were added and

kept at 4°C over-night. Cells were then washed in PBST (PBS + 0.1% Tween20) and secondary conjugated antibodies were added and incubated at room temperature. Cells were washed, counter stained with DAPI and mounted on slides using DPX. The cells were then observed under a fluorescent microscope.

### **3.5.27. Expression of EMT markers using Flowcytometry**

The expression of EMT markers were also confirmed by flowcytometric analysis in the HaCaT cells. Adherent HaCaT cells were harvested using versene solution, followed by resuspension in PBS. The cells were fixed by 2% paraformaldehyde solution for 20 min at room temperature and permeabilized using a 0.1% saponin solution for 15 min at room temperature. The cell suspensions were subsequently washed in PBS by centrifugation at 1500 rpm for 5 min, followed by blocking with 1% BSA solution in PBS for 1 h. Primary antibody was then added and incubated overnight at 4°C. Secondary antibody was added and incubated at RT for 2 hours. Flowcytometry was performed using BD FACSCalibur. The primary conjugated antibodies used for flowcytometry were ECadherin [67A4] (FITC) (Genetex, 1:50) and Vimentin [VI-RE/1] (PEs) (Genetex, 1:500); while other primary antibodies were non-conjugated. For non-conjugated primary antibodies, secondary conjugated antibodies were used Goat anti-rabbit IgG (FITC) (Genetex, 1:500), Rabbit anti-mouse IgG (FITC) (Genetex, 1:500).

### **3.5.28. *in vitro* wound healing assay**

Confluent plates of HaCaT cells were scratched in a straight line in order to create a wound, using sterile pipette tip (200 µl). The width of the

inflicted wound was photographed aseptically using an inverted microscope, immediately after scratching, which is considered as the 0th hour. Plates were then incubated for 24 hours with desired treatment plans. After 24 hours, the plates were photographed again to assess the width of the wound. Wound healing was assessed by calculating the reduction of the scratch width of the inflicted wound after 24 hours. Reduction in the width of the wound was expressed as a percentage of wound closure, indicating the migration potential of the cells.

### **3.5.29. Transwell migration and invasion assay.**

The migration and invasive property of the HaCaT cells were determined by the Transwell assay. This assay was performed according to the laboratory protocol [Sarkar et al., 2016], inside a Boyden chamber consisting of transwell region, covered with a polyethylene terephthalate (PET) filter membrane having pore size of 8  $\mu\text{m}$ . Serum free cell suspension of  $10^5$  cells were seeded in the upper chamber; for migration assay the upper chamber was not coated with extra cellular protein matrix, whereas for invasion assay the upper chamber was coated with extra cellular protein matrix. The lower chamber was fed with medium containing 20% FBS, acting as a chemo-attractant. Cells were allowed to migrate/invade for 24 hours. The cells which reached the lower chamber were formalin fixed (4%) and stained with 0.5% crystal violet stain. Each field was counted thrice and the mean of three readings was recorded. The stained cells were then de-stained with 30% acetic acid to dissolve the crystal violet stain which was then collected and the absorbance was measured at 570 nm. Intensity of the stain is directly proportional to the migrated/ invaded cells.

### **3.5.30. Gelatin Zymography Assay.**

Invasiveness and activity of the Matrix Metalloproteases (MMP2 and 9) were estimated by performing the gelatin zymography assay in HaCaT cells. Control, iAs and BTE + iAs treated HaCaT cells were grown in serum free medium for 24 hours. This conditioned medium was collected, concentrated and electrophoresed on 10% SDS-PAGE gel with 0.1% gelatin. Gel was then washed 3 times using the renaturing buffer or the washing buffer (pH 7.5, 2.5% Triton X-100), followed by incubation overnight at 37°C in developing buffer (50 mM Tris-HCl pH 7.5, 5 mM CaCl<sub>2</sub>, and 200 mM NaCl). This facilitates digestion of the gelatin by the MMP's. The gel was then stained with 0.5% Coomassie Blue R-250 stain, in 30% methanol and 10% glacial acetic acid. The gel was then de-stained with 30% methanol and 10% acetic acid. Clear white bands of MMP 2 and 9 were observed against a dark background.

### **3.5.31. Docking studies**

The crystal structure of JARID1B (KDM5B) (PDB ID: 5FUN) was obtained from protein data bank (<https://www.rcsb.org>). This structure was used for studying small molecule inhibitors for the JmjC domain of JARID1B [Johansson et al., 2016]. The chemical structures of theaflavin (PubChem CID: 135403798) and theaflavin-3,3'-digallate (PubChem CID: 21146795) were downloaded from PubChem (<https://pubchem.ncbi.nlm.nih.gov/>). Protein and ligand preparations were done using Python Molecular Viewer (pmv), part of MGLTools from Scripps Institute [Sanner, 1999]. The PHD1-ARID domains were deleted from JARID1B structure (PDB ID: 5FUN) and it was considered suitable for our

study as the focus is on the JmjC domain. Johansson et al. used several supplementary ligands in their study which were removed from the PDB file for molecular dynamical simulations [Johansson et al., 2016]. These supplementary ligands are EDO (1,2 ethanediol), EPE (4-(2-hydroxyethyl)-1-piperazine ethanesulfonic acid), GZA (2-[(1-benzyl-1H-pyrazol-4-yl)oxy]pyrido[3,4-d]pyrimidin-4(3H)-one), metals (Mn, Zn, Na) and phosphate ion. The removal of these supplementary ligands had no effect on the protein structure, which was verified by superimposing the two structures. The protein was prepared by deleting water molecules, adding polar hydrogen and Gasteiger charges, and saved in the pdbqt format. The ligand was prepared by adding Gasteiger charges and saved in the pdbqt format. Docking was done using Webina, a web-based docking tool that runs in a browser using AutoDock Vina [Trott et al., 2010; Kochnev et al., 2020]. The centre ( $x = 88$ ,  $y = 66$ ,  $z = 11.6$ ) and size ( $x=30$ ,  $y=27$ ,  $z=32$ ) of the docking box were chosen to cover the JmjC domain of JARID1B. The top-9 docking poses for both theaflavin and theaflavin-3,3'-digallate were analysed for polar interactions using PyMol. The docking poses were extracted from the output using vina\_split, a tool in the AutoDock Vina software.

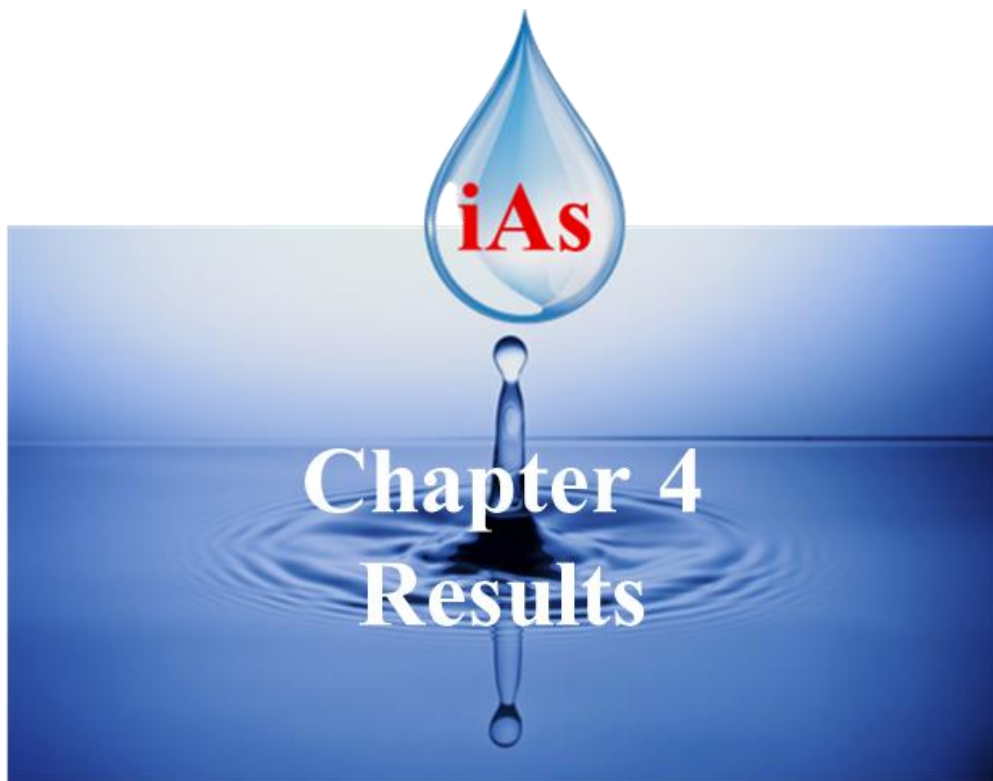
### **3.5.32. Molecular dynamical simulation**

Preparations of the protein-ligand systems for molecular dynamical simulation were done using Gromacs in-built tools [Abraham et al., 2015] version 2020.1-Ubuntu-2020.1-1 on a 64-bit, quad core Ubuntu system. The Bioexcel Building Block library [[https://mmb.irbbarcelona.org/biobb/availability/tutorials/md\\_setup](https://mmb.irbbarcelona.org/biobb/availability/tutorials/md_setup)] workflow was used for preparation of the protein-

ligand system, using python 3.7 and Jupyter Notebook. The Amber ff99sb forcefield was used, as this forcefield is considered to be appropriate for protein-ligand simulations. Short (10 ps) molecular dynamical simulations were done at the preparation stage to check the setup parameters. The Zeus supercomputer in Pawsey Supercomputing Facility in Perth, Western Australia was used for the Gromacs production runs (Intel Xeon E5-2690V3 “Haswell” processors, 12-cores, 2.6 Ghz). 24 MPI processes and 4 OpenMP threads in each MPI process were found to provide optimal performance. Each production simulation was run for 24 hours, providing approximately 37 nano seconds of simulation time. Molecular mechanics Poisson Boltzmann surface area (MM/PBSA), a widely used method to calculate the binding free energy between protein and ligands was used. Although it is not as accurate as alchemical free energy methods, it is considered to be more accurate than scoring functions used in docking and substantially much faster than the alchemical methods. MM/PBSA analysis was done using the `g_mmpbsa` tool [Kumar et al., 2014]. The docking movies were created using Gromacs trajectory files.

### **3.5.33. Statistical Analysis**

Statistical analysis was performed using IBM SPSS Statistics 22. One way ANOVA Dunnett's Test was performed to check the significance of the MTT results, while Tukey Test was performed to assess the significance between the control and other treatment groups.





**PRELIMINARY**  
**RESULTS**



## **4. Results**

### **A. PRELIMINARY RESULTS**

#### **4.1. Determination of the dose of iAs in Swiss albino mice.**

Table 4.1 represents the results of the pilot study, performed on the Swiss albino mice, for a period of 6 months, to ascertain the concentration of iAs for the study. From the table it is can be seen that initially the treatment of mice began with 4 doses of iAs (100 µg/l, 250 µg/l, 500 µg/l and 1000 µg/l). The dose of 1000 µg/l had to be discontinued because 80% of the treated mice died within 1 month of treatment. The work was carried forward with the remaining three doses. At the end of 6 months of treatment, keratotic lesions appeared on the skin of the mice which received 500 µg/l of iAs. Histological analysis of these lesions showed hyperplastic and dysplastic changes within the lesions. No lesions appeared on the skin of the mice which received 100 µg/l and 250 µg/l of iAs and histological analysis of the skin also revealed no prominent changes. Therefore, 500 µg/l was chosen as the dose of iAs which was to be administered to the mice for further experimentations.

#### **4.2. Polyphenol content of BTE**

According to cohort data collected over 10 years, it has been seen that consumption of 10 cups of tea per day by adult human male (70 kg) resulted in decrease of cancer incidences. 10 cups of tea may be approximated to 1000 ml and 2.5% infusion (based on 2.5 g of tea leaves required to brew 100 ml of water in a cup of tea) [Sinha et al., 2010]. Using the above estimation, the BTE used in the present study is 2.5% infusion. The polyphenolic contents of 2.5% infusion BTE were quantitated using HPLC. Different constituents of Catechins, EGCG [(-)- epigallocatechin gallate], EGC [(-)- epigallocatechin] and

**Table 4.1:** Pilot study to determine the dose of iAs in Swiss albino mice. The table below displays the four doses of iAs with which groups of mice were treated. Dose of 1000 µg/l was discontinued within one month due to high toxicity. Study was conducted with the remaining three doses for a period of 6 months. Out of the three doses, dysplastic lesions appeared only in 500 µg/l dose of iAs. Hence, subsequently the study was conducted with 500 µg/l dose of iAs.

Time in months	Observation	Dose of iAs (µg/l)			
		100	250	500	1000
1	Ectopic	-	-	-	80 % death
	Histology	No change	No change	No change	
3	Ectopic	-	-	Redness	Discontinued
	Histology	No visible change	No visible change	Mild dysplasia	
6	Ectopic	-	-	Small lesions	
	Histology	No visible change	Mild changes	Hyperplasia, dysplasia, keratosis	

ECG [(-)- epicatechin gallate] were separated using gradient mode; whereas TF [Theaflavin] was separated in isocratic mode. The concentrations (mg/ml) of the respective polyphenols have been provided in Table 4.2. Theaflavin was found to be the most abundant polyphenolic compound present in the BTE prepared in the laboratory for the experiments. The final concentration of BTE administered to Swiss albino mice was 0.33 mg/gm body weight. The concentration of BTE provided to HaCaT cells was 1  $\mu$ M (non-toxicity of the dose was confirmed by MTT assay).

#### **4.3. Mitigation of iAs induced damage by BTE using mathematical model.**

Mathematical modelling was performed to estimate the mitigation of iAs induced damage by BTE. Mathematical models determining the modulatory property of BTE against iAs induced cell damage and tumour growth have been prepared using the experimental data obtained from the present study [Srivastava et al., 2020]. Figure 4.1A displays a line graph which shows proportions of damaged cells, which occur due to oxidative stress in Swiss albino mice. The blue line shows the proportion of damaged cells in the iAs treated mice, while those belonging to the iAs+BTE treated mice have been shown by red line. The graph clearly shows that the damaged proportion of cells are reduced upon BTE administration. Modelling was performed by progressively considering complex factors. The first model used the differential equation of the standard decay model. It considered only the growth of damaged cells using the differential equation, with oxidative damage due to iAs and the mitigating factor of BTE opposing each other. Some of the parameters of this model were taken from existing literature on tumour growth. The predictions from this model were close to the experimental data. In the subsequent models,

**Table 4.2 :** The polyphenolic contents of BTE. Different constituents of Catechins, EGCG [(-)-epigallocatechin gallate, EGC [(-)- epigallocatechin] and ECG [(-)-epicatechin gallate] were separated using gradient mode; whereas TF [Theaflavin] was separated in isocratic mode. Concentrations (mg/ml) have been listed below in the table.

**Polyphenolic content of Black Tea Extract (2.5%)**

<b>Polyphenol</b>	<b>Concentration (mg/ml)</b>
<b>EGC</b>	0.24
<b>EGCG</b>	0.43
<b>ECG</b>	0.30
<b>TF</b>	0.97

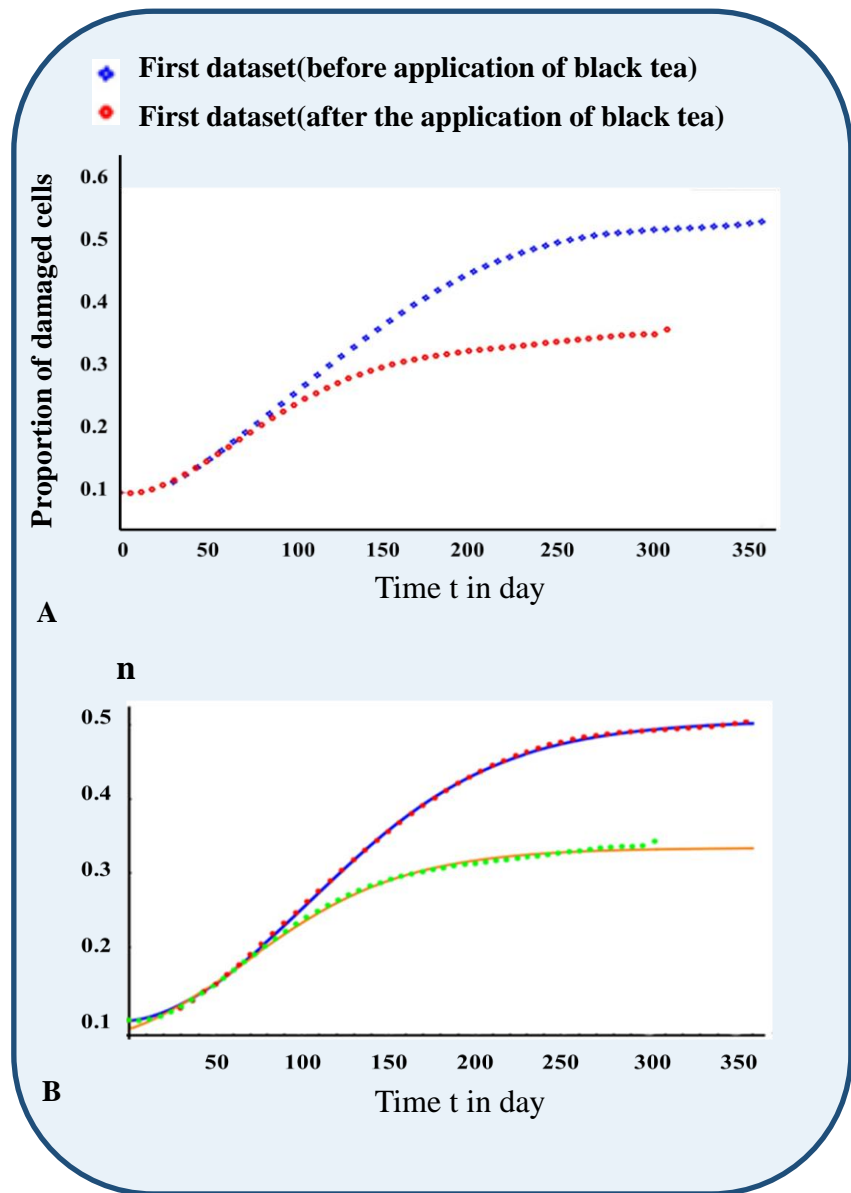


**Figure 4.1:** Mathematical modelling of mitigation of iAs induced damage by BTE. **Figure 4.1A** displays a line graph where the upper curve represents cell-damage proportion by iAs and the lower curve represents data from the group receiving iAs along with black tea. The amelioration i.e. limiting the extent of damage due to tea, is evident.

**Figure 4.1B** displays a line graph which shows fitting of curves to the given experimental data. Red and green dots represent experimental data and the blue and orange lines represent the fitted curves. Experimental data is in good agreement with the model.

more complex factors were introduced like the action of immune cells, and the delay in the activation of immune cells. The predictions from the most complex model matched with the experimental data very well. Figure 4.1B displays the line graph which represents fitting of the curves of mathematical model with the experimental data. The red and green dots in the graph represent the experimental data of iAs and iAs+BTE treated mice respectively, whereas, the blue and the orange lines represent the curves of the mathematical model. The dots and the curves matched very well, indicating that the experimental data is in agreement with the simulated mathematical model. Therefore, it can be stated that the mathematical models confirmed the experimental findings.

#### **4.4. Determination of iAs accumulation in the hair and nails of Swiss albino mice**

iAs accumulation in the hair and nails of the mice were estimated using AAS-VGA. Table 4.3 displays the amount of iAs accumulated in the hair and nails of the mice, which were chronically exposed to iAs for 330 days. From the results we can see that substantial amount of iAs gets accumulated in the hair and nails of the iAs treated mice, whereas no such accumulation of iAs was observed in the control mice. Therefore, we may say that, the development of tumour and other consequential effects observed in mice, may be due to accumulation of iAs.

#### **4.5. Determination of the dose of iAs and BTE for *in-vitro* treatment of the HaCaT cells**

Toxicity of logarithmic concentrations of iAs and BTE were tested on HaCaT cells employing MTT assay, results are depicted in Figure 4.2A and Figure 4.2B respectively. Exponentially growing HaCaT cells were treated with

**Table 4.3:** Arsenic accumulation in the hair and nail of mice were estimated using AAS-VGA and have been displayed in the table. Swiss albino mice were treated with iAs for 330 days and then their hair and nails were subjected to iAs estimation. Prominent accumulation of iAs was observed in the hair and nails of iAs treated mice. Minimum Reporting Limit (MRL) for iAs is 2 µg/l. Values below MRL are written as < 2 µg/l.

Parameter	Concentration (µg/l)			
	Control		Exposed	
Arsenic estimation	Nail	Hair	Nail	Hair
	<2	<2	3.95	37.2

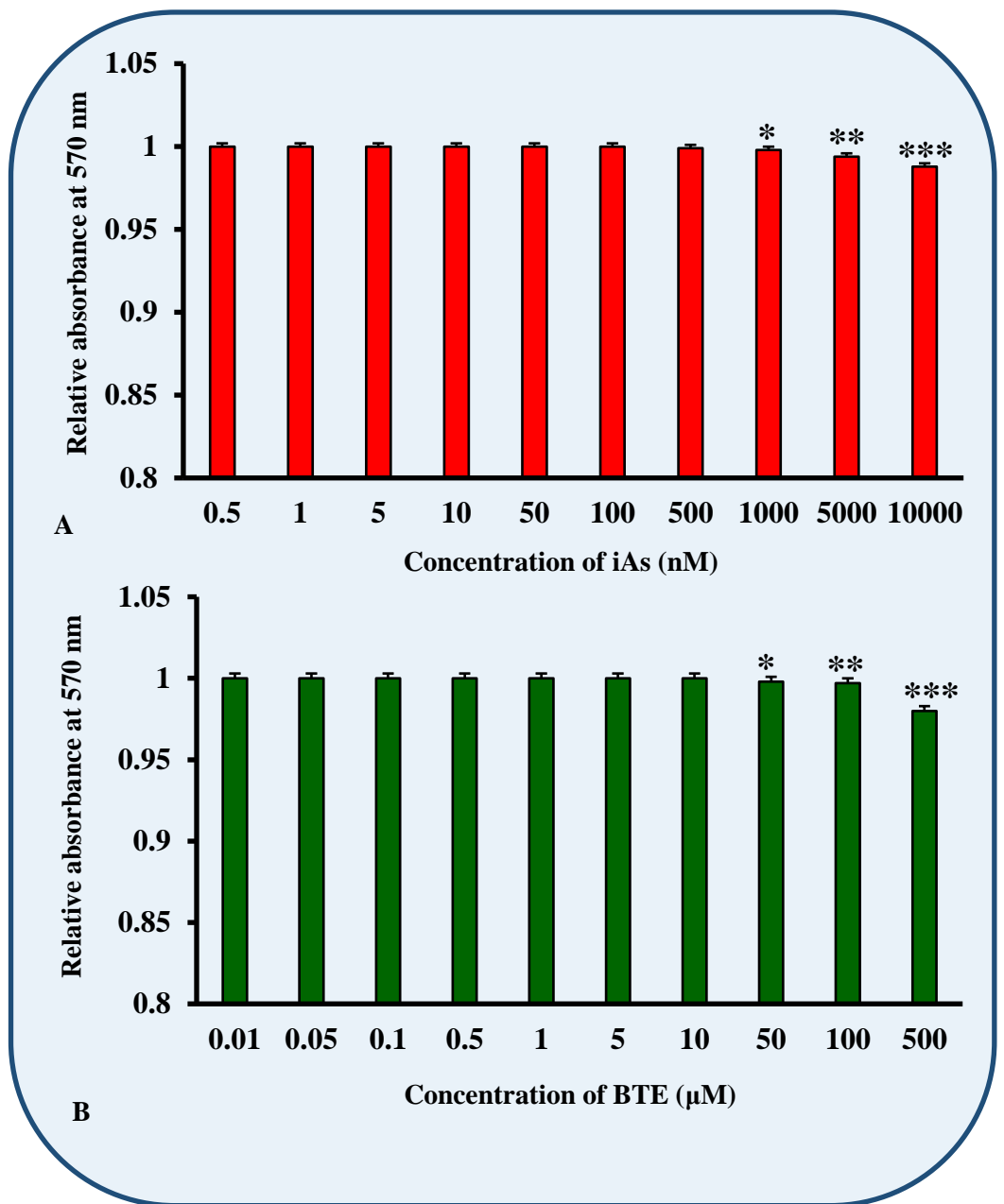


**Figure 4.2:** Toxicity of iAs and BTE at different doses and time points.

**Figure 4.2A** shows the toxicity of different concentrations of iAs employing MTT assay. Up to a concentration of 100 nM, iAs showed no toxicity for 48 h of treatment. Very little toxicity is seen at 1000 nM, 5000 nM and 10,000 nM which are insignificant at \* $p = 0.057$ , \*\* $p = 0.016$  and \*\*\* $p = 0.003$  respectively.

**Figure 4.2B** Shows the toxicity of different concentrations of BTE employing MTT assay. Up to 10  $\mu\text{M}$  concentration of BTE, there has been no toxicity, marginal toxicity was noted at 50  $\mu\text{M}$ , 100  $\mu\text{M}$  and 500  $\mu\text{M}$  which are insignificant at \* $p = 0.595$ , \*\* $p = 0.461$  and \*\*\* $p = 0.006$  respectively.

Values are represented as mean of three independent experiments  $\pm$ S.D.



iAs or BTE for 48 h. A concentration of 100 nM of iAs was chosen to be administered to the HaCaT cells, which showed no toxicity. This dose is in accordance with the finding of other groups [Banerjee et al., 2021]. MTT assay with different concentrations of BTE was performed to choose a non-toxic dose; from Figure 4.2B, a concentration of 1  $\mu$ M was selected for treatment of the HaCaT cells.

Biochemical parameters, like alanine transaminase (ALT) or serum glutamate pyruvate transaminase (SGPT), aspartate aminotransferase (AST) or serum glutamic-oxaloacetic transaminase (SGOT), creatinine and urea have been estimated from serum sample using available kits in the Biochemistry department of Chittaranjan National Cancer Institute, Kolkata. AST, ALT values in control Swiss albino mice were  $149.44 \pm 10.2$  U/l and  $47.28 \pm 3.26$  U/l respectively and the values remained more or less similar after treatment with the selected dose of iAs (500  $\mu$ g/l) and BTE (0.33 mg/gm body weight) at different time points. The changes were not significant. Creatinine level was  $0.6 \pm 0.02$  mg/dl, whereas the urea level was  $30.22 \pm 1.8$  mg/dl. Treatment with iAs and BTE, alone or in combination did not affect the creatinine and urea level significantly. Haematological parameters were also checked. Haemoglobin (Hb) was not affected by iAs or BTE at the doses chosen for the study. Total Leukocyte Count (TLC), which is an indicator of several disorders, was also evaluated and found to be normal at the doses selected for the study. Hence, 500  $\mu$ g/l of iAs and 0.33 mg/gm body weight BTE, alone or in conjunction did not affect the health of the Swiss albino mice.



***in vivo model***

## **B. *in vivo* RESULTS**





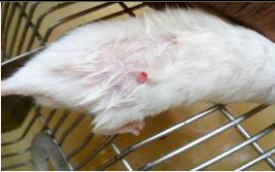










### **4.6. Development of skin lesions and tumour growth dynamics**

Figure 4.3 displays the representative photographs of the control, iAs and iAs+BTE treated mice at different timepoints of treatment. No lesions were observed after 30 days of treatment by iAs. Lesions started appearing on the shaved skin of the iAs treated mice after 90 days of treatment. After 180 days of treatment by iAs, lesions grew further; minute lesions appeared on the iAs +BTE treated mice. However, lesions in iAs treated group of animals were visibly prominent, more in number, covering a greater surface area of the skin. At 270 days of treatment, lesions of the iAs treated mice developed further and ulcerative growth were observed. In iAs+BTE group of mice scattered lesions were observed, which were smaller in size and number. After 330 days of treatment, the lesion of the iAs group appeared fluid filled, highly ulcerative and covering a large surface area. BTE counterpart at 330 days only displayed smaller lesions with no signs of ulceration or invasion.

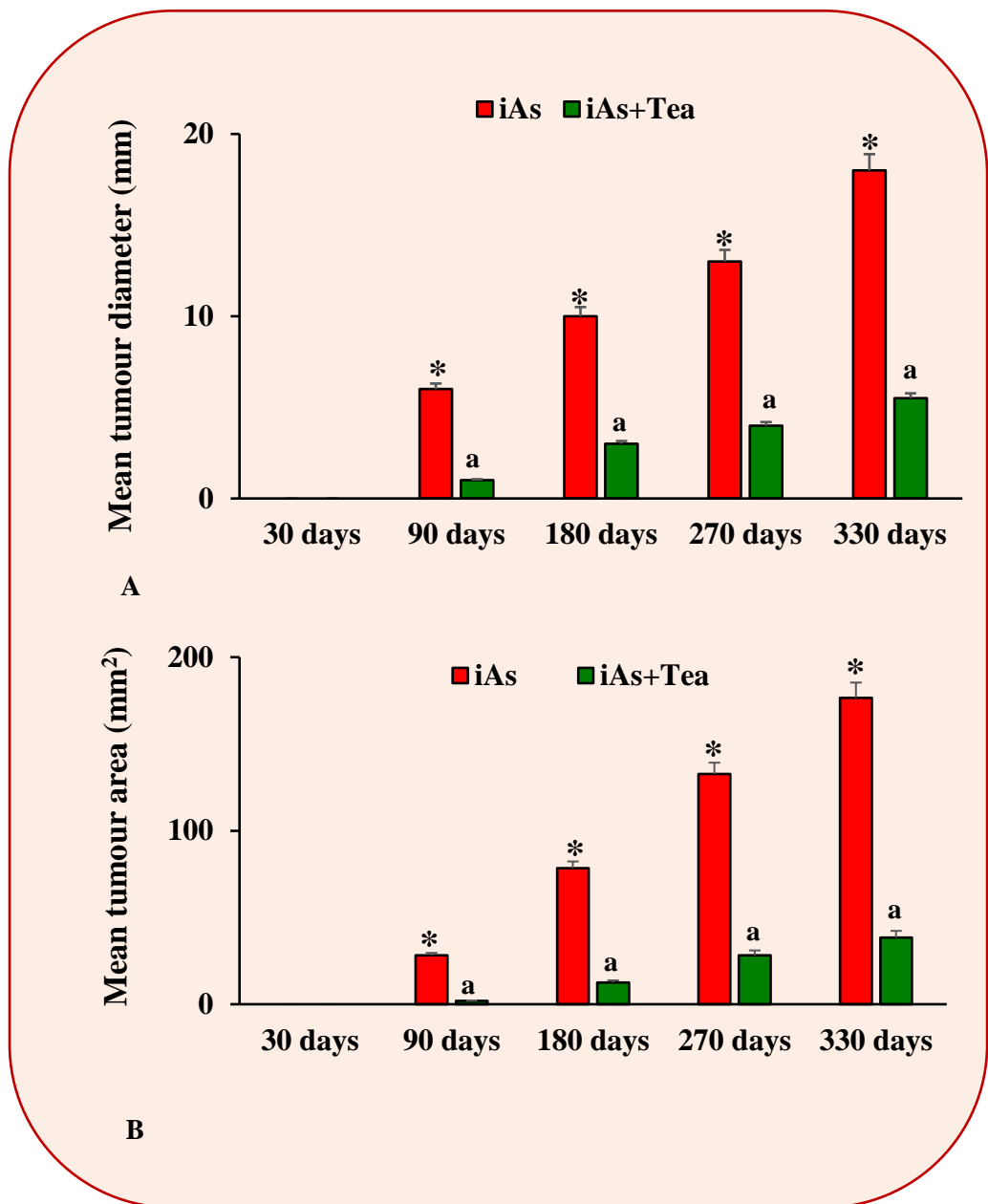
The diameter and area of the tumours of different treatment groups of mice have been depicted by bar graph, respectively in the Figures 4.4A and 4.4B. It can be clearly seen that with chronic exposure of iAs, the diameter (A) and area of the tumours (B) in the iAs treated mice were significantly ( $p < 0.0001$ ) higher than that of the mice which were administered BTE. No lesions were observed in the control mice group, as well after treatment for 30 days.

### **4.7. Histological analysis of tumour development**

Photographs displaying histological analysis of the control, iAs and iAs+BTE treated mice skin tissue, at different timepoints of treatment have been displayed in Figure 4.5. Hyperplastic changes were first observed in the iAs

No of Days	Control	iAs	iAs+BTE
30			
90			
180			
270			
330			

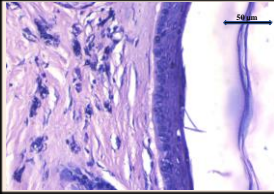
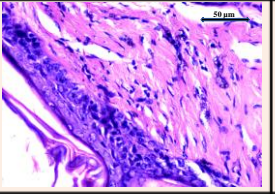
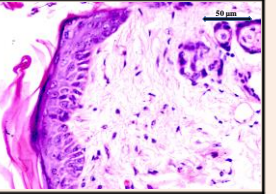
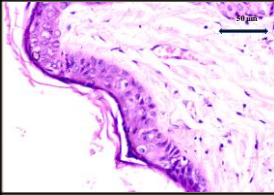
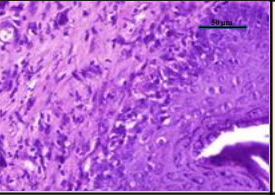
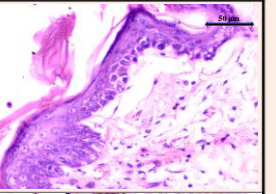
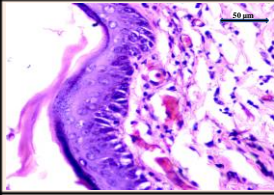
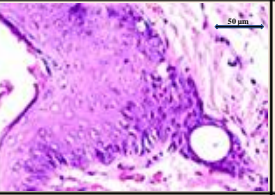
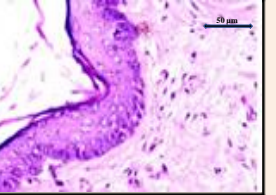
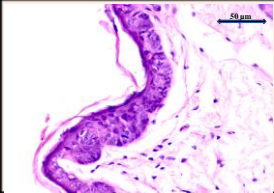
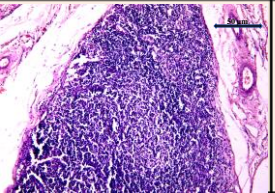
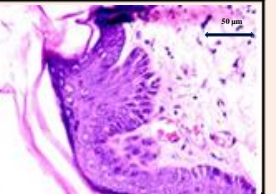
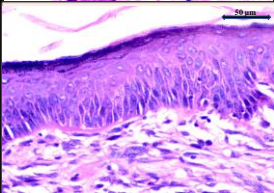
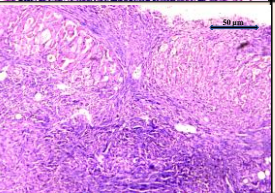
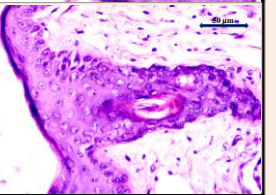
**Figure 4.3:** Development of skin lesions due to iAs exposure. Representative photographs of tumour development in control, iAs and iAs+BTE treated mice, at 30, 90, 180, 270 and 330 days of treatment, have been displayed in the figure. From the photographs it can be seen that lesions started to develop in the iAs treated mice from 90 days onwards, which became prominent at 180 days. Large and keratotic lesions developed at 270 days and ulcerative, fluid filled massive tumours at 330 days of treatment were evident. Minute lesions appeared on the iAs+BTE treated mice at 180 days of treatment which were scattered at 270 days of treatment. At 330 days, the lesions were prominent but showed no signs of keratosis or ulceration. No lesions developed on the skin of the control mice.



**Figure 4.4:** Measurement of tumour size in Swiss albino mice.

**Figure 4.4A** displays a bar graph depicting tumour diameter, in Swiss albino mice, recorded at 30, 90, 180, 270 and 330 days of treatment, in the iAs and iAs+BTE treated mice. The diameter has been measured using vernier calipers and displayed as mean of three independent experiments  $\pm$  S.D.

**Figure 4.4B** displays a bar graph representing area of tumour, which was measured in Swiss albino mice, at 30, 90, 180, 270 and 330 days of treatment. The data has been represented as mean of three independent experiments  $\pm$  S.D. There was no visible tumour at 30 days, therefore, increase in diameter has been calculated with respect to the one obtained at 90 days. Increase in diameter and tumour area are significant at  $*p < 0.0001$ . Intervention with BTE, resulted in appreciable decrease in tumour diameter and area, which are significant at  $^ap < 0.0001$ , with respect to the iAs treated mice.

Time in days	Treatment		
	Control	iAs	iAs+BTE
30			
90			
180			
270			
330			

**Figure 4.5:** Histopathological studies during development of iAs induced skin carcinogenesis at different stages. Tissue Sections were stained by hematoxylin & eosin and visualized under a light microscope. Tissue sections indicate hyperplastic changes at 90 days of iAs exposure, which further developed to dysplasia at 180 days, along with appearance of keratin pearls. At 270 days of exposure, in situ carcinogenesis was observed, which further developed into invasive SCC at 330 days. In BTE intervention group, no changes have been observed upto 90 days, beyond which mild hyperplastic changes were observed at 180 days. Low grade dysplastic changes were seen at 270 and 330 days, including formation of keratin pearls. Representative photographs were captured using a bright field microscope at 400x magnification.

treated mice group after 90 days of treatment, while appearance of keratin pearls, prominent dysplastic changes and thickening of the epidermis were visible at 180 days. No definitive abnormal changes were observed in the epidermal architecture of the iAs+BTE treated mice at 90 days of treatment whereas slight hyperplastic changes were observed at 180 days. Histological analysis at 270 days of treatment in the iAs treated mice revealed development of in-situ carcinoma with appearance of parakeratosis, loss of epidermal layers and presence of deeply stained aggressive nuclei. These histological changes further aggravate into invasive squamous cell carcinoma at 330 days in the iAs treated mice, showing loss of entire epidermal structure and prominent infiltration of the deeply stained nuclei covering more than 2/3rd proportion of the underlying dermis. The lesions of the iAs+BTE treated mice showed thickening of the epidermal layers, development of dysplastic changes along with mild keratinisation at 270 and 330 days respectively but none of them progressed beyond this stage. The BTE administered mice did not show development of in-situ or invasive carcinoma within them even beyond the treatment period of 330 days.

#### **4.8. Estimation of ROS generation**

Results of the spectrofluorometric analysis of ROS in the leukocytes of mice, belonging to different treatment groups, at specific time intervals, have been displayed as a bar graph in the Figure 4.6A. Results indicate that the ROS generation in the iAs treated mice was remarkably higher than the control mice at all the timepoints of treatment. In the iAs+BTE administered mice, the extent of ROS generation was much less than the iAs group, hinting at quenching of excess ROS generation by iAs.



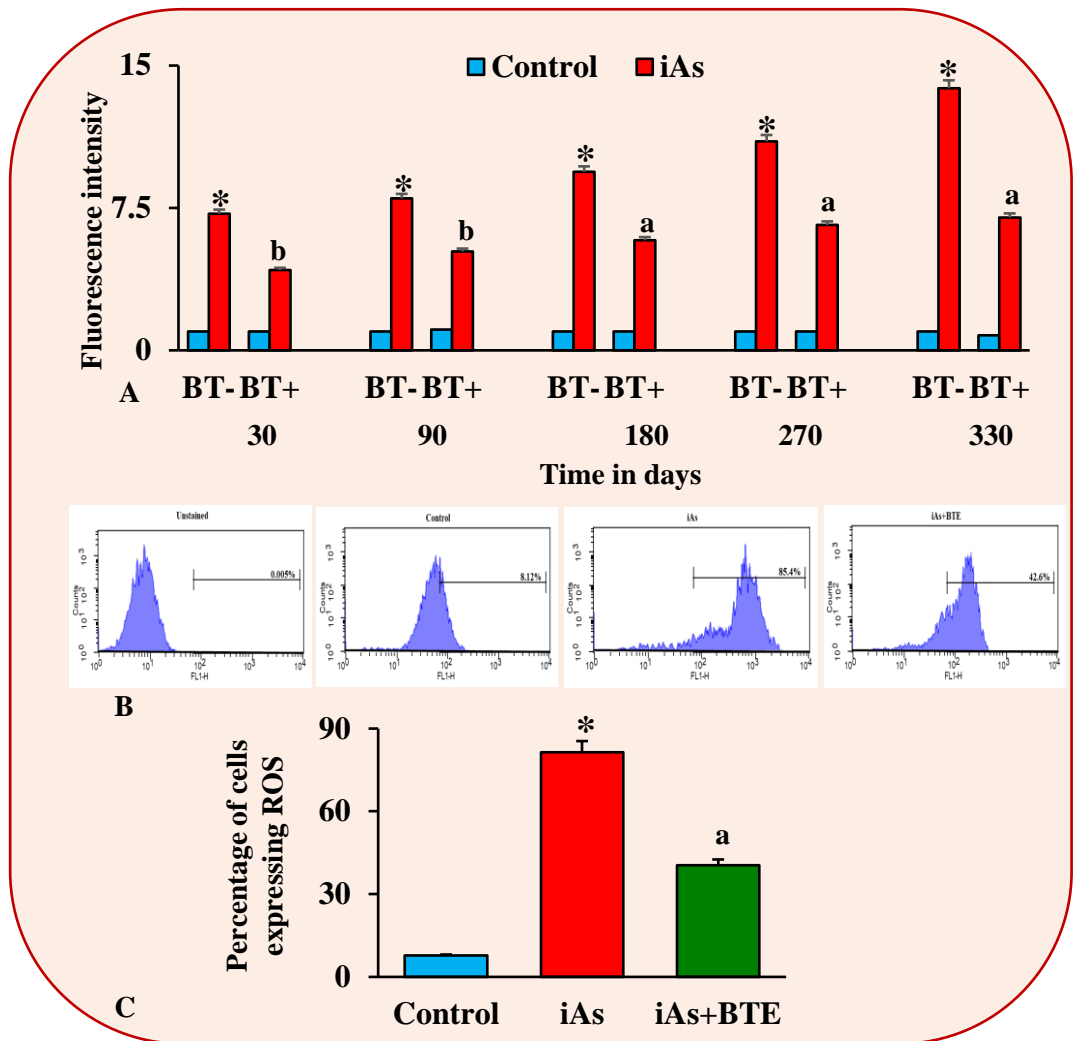


**Figure 4.6:** Determination of Reactive Oxygen Species (ROS) by spectrofluorimetric & flowcytometric studies using 2',7'-dichlorofluorescein diacetate (DCFDA).

**Figure 4.6A** displays a bar graph representing ROS generation in the leukocytes of control, iAs and iAs+BTE treated Swiss albino mice, at 30, 90, 180, 270 and 330 days of treatment. Results indicate higher ROS generation in mice chronically treated with iAs, which is much less in the iAs+BTE group.

**Figure 4.6B** displays histograms representing the percentage of ROS generating leukocytes, in Swiss albino mice, as assessed by flowcytometric studies, at 330 days of treatment. The histogram of iAs treated mice shows a prominent right shift of the fluorescence channel-1 peak with respect to the control, indicating excess ROS generation. Histogram peak of iAs + BTE treated mice shows a left shift, compared to the iAs treated mice, suggesting quenching of ROS. The proportions of leukocytes expressing ROS in the control, iAs and iAs + BTE treated mice are 8.12%, 85.4%, and 42.6%, respectively.

**Figure 4.6C** displays a bar graph indicating the mean percentages of ROS generating cells in the control, iAs and iAs +BTE treated mice. Displayed results are mean of three independent experiments  $\pm$ S.D. Increase in ROS generation, in iAs treated mice is significant at  $*p < 0.0001$ , with respect to the control. Decrease in ROS generated in the iAs+BTE group is significant at  $^b p < 0.001$  and highly significant at  $^a p < 0.0001$ , with respect to the iAs treated mice.



Flowcytometric analysis of ROS generation in the leukocytes of the control, iAs and iAs+BTE treated mice, at 330 days, have been displayed as representative histograms in the Figure 4.6B. Mean percentages of ROS generating cells, as assessed by Flowcytometry, was represented as a bar graph in the Figure 4.6C. The flowcytometric analysis and the bar graph reiterates our spectrofluorometric results and show that with chronic exposure to iAs there is significant ( $p < 0.0001$ ) increase in ROS generation which is significantly ( $p < 0.0001$ ) quenched upon BTE administration.

#### **4.9. Estimation of RNS generation**

Spectrophotometric analysis of RNS generation has been displayed as a bar graph in the Figure 4.7. The results indicate that RNS generation was significantly high in iAs treated mice, while in iAs+BTE treated mice it was appreciably reduced. This result suggests that BTE intervention reduces the RNS generated due to iAs exposure.

#### **4.10. Estimation of DNA damage using micronuclei assay**

DNA damage has been estimated using the micronuclei assay. Figure 4.8A depicts a bar graph which represents frequency of micronuclei formation per 1000 binucleate cells, estimated in the haematopoietic cells of the mice. Chronic exposure to iAs leads to significant ( $p < 0.0001$ ) increase in the micronuclei frequency, at 180, 270 and 330 days, compared to the control mice. Administration of BTE have been found to significantly ( $p < 0.0001$ ) reduce micronuclei frequency in the iAs treated mice at 180, 270 and 330 days. BTE appears to prevent micronuclei formation in the iAs treated mice. The representative photographs of micronuclei formation using Giemsa and Hoechst 33342 staining have been depicted in Figure 4.8B.

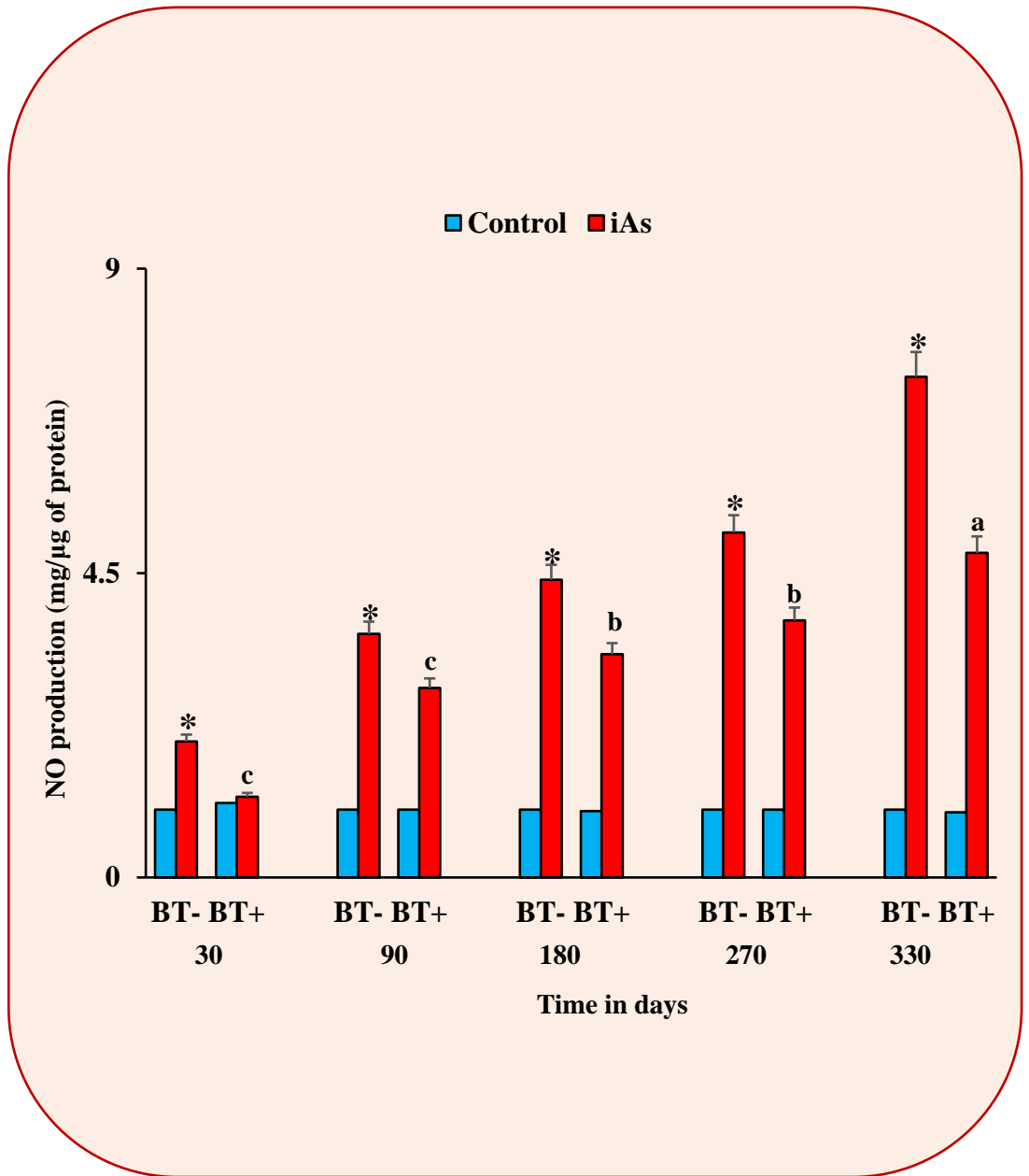


**Figure 4.7:** Determination of Reactive Nitrogen Species (RNS) generation using spectrophotometric analysis. The figure displays a bar graph representing RNS generation in control, iAs and iAs+BTE treated Swiss albino mice, measured at 30, 90, 180, 270 and 330 days of treatment. Greiss reagent was used to determine generation of RNS. Chronic iAs exposure results in excess RNS generation which appears to be quenched in the iAs+BTE treated mice. Values are mean of three independent experiments  $\pm$ S.D.. Increase in RNS generation, in iAs treated mice is significant at  $*p < 0.0001$ , with respect to the control. Decrease in RNS generated in the iAs+BTE group is significant at  $^c p < 0.05$ ,  $^b p < 0.001$  and highly significant at  $^a p < 0.0001$ , with respect to the iAs treated mice.

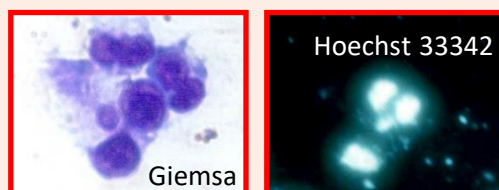
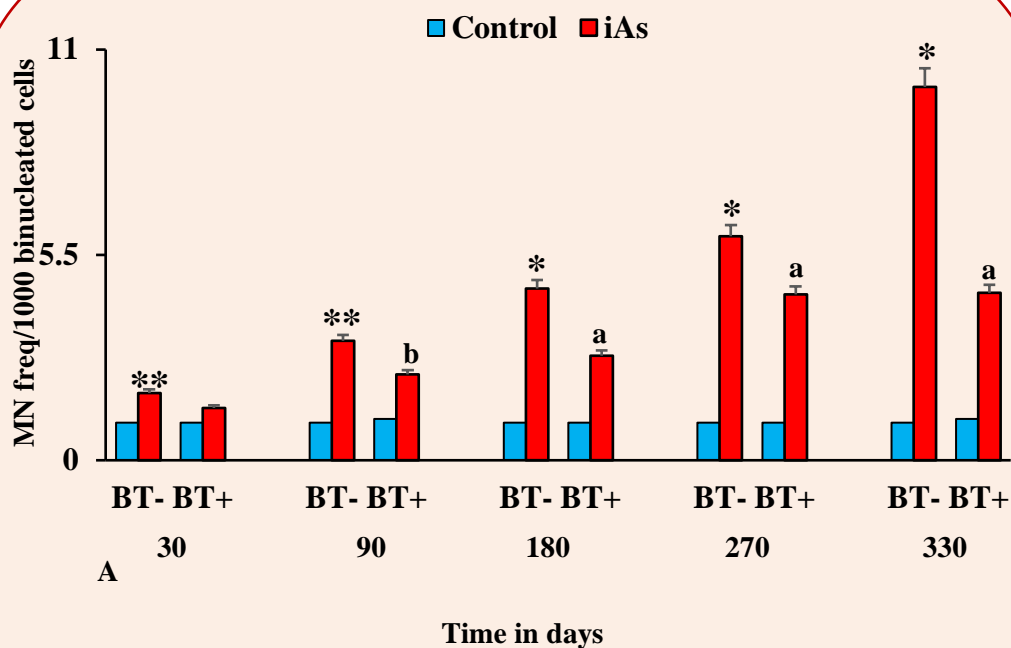


**Figure 4.8:** Determination of DNA damage using micronuclei assay.

**Figure 4.8A** displays a bar graph representing frequency of micronuclei formed per 1000 binucleated cells, in the leukocytes of Swiss albino mice, at 30, 90, 180, 270 and 330 days of treatment. Chronic exposure to iAs led to elevated micronuclei frequency, while treatment with iAs+BTE resulted in its prominent suppression. Values are mean of three independent experiments  $\pm$ S.D. Increase in micronuclei frequency in the iAs treated mice is significant at  $^{**}p < 0.001$  and highly significant at  $^{*}p < 0.0001$ , with respect to the control mice. Decrease in micronuclei frequency, in the iAs+BTE treated mice is significant at  $^{b}p < 0.001$  and highly significant at  $^{a}p < 0.0001$ , with respect to the iAs treated mice.

**Figure 4.8B** displays representative images of micronuclei formation, stained with 5% Giemsa and Hoechst 33342 (1  $\mu$ g/ml) respectively. Images of Giemsa stained slides were captured under a bright field microscope while those of Hoechst 33342 were captured under a fluorescent microscope. The images were captured at 1000X magnification.

#### **4.11. Estimation of DNA damage using single cell gel electrophoresis/ Comet assay**

DNA damage has also been estimated by single cell gel electrophoresis assay. Figure 4.9A displays a bar graph showing change in comet tail length with respect to increase in treatment time. During electrophoresis, the damaged DNA appears like a comet under the microscope and the length of the tail indicates extent of damaged DNA. From the bar graph it is evident that, in chronically iAs exposed mice, there is significant ( $p < 0.0001$ ) increase in comet tail length compared to that of the control group. Intervention by BTE led to reduction of comet tail length which was significant at 180 ( $p < 0.001$ ), 270 ( $p < 0.0001$ ) and 330 ( $p < 0.0001$ ) days of treatment.

Figure 4.9B depicts a bar graph representing Olive tail moment of the electrophoresed leukocytes isolated from mice, with respect to increase in treatment time. Olive tail moment is an effective index to measure DNA damage, which is calculated as the product of percentage of DNA in the tail and corresponding comet tail length. The Olive tail moment increases significantly ( $p < 0.0001$ ) in the iAs treated mice at 180, 270 and 330 days of treatment, whereas, in the BTE administered mice, there is significant ( $p < 0.0001$ ) reduction in the olive tail moment, at 180, 270 and 330 days of treatment, compared to the iAs treated mice. These results indicate that chronic exposure to iAs leads to increase in DNA damage while BTE inhibits it. Representative comet assay images of the control, iAs and iAs+BTE treatment groups have depicted in the Figure 4.9C.

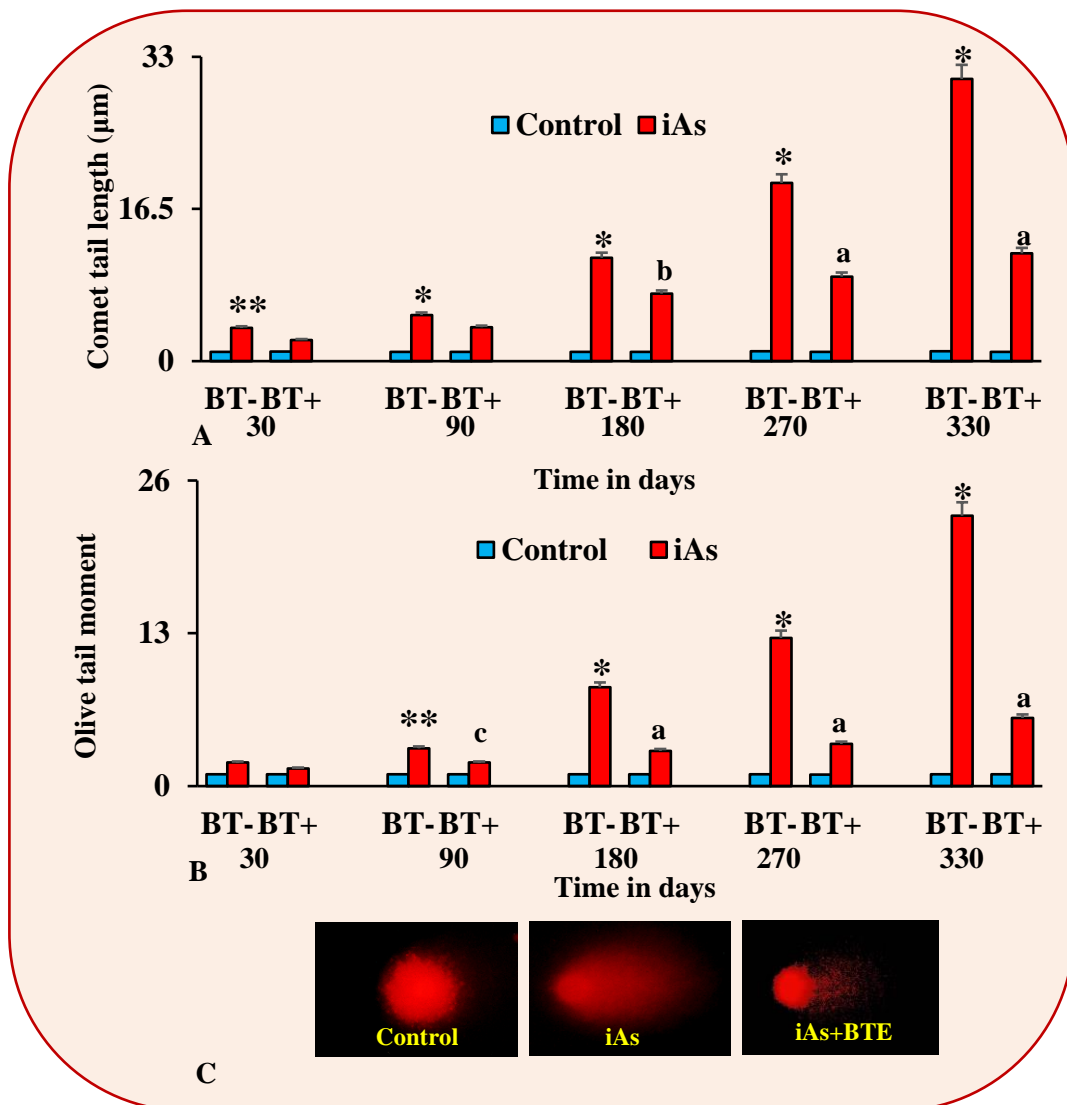


**Figure 4.9:** Determination of DNA damage using Single Cell Gel Electrophoresis (SCGE) or comet assay.

**Figure 4.9A** displays a bar graph representing mean comet tail length, in the leukocytes of Swiss albino mice, at 30, 90, 180, 270 and 330 days of treatment. Comet tail length is measured in  $\mu\text{m}$ . In iAs treated mice, it increases greatly with increase in treatment time while its is effectively decreased in the iAs+BTE treated mice.

**Figure 4.9B** displays a bar graph representing mean olive tail moment, in the leukocytes of Swiss albino mice, at 30, 90, 180, 270 and 330 days of treatment. Olive tail moment in iAs treated mice, is significantly elevated with increase in treatment time while its is suppressed in the iAs+BTE treated mice. Increase in comet tail length and olive tail moment in the iAs treatment group, is significant at  $**p < 0.001$  and highly significant at  $*p < 0.0001$ , compared to the control mice. Decrease of comet tail length and olive tail moment in the iAs+BTE treated mice is significant at  $^c p < 0.05$ ,  $^b p < 0.001$  and highly significant at  $^a p < 0.0001$ . Obtained values are mean of three independent experiments  $\pm$  S.D.

**Figure 4.9C** displays representative images of comet formation in the respective treatment groups. The cells were stained with Ethidium Bromide and observed under a fluorescent microscope. The images were captured at 400X.

#### **4.12. Estimation of Lipid damage by Lipid peroxidation Assay.**

Lipid peroxidation is measured by moles of malondialdehyde (MDA) generated which gives an estimation of lipid damage. Figure 4.10A depicts a bar graph showing moles of MDA generated in the different treatment groups of mice, at different treatment time points. The results indicate that MDA generation in the iAs treated mice increases significantly ( $p < 0.0001$ ) at 180, 270 and 330 days of treatment, while in the BTE administered mice, there is significant ( $p < 0.0001$ ) decrease of MDA generation at 180, 270 and 330 days of treatment. The results imply that lipid peroxidation increases upon iAs treatment, while intervention by BTE reduces this effect.

#### **4.13. Estimation of protein damage by protein carbonyl formation**

Protein damage is assessed by protein carbonyl formation and Figure 4.10B depicts a bar graph which represents fold change in protein carbonyl content of mice at different treatment time points. Results indicate increase of protein carbonyl formation upon chronic iAs exposure is significant ( $p < 0.001$ ) at 180, 270 and 330 days of treatment. Administration of BTE has been found to significantly reduce the protein carbonyl content at 180 ( $p < 0.001$ ), 270 ( $p < 0.0001$ ) and 330 ( $p < 0.0001$ ) days, indicating that BTE inhibits iAs induced protein damage by preventing protein carbonyl formation.

#### **4.14. Estimation of antioxidant capacity.**

Total antioxidative capacity and the activity of specific antioxidant enzymes like Catalase, SOD, GPx, GR, and GST have been represented as bar graphs in the Figures 4.11, 4.12A, 4.12B, 4.12C, 4.13A and 4.13B respectively. From the bar graphs it can be seen that, with chronic exposure to iAs, there is a reduction in total antioxidative capacity, as well as in the activity of respective

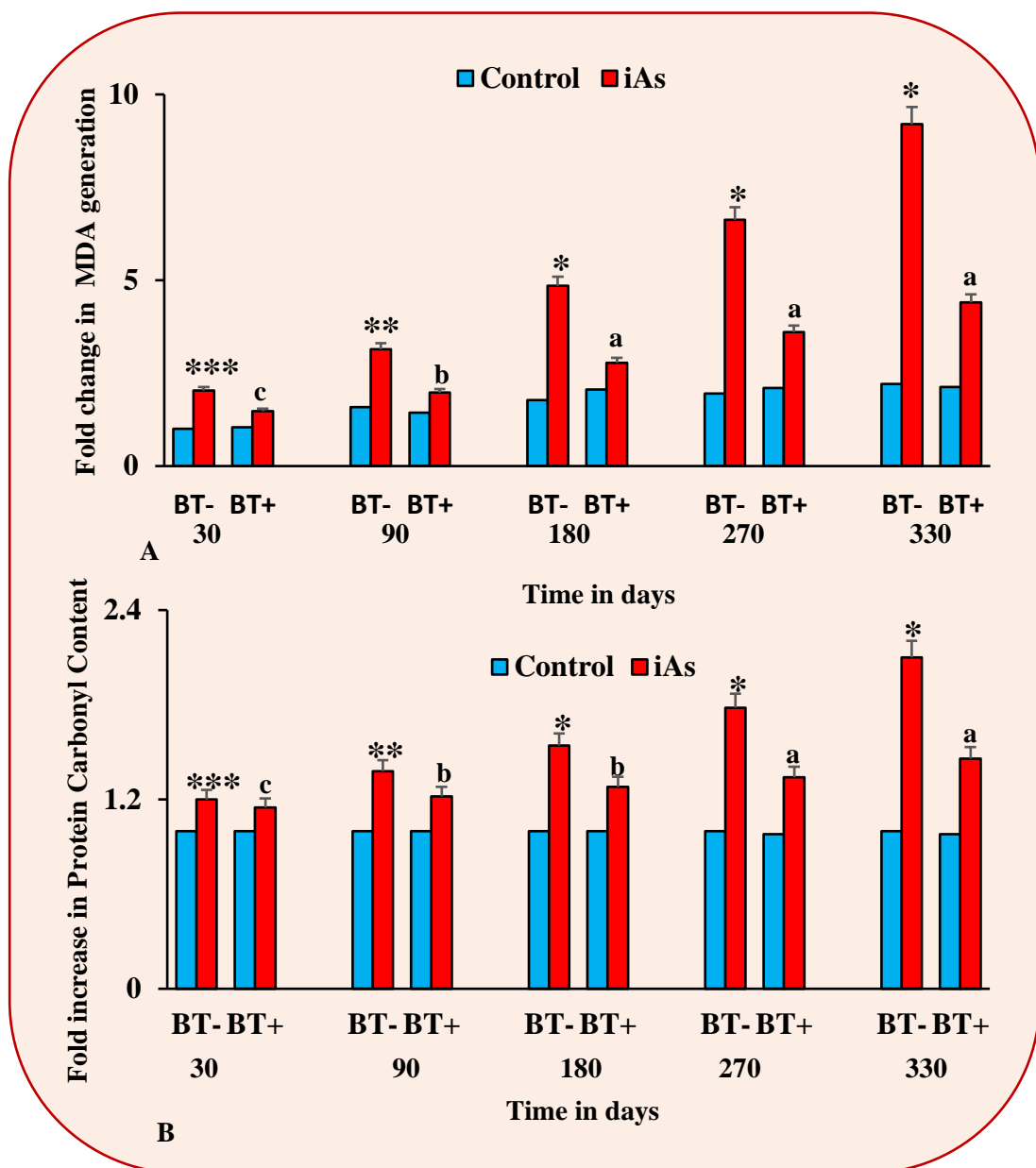


**Figure 4.10:** Determination of lipid and protein damage.

**Figure 4.10A** displays a bar graph showing fold change in MDA generation, in the tissues of Swiss albino mice, at 30, 90, 180, 270 and 330 days of treatment. MDA generation increased with chronic iAs exposure, while in the iAs+BTE treated mice, it is greatly decreased.

**Figure 4.10B** displays a bar graph showing fold change in protein carbonyl content at 30, 90, 180, 270 and 330 days of treatment. Protein carbonyl formation showed an increasing trend with chronic iAs treatment, while intervention with BTE effectively reduced it. Fold increase in MDA generation and protein carbonyl content, in the iAs treated mice is significant at \*\*\* $p < 0.05$ , \*\* $p < 0.001$  and \* $p < 0.0001$ , with respect to the control group. Fold decrease in MDA and protein carbonyl formation, in the iAs+BTE treated mice is significant at  $c p < 0.05$ ,  $b p < 0.001$  and  $a p < 0.0001$ , with respect to iAs group. Values are displayed as mean of three independent experiments  $\pm$ S.D.

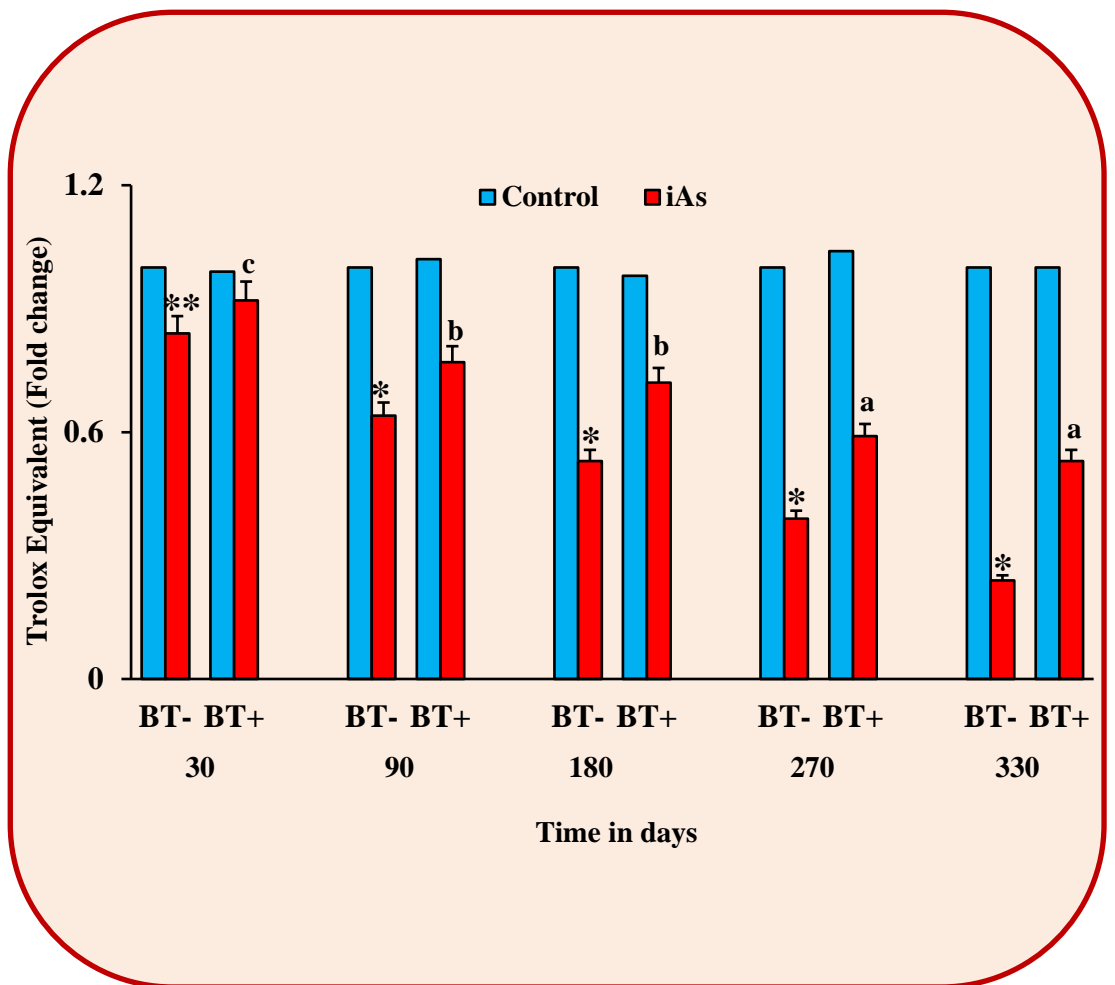


**Figure 4.11:** Determination of total antioxidant activity. Total antioxidant capacity was expressed as Trolox equivalent (Compared against the antioxidant capacity of Trolox, a tocopherol analogue). The bar graph displayed in the figure represents fold change of total antioxidative capacity, of the tissue lysates of Swiss albino mice, measured at 30, 90, 180, 270 and 330 days of treatment. Chronic iAs exposure results in prominent lowering of the total antioxidative capacity, while administration of BTE increased it effectively. Fold decrease of Trolox equivalent, in iAs treated mice, is significant at  $**p < 0.001$  and highly significant at  $*p < 0.0001$ , with respect to the control mice tissues. Fold increase of Trolox equivalent, in iAs+BTE treated mice, is significant at  $^c p < 0.05$ ,  $^b p < 0.001$  and highly significant at  $^a p < 0.0001$ , with respect to the iAs treatment group. Values are calculated as mean of three independent experiments  $\pm$ S.D.



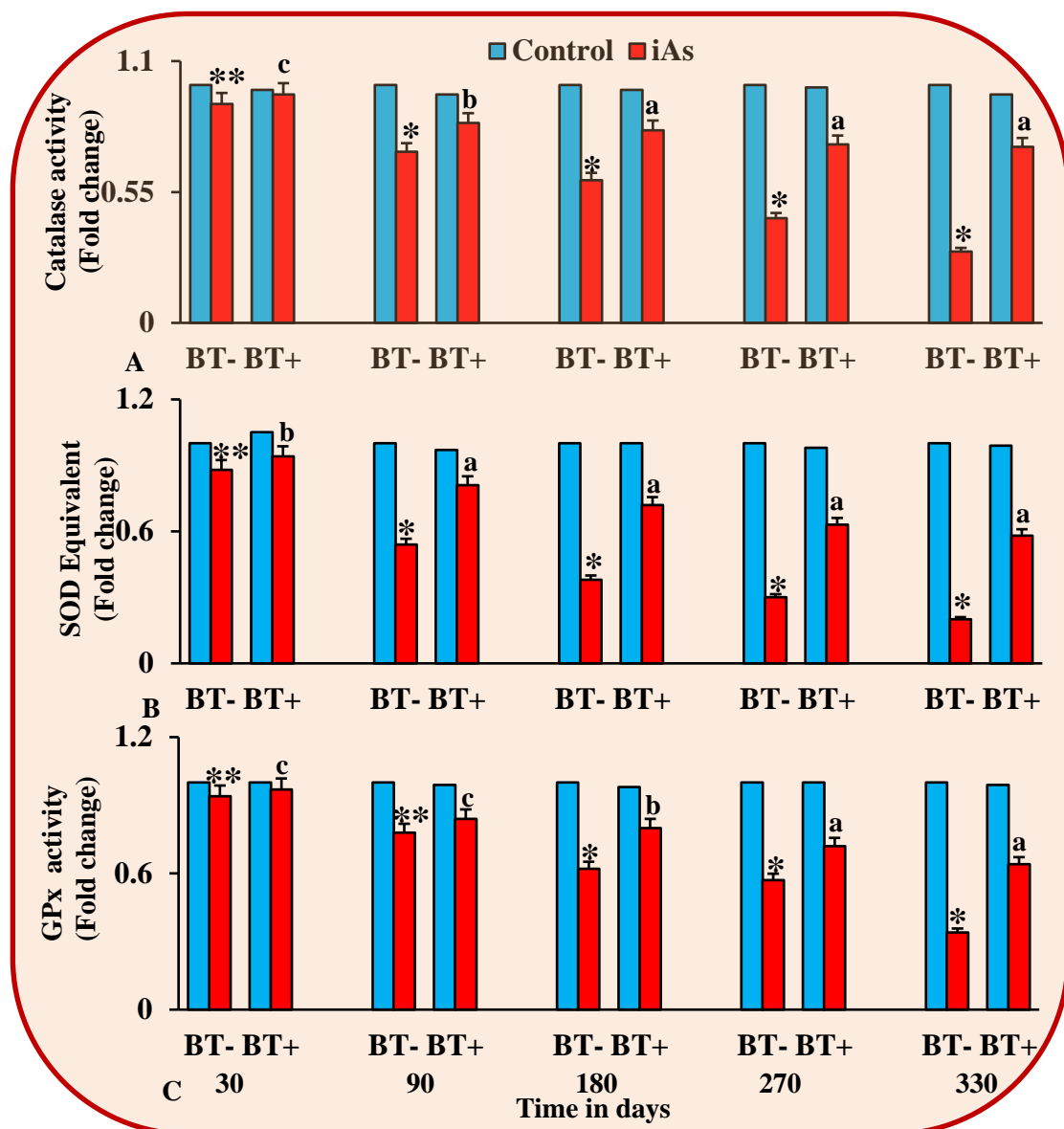


**Figure 4.12:** Determination of the activity of Catalase, SOD and GPx.

**Figure 4.12A** displays a bar graph showing fold change of Catalase activity, as measured in the tissue lysates of Swiss albino mice, at 30, 90, 180, 270 and 330 days of treatment. Catalase activity decreases remarkably in the iAs treated mice, while it is considerably high in the iAs+BTE treated mice.

**Figure 4.12B** displays fold change in SOD activity, in Swiss albino mice, at 30, 90, 180, 270 and 330 days of treatment. Chronic iAs treatment results in effective suppression of SOD activity, while BTE treatment elevates its activity.

**Figure 4.12C** displays fold change of GPx activity, of Swiss albino mice, measured at 30, 90, 180, 270 and 330 days of treatment. Prolonged exposure to iAs results in prominent reduction in GPx activity, while in the iAs+BTE treated mice it is increased. Reduction of Catalase, SOD and GPx activity in the iAs treated mice is significant at  $**p < 0.001$  and highly significant at  $*p < 0.0001$ , with respect to the control mice. Increase in Catalase, SOD and GPx activity in the iAs+BTE treated mice, is significant at  $^cp < 0.05$ ,  $^bp < 0.001$  and  $^ap < 0.0001$ , with respect to the iAs treatment group. Values are calculated as mean of three independent experiments  $\pm$  S.D.

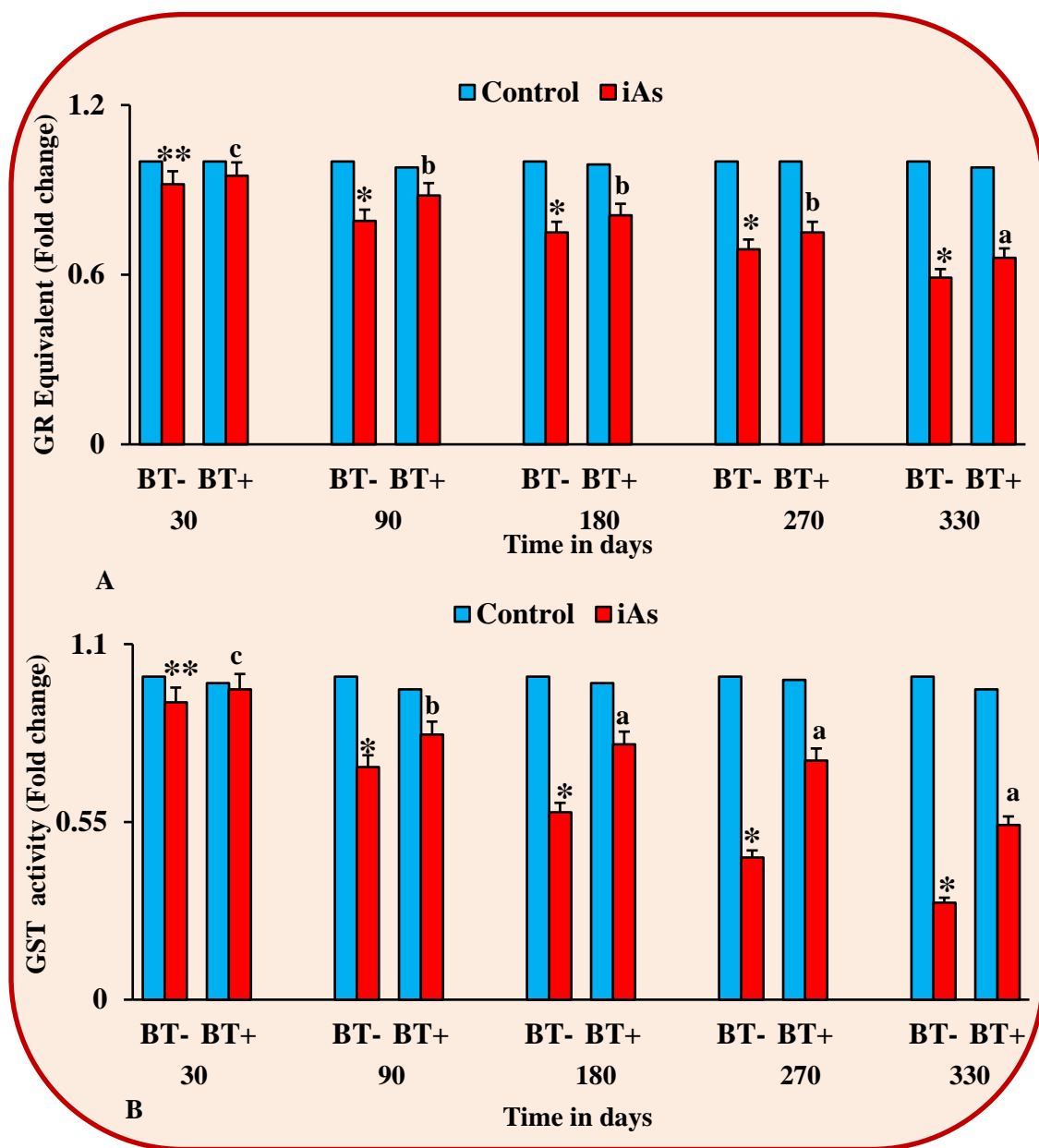


**Figure 4.13:** Determination of the activity of GR and GST.

**Figure 4.13A** displays a bar graph showing fold change in activity of GR, in the tissues of Swiss albino mice, at 30, 90, 180, 270 and 330 days of treatment. Prominent reduction in activity of GR has been observed in the tissues of mice chronically treated with iAs, whereas the activity GR has been increased in the iAs+BTE treated mice.

**Figure 4.13B** displays a bar graph showing fold change in GST activity, in the tissues of Swiss albino mice, at 30, 90, 180, 270 and 330 days of treatment. iAs treated mice showed lowering of GST activity which is elevated in the iAs+BTE group of mice.

Decrease in activity of GR and GST is significant at  $**p < 0.001$  and highly significant at  $*p < 0.0001$ , with respect to the control mice. Increase in activity of GR and GST is significant at  $^cp < 0.05$ ,  $^bp < 0.001$  and highly significant at  $^ap < 0.0001$ , with respect to the iAs treated mice. The values are calculated as mean of three independent experiments  $\pm$ S.D.

antioxidant enzymes (Catalase, SOD, GPx, GR, and GST). In the BTE administered mice, there is prominent upregulation of total antioxidant activity as well as of the respective antioxidant enzymes, indicating that BTE promotes antioxidative machinery which is downregulated by iAs.

#### **4.15. Estimation of DNA repair capacity and expression of repair enzymes.**

Bar-graph depicted in Figure 4.14 represents DNA repair capacity of the lymphocytes isolated from the different treatment groups of mice. The results indicate significant ( $p < 0.0001$ ) downregulation of DNA repair capacity upon chronic iAs exposure at 90, 180, 270 and 330 days of treatment. In the BTE administered mice, the repair capacity is significantly ( $p < 0.0001$ ) upregulated, in comparison to the iAs treated mice. This indicates upregulation of iAs impaired DNA repair capacity due to administration of BTE.

Figure 4.15 displays representative immunoblot images of different repair enzymes, isolated from mice tissues. Fold change in band intensities of these repair enzymes have been displayed in Table 4.4. These results indicate that with chronic exposure to iAs, there is prominent downregulation in the expression of repair enzymes belonging to BER pathway (PARP1, XRCC1, Ligase I), NER pathway (ERCC1, ERCC2 and XPA) and NHEJ pathway (DNA PKcs, Ligase IV and Ku70) with the exception of OGG1. OGG1, belonging to the BER pathway, shows significant ( $p < 0.0001$ ) upregulation upon chronic iAs exposure. Upon iAs+BTE administration, the expressions of repair enzymes are significantly ( $p < 0.0001$ ) upregulated, with the exception of OGG1. OGG1 shows significant ( $p < 0.0001$ ) downregulation upon BTE administration. The obtained results indicate that, BTE reverses the effect of iAs by enhancing the activity of DNA repair enzymes.

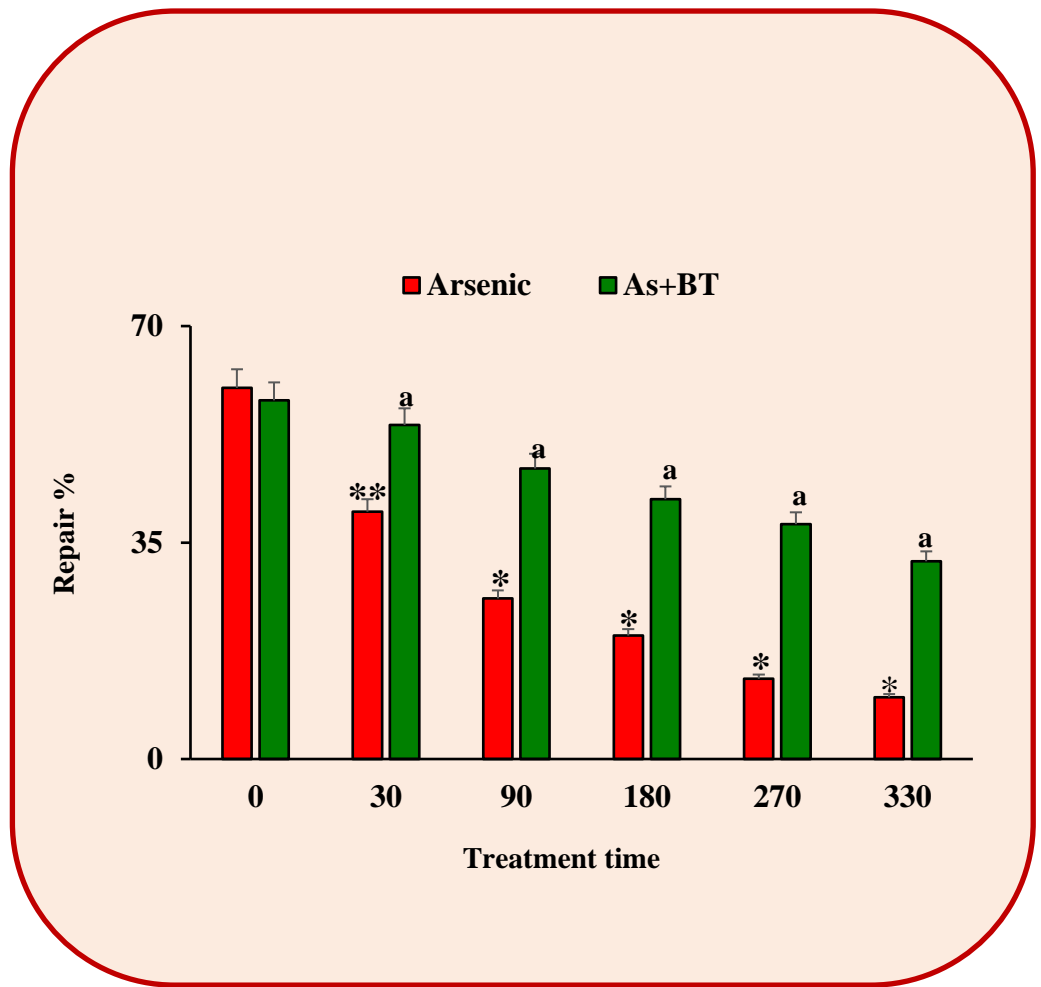


**Figure 4.14:** Determination of DNA repair potential. The bar graph displayed in the figure represents the percentage of DNA repair, in the lymphocytes of Swiss albino mice, at 30, 90, 180, 270 and 330 days of treatment. The repair % decreases remarkably in the iAs treated mice, while it is effectively increased in the iAs+BTE treated mice. Decrease in repair % in the iAs treated mice, is significant at \*\* $p < 0.001$  and highly significant at \* $p < 0.0001$  with respect to the control mice. Increase in repair % in the iAs+BTE treated mice is significant at <sup>a</sup> $p < 0.0001$ , compared to the iAs group. Values are mean of three independent experiments  $\pm$ S.D.

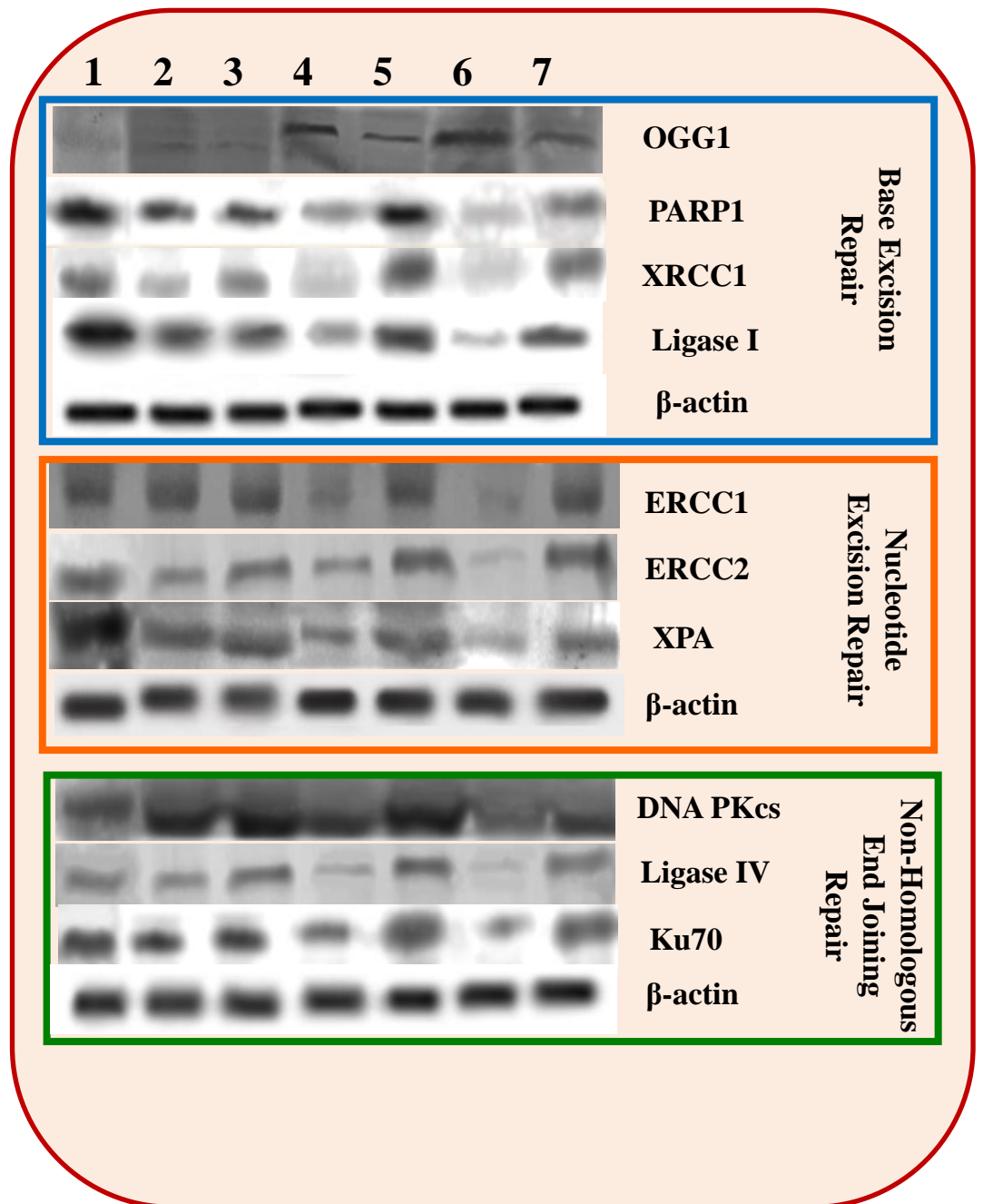


**Figure 4.15:** Determination of the expression of DNA repair enzymes. Representative immunoblot images of DNA repair enzymes belonging to the BER (namely OGG1, PARP1, XRCC1, DNA ligase I), NER (ERCC1, ERCC2, XPA) and NHEJ (DNA PKcs, Ku70 and Ligase IV) pathway have been displayed in the figure. Lane 1 represents immunoblot of control mice, Lanes 2, 4, 6 represent immunoblots of iAs treated mice iAs at 30, 180 and 330 days of treatment respectively. Lanes 3,5,7 represent immunoblots of iAs+BTE treated mice, at 30, 180 and 330 days respectively.  $\beta$ -actin was used as a loading control.

**Table 4.4.** Fold change in mean band intensities of different repair enzymes belonging to BER, NER and NHEJ repair pathway. Table below lists the fold change in mean band intensities, of the immunoblots, of different repair enzymes in Swiss albino mice at 30, 180 and 330 days of treatment. Prominent downregulation of repair enzymes was observed in mice chronically treated with iAs, whereas in the BTE administered mice, it was remarkably upregulated, except for OGG1. OGG1 showed upregulation upon iAs treatment and downregulation in the iAs+BTE treated mice. Values are mean of three independent experiments  $\pm$ S.D.

Repair Enzyme	Control	30 days		180 days		330 days	
		iAs	iAs+BTE	iAs	iAs+BTE	iAs	iAs+BTE
OGG1	1	1.26 $\pm$ .05	1.14 $\pm$ .02 <sup>c</sup>	1.48 $\pm$ .09 <sup>*</sup>	1.20 $\pm$ .04 <sup>a</sup>	1.68 $\pm$ .07 <sup>*</sup>	1.11 $\pm$ .03 <sup>a</sup>
PARP1	1	0.62 $\pm$ .01	0.62 $\pm$ .09 <sup>b</sup>	0.40 $\pm$ .05 <sup>*</sup>	0.69 $\pm$ .04 <sup>a</sup>	0.21 $\pm$ .01 <sup>*</sup>	0.63 $\pm$ .02 <sup>a</sup>
XRCC1	1	0.60 $\pm$ .03 <sup>**</sup>	0.76 $\pm$ .09 <sup>b</sup>	0.46 $\pm$ 0.5 <sup>*</sup>	0.94 $\pm$ .05 <sup>a</sup>	0.34 $\pm$ .01 <sup>*</sup>	0.88 $\pm$ .07 <sup>a</sup>
Ligase I	1	0.43 $\pm$ .04 <sup>**</sup>	0.54 $\pm$ .02 <sup>a</sup>	0.28 $\pm$ .08 <sup>*</sup>	0.68 $\pm$ .06 <sup>a</sup>	0.13 $\pm$ .06 <sup>*</sup>	0.52 $\pm$ .01 <sup>a</sup>
ERCC1	1	0.99 $\pm$ .01	0.99 $\pm$ .01	0.72 $\pm$ .09 <sup>**</sup>	0.96 $\pm$ .07 <sup>b</sup>	0.63 $\pm$ .05 <sup>*</sup>	0.90 $\pm$ .03 <sup>a</sup>
ERCC2	1	0.70 $\pm$ .02 <sup>**</sup>	0.84 $\pm$ .03 <sup>b</sup>	0.60 $\pm$ .06 <sup>*</sup>	0.90 $\pm$ .04 <sup>a</sup>	0.42 $\pm$ .01 <sup>*</sup>	0.82 $\pm$ .06 <sup>a</sup>
XPA	1	0.74 $\pm$ .09 <sup>***</sup>	0.79 $\pm$ .03 <sup>b</sup>	0.42 $\pm$ .02 <sup>*</sup>	0.64 $\pm$ .03 <sup>a</sup>	0.24 $\pm$ .07 <sup>*</sup>	0.51 $\pm$ .03 <sup>a</sup>
DNA Pkc	1	0.90 $\pm$ .02	0.96 $\pm$ .05 <sup>c</sup>	0.78 $\pm$ .03 <sup>**</sup>	0.90 $\pm$ .06 <sup>b</sup>	0.66 $\pm$ .05 <sup>*</sup>	0.85 $\pm$ .08 <sup>a</sup>
Ligase IV	1	0.54 $\pm$ .09 <sup>*</sup>	0.78 $\pm$ .04 <sup>a</sup>	0.40 $\pm$ .03 <sup>*</sup>	0.89 $\pm$ .09 <sup>a</sup>	0.28 $\pm$ .03 <sup>*</sup>	0.89 $\pm$ .08 <sup>a</sup>
Ku70	1	0.72 $\pm$ .04 <sup>**</sup>	0.83 $\pm$ .06 <sup>b</sup>	0.58 $\pm$ .03 <sup>*</sup>	0.94 $\pm$ .05 <sup>a</sup>	0.38 $\pm$ .01 <sup>*</sup>	0.78 $\pm$ .07 <sup>a</sup>

**Note:** Modulation of band intensities in the iAs treated mice, with respect to the control, is significant at <sup>\*</sup>p<0.0001, <sup>\*\*</sup>p<0.001 and <sup>\*\*\*</sup>p<0.05.

Modulation of band intensities in the iAs+BTE administered mice, with respect to the iAs treatment group, is significant at <sup>a</sup>p<0.0001, <sup>b</sup>p<0.001 and <sup>c</sup>p<0.05

#### **4.16. Estimation of the activity and expression of inflammatory cytokines.**

The bar graphs depicted in Figures 4.16A and 4.16B represent fold change in activity of pro-inflammatory cytokines like TNF- $\alpha$ , IL2, IL6, IL8, IL13, IL17a and IL22 as well as of anti-inflammatory cytokine like IL10. The results indicate that with chronic exposure of iAs the activity of pro-inflammatory cytokines increases prominently, while administration of BTE significantly reduces their activity. The activity of anti-inflammatory cytokine IL10 is diminished upon chronic iAs treatment, which is upregulated due to intervention by BTE.

Figure 4.17 displays the representative immunoblot bands of the respective pro- and anti-inflammatory cytokines, at different time points of iAs and iAs+BTE treated mice. Fold change in band intensities, of the immunoblots, of respective pro- and anti-inflammatory cytokines have been summarised in the Table 4.5. The results of the immunoblot assays reveal that, the expression of pro-inflammatory cytokines increase prominently with chronic iAs treatment, whereas BTE intervention decreases them. The expression of anti-inflammatory cytokine IL10, decreases upon chronic iAs exposure and increases effectively upon BTE treatment. The results of the cytokine activity assay and immunoblot assay appear to be in unison which suggests that chronic iAs exposure induces the activity and expression of pro-inflammatory cytokines and reduces that of the anti-inflammatory cytokine, which appears to be reversed by BTE.

#### **4.17. Estimation of the activity and expression of two sub-units of NF $\kappa$ B (p50 and p65)**

The bar graphs depicted in Figures 4.18A and 4.18B represent the fold change in activity of the two subunits of NF $\kappa$ B, namely p50 and p65, in

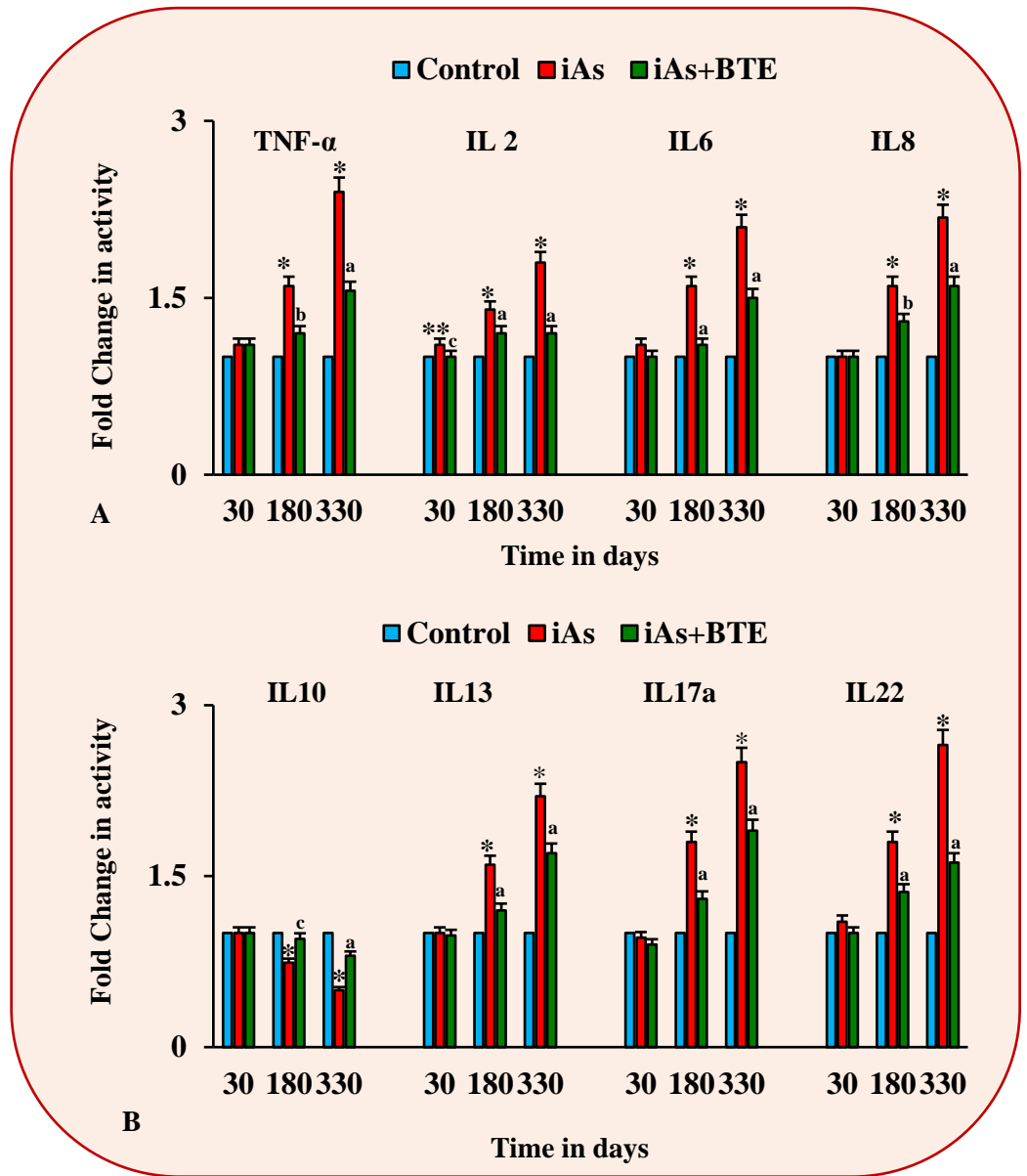


**Figure 4.16:** Determination of the activity of pro- and anti-inflammatory cytokines. **Figure 4.16A** displays a bar graph representing fold change, in mean band intensities of pro-inflammatory cytokine TNF- $\alpha$ , IL2, IL6 and IL8, in Swiss albino mice, at 30, 180 and 330 days of treatment. Mice chronically treated with iAs showed prominent elevation of the activity of these pro-inflammatory cytokines, whereas, in the iAs+BTE treated mice, it was effectively suppressed.

**Figure 4.16B** displays a bar graph representing fold change in mean band intensities of anti-inflammatory cytokine IL10 and of pro-inflammatory cytokines IL13, IL17a and IL22. Chronic iAs treatment resulted in suppression of IL10 and elevation of IL13, IL17a and IL22, which was reversed in the BTE treated mice. Modulation of activity of cytokines, in the iAs treated mice is significant at  $**p < 0.001$  and highly significant at  $*p < 0.0001$ , with respect to the control mice. Modulation of activity of cytokines, in the iAs+BTE treated mice is significant at  $^cp < 0.05$ ,  $^bp < 0.001$  and highly significant at  $^ap < 0.0001$ , with respect to the iAs group. Values are mean of three independent experiments  $\pm$ S.D.



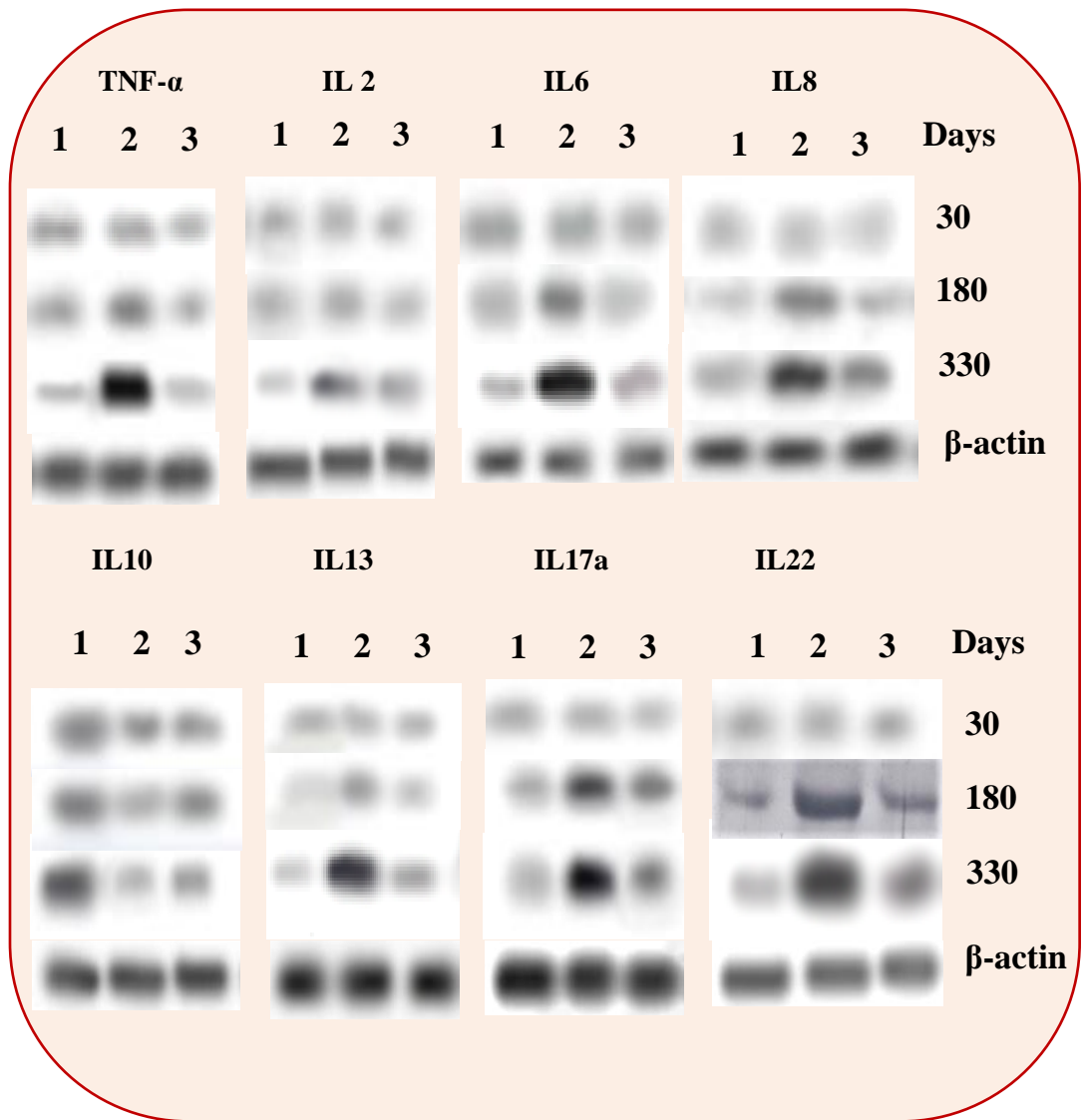


**Figure 4.17:** Determination of the expression of pro-inflammatory (TNF- $\alpha$ , IL2, IL6, IL8, IL13, IL17a and IL22) and anti-inflammatory (IL10) cytokine by immunoblotting assay. Representative immunoblot images of Pro- and anti-inflammatory cytokines, assessed at 30,180 and 330 days of treatment, in Swiss albino mice, has been displayed in the figure. Lanes 1, 2 and 3 represent control, iAs and iAs+BTE treated mice respectively. Expression of pro-inflammatory cytokines increased while that of anti-inflammatory cytokine decreased upon iAs treatment, which appeared to be reversed in the iAs+BTE treated mice.  $\beta$ -actin was used as a loading control.

**Table 4.5:** Fold change in mean band intensities of different pro and anti-inflammatory cytokines. Fold change in mean band intensities of pro-inflammatory cytokines like TNF- $\alpha$ , IL2, IL6, IL8, IL13, IL17a, IL22 and anti-inflammatory cytokine IL10, at 30, 180 and 330 days of treatment, have been listed in the table below. Chronic treatment with iAs resulted in increase in band intensity of pro-inflammatory cytokines and decrease in band intensity of IL10. In the iAs+BTE treated mice it appears to be reversed. Band intensities are mean of three independent experiments  $\pm$ S.D.

Cytokines	Days	Control	Arsenic	As+Tea
TNF- $\alpha$	30	1	1.1	1
	180	1	1.45 $\pm$ .03**	1.2 $\pm$ .01
	330	1	2.5 $\pm$ .094*	1.4 $\pm$ .08 <sup>a</sup>
IL2	30	1	1	1
	180	1	1.5 $\pm$ .042**	1.28 $\pm$ .05 <sup>c</sup>
	330	1	1.7 $\pm$ .045**	1.2 $\pm$ .024 <sup>a</sup>
IL6	30	1	1.2 $\pm$ .012	1.1 $\pm$ .01
	180	1	1.6 $\pm$ .022**	1.2 $\pm$ .014 <sup>b</sup>
	330	1	2.3 $\pm$ .072*	1.8 $\pm$ .046 <sup>a</sup>
IL8	30	1	1	1
	180	1	1.5 $\pm$ .013**	1.2 $\pm$ .011 <sup>c</sup>
	330	1	2.2 $\pm$ .014*	1.6 $\pm$ .018 <sup>b</sup>
IL10	30	1	1	1
	180	1	0.68 $\pm$ .021**	0.9 $\pm$ .019 <sup>b</sup>
	330	1	0.46 $\pm$ .01*	0.78 $\pm$ .014 <sup>a</sup>
IL13	30	1	1.1	1.1
	180	1	1.8 $\pm$ .023*	1.3 $\pm$ .012 <sup>b</sup>
	330	1	2.3 $\pm$ .034*	1.9 $\pm$ .019 <sup>b</sup>
IL17a	30	1	1	0.96
	180	1	1.9 $\pm$ .06*	1.4 $\pm$ .011 <sup>b</sup>
	330	1	2.4 $\pm$ .098*	2 $\pm$ .05 <sup>b</sup>
IL22	30	1	0.98	1
	180	1	1.8 $\pm$ .02*	1.28 $\pm$ .03 <sup>c</sup>
	330	1	2.5 $\pm$ .041*	1.5 $\pm$ .017 <sup>a</sup>

**Note:** Modulation of band intensities in the iAs treated mice, with respect to the control, is significant at \* $p$ <0.0001 and \*\* $p$ <0.001.

Modulation of band intensities in the iAs+BTE administered mice, with respect to the iAs treatment group, is significant at <sup>a</sup> $p$ <0.0001, <sup>b</sup> $p$ <0.001 and <sup>c</sup> $p$ <0.05.

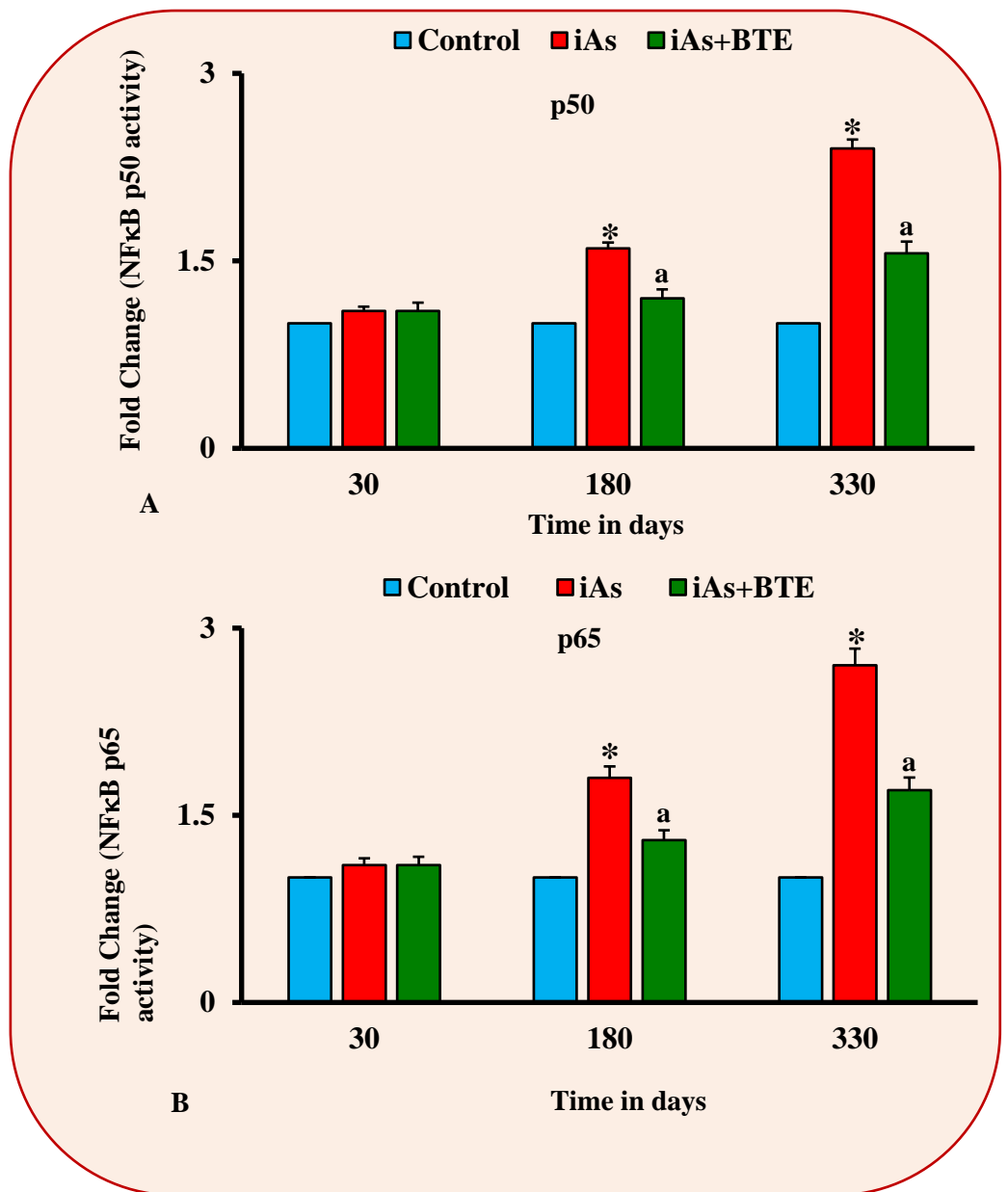


**Figure 4.18:** Fold change in activity of p50 and p65.

**Figure 4.18A** displays a bar graph which represents fold change in activity of p50, a subunit of NFκB, in the tissues of Swiss albino mice, at 30, 180 and 330 days of treatment.

**Figure 4.18B** displays a bar graph representing fold change in activity of p65, another subunit of NFκB, at 30, 180 and 330 days of treatment.

The activity of p50 and p65 increased upon chronic treatment with iAs, whereas, in the BTE administered mice, it was reduced. Fold increase in activity, in the iAs treated mice is significant at  $*p < 0.0001$ , with respect to the control mice. Fold change (decrease) in activity in the iAs+BTE treated mice is significant at  $^ap < 0.0001$ , with respect to the iAs group. The values are mean of three independent experiments  $\pm$ S.D.

Swiss albino mice, at different timepoints of treatment. The results clearly indicate that upon chronic iAs exposure, the activity of p50 and p65 increases significantly ( $p < 0.0001$ ) at 180 and 330 days of treatment, while administration of BTE reduces it significantly ( $p < 0.0001$ ). Figure 4.19 displays representative immunoblot images of p50 and p65 at different time points of treatment. Fold change in band intensities of p50 and p65 at 30, 180 and 330 days of treatment, have been displayed as a bar graph in the Figures 4.20A and 4.20B respectively. The results indicate that, the expression of p50 and p65 increases significantly ( $p < 0.0001$ ) at 180 and 330 days of iAs exposure while it is significantly ( $p < 0.0001$ ) downregulated upon BTE intervention. The results indicate upregulation of the expression and activity of p50 and p65 with chronic iAs treatment and their downregulation by BTE administration.

#### **4.18. Modulation of TGF- $\beta$ pathway in Swiss albino mice.**

Expression of TGF- $\beta$  and its downstream signalling proteins have been assessed by the immunoblotting assay at 330 days of treatment. Representative immunoblots images of TGF- $\beta$  and its canonical (Smad) and non-canonical (PI3K-AKT, MAPK) signalling intermediates are depicted in Figures 4.21A, 4.22A, 4.23A and 4.24A. Fold changes in band intensities of these proteins have been represented as bar graph in Figures 4.21B, 4.22B, 4.23B and 4.24B. Results show significant ( $p < 0.0001$ ) upregulation of TGF- $\beta$  upon iAs exposure. The change in expression of TGF- $\beta$  in the BTE administered mice was not significant ( $p = 0.065$ ). The bar graph depicted in Figure 4.22B shows downregulation of pSmad2, pSmad3 and pSmad4 upon chronic iAs exposure, which was upregulated in the iAs+BTE treated mice. Immunoblot results displayed as a bar graph in Figure 4.23B reveals downregulation of

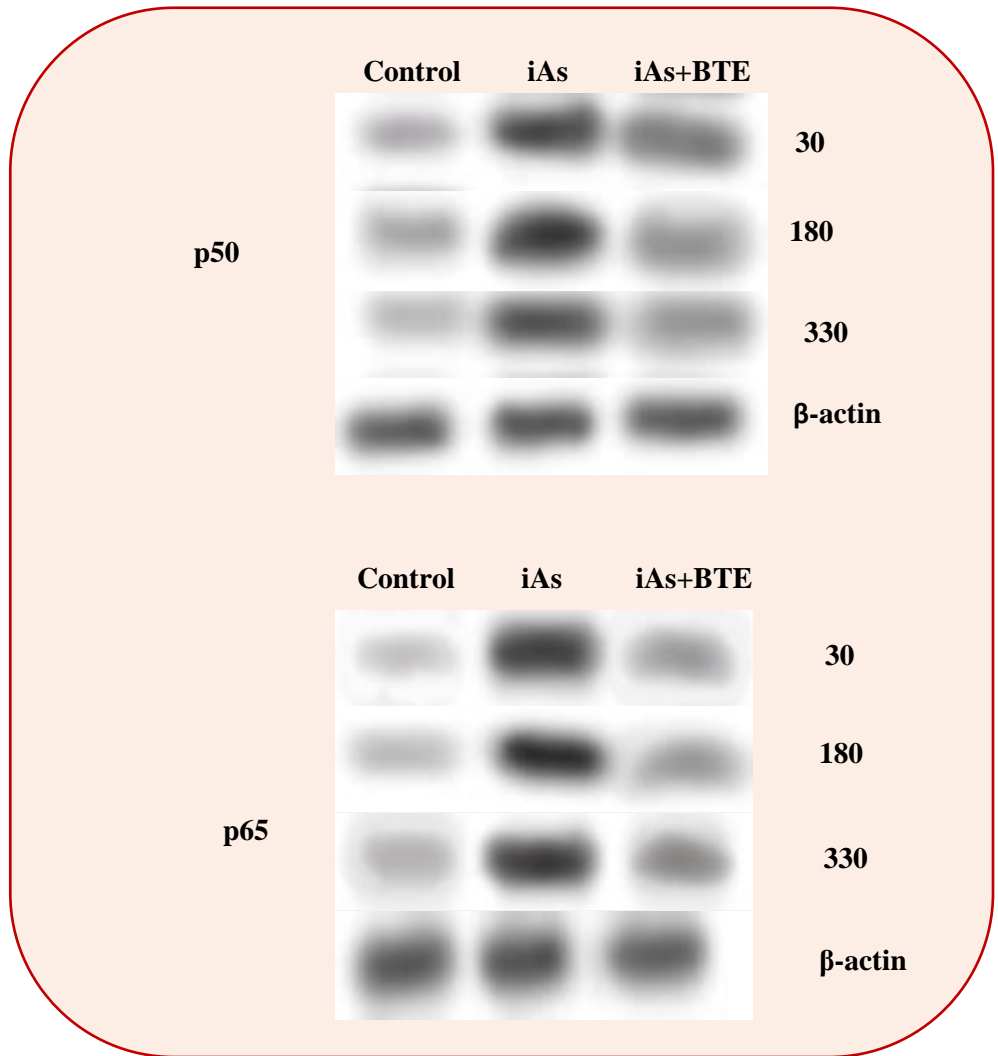


**Figure 4.19:** Determination of the expression of p50 and p65 subunits of NFκB. Representative immunoblot images of p50 and p65 subunits of NFκB, assessed at 30,180 and 330 days of treatment, in Swiss albino mice, has been displayed in the figure. Expression of p50 and p65 increased upon chronic iAs treatment, which decreases effectively in the iAs+BTE treated mice. β-actin was used as a loading control.

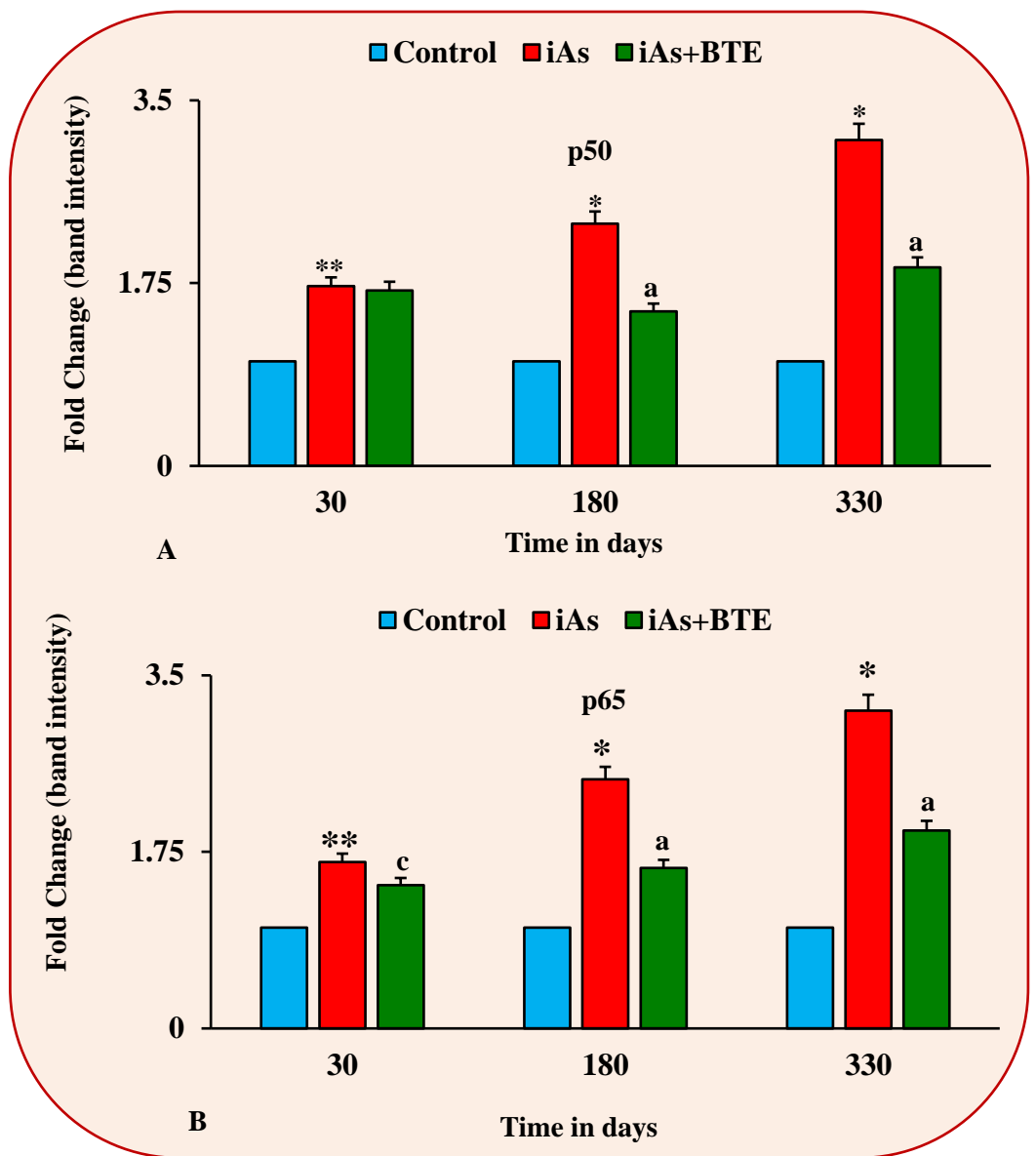


**Figure 4.20:** Fold change in mean band intensities of p50 and p65.

**Figure 4.20A** displays a bar graph which represents fold change in mean band intensity of p50, in the tissues of Swiss albino mice, at 30, 180 and 330 days of treatment.

**Figure 4.20B** displays a bar graph representing fold change in mean band intensity of p65 at 30, 180 and 330 days of treatment.

Band intensities of p50 and p65 increases upon chronic treatment with iAs, whereas, in the BTE administered mice, it was reduced. Fold increase in band intensity, in the iAs treated mice, is significant at \*\* $p < 0.001$  and \* $p < 0.0001$ , with respect to the control mice. Fold decrease in band intensity, in the iAs+BTE treated mice is significant at <sup>c</sup> $p < 0.05$  and <sup>a</sup> $p < 0.0001$ , with respect to the iAs group. The values are mean of three independent experiments  $\pm$ S.D.

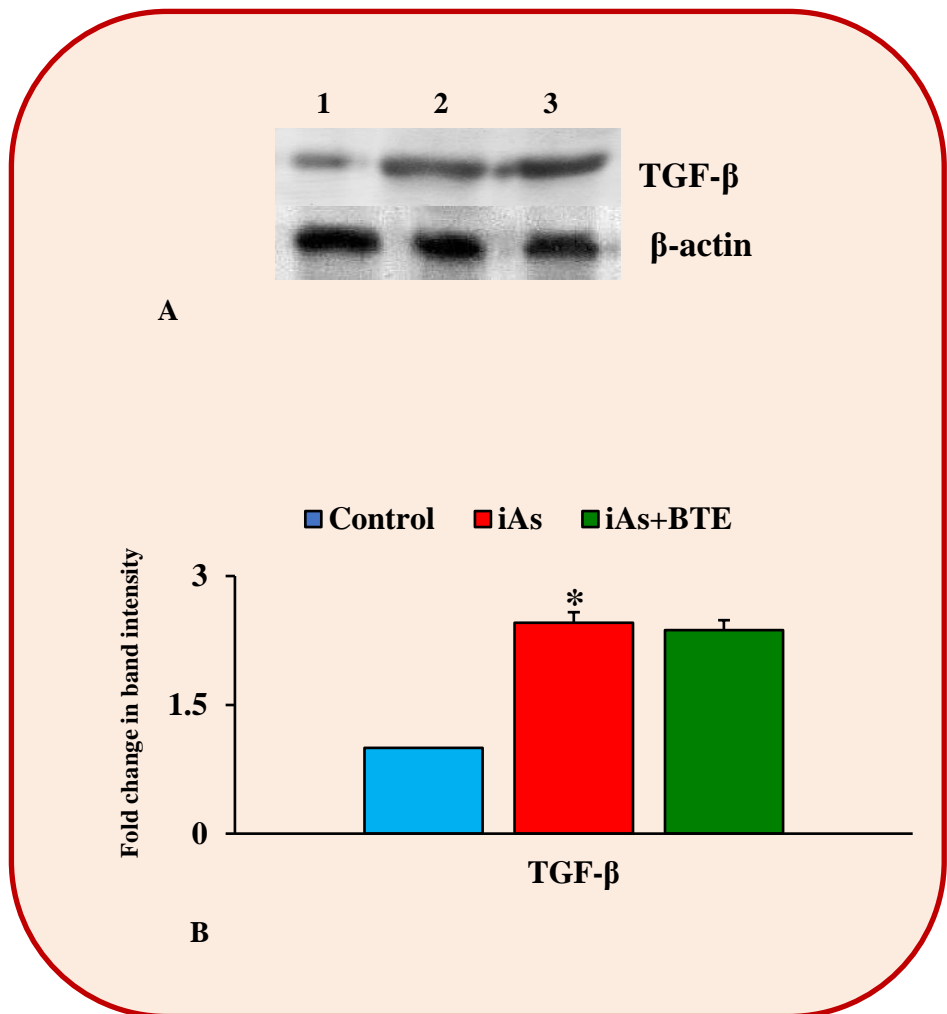


**Figure 4.21:** Estimation of the expression of TGF- $\beta$ .

**Figure 4.21A** displays the representative immunoblot images of TGF- $\beta$  extracted from the tissues of Swiss albino mice, at 330 days of treatment. Lanes 1, 2 and 3 represent control, iAs and iAs+BTE treated mice.  $\beta$ -actin was used as a loading control.

**Figure 4.21B** displays a bar graph representing the fold change in mean band intensity, of TGF- $\beta$ , in control, iAs and iAs+BTE treated mice. Expression of TGF- $\beta$  is very high in the iAs treated mice, which also remains high in the iAs+BTE treated mice. Fold increase in band intensity, in the iAs treated mice, is significant at  $*p < 0.0001$ , with respect to the control mice. Values are mean of three independent experiments  $\pm$ S.D.

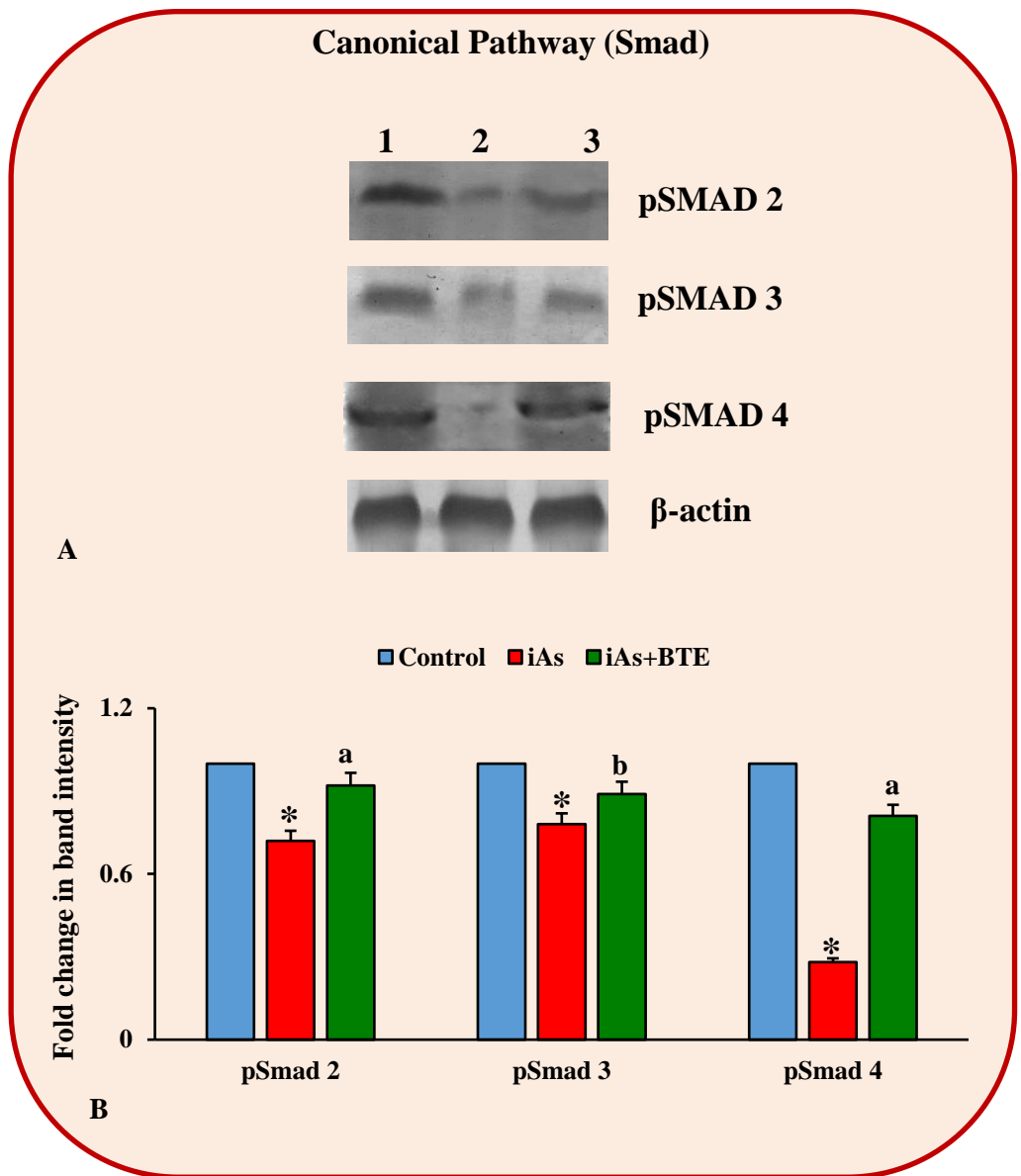


**Figure 4.22:** Estimating the expression of signalling intermediates of the Smad pathway (canonical pathway of TGF- $\beta$ ).

**Figure 4.22A** displays the representative immunoblot images of phospho-Smad2, phospho-Smad3 and phospho-Smad4, at 330 days of treatment. Lanes 1, 2 and 3 represent control, iAs and iAs+BTE treated mice respectively.  $\beta$ -actin was used as a loading control.

**Figure 4.22B** displays a bar graph showing fold change in mean band intensities of phospho-Smad2, phospho-Smad3 and phospho-Smad4. iAs treatment results in downregulation of phospho-Smad2, phospho-Smad3 and phospho-Smad4, while BTE administration reverses it. Fold decrease in band intensity, in the iAs treated mice, is significant at  $^*p < 0.0001$ , with respect to the control mice. Fold increase in band intensity, in the iAs+BTE treated mice, is significant at  $^ap < 0.0001$ , in comparison to the iAs group. Values are mean of three independent experiments  $\pm$ S.D.



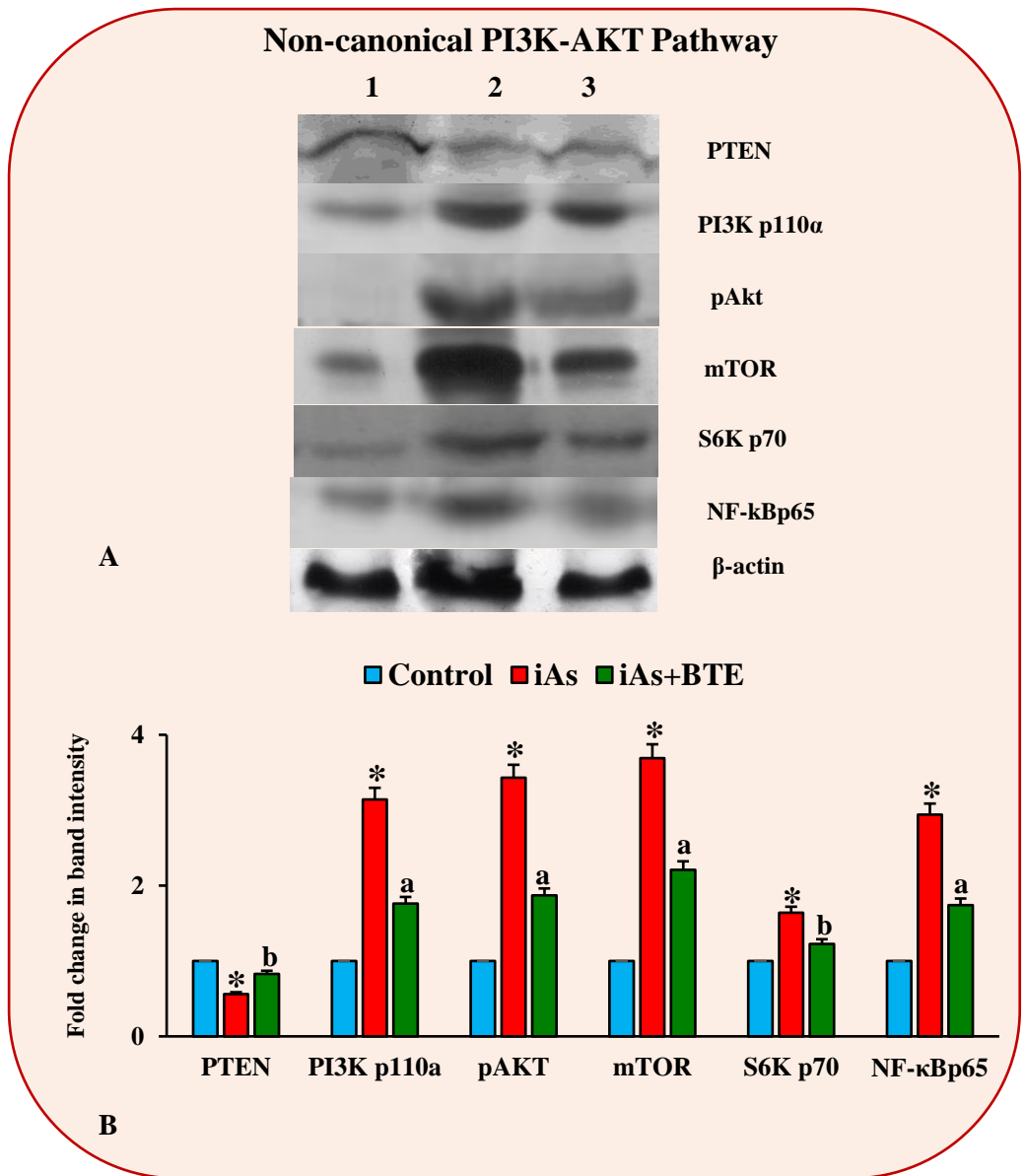


**Figure 4.23:** Estimating the expression of signalling intermediates of the PI3K-AKT pathway (non-canonical pathway of TGF-β).

**Figure 4.23A** displays the representative immunoblot images of PTEN, PI3K, phospho-AKT, mTOR, S6K, and p65, at 330 days of treatment. Lanes 1, 2 and 3 represent control, iAs and iAs+BTE treated mice respectively. β-actin was used as a loading control.

**Figure 4.23B** displays a bar graph showing fold change in mean band intensities of PTEN, PI3K, phospho-AKT, mTOR, S6K, and p65. iAs treatment results in downregulation of PTEN with simultaneous upregulation of PI3K, phospho-AKT, mTOR, S6K and p65. In the iAs+BTE treated mice, this expression pattern is reversed. Modulation of band intensity, in the iAs treated mice, is significant at <sup>\*</sup>p<0.0001, with respect to the control mice. Modulation of band intensity, in the iAs+BTE treated mice, is significant at <sup>b</sup>p<0.001 and <sup>a</sup>p<0.0001, in comparison to the iAs group. Values are mean of three independent experiments ±S.D.

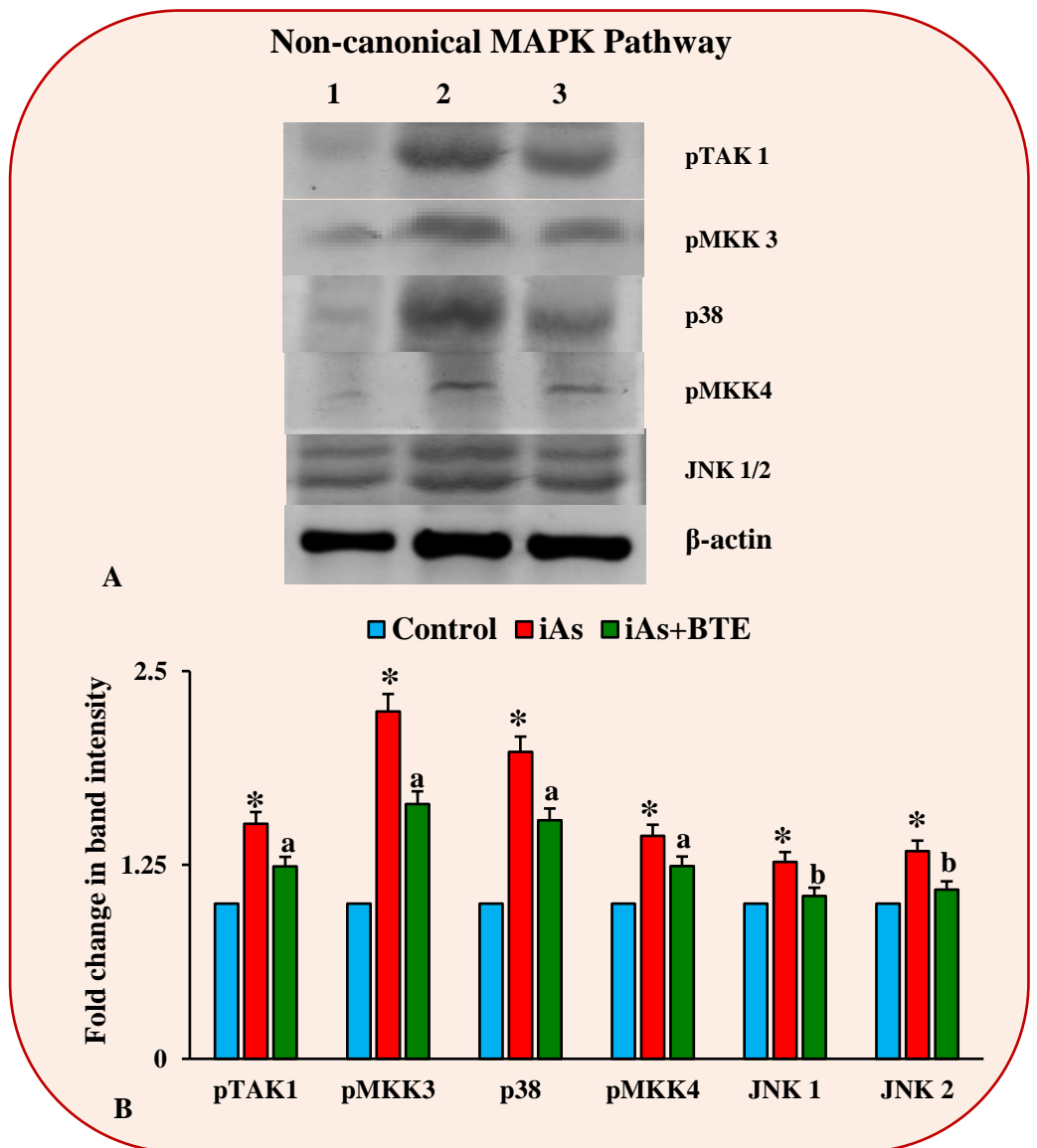


**Figure 4.24:** Estimating the expression of signalling intermediates of the MAPK pathway (non-canonical pathway of TGF-β).

**Figure 4.24A** displays the representative immunoblot images of phospho-TAK1, phospho-MKK3, phospho-p38, phospho-MKK4, JNK1 and JNK2. Lanes 1, 2 and 3 represent control, iAs and iAs+BTE treated mice respectively. β-actin was used as a loading control.

**Figure 4.24B** displays a bar graph showing fold change in mean band intensities of phospho-TAK1, phospho-MKK3, phospho-p38, phospho-MKK4, JNK1 and JNK2. iAs treatment results in upregulation of phospho-TAK1, phospho-MKK3, phospho-p38, phospho-MKK4, JNK1 and JNK2, which appears to be reversed in the BTE administered mice. Fold increase of band intensity, in the iAs treated mice, is significant at <sup>\*</sup>p<0.0001, with respect to the control mice. Fold decrease of band intensity, in the iAs+BTE treated mice, is significant at <sup>b</sup>p<0.001 and <sup>a</sup>p<0.0001, in comparison to the iAs group. Values are mean of three independent experiments ±S.D.

PTEN with subsequent significant upregulation of PI3Kp110 $\alpha$ , pAKT, mTOR, S6Kp70 and NF $\kappa$ Bp65 subunit, in the iAs treatment group. In the iAs+BTE treated mice, this expression pattern is reversed. This indicates upregulation of the PI3K-AKT pathway upon chronic iAs treatment, while administration of BTE results in modulation of this signalling pathway of TGF- $\beta$ .

Immunoblot results of the MAPK pathway, depicted as a bar graph in Figure 4.24B shows elevated expression of pTAK1, pMKK3, p38, pMKK4 and JNK in the iAs treated mice, indicating upregulation of the MAPK pathway. In the iAs+BTE administered mice, the elevated expressions of these signalling proteins were lowered suggesting downregulation of the MAPK pathway.

Chronic iAs exposure led to upregulation of the TGF- $\beta$ , downregulation of the Smad pathway, with simultaneous upregulation of PI3K-AKT and MAPK pathways, suggesting that upon iAs treatment, TGF- $\beta$  transmits its downstream signalling mainly via the non-canonical (PI3K-AKT and MAPK) pathways. In the iAs+BTE treated mice, expression of TGF- $\beta$  remains high along with signalling intermediates of the Smad pathway; whereas, expression of the signalling intermediates of the PI3K-AKT and MAPK pathways are low.

#### **4.19. Investigation of EMT induction by Immunoblotting and semi-quantitative RT-PCR**

Immunoblotting and semi-quantitative RT-PCR have been performed to investigate the induction of EMT in Swiss albino mice, at 330 days of treatment. Figures 4.25A, 4.26A, 4.27A and 4.28A display the representative immunoblot images of the respective EMT markers, while Figures 4.25C, 4.26C, 4.27C and 4.28C display the representative semi-quantitative RT-PCR

## Epithelial markers of EMT

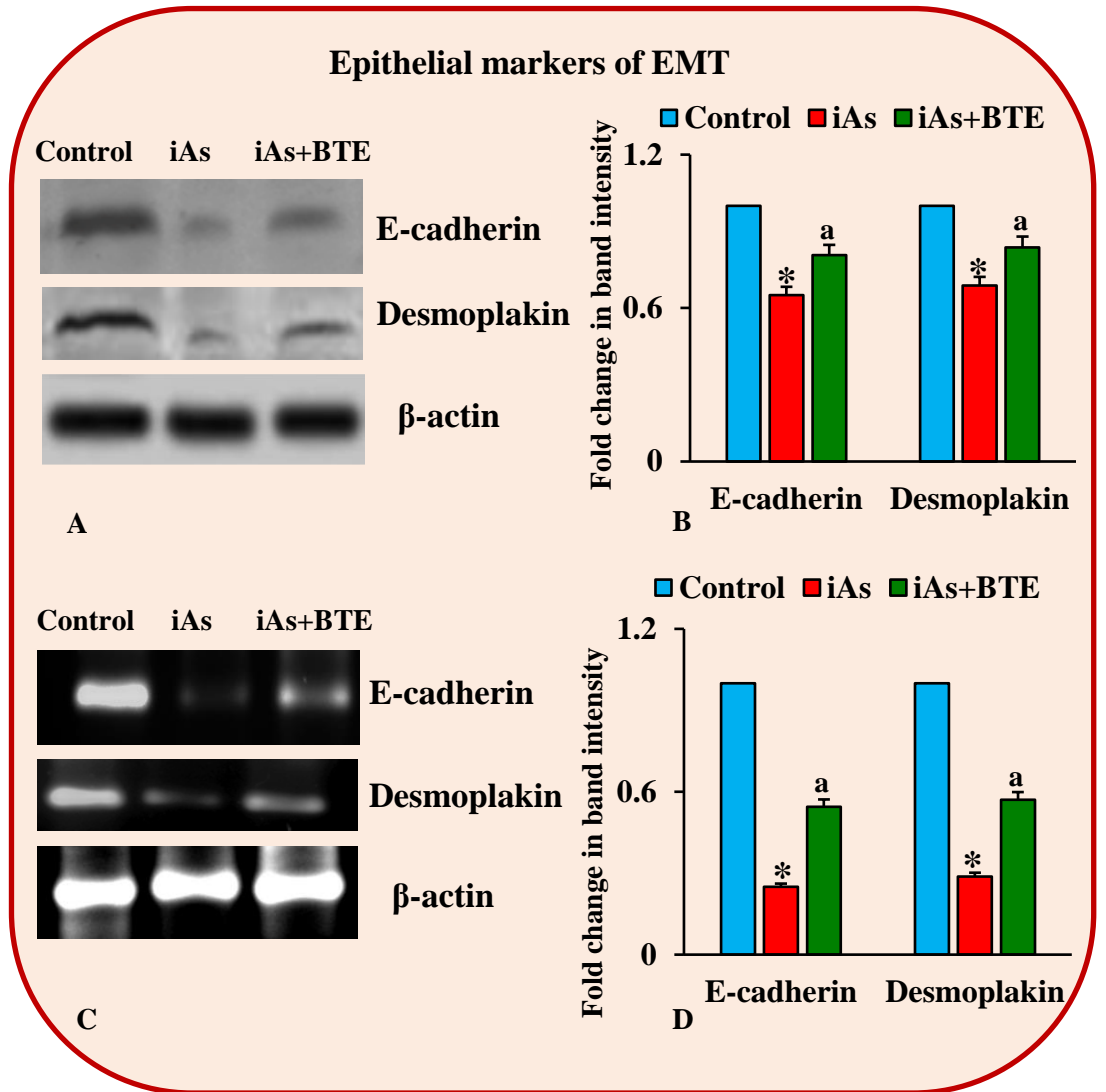


**Figure 4.25:** Estimating the expression of epithelial markers E-cadherin and Desmoplakin.

**Figure 4.25A** displays the representative immunoblot images of epithelial markers, E-cadherin and Desmoplakin, in Swiss albino mice at 330 days of treatment.

**Figure 4.25B** displays a bar graph representing the fold change in band intensities of the respective epithelial markers. iAs treatment leads to downregulation of epithelial markers, while BTE administration upregulates them.

**Figure 4.25C** displays the representative RT-PCR bands of the respective epithelial markers.

**Figure 4.25D** displays a bar graph showing fold change in RT-PCR band intensities, of E-cadherin and Desmoplakin. Chronic iAs treatment results in lowering of the RT-PCR band intensities, of epithelial markers, whereas, administration of BTE increases them. Reduction of band intensities, in the iAs treated mice, is significant at  $*p < 0.0001$ , with respect to the control mice. Promotion of band intensity, in the iAs+BTE treated mice, is significant at  $^ap < 0.0001$ .  $\beta$ -actin was used as a loading control. Values are mean of three independent experiments  $\pm$ S.D.

## Mesenchymal markers of EMT

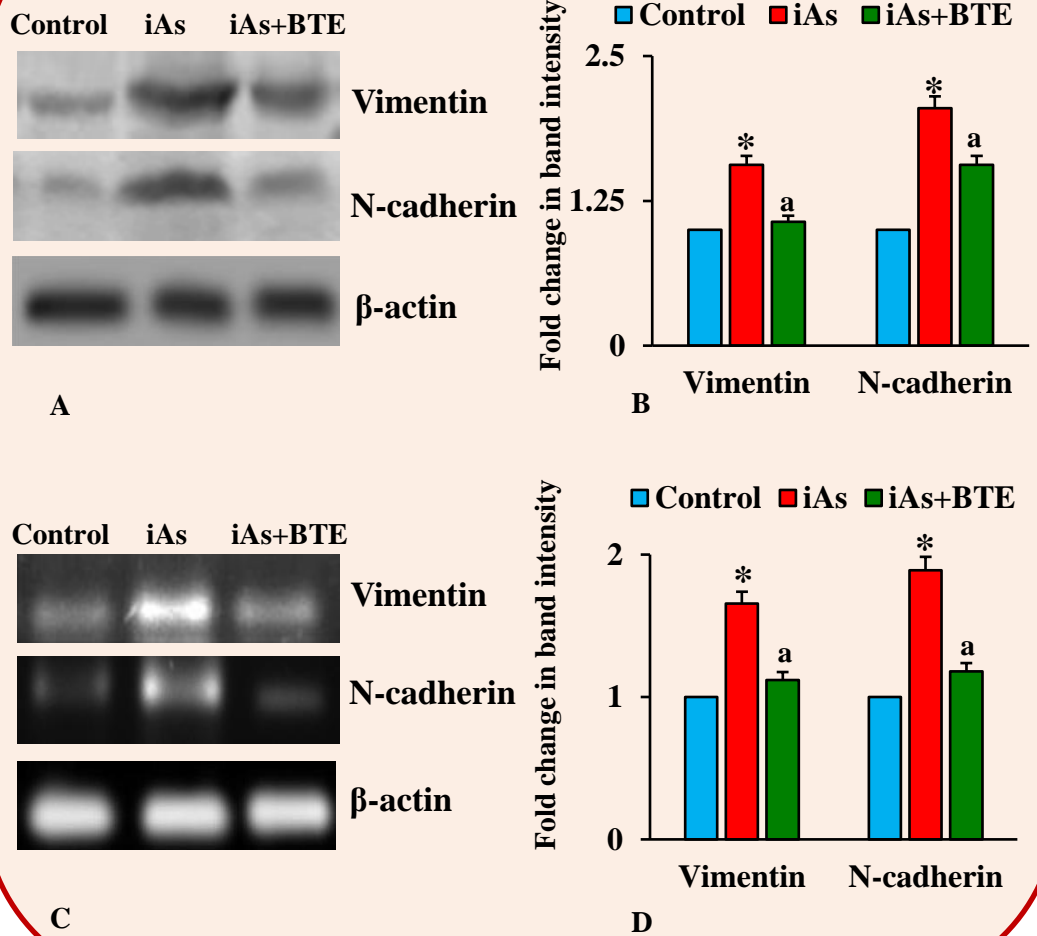


**Figure 4.26:** Estimating the expression of mesenchymal markers Vimentin and N-cadherin.

**Figure 4.26A** displays the representative immunoblot images of mesenchymal markers Vimentin and N-cadherin, in Swiss albino mice at 330 days of treatment.

**Figure 4.26B** displays a bar graph representing the fold change in band intensities of the respective mesenchymal markers. iAs treatment leads to upregulation of mesenchymal markers, while BTE administration downregulates them.

**Figure 4.26C** displays the representative RT-PCR bands of the respective mesenchymal markers.

**Figure 4.26D** displays a bar graph showing fold change in RT-PCR band intensities, of Vimentin and N-cadherin. Chronic iAs treatment results in elevation of the RT-PCR band intensities, of the mesenchymal markers, whereas, administration of BTE suppresses them. Elevation of band intensities, in the iAs treated mice, is significant at  $*p < 0.0001$ , with respect to the control mice. Suppression of band intensity, in the iAs+BTE treated mice, is significant at  $^ap < 0.0001$ .  $\beta$ -actin was used as a loading control. Values are mean of three independent experiments  $\pm$ S.D.

### Mesenchymal markers of EMT (Contd.)

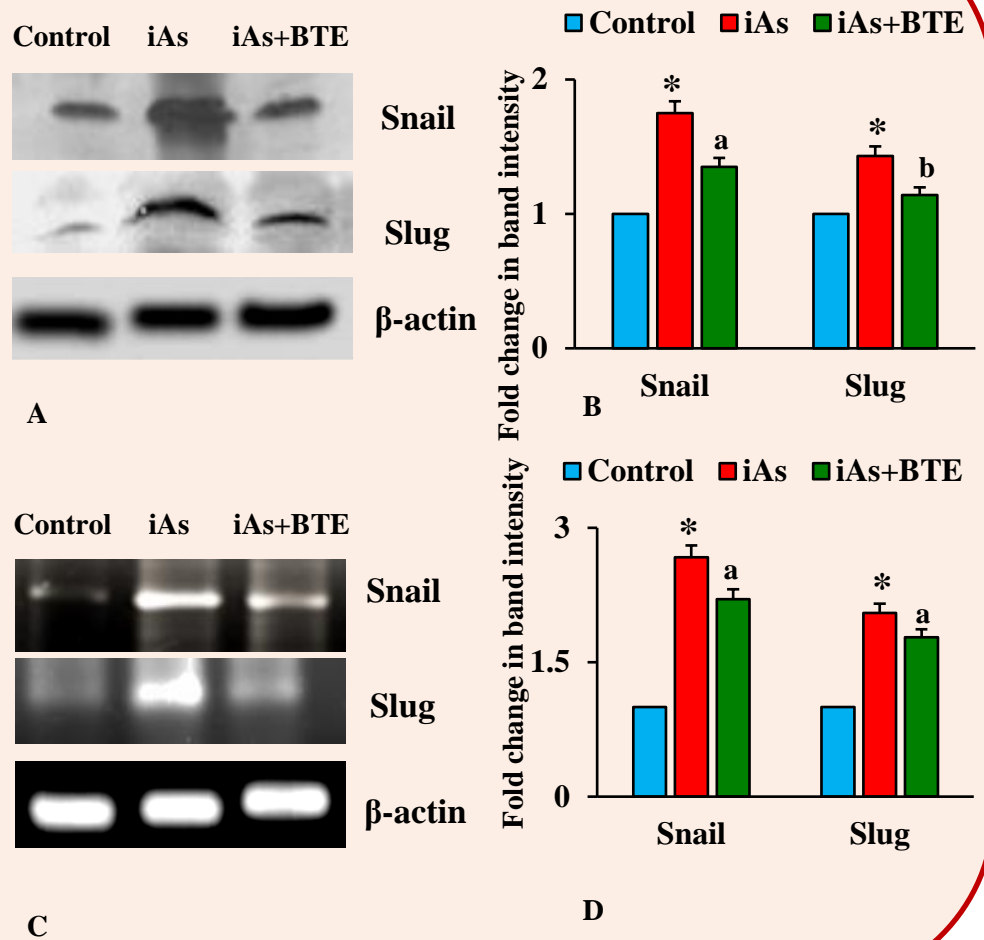


**Figure 4.27:** Estimating the expression of mesenchymal transcription factors Snail and Slug.

**Figure 4.27A** displays the representative immunoblot images of mesenchymal markers Snail and Slug, in Swiss albino mice at 330 days of treatment.

**Figure 4.27B** displays a bar graph representing the fold change in band intensities of the respective mesenchymal markers. iAs treatment leads to upregulation of mesenchymal markers, while BTE administration downregulates them.

**Figure 4.27C** displays the representative RT-PCR bands of the respective mesenchymal markers.

**Figure 4.27D** displays a bar graph showing fold change in RT-PCR band intensities, of Snail and Slug. Chronic iAs treatment results in elevation of the RT-PCR band intensities, of the mesenchymal markers, whereas, administration of BTE suppresses them. Elevation of band intensities, in the iAs treated mice, is significant at  $*p < 0.0001$ , with respect to the control mice. Suppression of band intensity, in the iAs+BTE treated mice, is significant at  $^ap < 0.0001$  and  $^bp < 0.001$ .  $\beta$ -actin was used as a loading control. Values are mean of three independent experiments  $\pm$ S.D.

## Mesenchymal markers of EMT (Contd.)

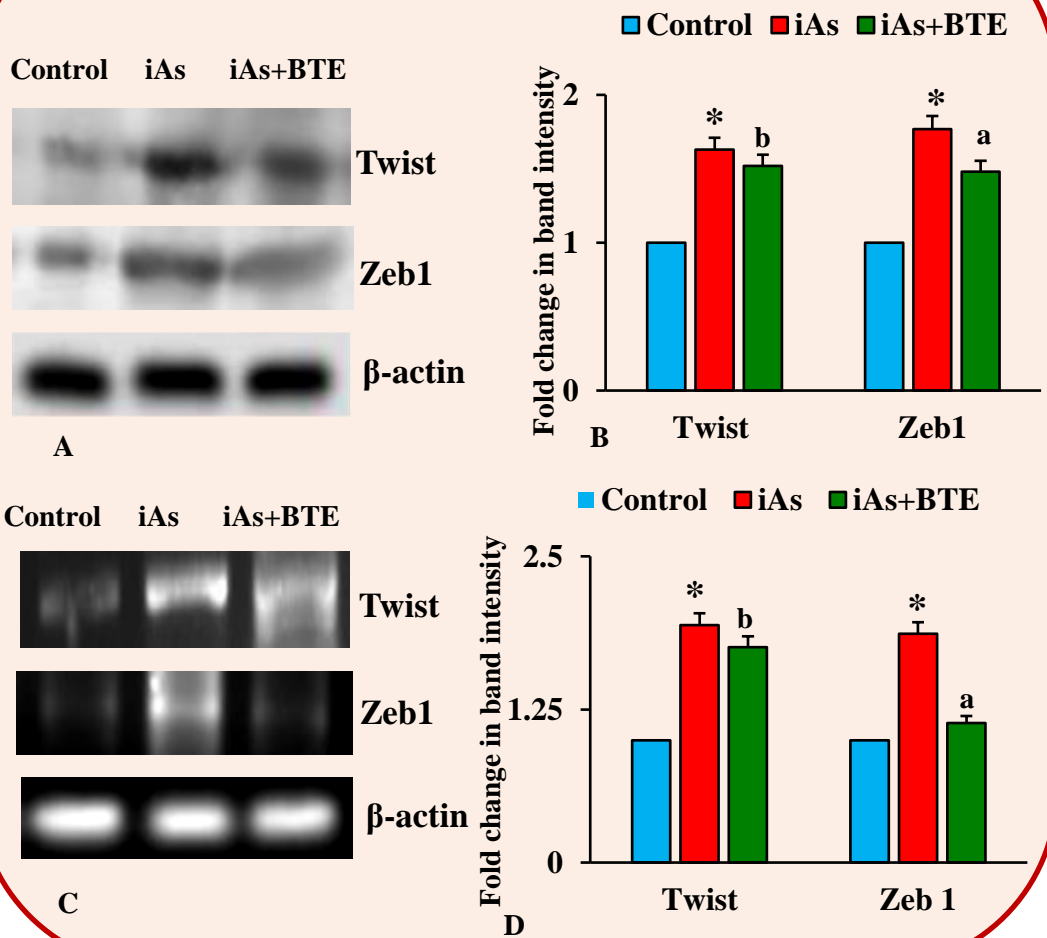


**Figure 4.28:** Estimating the expression of mesenchymal transcription factors Twist and Zeb.

**Figure 4.28A** displays the representative immunoblot images of mesenchymal transcription factors Twist and Zeb 1, in Swiss albino mice at 330 days of treatment.

**Figure 4.28B** displays a bar graph representing the fold change in band intensities of the respective mesenchymal markers. iAs treatment results in upregulation of mesenchymal markers, while BTE administration downregulates them.

**Figure 4.28C** displays the representative RT-PCR bands of the respective mesenchymal markers.

**Figure 4.28D** displays a bar graph showing fold change in RT-PCR band intensities, of Twist and Zeb 1. Chronic iAs treatment results in increase of the RT-PCR band intensities, of Twist and Zeb 1, whereas, administration of BTE decreases them.

Fold increase of band intensities, in the iAs treated mice, is significant at  $*p < 0.0001$ , with respect to the control mice. Fold decrease of band intensity, in the iAs+BTE treated mice, is significant at  $*p < 0.0001$  and  $^b p < 0.001$ , with respect to the iAs treatment group.  $\beta$ -actin was used as a loading control. Values are mean of three independent experiments  $\pm$ S.D.

blots of the corresponding EMT markers. The bar graph in the Figures 4.25B, 4.26B, 4.27B and 4.28B represent the fold change in band intensities of the respective EMT marker immunoblots. The bar graph in the Figures 4.25D, 4.26D, 4.27D and 4.28D shows the fold change in intensities of the PCR bands of the respective EMT markers. Immunoblot and RT-PCR results show a prominent downregulation of the epithelial markers (E-cadherin and Desmoplakin) in the iAs treated mice with the subsequent upregulation of mesenchymal markers (Vimentin, N-cadherin, Snail, Slug, Twist and Zeb), indicating induction of EMT. In the iAs+BTE administered mice, this phenomenon appears to be reversed, the expressions of epithelial markers remain high while the expression of mesenchymal markers are reduced effectively, suggesting that BTE inhibited induction of EMT.

#### **4.20. Investigation of EMT induction by IHC.**

Figures 4.29, 4.30, 4.31 and 4.32 display representative IHC images of the respective EMT markers in the tissues of the control, iAs and iAs+BTE treated mice, at 330 days of treatment. Tables 4.6, 4.7, 4.8 and 4.9 display the Allred scores of the respective EMT markers, which were used to quantify the IHC results. The IHC results clearly indicate downregulation of the epithelial markers (E-cadherin and Desmoplakin) and upregulation of mesenchymal markers (Vimentin, N-cadherin, Snail, Slug, Twist and Zeb) in the tissues of the iAs treated mice. In the iAs+BTE treated mice, the expression of epithelial markers is upregulated and mesenchymal markers is downregulated. These results reverberate the immunoblot and RT-PCR results, where iAs have been found to induce EMT, which was inhibited by BTE.



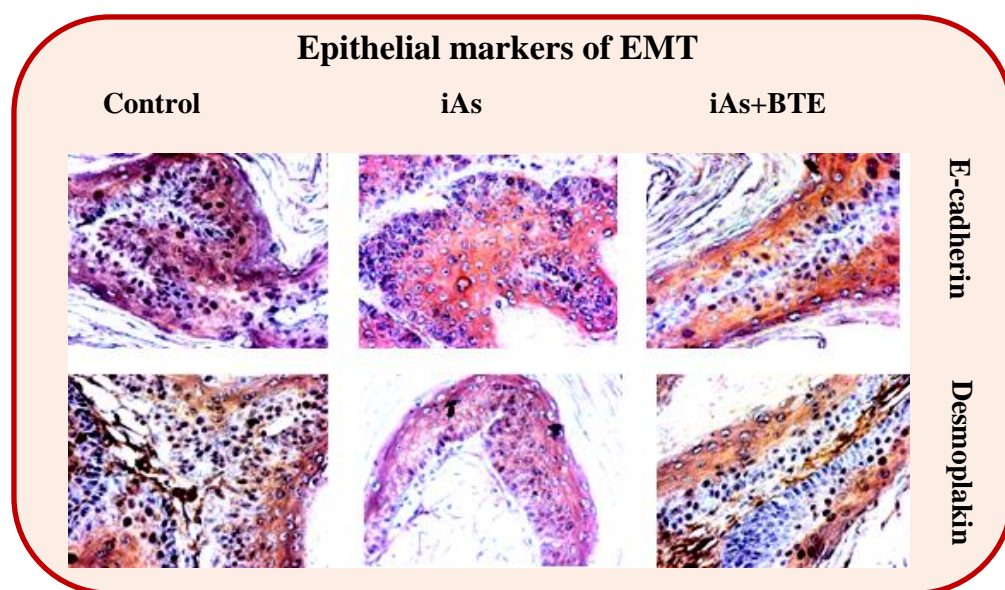


**Figure 4.29:** Assessment of EMT marker expression by IHC. Representative IHC images of the respective EMT markers in control, iAs, and iAs + BTE treated mice have been displayed. The results suggest downregulation of epithelial markers (E-cadherin and desmoplakin) in iAs treated mice and its reversal in iAs + BTE treated mice. IHC was performed on formalin fixed, paraffin embedded, mouse skin tissues, which after incubating with antibodies, were stained with diaminobenzidine. Images were captured with a bright field microscope at 400x. Fifty fields were analyzed for each marker from each treatment group and representative photographs for epithelial markers have been depicted.

**Table 4.6:** Quantification of Immunohistochemistry results using Allred scoring. Allred score of the epithelial markers, E-cadherin and Desmoplakin, in the control, iAs and iAs + BTE treated mice has been tabulated. Values are presented as mean  $\pm$  SD.

EMT markers	Control	iAs	iAs+BTE
<b>E-cadherin</b>	$8 \pm 0.36$	$3 \pm 0.09^*$	$5 \pm 0.11^a$
<b>Desmoplakin</b>	$7 \pm 0.24$	$4 \pm 0.18^*$	$6 \pm 0.17^a$

Allred scores of the iAs treated mice are significant at  $^*p < 0.0001$ , with respect to the control mice.

Allred scores of the iAs+BTE treated mice are significant at  $^ap < 0.0001$ , with respect to the iAs treatment group.

### Mesenchymal markers of EMT

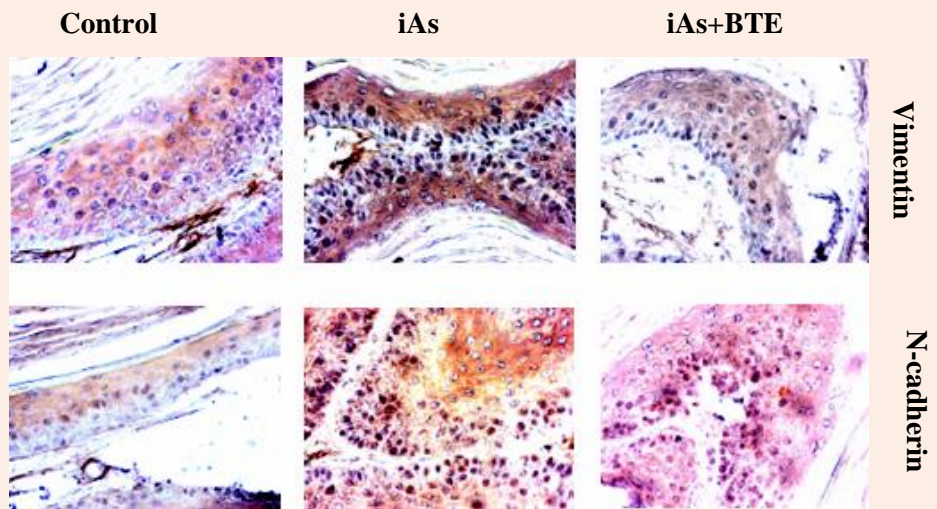


**Figure 4.30:** Assessment of EMT marker expression by IHC. Representative IHC images of the EMT markers in control, iAs, and iAs + BTE treated mice have been displayed. The results suggest upregulation of mesenchymal markers (Vimentin and N-cadherin) in iAs treated mice and its downregulation in iAs + BTE treated mice. IHC was performed on formalin fixed, paraffin embedded, mouse skin tissues, which after incubating with antibodies, were stained with diaminobenzidine. Images were captured with a bright field microscope at 400x. Fifty fields were analysed for each marker from each treatment group and representative photographs of the mesenchymal markers have been depicted.

**Table 4.7:** Quantification of Immunohistochemistry results using Allred scoring. Allred score of the mesenchymal markers, Vimentin and N-cadherin, in the control, iAs and iAs + BTE treated mice has been tabulated. Values are presented as mean  $\pm$  SD.

EMT markers	Control	iAs	iAs+BTE
Vimentin	2 $\pm$ 0.12	7 $\pm$ 0.30*	4 $\pm$ 0.20 <sup>a</sup>
N-cadherin	1 $\pm$ 0.03	6 $\pm$ 0.25*	4 $\pm$ 0.08 <sup>a</sup>

Allred scores of the iAs treated mice are significant at \* $p < 0.0001$ , with respect to the control mice.

Allred scores of the iAs+BTE treated mice are significant at <sup>a</sup> $p < 0.0001$ , with respect to the iAs treatment group.

### Mesenchymal markers of EMT continued

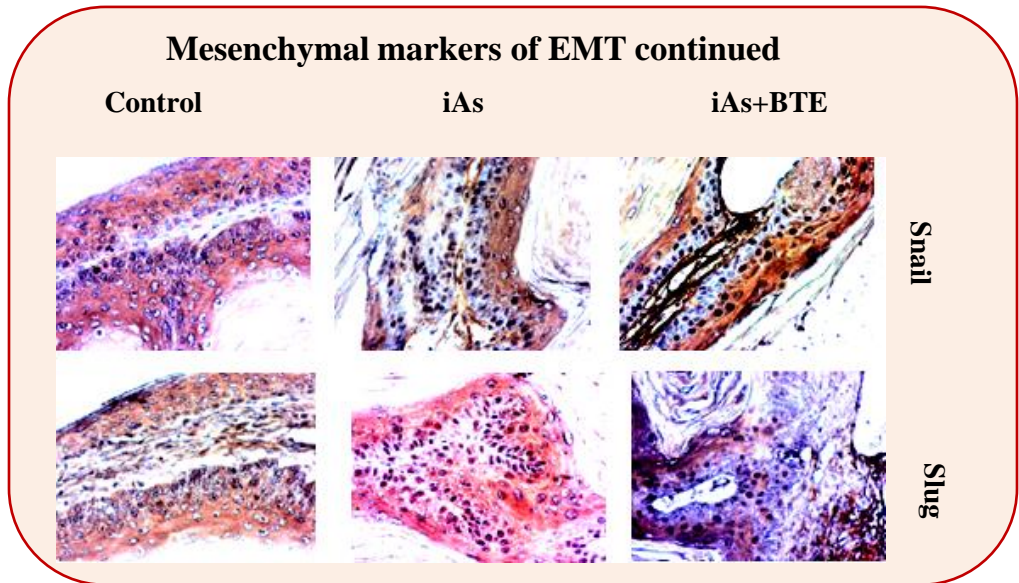


**Figure 4.31:** Assessment of EMT marker expression by IHC. Representative IHC images of the EMT markers in control, iAs, and iAs + BTE treated mice have been displayed. The results suggest upregulation of mesenchymal markers (Snail and Slug) in iAs treated mice and its downregulation in iAs + BTE treated mice. IHC was performed on formalin fixed, paraffin embedded, mouse skin tissues, which after incubating with antibodies, were stained with diaminobenzidine. Images were captured with a bright field microscope at 400x. Fifty fields were analyzed for each marker from each treatment group and representative photographs of the mesenchymal markers have been depicted.

**Table 4.8:** Quantification of Immunohistochemistry results using Allred scoring. Allred score of the mesenchymal markers, Snail and Slug, in the control, iAs and iAs + BTE treated mice has been tabulated. Values are presented as mean  $\pm$  SD.

EMT markers	Control	iAs	iAs+BTE
Snail	4 $\pm$ 0.18	8 $\pm$ 0.28*	5 $\pm$ 0.23 <sup>a</sup>
Slug	3 $\pm$ 0.11	8 $\pm$ 0.33*	6 $\pm$ 0.25 <sup>b</sup>

Allred scores of the iAs treated mice are significant at \* $p < 0.0001$ , with respect to the control mice.

Allred scores of the iAs+BTE treated mice are significant at <sup>a</sup> $p < 0.0001$  and <sup>b</sup> $p < 0.001$  with respect to the iAs treatment group.

### Mesenchymal markers of EMT continued

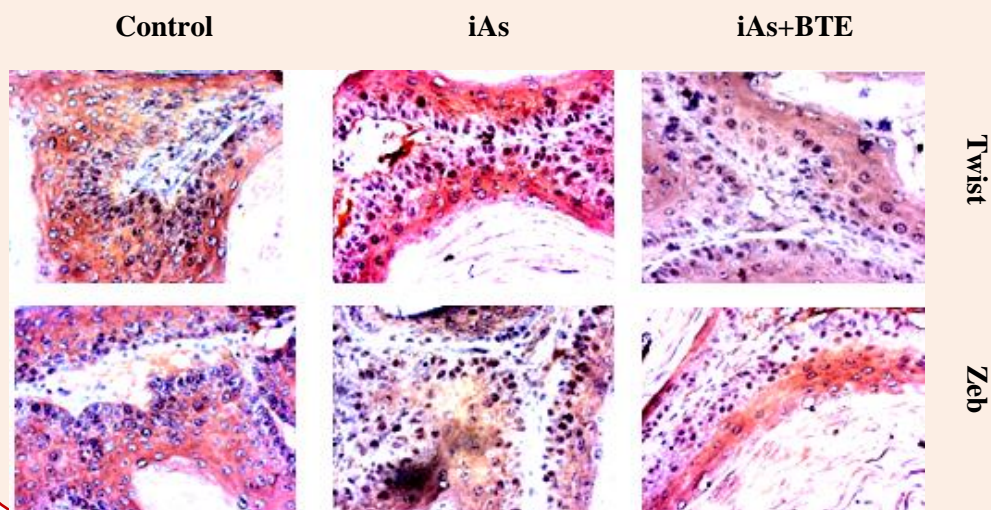


**Figure 4.32:** Assessment of EMT marker expression by IHC. Representative IHC images of the EMT markers in control, iAs, and iAs + BTE treated mice have been displayed. The results suggest upregulation of mesenchymal markers (Twist and Zeb) in iAs treated mice and its downregulation in iAs + BTE treated mice. IHC was performed on formalin fixed, paraffin embedded, mouse skin tissues, which after incubating with antibodies, were stained with diaminobenzidine. Images were captured with a bright field microscope at 400x. Fifty fields were analyzed for each marker from each treatment group and representative photographs of the mesenchymal markers have been depicted.

**Table 4.9:** Quantification of Immunohistochemistry results using Allred scoring. Allred score of the mesenchymal markers, Twist and Zeb, in the control, iAs and iAs + BTE treated mice has been tabulated. Values are presented as mean  $\pm$  SD.

EMT markers	Control	iAs	iAs+BTE
Twist	2 $\pm$ 0.08	6 $\pm$ 0.18*	4 $\pm$ 0.18 <sup>a</sup>
Zeb 1	3 $\pm$ 0.12	7 $\pm$ 0.22*	4 $\pm$ 0.05 <sup>a</sup>

Allred scores of the iAs treated mice are significant at \* $p < 0.0001$ , with respect to the control mice.

Allred scores of the iAs+BTE treated mice are significant at <sup>a</sup> $p < 0.0001$ , with respect to the iAs treatment group.

#### **4.21. Global methylation status of H3K4.**

The bar graph displayed in Figure 4.33 represents the global methylation status of H3K4 loci in the tissues of the control, iAs and iAs+BTE treated mice, at 330 days of treatment. The methylation of H3K4 loci was significantly ( $p < 0.0001$ ) low in the iAs treated mice, in comparison to the control group. In the iAs+BTE administered mice, H3K4 global methylation was significantly ( $p < 0.0001$ ) higher than the iAs group, indicating that, BTE inhibited iAs induced global demethylation of the H3K4 loci.

#### **4.22. Assessment of epigenetic histone marks and their modifiers via Immunoblot assay (methyltransferases, demethylases and acetyltransferases)**

Representative Immunoblot images of histone acetylation mark H4K16ac and its acetyl transferase MYST1, at 330 days of treatment, in Swiss albino mice, have been depicted in the Figure 4.34A and their respective band intensities have been displayed as a bar graph in Figure 4.34B. The results indicated that, upon chronic exposure to iAs, the expression of H4K16ac and MYST1 is significantly ( $p < 0.0001$ ) downregulated while upon BTE intervention, the results are reversed.

Representative Immunoblot images of histone mark H3K27me3, its methyl transferase EZH2, JARID2 and its demethylase KDM6A have been depicted in Figure 4.35A. The band intensities of these histone marks and their modifiers have been represented as a bar graph in the Figure 4.35B. The obtained results suggest that, chronic iAs treatment leads to significant ( $p < 0.0001$ ) upregulation of H3K27me3, EZH2, JARID2 and downregulation of KDM6A. This expression profile is reversed in the iAs+BTE treated mice.



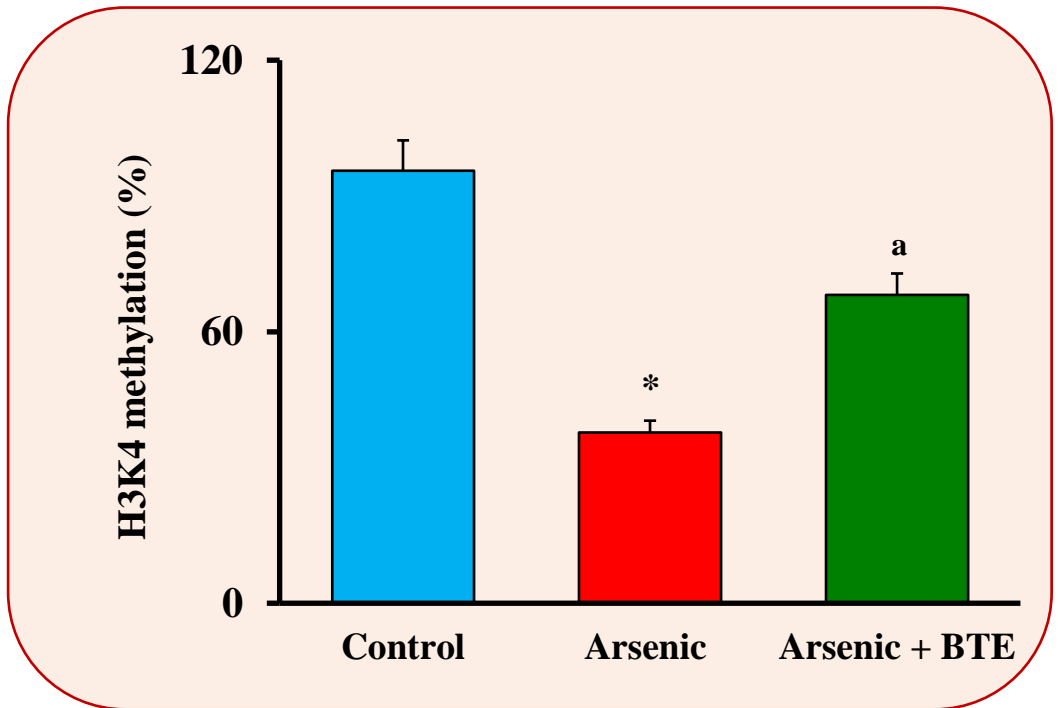


**Figure 4.33:** Global methylation at H3K4 loci.

Global methylation has been depleted to 0.4-fold by exposure to iAs for 330 days. Reduced methylation at H3K4 loci has been increased by BTE administration. Values are average of three independent experiments  $\pm$  SD. Reduction in global H3K4 methylation is significant with respect to control at  $^*p < 0.0001$ ; enhancement of the same by BTE is significant at  $^ap < 0.0001$ .

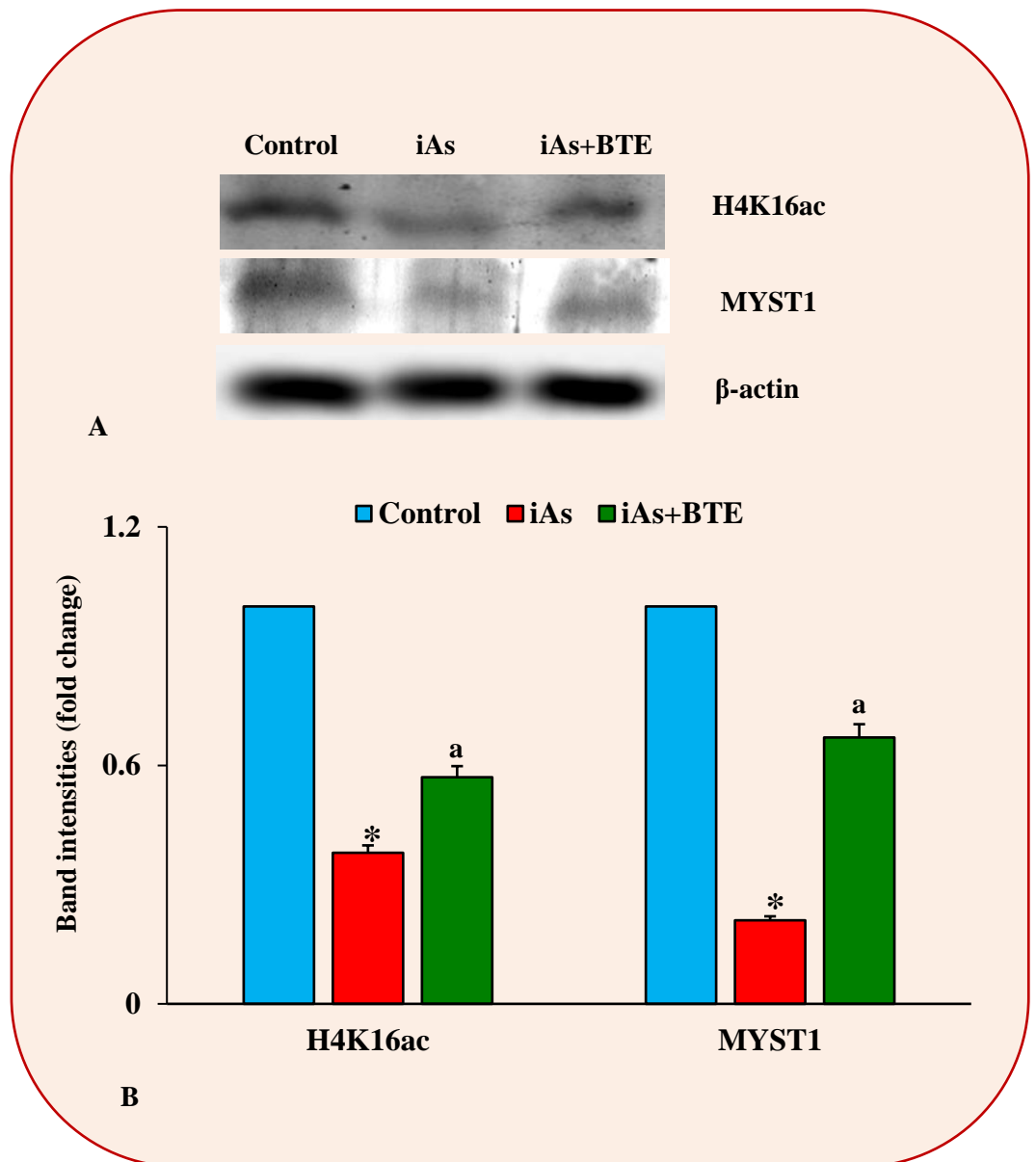


**Figure 4.34:** Estimation of the expression of H4K16ac and its acetyltransferase MYST1.

**Figure 4.34A** displays the representative immunoblot images of H4K16ac and its acetyltransferase MYST1, in control, iAs and iAs+BTE treated Swiss albino mice, at 330 days of treatment.  $\beta$ -actin was used as a loading control.

**Figure 4.34B** displays a bar graph representing fold change in mean band intensities of H4K16ac and its acetyltransferase MYST1, in control, iAs and iAs+BTE treated Swiss albino mice, at 330 days of treatment. Downregulation of H4K16ac and MYST1 have been observed in the iAs treated mice, which were upregulated upon BTE administration. Fold change (decrease) in band intensities of the iAs treated mice is significant at  $*p < 0.0001$ , with respect to the control mice. Fold change (increase) in band intensities of the iAs+BTE treated mice is significant at  $^ap < 0.0001$ , with respect to the iAs treatment group.

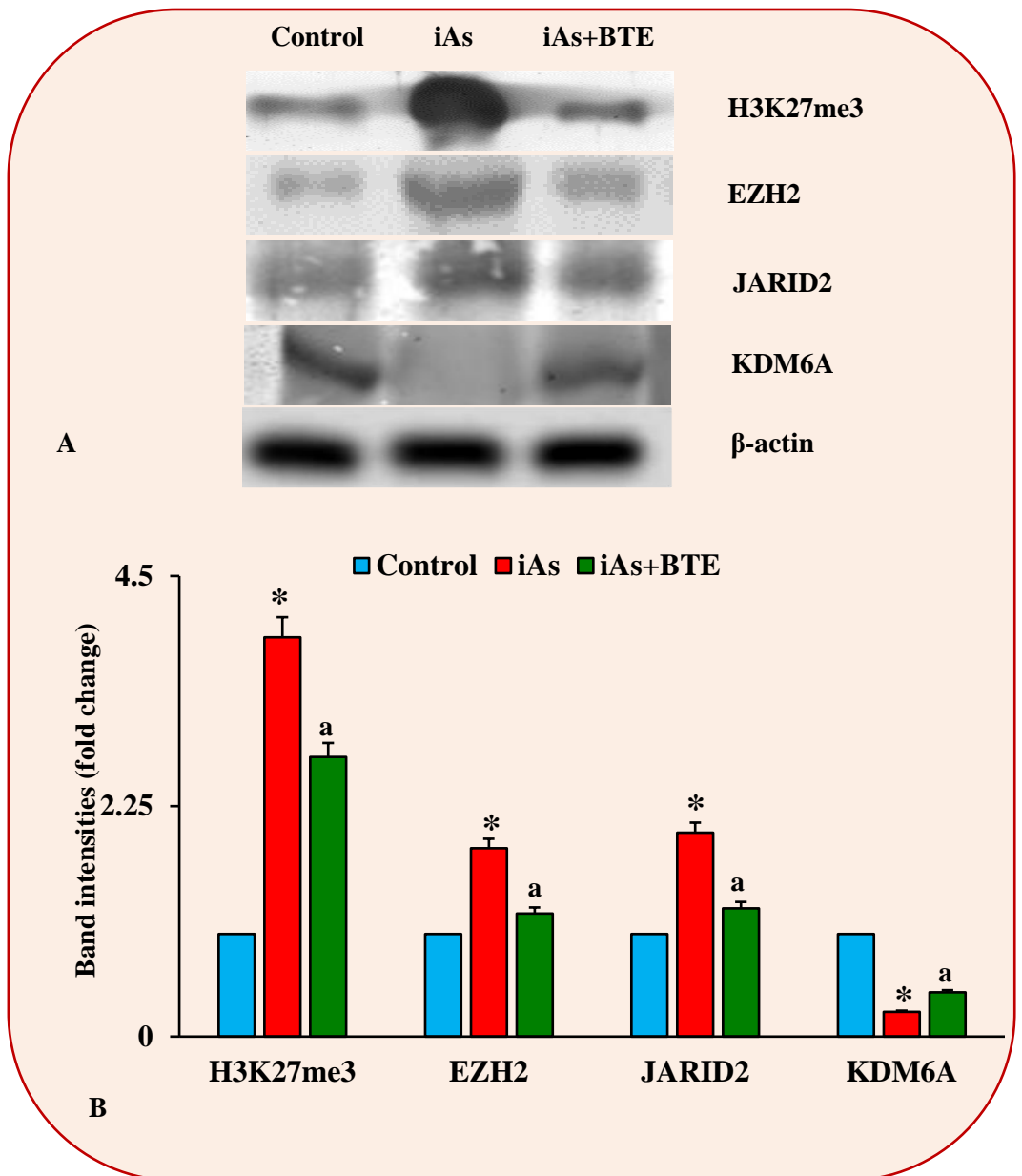


**Figure 4.35:** Estimation the expression of H3K27me3, its methyltransferase EZH2, JARID2 and its demethylase KDM6A.

**Figure 4.35A** displays the representative immunoblot images of H3K27me3, EZH2, JARID2 and KDM6A, in control, iAs and iAs+BTE treated Swiss albino mice, at 330 days of treatment.  $\beta$ -actin was used as a loading control.

**Figure 4.35B** displays a bar graph representing fold change in mean band intensities of H3K27me3, EZH2, JARID2 and KDM6A, in control, iAs and iAs+BTE treated Swiss albino mice, at 330 days of treatment. Upregulation of H3K27me3, EZH2 and JARID2 with simultaneous downregulation of KDM6A have been observed in the iAs treated mice. In the iAs+BTE treated mice, this expression pattern was reversed. Modulation of band intensities in the iAs treated mice is significant at  $^*p < 0.0001$ , with respect to the control mice. Modulation of band intensities in the iAs+BTE treated mice is significant at  $^ap < 0.0001$ , with respect to the iAs treatment group.



The Figure 4.36A depicts the representative immunoblot images of the histone mark H3K4me1, its methyl transferase MLL3 and demethylase LSD1. The bar graph in the Figure 4.36B represents the band intensities of these respective proteins. The obtained results indicate upregulation of H3K4me1 and MLL3 in the iAs administered mice while their expression is suppressed upon BTE administration. The expression of the demethylase LSD1 is not altered in the iAs and iAs+BTE treated mice.

Figure 4.37A depicts the representative immunoblot band images of the histone mark H3K4me3, its methyltransferase MLL1 and its specific demethylase JARID1B. The mean band intensities of these immunoblots have been represented as a bar graph in the figure 4.37B. The results indicate that upon chronic iAs exposure, the expression of H3K4me3 histone mark and its methyltransferase MLL1 is significantly ( $p < 0.0001$ ) downregulated, while that of the demethylase JARID1B is upregulated ( $p < 0.0001$ ). In the iAs+BTE administered mice, the expression of H3K4me3 and MLL1 is upregulated but anomalously the expression of demethylase JARID1B also remains high.

#### **4.23. Assessment of epigenetic histone marks and their modifiers via IHC**

The expression of the histone marks and their modifiers, within the mice tissues, have also been assessed by IHC assay. The representative IHC images of these histone marks along with their modifiers have been depicted in the Figures 4.38, 4.39, 4.40 and 4.41. The IHC results were quantified using Allred scoring system and the Allred scores of the respective histone marks and their modifiers have been displayed in the Tables 4.10, 4.11, 4.12 and 4.13. Results of the IHC assay reiterated the immunoblot assay results. IHC assay also

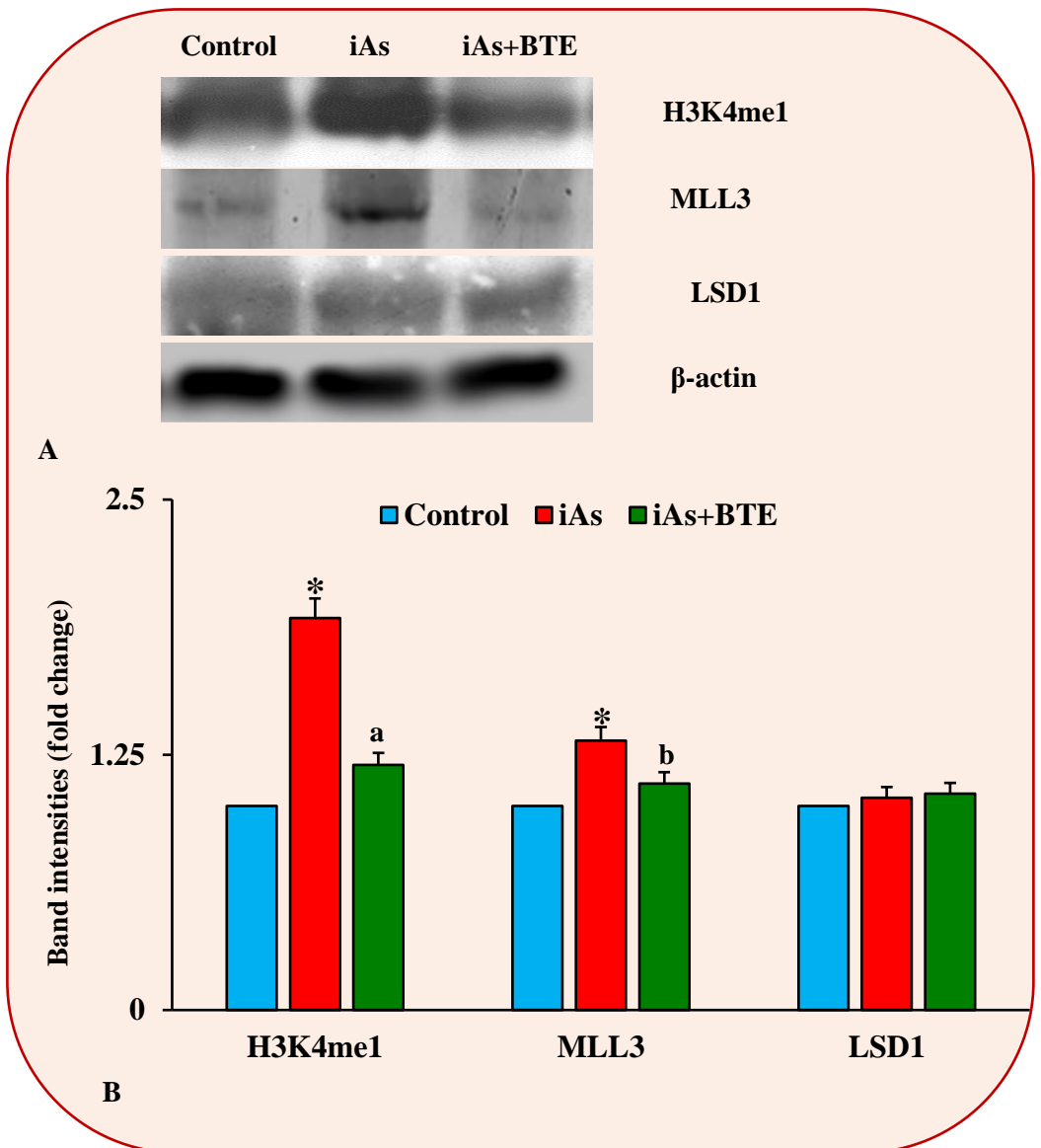


**Figure 4.36:** Estimating the expression of H3K4me1, its methyltransferase MLL3 and demethylase LSD1.

**Figure 4.36A** displays the representative immunoblot images of H3K4me1, MLL3 and LSD1, in control, iAs and iAs+BTE treated Swiss albino mice, at 330 days of treatment.  $\beta$ -actin was used as a loading control.

**Figure 4.36B** displays a bar graph representing fold change in mean band intensities of H3K4me1, MLL3 and LSD1, in control, iAs and iAs+BTE treated Swiss albino mice, at 330 days of treatment. Upregulation of H3K4me1 and MLL3 were observed in the iAs treated mice, which were found to be downregulated in the iAs+BTE treated mice. No significant change in expression of LSD1 was observed in the control, iAs and iAs+BTE treated mice.

Fold change (increase) of band intensities in the iAs treated mice is significant at  $*p < 0.0001$ , with respect to the control mice. Fold change (decrease) of band intensities in the iAs+BTE treated mice is significant at  $^ap < 0.0001$  and  $^bp < 0.001$ , with respect to the iAs treatment group.

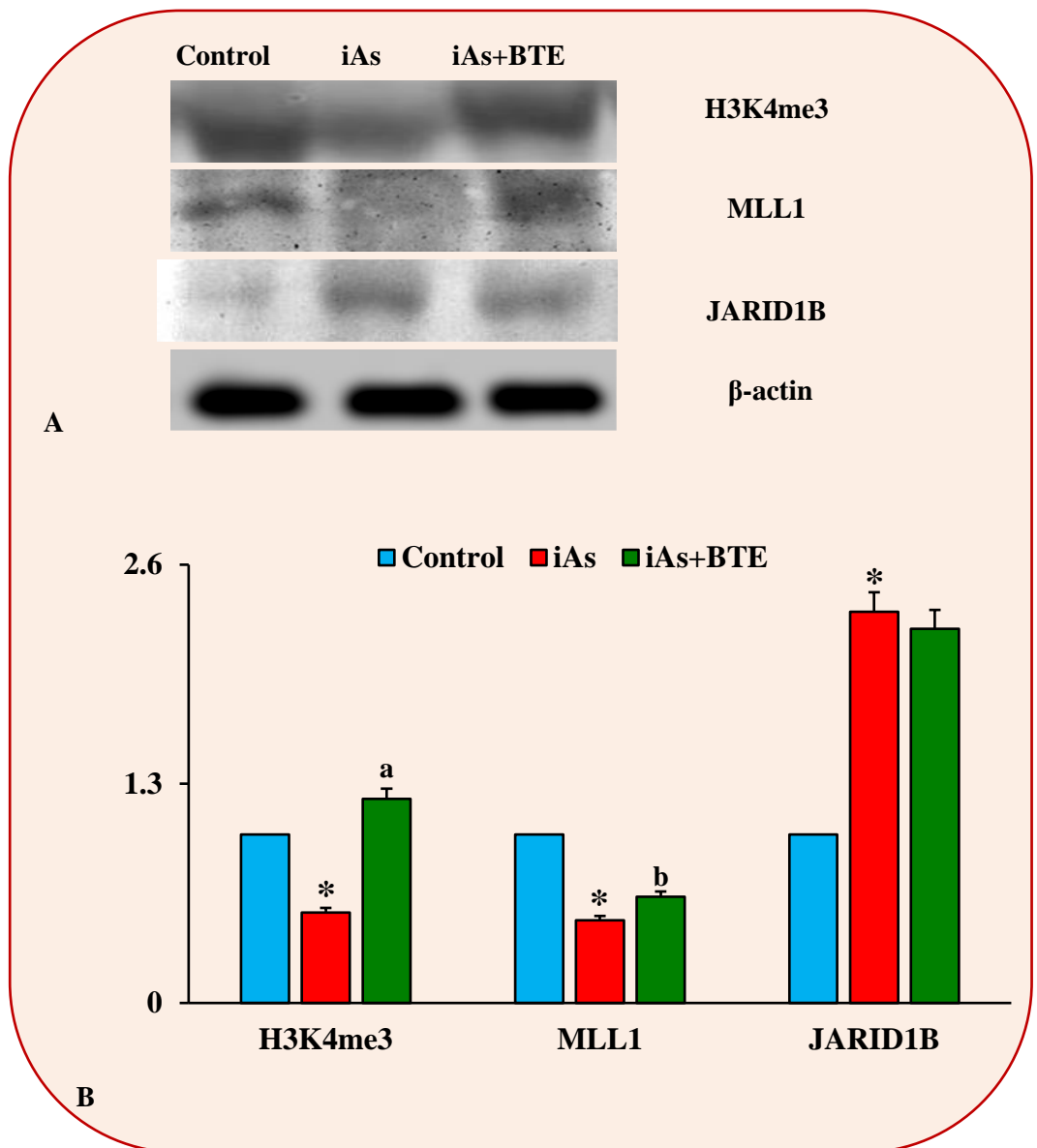


**Figure 4.37:** Estimating the expression of H3K4me3, its methyltransferase MLL1 and its specific demethylase JARID1B.

**Figure 4.37A** displays the representative immunoblot images of H3K4me3, MLL1 and JARID1B, in control, iAs and iAs+BTE treated Swiss albino mice, at 330 days of treatment.  $\beta$ -actin was used as a loading control.

**Figure 4.37B** displays a bar graph representing fold change in mean band intensities of H3K4me3, MLL1 and JARID1B, in control, iAs and iAs+BTE treated Swiss albino mice, at 330 days of treatment. Downregulation of H3K4me3 and MLL1 with simultaneous upregulation of JARID1B were observed in the iAs treated mice. In the iAs+BTE treated mice, the expression of H3K4me3 and MLL1 was upregulated but no significant modulation was observed in the expression of JARID1B.

Modulation of band intensities in the iAs treated mice is significant at  $^*p < 0.0001$ , with respect to the control mice. Modulation of band intensities in the iAs+BTE treated mice is significant at  $^ap < 0.0001$  and  $^bp < 0.001$ , with respect to the iAs treatment group.

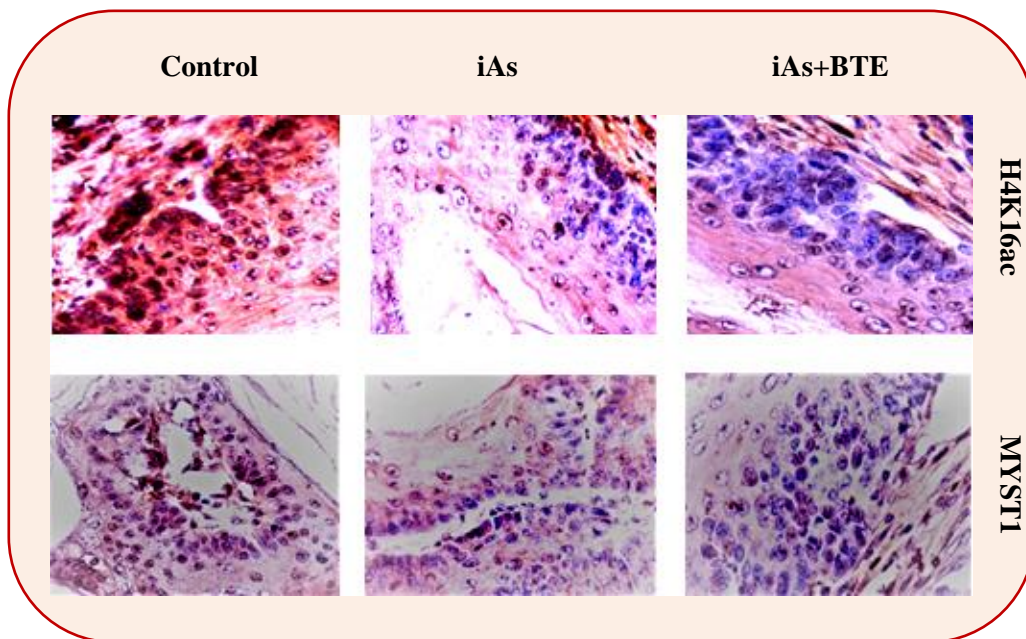


**Figure 4.38:** : Assessment of H4K16ac and methyl transferase MYST1 expression by IHC. Representative IHC images of the H4K16ac and MYST1 in control, iAs, and iAs + BTE treated mice have been displayed. The results suggest downregulation of H4K16ac and MYST1 in iAs treated mice and its upregulation in iAs + BTE treated mice. IHC was performed on formalin fixed, paraffin embedded, mouse skin tissues, which after incubating with antibodies, were stained with diaminobenzidine. Images were captured with a bright field microscope at 400x. Fifty fields were analyzed for each marker from each treatment group and representative photographs have been depicted.

**Table 4.10:** Quantification of Immunohistochemistry results using Allred scoring. Allred score of H4K16ac and MYST1 , in the control, iAs and iAs + BTE treated mice has been tabulated. Values are presented as mean  $\pm$  SD.

Proteins	Control	Arsenic (iAs)	iAs + BTE
H4K16ac	7 $\pm$ 0.45	4 $\pm$ 0.50*	5 $\pm$ 0.32 <sup>b</sup>
MYST1	7 $\pm$ 0.45	4 $\pm$ 0.50*	6 $\pm$ 0.50 <sup>a</sup>

Allred scores of the iAs treated mice are significant at \* $p < 0.0001$ , with respect to the control mice.

Allred scores of the iAs+BTE treated mice are significant at <sup>a</sup> $p < 0.0001$  and <sup>b</sup> $p < 0.001$ , with respect to the iAs treatment group.

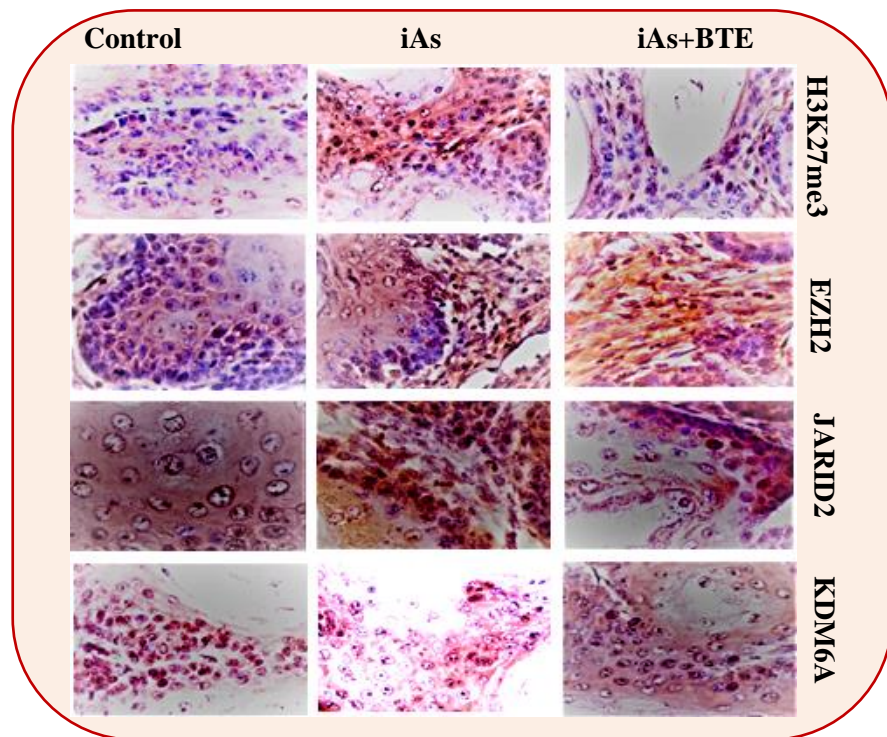


**Figure 4.39:** Assessment of H3K27me3, its methyltransferase EZH2, JARID2 and its demethylase KDM6A by IHC. Representative IHC images of H3K27me3, EZH2, JARID2 and KDM6A in control, iAs, and iAs + BTE treated mice have been displayed. Upregulation of H3K27me3, EZH2 and JARID2 with simultaneous downregulation of KDM6A in iAs treated mice was seen, which was reversed by BTE. IHC was performed on mouse skin tissues, which after incubating with antibodies, were stained with diaminobenzidine. Images were captured in a bright field microscope at 400x. Fifty fields were analyzed for each marker from each treatment group and representative images have been depicted.

**Table 4.11:** Quantification of Immunohistochemistry results using Allred scoring. Allred score (AS) of H3K27me3, EZH2, JARID2 and KDM6A, in the control, iAs and iAs + BTE treated mice has been tabulated. Values are presented as mean  $\pm$  SD.

Proteins	Control	Arsenic (iAs)	iAs + BTE
H3K27me3	4 $\pm$ 0.54	8 $\pm$ 0.21*	6 $\pm$ 0.45 <sup>a</sup>
EZH2	4 $\pm$ 0.44	8 $\pm$ 0.21*	6 $\pm$ 0.45 <sup>a</sup>
JARID2	5 $\pm$ 0.45	7 $\pm$ 0.31*	6 $\pm$ 0.45 <sup>b</sup>
KDM6A	7 $\pm$ 0.45	5 $\pm$ 0.50*	6 $\pm$ 0.21 <sup>b</sup>

AS of the iAs treated mice are significant at \* $p$ <0.0001, with respect to the control. AS of the iAs+BTE treated mice are significant at <sup>a</sup> $p$ <0.0001 and <sup>b</sup> $p$ <0.001, with respect to the iAs treatment group.

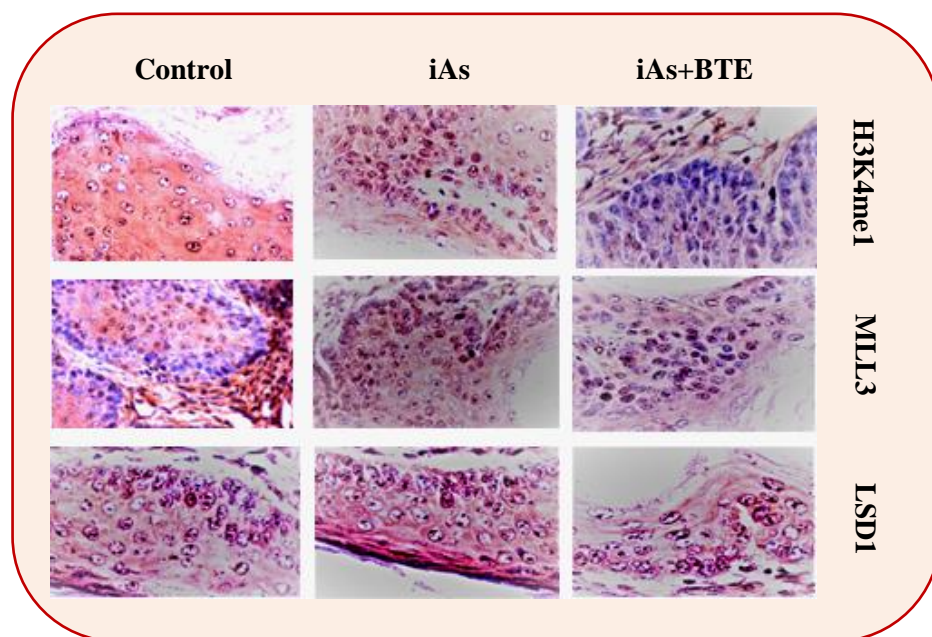


**Figure 4.40:** Assessment of H3K4me1, its methyltransferase MLL3 and demethylase LSD1 by IHC. Representative IHC images of H3K4me1, MLL3 and LSD1 in control, iAs, and iAs + BTE treated mice have been displayed. The results suggest upregulation of H3K4me1 and MLL3 in iAs treated mice and their downregulation in iAs + BTE treated mice. LSD1 shows no modulation of expression in control, iAs and iAs+BTE treated mice. IHC was performed on formalin fixed, paraffin embedded, mouse skin tissues, which after incubating with antibodies, were stained with diaminobenzidine. Images were captured with a bright field microscope at 400x. Fifty fields were analyzed for each marker from each treatment group and representative photographs have been depicted.

**Table 4.12 :** Quantification of Immunohistochemistry results using Allred scoring. Allred score of H3K4me1, MLL3 and LSD1, in the control, iAs and iAs + BTE treated mice has been tabulated. Values are presented as mean  $\pm$  SD

Proteins	Control	Arsenic (iAs)	iAs + BTE
H3K4me1	5 $\pm$ 0.45	7 $\pm$ 0.38*	6 $\pm$ 0.32 <sup>b</sup>
MLL3	6 $\pm$ 0.45	7 $\pm$ 0.45**	6 $\pm$ 0.38 <sup>b</sup>
LSD1	6 $\pm$ 0.45	6 $\pm$ 0.55	5 $\pm$ 0.62

Allred scores of the iAs treated mice are significant at \* $p < 0.0001$  and \*\* $p < 0.001$ , with respect to the control mice.

Allred scores of the iAs+BTE treated mice are significant at <sup>b</sup> $p < 0.001$ , with respect to the iAs treatment group.



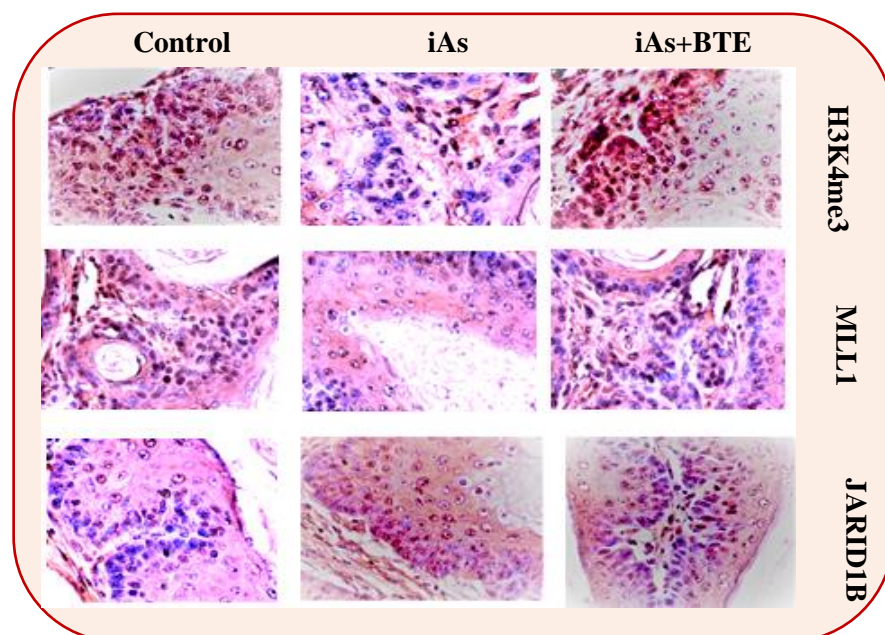


**Figure 4.41:** Assessment of H3K4me3, its methyltransferase MLL1 and its specific demethylase JARID1B by IHC. Representative IHC images of H3K4me3, MLL1 and JARID1B in control, iAs, and iAs + BTE treated mice have been displayed. The results suggest downregulation of H3K4me1 and MLL3 in iAs treated mice with simultaneous upregulation of JARID1B. In the iAs+BTE treated mice, H3K4me3 and MLL1 are upregulated, while JARID1B remains high. BTE fails to modulate the expression of JARID1B. IHC was performed on formalin fixed, paraffin embedded, mouse skin tissues, which after incubating with antibodies, were stained with diaminobenzidine. Images were captured with a bright field microscope at 400x. Fifty fields were analyzed for each marker from each treatment group and representative photographs have been depicted.

**Table 4.13:** Quantification of Immunohistochemistry results using Allred scoring. Allred score of H3K4me3, MLL1 and JARID1B , in the control, iAs and iAs + BTE treated mice has been tabulated. Values are presented as mean  $\pm$  SD

Proteins	Control	Arsenic (iAs)	iAs + BTE
H3K4me3	7 $\pm$ 0.38	4 $\pm$ 0.45*	6 $\pm$ 0.45 <sup>a</sup>
MLL1	7 $\pm$ 0.45	5 $\pm$ 0.50*	6 $\pm$ 0.32 <sup>b</sup>
JARID1B	4 $\pm$ 0.63	6 $\pm$ 0.63*	6 $\pm$ 0.91

Allred scores of the iAs treated mice are significant at \* $p$ <0.0001, with respect to the control mice.

Allred scores of the iAs+BTE treated mice are significant at <sup>a</sup> $p$ <0.0001 and <sup>b</sup> $p$ <0.001, with respect to the iAs treatment group.

confirmed the anomalous high expression of JARID1B in the iAs+BTE treated mice, therefore, we may say that the immunoblot and IHC results are in unison.

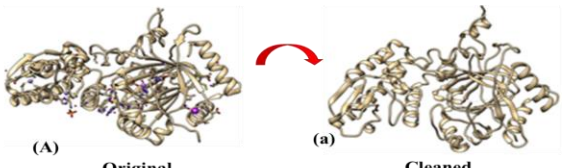
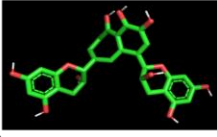
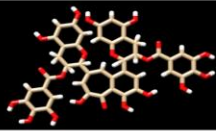
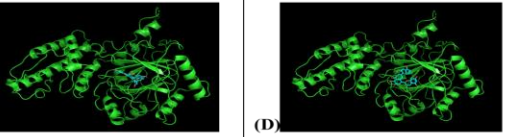
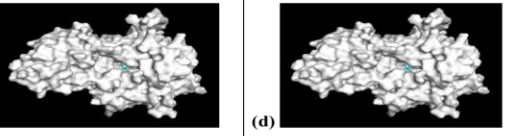
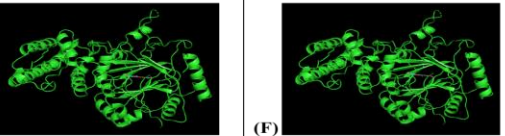
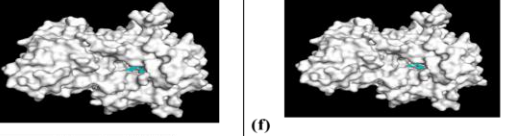
#### **4.24. Estimating the activity of JARID1B by in-silico docking studies.**

Initial docking of JARID1B and theaflavin was done in the presence of the supplementary ligands with high docking affinity. Fe(II) ion was replaced by Mn(II) ion, and several C and H atoms of theaflavin were docked less than 2 Å from the Mn(II) ion. Both theaflavin and theaflavin-3,3'-digallate were docked after removing the supplementary ligands. The structure of JARID1B (PDB id: 5FUN) downloaded from PDB with additional ligands and the corresponding cleaned structure of the same are shown in Figure 4.42. Both theaflavin and theaflavin-3,3'-digallate were docked after removing the supplementary ligands (Figure 4.42), with high affinities (-9.7 kCal/mole and -11.5 kCal/mole respectively). Top two poses of cleaned protein docked with theaflavin and theaflavin-3,3'-digallate are shown in Figure 4.42. Analysis using PyMol showed at least one hydrogen bond and several medium range (<10 Å) polar interactions. Two beta sheets each from either side of the JmjC domain were within 5 Å distance from the docked ligands (theaflavin and theaflavin-3,3'-digallate).

#### **4.25. Estimating the strength of the JARID1B and Theaflavin-3,3'-digallate docking using molecular simulation studies.**

MM/PBSA calculations were done on the trajectories of the systems between 30-31 ns from the production run. The time evolution of the RMSDs shows the systems to be fairly stabilized during this period. The lower the calculated binding energy, the stronger the ligand is expected to bind to the protein. From our calculations (Figure 4.42) it appears that the binding affinity



<p><b>Original and cleaned structures of JARID1B</b></p>	 <p>(A) Original (a) Cleaned</p>					
<p><b>Ligand</b></p>	 <p>Theaflavin (B)</p>	 <p>Theaflavin-3,3'-digallate (b)</p>				
<p><b>Pose 1</b></p>	<p><b>Cartoon</b></p>  <p>(C) (D)</p> <p><b>Solid</b></p>  <p>(e) (d)</p> <p><b>MM/PBSA analysis kJ/mole</b></p> <table border="0"> <tr> <td style="vertical-align: middle;">{</td> <td> <b>MM Energy:</b> <math>-135.77 \pm 0.74</math>  <b>Polar Energy:</b> <math>118.67 \pm 0.65</math>  <b>Nonpolar Energy:</b> <math>-12.68 \pm 0.06</math> </td> <td style="vertical-align: middle;">{</td> <td> <b>MM Energy:</b> <math>-137.17 \pm 0.75</math>  <b>Polar Energy:</b> <math>104.92 \pm 0.65</math>  <b>Nonpolar Energy:</b> <math>-12.55 \pm 0.05</math> </td> </tr> </table>		{	<b>MM Energy:</b> $-135.77 \pm 0.74$ <b>Polar Energy:</b> $118.67 \pm 0.65$ <b>Nonpolar Energy:</b> $-12.68 \pm 0.06$	{	<b>MM Energy:</b> $-137.17 \pm 0.75$ <b>Polar Energy:</b> $104.92 \pm 0.65$ <b>Nonpolar Energy:</b> $-12.55 \pm 0.05$
{	<b>MM Energy:</b> $-135.77 \pm 0.74$ <b>Polar Energy:</b> $118.67 \pm 0.65$ <b>Nonpolar Energy:</b> $-12.68 \pm 0.06$	{	<b>MM Energy:</b> $-137.17 \pm 0.75$ <b>Polar Energy:</b> $104.92 \pm 0.65$ <b>Nonpolar Energy:</b> $-12.55 \pm 0.05$			
<p><b>Pose 2</b></p>	<p><b>Cartoon</b></p>  <p>(E) (F)</p> <p><b>Solid</b></p>  <p>(e) (f)</p> <p><b>MM/PBSA analysis kJ/mole</b></p> <table border="0"> <tr> <td style="vertical-align: middle;">{</td> <td> <b>MM Energy:</b> <math>-162.60 \pm 1.15</math>  <b>Polar Energy:</b> <math>136.01 \pm 0.94</math>  <b>Nonpolar Energy:</b> <math>-13.09 \pm 0.06</math> </td> <td style="vertical-align: middle;">{</td> <td> <b>MM Energy:</b> <math>-116.36 \pm 0.72</math>  <b>Polar Energy:</b> <math>92.48 \pm 0.62</math>  <b>Nonpolar Energy:</b> <math>-11.61 \pm 0.05</math> </td> </tr> </table>		{	<b>MM Energy:</b> $-162.60 \pm 1.15$ <b>Polar Energy:</b> $136.01 \pm 0.94$ <b>Nonpolar Energy:</b> $-13.09 \pm 0.06$	{	<b>MM Energy:</b> $-116.36 \pm 0.72$ <b>Polar Energy:</b> $92.48 \pm 0.62$ <b>Nonpolar Energy:</b> $-11.61 \pm 0.05$
{	<b>MM Energy:</b> $-162.60 \pm 1.15$ <b>Polar Energy:</b> $136.01 \pm 0.94$ <b>Nonpolar Energy:</b> $-13.09 \pm 0.06$	{	<b>MM Energy:</b> $-116.36 \pm 0.72$ <b>Polar Energy:</b> $92.48 \pm 0.62$ <b>Nonpolar Energy:</b> $-11.61 \pm 0.05$			

**Figure 4.42:** Docking results of JARID1B. (A) The original structure of JARID1B (PDB id: 5FUN) downloaded from PDB with additional ligands; (a) The cleaned structure of JARID1B (PDB id: 5FUN) downloaded from PDB with additional ligands; (B) Chemical structure of theaflavin; (b) Chemical structure of theaflavin- 3,3'-digallate; (C) The best docking pose of theaflavin with JARID 1B (cartoon rendering); (c) The best docking pose of theaflavin with JARID 1B (solid rendering); (D) The best docking pose of theaflavin-3,3'-digallate with JARID 1B (cartoon rendering); (d) The best docking pose of theaflavin-3,3'-digallate with JARID 1B (solid rendering). (E) The 2<sup>nd</sup> best docking pose of theaflavin with JARID 1B (cartoon rendering); (e) The 2<sup>nd</sup> best docking pose of theaflavin with JARID 1B (solid rendering); (F) The 2<sup>nd</sup> best docking pose of theaflavin-3,3'-digallate with JARID 1B (cartoon rendering); (f) The 2<sup>nd</sup> best docking pose of theaflavin-3,3'-digallate with JARID 1B (solid rendering). The corresponding MM/PBSA analyses results have been shown below the figures.

of theaflavin-3,3'-digallate for the JmjC domain of JARID1B is higher than theaflavin.

Time evolution and variation in different energy components as observed from molecular dynamical simulations of JARID1B with theaflavin-3,3'-digallate for the top docking pose are shown in Figure 4.43. We chose to include the results for the top docking pose of theaflavin-3,3'-digallate due to its higher affinity for docking with JARID1B.

#### **4.26. Histological analysis of the co-carcinogenicity of iAs.**

Figure 4.44 displays the representative haematoxylin and eosin-stained images of histological analysis, of DMBA and DMBA+iAs treated Swiss albino mice, at different time points. The study was performed to analyse the co-carcinogenicity of iAs. Analysis of the skin tissue and lesions of the DMBA treated mice revealed development of hyperplasia, dysplasia, in-situ carcinoma and invasive carcinoma at 60, 120, 240 and 300 days respectively. The DMBA+iAs treated mice developed severe dysplasia at 60 days of treatment, in-situ carcinoma at 120 days and invasive carcinoma at 240 days. Invasive carcinogenic histological modifications were visible in the DMBA treated mice only after 300 days of treatment, whereas in the DMBA+iAs treated mice it was achieved at 240 days. This result highlights the co-carcinogenic potential of iAs where it enhances the carcinogenicity of DMBA, by early development of invasive carcinoma.

#### **4.27. Assessment of ROS generation, DNA, lipid and protein damage in DMBA and DMBA+iAs treated mice.**

The line graphs represented in the Figures 4.45A, 4.45B, 4.46A and 4.46B represent estimation of ROS generation, DNA damage (Comet assay,

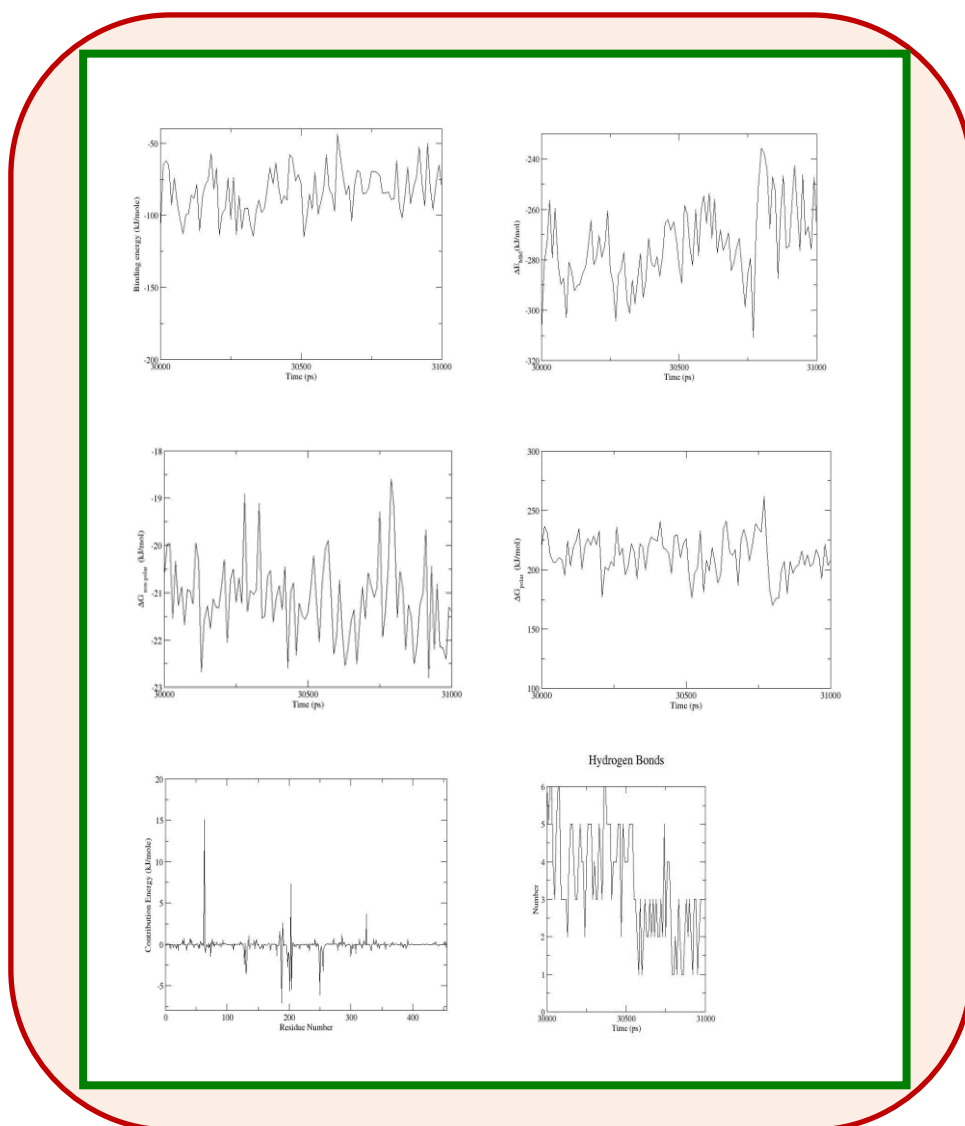


**Figure 4.43:** Analysis of different energy values for the binding of the top pose of theaflavin-3,3'-digallate with JARID1B between 30-31 ns of Gromacs simulation. (a) total binding energy-low total binding energy indicates stable docking; (b) MM energy; (c) non-polar binding energy; (d) polar binding energy; (e) per residue binding energy; (f) hydrogen bonds—the graph shows up to 6 hydrogen bonds, and at least 1 hydrogen bond during the simulation period between 30-31 ns.

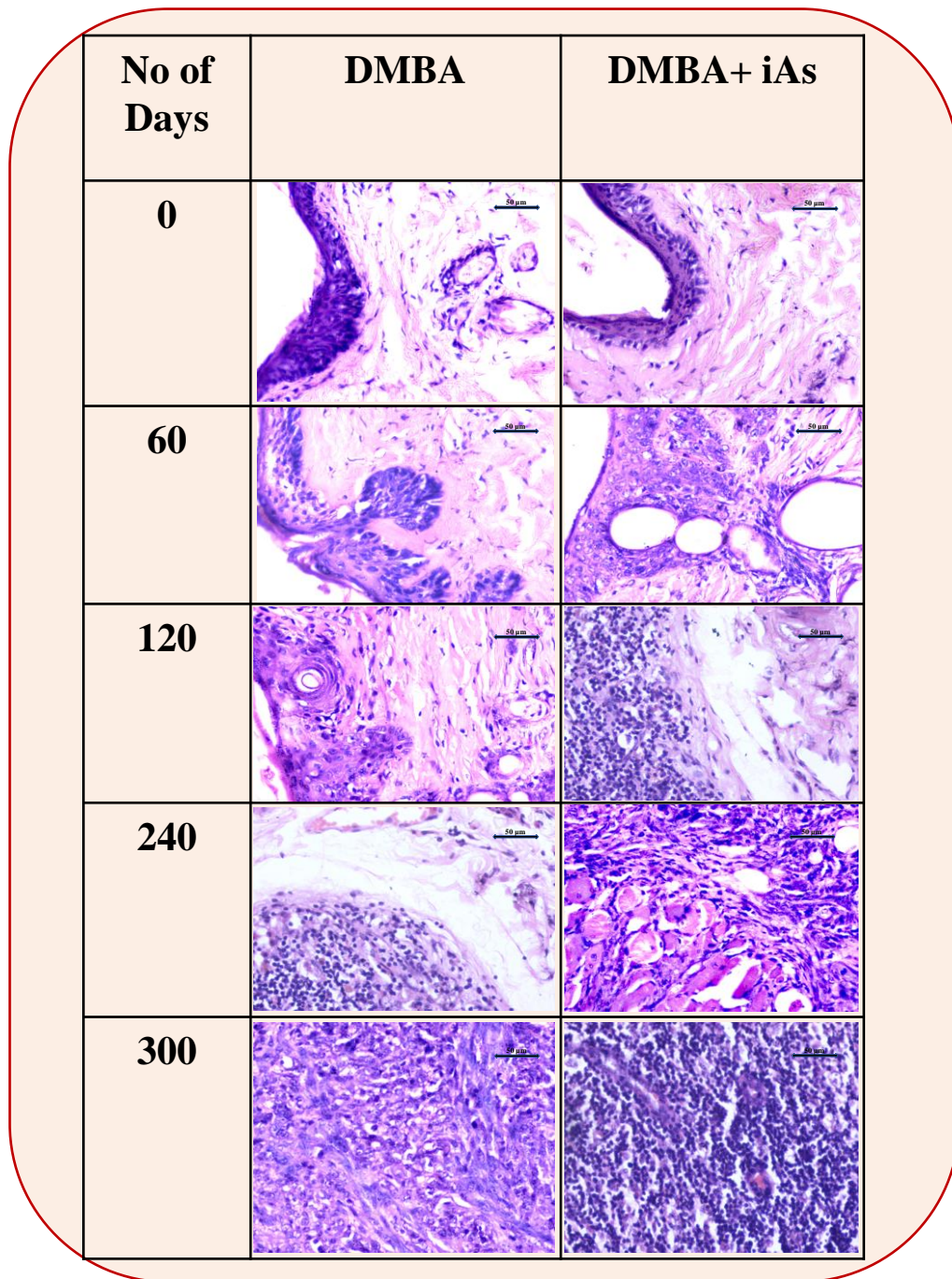


**Figure 4.44:** Histopathological studies during development of carcinogenesis at different time points. Tissue sections were stained by haematoxylin and eosin, visualised under a light microscope. Histological analysis reveals development of hyperplasia, dysplasia, in-situ carcinoma and invasive carcinoma at 0, 60, 120, 240 and 300 days respectively for DMBA treated group. In DMBA+iAs treatment group, dysplasia, in-situ carcinoma and invasive carcinoma were observed at 60, 120 and 240 days respectively; beyond 240 days (upto 300 days) of DMBA+iAs treatment, most of the mice died and histological analysis revealed presence of severe invasive carcinoma in them. Representative photographs were captured at 400x magnification.

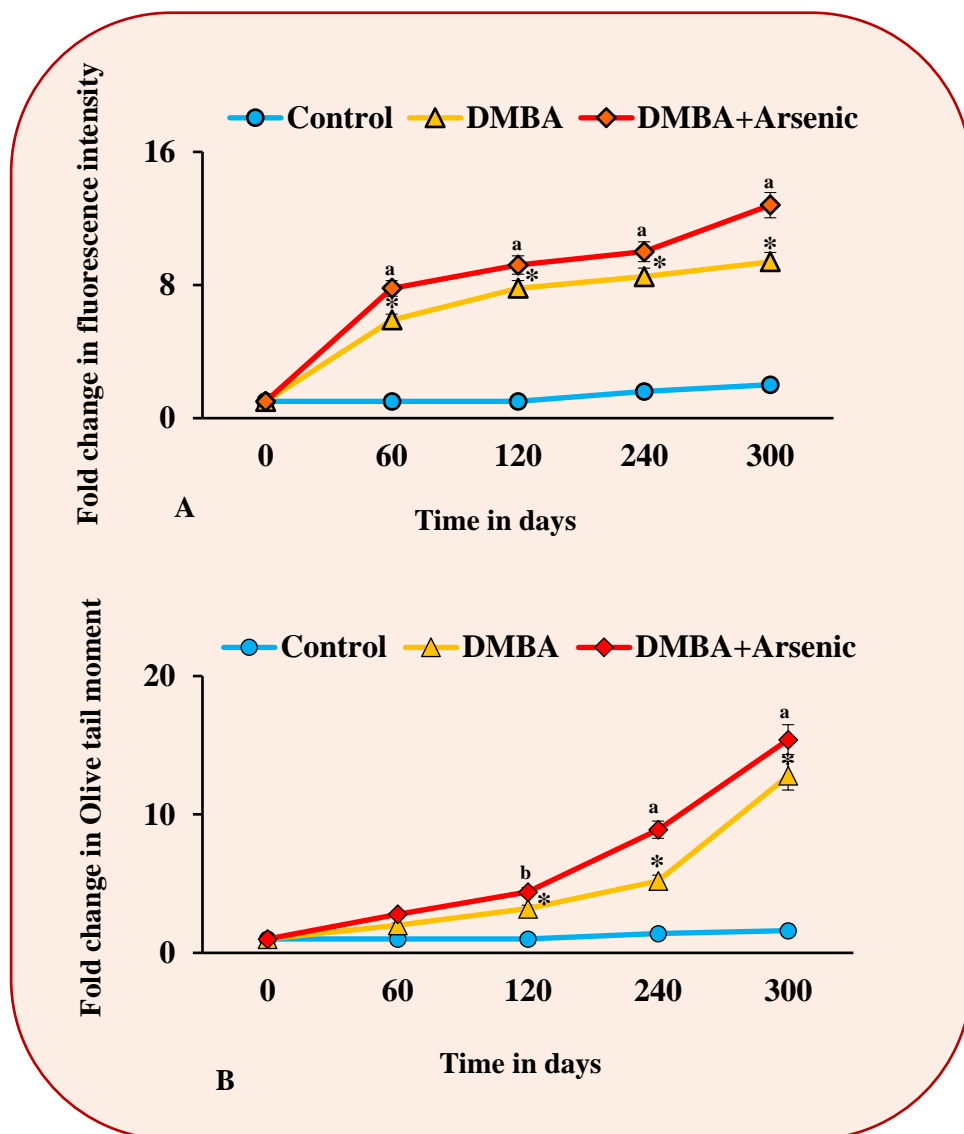


**Figure 4.45:** Estimation of ROS generation and DNA damage by DMBA alone or in conjunction with iAs

**Figure 4.45A** represents a line graph displaying ROS generation in the control, DMBA and DMBA+iAs treated Swiss albino mice, using spectrofluorometer, at 0, 60, 120, 240 and 300 days respectively. ROS generated in the DMBA+iAs treated mice is higher than DMBA treated group. The cells were stained with DCFDA.

**Figure 4.45B** represents a line graph displaying Olive tail moment, estimated in the leukocytes of the Swiss albino mice, at 0, 60, 120, 240 and 300 days of treatment. Olive tail moment is used to measure DNA damage and is estimated by Comet assay. DNA damage is higher in the DMBA+iAs treated group, than the DMBA treated mice.

Values are average of three independent experiments  $\pm$  SD.

Increase of ROS generation and Olive tail moment in the DMBA treated group is significant at  $*p < 0.0001$ , with respect to the control group.

Increase of ROS generation and Olive tail moment in the DMBA+iAs treated mice is significant at  $^ap < 0.0001$  and  $^bp < 0.001$ , with respect to the DMBA group.

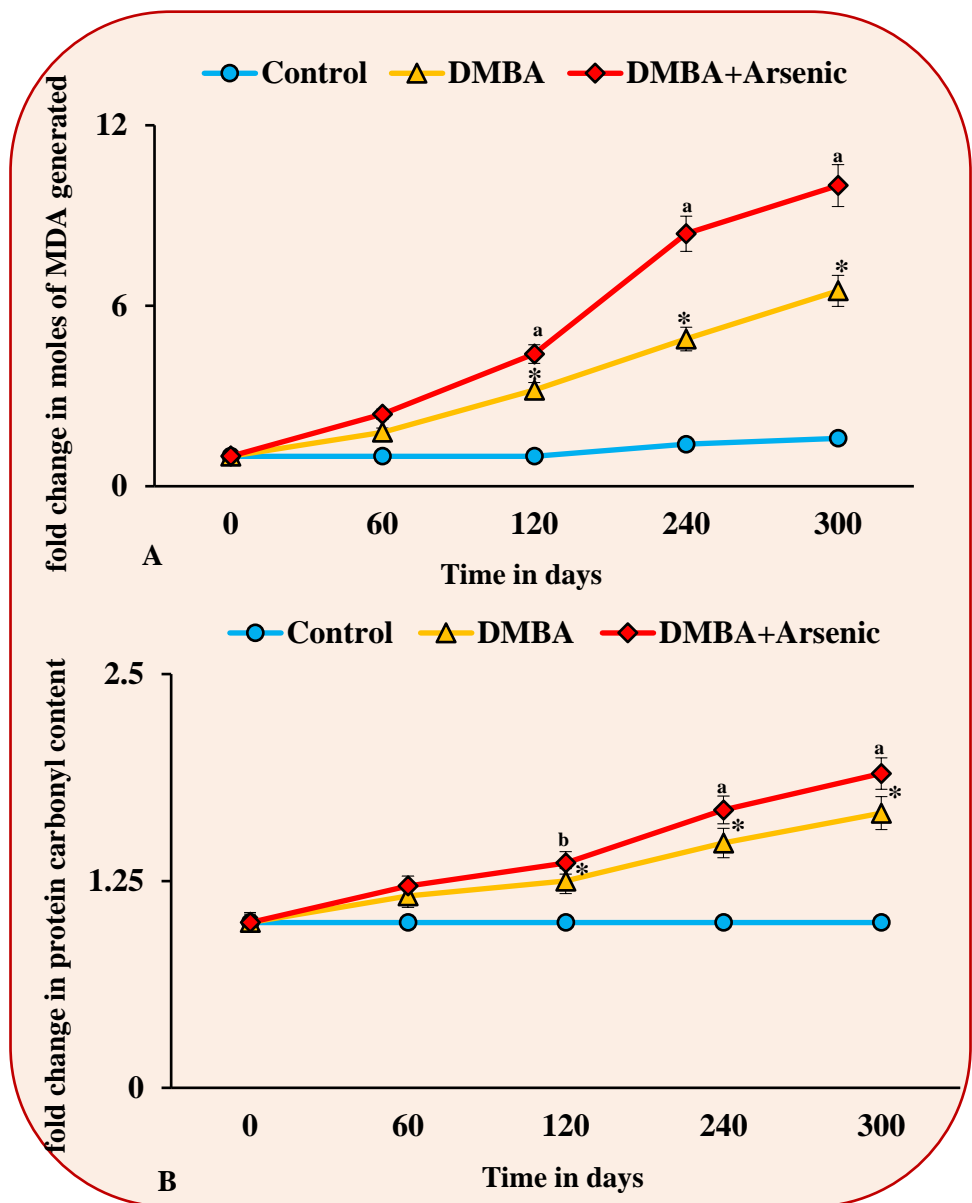


**Figure 4.46:** Estimation of lipidperoxidation generation and protein carbonyl content by DMBA alone or in conjunction with iAs

**Figure 4.46A** represents a line graph displaying MDA generation in the control, DMBA and DMBA+iAs treated Swiss albino mice, using spectrophotometer, at 0, 60, 120, 240 and 300 days respectively. MDA generated in the DMBA+iAs treated mice is higher than DMBA treated group.

**Figure 4.46B** represents a line graph displaying protein carbonyl content estimated in the tissue lysate of the Swiss albino mice, at 0, 60, 120, 240 and 300 days of treatment. Protein carbonyl content is higher in the DMBA+iAs treated group, than the DMBA treated mice.

Values are average of three independent experiments  $\pm$  SD.

Increase of MDA generation and protein carbonyl content in the DMBA treated group is significant at  $^*p < 0.0001$ , with respect to the control group.

Increase of MDA generation and protein carbonyl content in the DMBA+iAs treated mice is significant at  $^ap < 0.0001$  and  $^bp < 0.001$ , with respect to the DMBA group.

Olive tail moment), lipid peroxidation and protein carbonyl formation in the DMBA and DMBA+iAs treated mice. The results indicate that ROS generation, DNA , lipid and protein damage in the DMBA+iAs treated mice is prominently higher than the DMBA treated mice. According to these results, iAs enhances cellular damage caused by DMBA thus its carcinogenic ability.

**4.28. Estimation of total antioxidative capacity in DMBA and DMBA+iAs treated mice.**

The line graph in Figure 4.47 shows the total antioxidative capacity of DMBA and DMBA+iAs treated mice. The results indicate that antioxidative capacity in the DMBA+iAs treated mice is much lower than the DMBA treated mice. These findings suggest that iAs decreases the antioxidative capacity further, promoting free radical accumulation and cellular damage than DMBA alone could do.

**4.29. Assessment of the activity of pro-inflammatory cytokines and two subunits of NFκB p50 and p65.**

The bar graphs in the Figures 4.48A and 4.48B represents the activity of the pro-inflammatory cytokines TNF- $\alpha$ , IL6, IL17a and IL22. The results of these activity assays indicate that activity of pro-inflammatory cytokines is definitively upregulated in the DMBA+iAs treated mice than the DMBA group. The bar graph in the Figure 4.49 shows that, the activity of p50 and p65 is higher in the DMBA+iAs treated mice group than the DMBA treated group. These results highlight that iAs increases the carcinogenicity of DMBA by greatly upregulating the activity of pro-inflammatory cytokines and their downstream transcription factors.

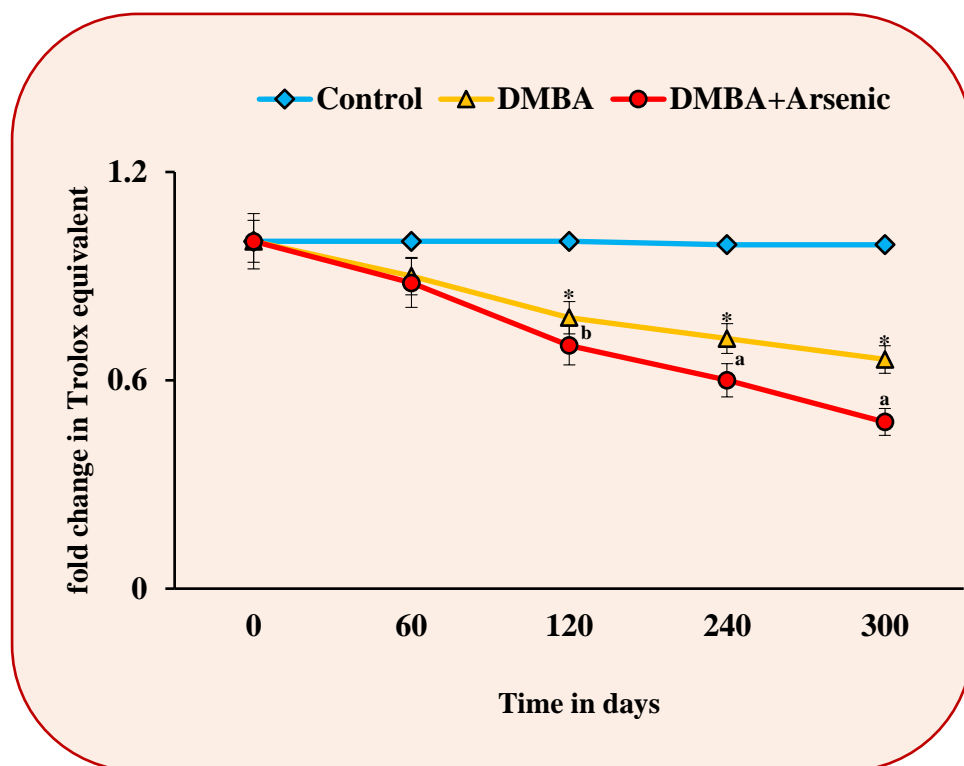


**Figure 4.47:** Estimation of total antioxidant capacity by DMBA alone or in conjunction with iAs. Total antioxidant capacity was expressed as Trolox equivalent (Compared against the antioxidant capacity of Trolox, a tocopherol analogue). The line graph displays fold change in Trolox equivalent, in control, DMBA and DMBA+iAs treated Swiss albino mice, at 0, 60, 120, 240 and 300 days respectively. Total antioxidant capacity of the DMBA+iAs treated mice is lower than that of the DMBA treatment group. Values are mean of three independent experiments  $\pm$  SD.

Lowering of total antioxidant capacity in the DMBA treated mice is significant at  $^*p < 0.0001$ , with respect to the control group.

Lowering of total antioxidant capacity in the DMBA+iAs treated mice is significant at  $^ap < 0.0001$  and  $^bp < 0.001$ , with respect to the DMBA treated mice.



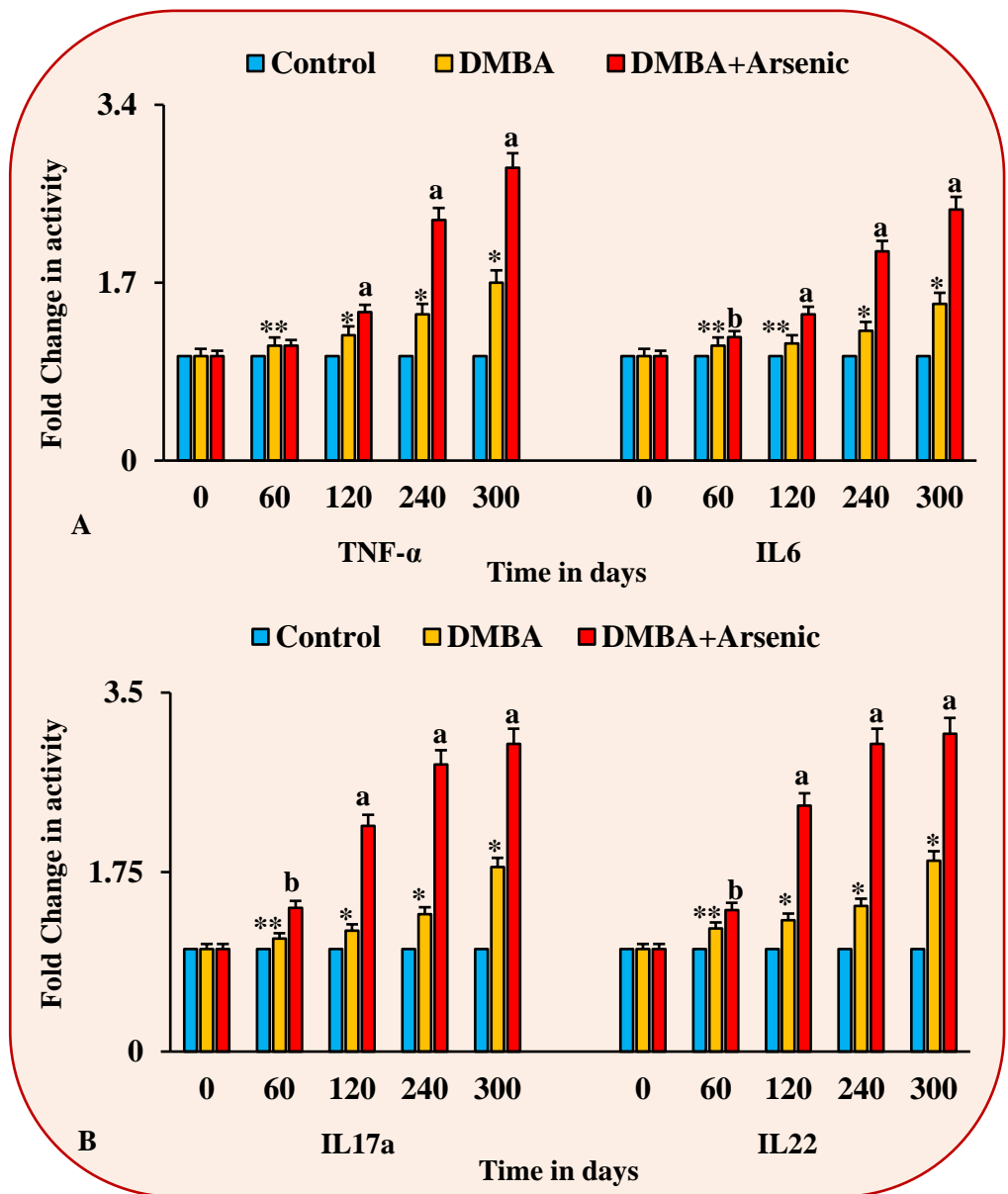


**Figure 4.48:** Estimating the activity of pro-inflammatory cytokines like TNF- $\alpha$ , IL6, IL17a and IL22 by DMBA alone or in conjunction with iAs.

**Figure 4.48A** displays a bar graph showing fold change in activity of TNF- $\alpha$  and IL6, in the control, DMBA and DMBA+iAs treated Swiss albino mice at 0, 60, 120, 240 and 300 days of treatment. The activity of TNF- $\alpha$  and IL6 in DMBA+iAs treated mice is much higher than that of the DMBA group.

**Figure 4.48B** displays a bar graph showing fold change in activity of proinflammatory cytokines like IL17a and IL22, in the control, DMBA and DMBA+iAs treated mice at 0, 60, 120, 240 and 300 days of treatment. Activity of IL17a and IL22 appear to be elevated in the DMBA+iAs treated mice with respect to the DMBA group.

Values are mean of three independent experiments  $\pm$  SD. Increase of activity in the DMBA treated group is significant at \* $p < 0.0001$  and \*\* $p < 0.001$ , with respect to the control group. Increase of activity in the DMBA+iAs treated mice is significant at <sup>a</sup> $p < 0.0001$  and <sup>b</sup> $p < 0.001$ , with respect to the DMBA group

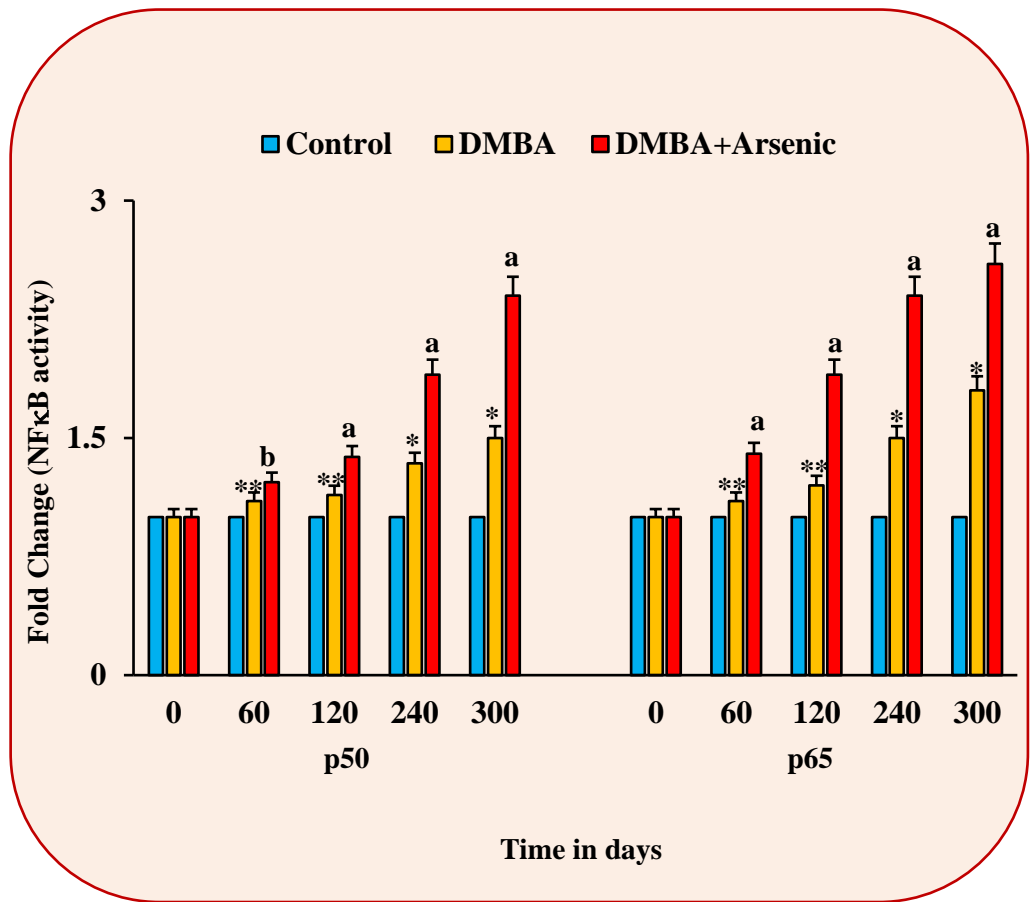


**Figure 4.49:** Estimating the activity of p50 and p65, two subunits of NFκB, by DMBA alone or in conjunction with iAs. The figure displays a bar graph showing fold change in activity of p50 and p65, in the control, DMBA and DMBA+iAs treated mice at 0, 60, 120, 240 and 300 days of treatment. Activity of p50 and p65 appear to be elevated in the DMBA+iAs treated mice with respect to the DMBA group. Values are mean of three independent experiments  $\pm$  SD. Increase of activity in the DMBA treated group is significant at \* $p < 0.0001$  and \*\* $p < 0.001$ , with respect to the control group. Increase of activity in the DMBA+iAs treated mice is significant at <sup>a</sup> $p < 0.0001$  and <sup>b</sup> $p < 0.001$ , with respect to the DMBA group

A microscopic image of a cell culture, likely a monolayer of cells, is centered within a circular frame. The cells are densely packed and exhibit a granular, purple-hued appearance. The circular frame is set against a light green background with rounded corners. The text "in vitro model" is overlaid in red, italicized font across the center of the cell culture image.

***in vitro model***

### **C. *in vitro* RESULTS**

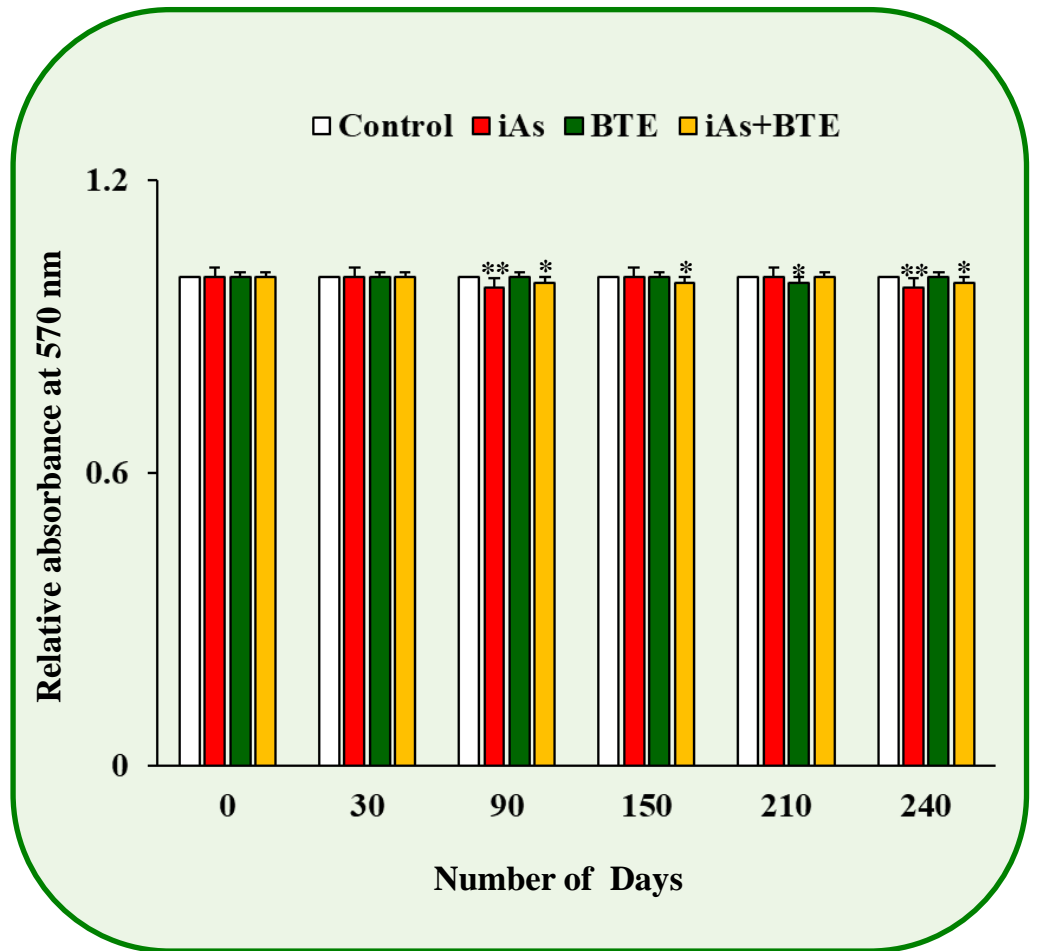
#### **4.30. Assessment of non-toxicity of the selected doses used to treat HaCaT cells.**

The bar graph shown in the Figure 4.50 shows viability of the cells treated with the selected doses of iAs (100 nM), BTE (1  $\mu$ M) and iAs + BTE (100 nM+ 1  $\mu$ M), at different time points of treatment (30, 90, 150, 210 and 240 days). The result of the viability assay showed that the administered doses of iAs (100 nM), BTE (1  $\mu$ M) and that of iAs + BTE (100 nM + 1  $\mu$ M) showed no toxicity in HaCaT cells throughout the study.

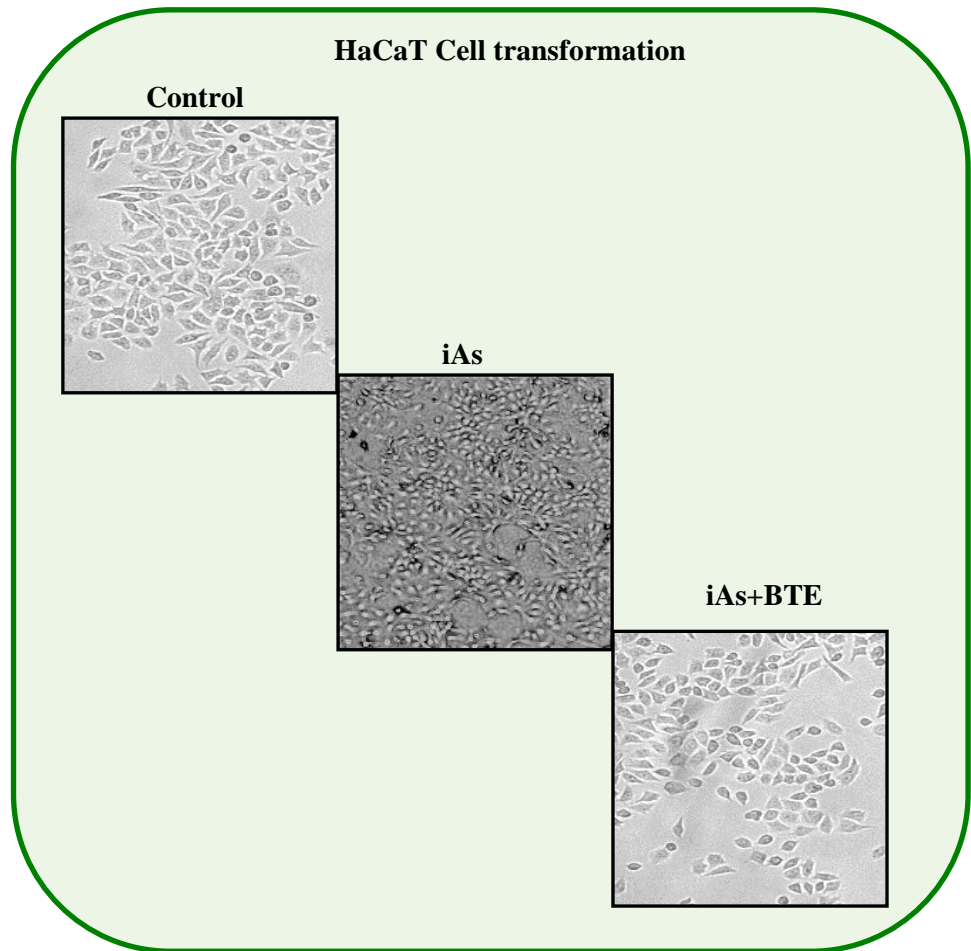
#### **4.31. Cell transformation and alteration of doubling time of HaCaT cells.**

Figure 4.51 displays the photographs of the control, iAs, iAs+BTE treated cells at the end of 240 days. The images show that, iAs treated cells had altered morphology compared to the control cells, these cells seemed to pile up and form dense aggregates. Some of these cells grew on top of other cells indicating loss of contact inhibition. BTE treated cells did not show any morphological transformation, nor loss of contact inhibition, even after receiving the similar dose of iAs for the same time period.

Table 4.14 displays the doubling time of the HaCaT cells in hours at different time points of treatment. Fold change in doubling time has been displayed as a line graph in the Figure 4.52. These results clearly indicate that with chronic treatment of iAs, the doubling time of the cells was significantly ( $p < 0.0001$ ) reduced at 150, 210 and 240 days of treatment. The iAs+BTE treated HaCaT cells did not show such prominent reduction of doubling time, rather these cells had significantly ( $p < 0.0001$ ) higher doubling time than their iAs treated counterparts.



**Figure 4.50:** Toxicity of iAs, BTE and iAs + BTE at different time points. The figure displays a bar graph representing the toxicity of the selected doses of iAs (100 nM), BTE (1  $\mu$ M) and iAs + BTE (100 nM + 1  $\mu$ M) at different time points of treatment (0, 30, 90, 150, 210 and 240 days respectively), with respect to the control. The toxicities were insignificant at (\* $p=0.012$ , \*\* $p=0.006$ ). Values are mean of three independent experiments  $\pm$  SD.



**Figure 4.51:** Transformation of HaCaT cells. The figure depicts morphological transformation of HaCaT cells at 240 days of exposure. iAs exposed HaCaT cells showed piling up, aggregation and loss of contact inhibition at 240 days. These transformations are not observed in control and iAs + BTE treated cells. Images were captured at 200x.

**Table 4.14:** Doubling time of the HaCaT cells. Doubling time of control, iAs and iAs+BTE treated HaCaT cells at different time points of treatment have been depicted in tabular form. iAs transformed cells showed much lowered doubling time than the iAs+BTE treated cells.

Treatment	Doubling time at different treatment time points					
	0 days	30 days	90 days	150 days	210 days	240 days
Control	28	28	28	28	27.44	27.16
iAs	28	27.72	25.2	22.4	19.04	14
iAs+BTE	28	28	26.88	25.76	25.2	24.64

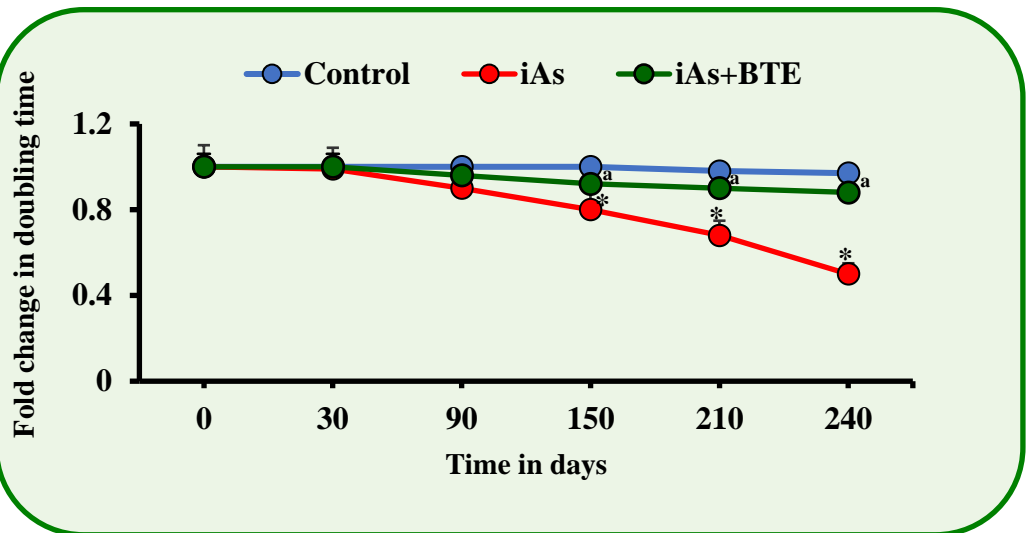


**Figure 4.52:** Fold change in doubling time. The line graph depicts fold change in doubling time in the control, iAs and iAs+BTE treated HaCaT cells, at 0, 30, 90, 150, 210 and 240 days of treatment. iAs transformed cells showed much lowered doubling time than the iAs+BTE group. Values are mean of three independent experiments  $\pm$  SD.

Lowering of doubling time in the iAs treated cells is significant at  $*p < 0.0001$ , with respect to the control cells.

Increase of doubling time in the iAs+BTE treated cells is significant at  $^ap < 0.0001$ , with respect to the iAs treatment group.

#### **4.32. Estimation of the proliferative index.**

Proliferative index of the HaCaT cells were assessed by performing the immunoblot assay for the proliferative marker Ki-67. The representative immunoblot images of Ki-67, in the iAs and iAs+BTE treated cells, at different time points of treatment, have been displayed in the Figure 4.53A. The line graph depicted in the Figure 4.53B represents the fold change in band intensity of Ki-67. Immunoblot results indicate that, with chronic treatment of iAs, the expression of Ki-67 increased significantly at 150 ( $p<0.001$ ), 210 ( $p<0.0001$ ) and 240 ( $p<0.0001$ ) days. In the iAs+BTE treated cells, the expression of Ki-67 was significantly lower at 150 ( $p<0.001$ ), 210 ( $p<0.0001$ ) and 240 ( $p<0.0001$ ) days, than the iAs treated cells, suggesting that the BTE treated cells did not have high proliferative index as observed upon chronic iAs treatment.

#### **4.33. Estimation of ROS generation in the HaCaT cells.**

The bar graph depicted in the Figure 4.54A represents the spectrofluorometric estimation of ROS generation in the HaCaT cells. The results clearly indicate that upon chronic treatment with iAs, free radical generation is effectively upregulated, while in the BTE treated counterpart, the generation of free radicals seems to be prominently quenched. Representative histograms images visible in the Figure 4.54B, depicts the estimation of ROS generation by flowcytometric analysis, at 240 days of treatment. The flowcytometric studies of ROS generation in HaCaT cells also reverberate our spectrofluorometric results, suggesting higher ROS generation in the iAs treated cells and its effective quenching in the BTE treated cells.



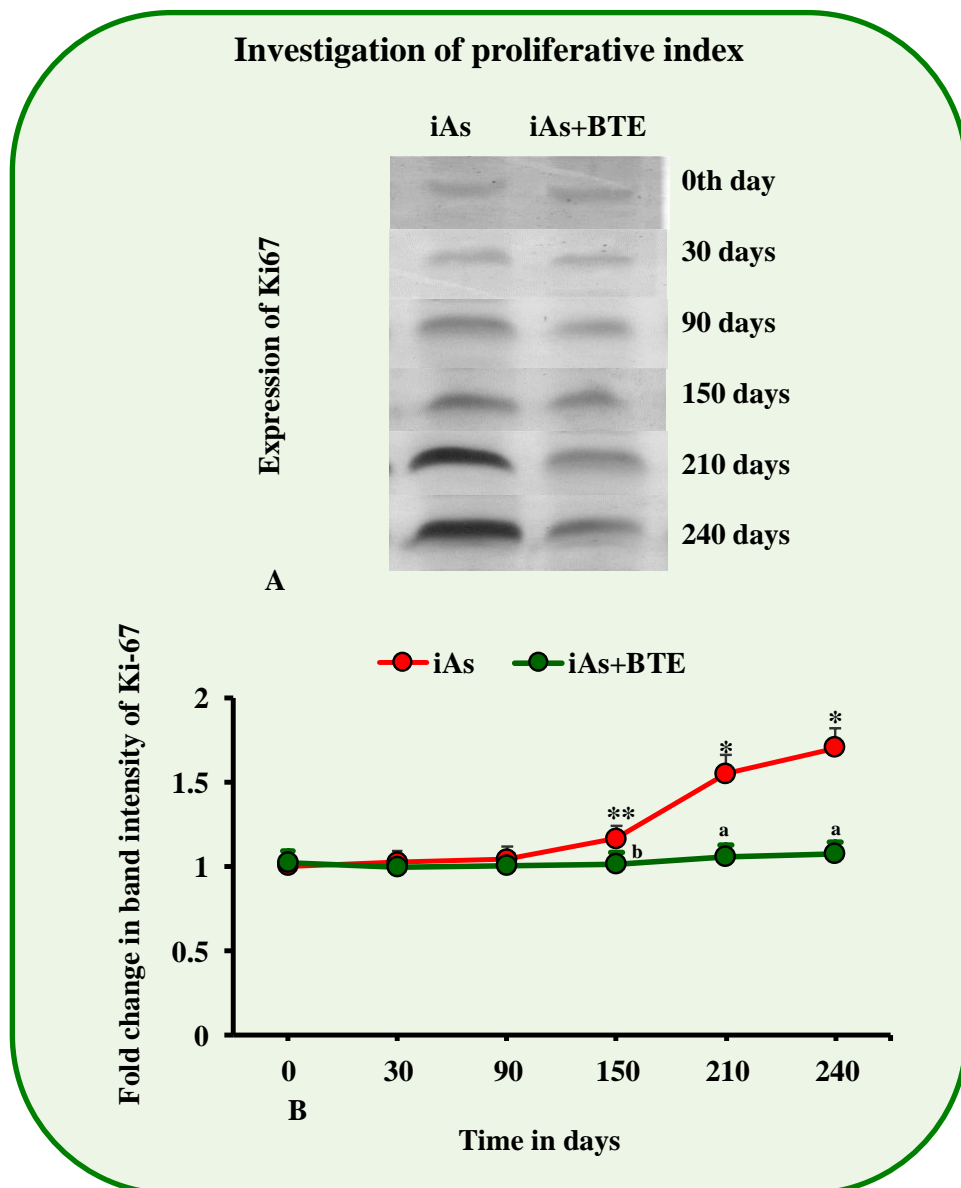


**Figure 4.53:** Estimating the proliferative index of HaCaT cells.

**Figure 4.53A** displays representative images of the immunoblot bands for Ki-67 in iAs and iAs + BTE treated HaCaT cells, at 0, 30, 90, 150, 210 and 240 days respectively.

**Figure 4.53B** represents fold change in mean band intensities of Ki-67 in a linear graph.

Values are mean of three independent experiments  $\pm$  SD.

Fold change (increase) of mean band intensities of the iAs treated cells is significant at  $^*p < 0.0001$  and  $^{**}p < 0.001$ , with respect to the control cells.

Fold change (decrease) of mean band intensities of the iAs+BTE treated cells is significant at  $^ap < 0.0001$  and  $^bp < 0.001$ , with respect to the iAs treatment group.

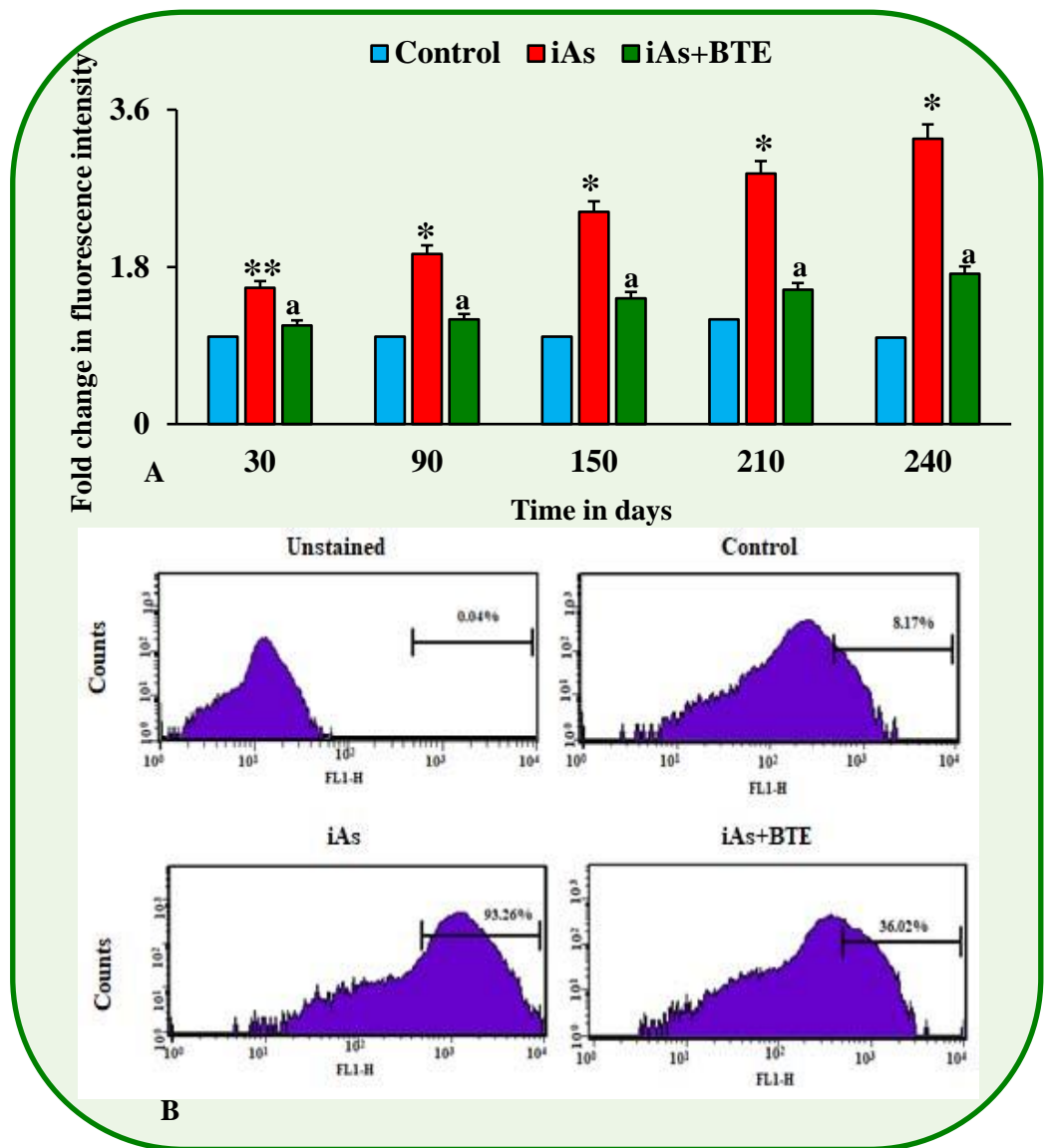


**Figure 4.54:** Determination of ROS by spectrofluorimetric & flowcytometric analysis in HaCaT cells.

**Figure 4.54A** displays a bar graph representing ROS generation in the control, iAs and iAs+BTE treated HaCaT cells, at 30, 90, 150, 210 and 240 days of treatment. Results indicate higher ROS generation in cells treated with iAs, which is much less in the iAs+BTE group.

**Figure 4.54B** displays histograms representing the percentage of ROS generating HaCaT cells, as assessed by flowcytometric studies, at 240 days of treatment. The histogram of iAs transformed cells shows a prominent right shift of the fluorescence channel-1 peak with respect to the control, indicating excess ROS generation. Histogram peak of iAs + BTE treated cells shows a left shift, compared to the iAs group, suggesting quenching of ROS. The proportions of ROS generating cells in the control, iAs and iAs + BTE treatment groups are 8.17%, 93.26%, and 36.02%, respectively.

Values are mean of three independent experiments  $\pm$ S.D. Increase in ROS generation, in iAs treated cells is significant at  $*p < 0.0001$  and  $**p < 0.001$ , with respect to the control. Decrease in ROS generated in the iAs+BTE group is significant at  $^ap < 0.0001$ , with respect to the iAs treated cells.

#### **4.34. Estimation of RNS generation in HaCaT cells.**

The bar graph displayed in the Figure 4.55 represents the spectrophotometric analysis of RNS generation in the HaCaT cells. RNS generation was measured using Griess' reagent. According to the obtained results, chronic treatment with iAs resulted in excess RNS generation in the HaCaT cells which appeared to be effectively quenched in the iAs+BTE treated cells.

#### **4.35. Estimation of DNA damage in HaCaT cells.**

DNA damage in HaCaT cells has been estimated by both micronuclei assay and comet assay. The bar graph depicted in Figure 4.56A represents the frequency of micronuclei formation per 1000 binucleated cells. The representative photographs of micronuclei formation using Giemsa and Hoechst 33342 staining have been depicted in Figure 4.56B. According to the obtained results, the frequency of micronuclei formation in the iAs treated cells is significantly ( $p < 0.0001$ ) higher than the control HaCaT cells, at every time point of treatment. In the iAs+BTE treated cells, the frequency of micronuclei formation is significantly ( $p < 0.0001$ ) lower, than the iAs treated cells, indicating that BTE inhibits micronuclei formation and induction of DNA damage.

The bar graphs depicted in the Figures 4.57A and 4.57B represents comet tail length and Olive tail moment of the comet assays performed on the HaCaT cells. The results clearly suggest an increase in comet tail length and Olive tail moment of the iAs treated cells, indicating increased DNA damage. In the iAs+BTE treated cells, significant reduction of tail length and Olive tail moment hint at inhibition of DNA damage by BTE. Therefore, it may be

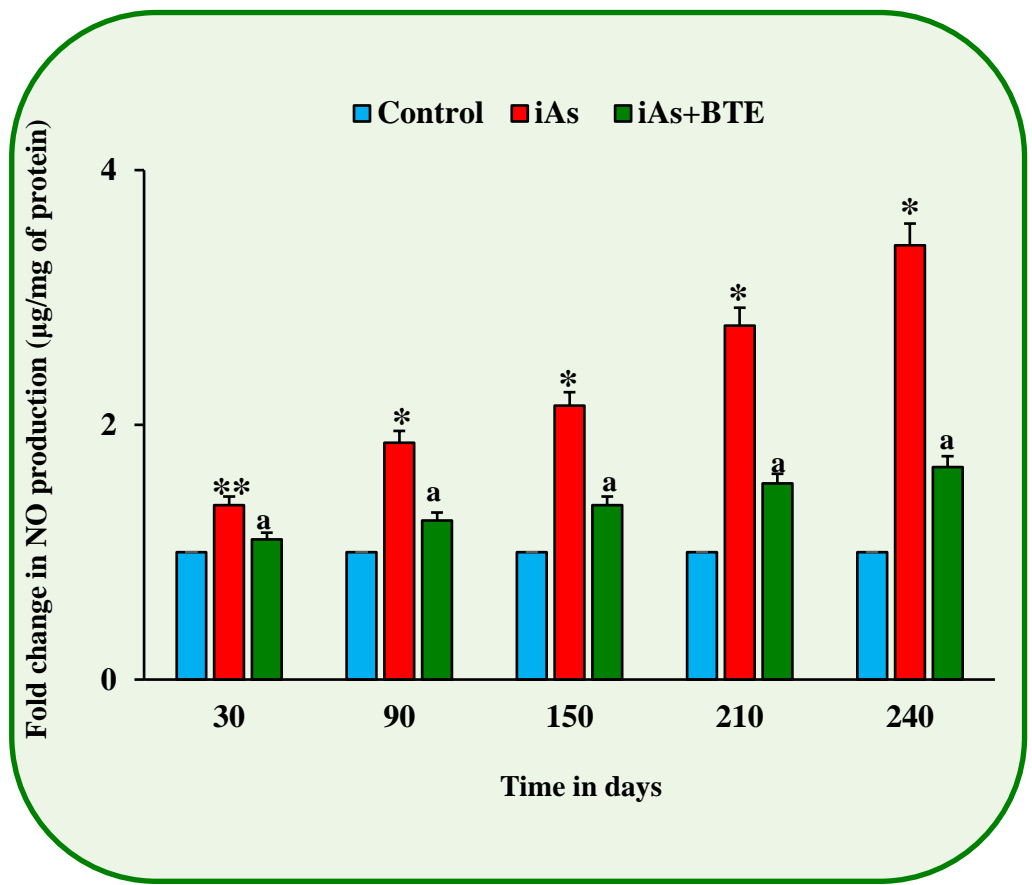


**Figure 4.55:** Determination of Reactive Nitrogen Species (RNS) generation using spectrophotometric analysis. The figure displays a bar graph representing RNS generation in control, iAs and iAs+BTE treated HaCaT cells, measured at 30, 90, 150, 210 and 240 days of treatment. Greiss reagent was used to determine generation of RNS. Chronic iAs exposure results in excess RNS generation which appears to be quenched in the iAs+BTE treated cells.

Values are mean of three independent experiments  $\pm$ S.D.

Increase in RNS generation, in iAs treated cells is significant at \* $p < 0.0001$  and \*\* $p < 0.001$ , with respect to the control.

Decrease in RNS generation in the iAs+BTE group is significant at <sup>a</sup> $p < 0.0001$ , with respect to the iAs treated cells.

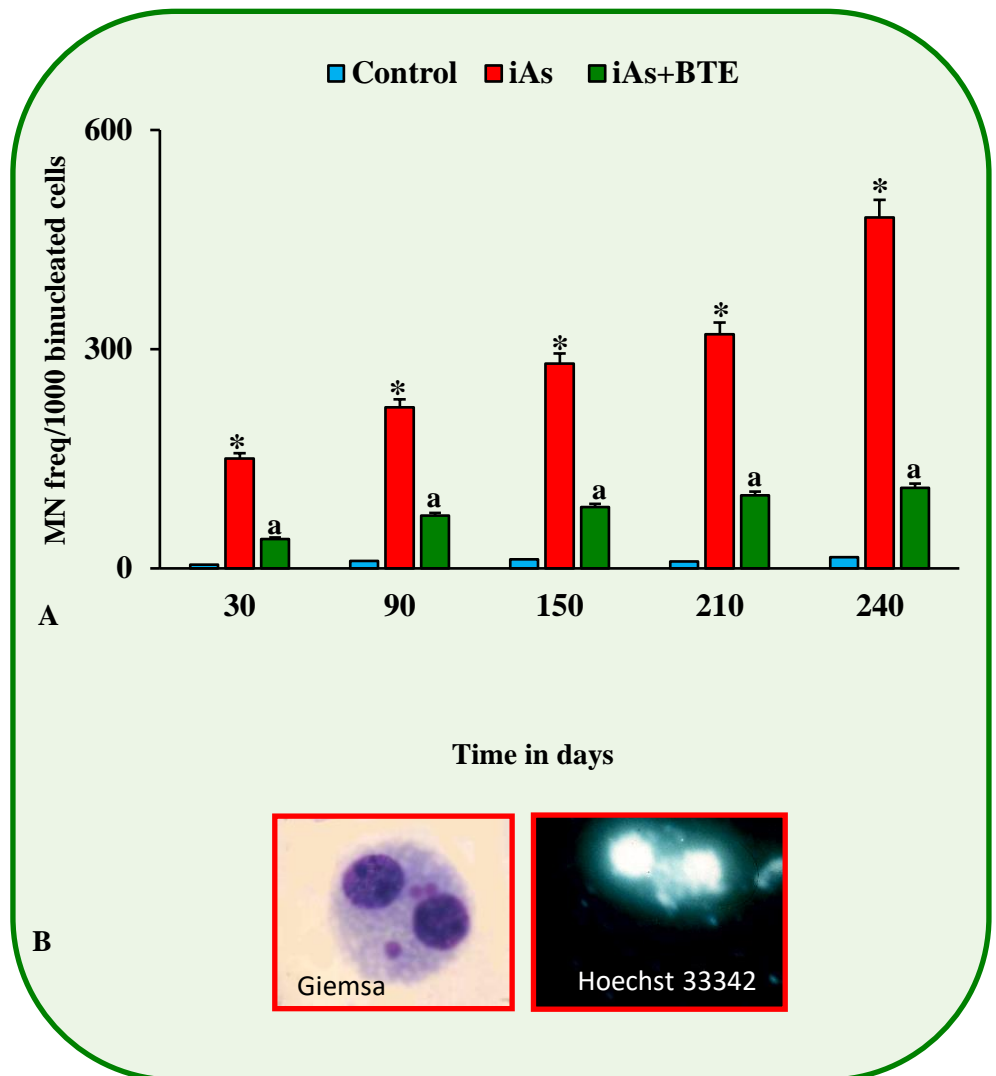


**Figure 4.56:** Determination of DNA damage using micronuclei assay.

**Figure 4.56A** displays a bar graph representing frequency of micronuclei formed per 1000 binucleated cells, in the HaCaT cells, at 30, 90, 150, 210 and 240 days of treatment. Chronic exposure to iAs led to elevated micronuclei frequency, while treatment with iAs+BTE resulted in its prominent suppression. Values are mean of three independent experiments  $\pm$ S.D.

Increase in micronuclei frequency in the iAs treated cells is significant at  $^*p < 0.0001$ , with respect to the control cells.

Decrease in micronuclei frequency, in the iAs+BTE treated cells is significant at  $^*p < 0.0001$ , with respect to the iAs treated cells.

**Figure 4.56B** displays representative images of micronuclei formation, stained with 5% Giemsa and Hoechst 33342 ( $1\mu\text{g/ml}$ ) respectively. Images of Giemsa stained slides were captured under a bright field microscope while those of Hoechst 33342 were captured under a fluorescent microscope. The images were captured at 1000X magnification

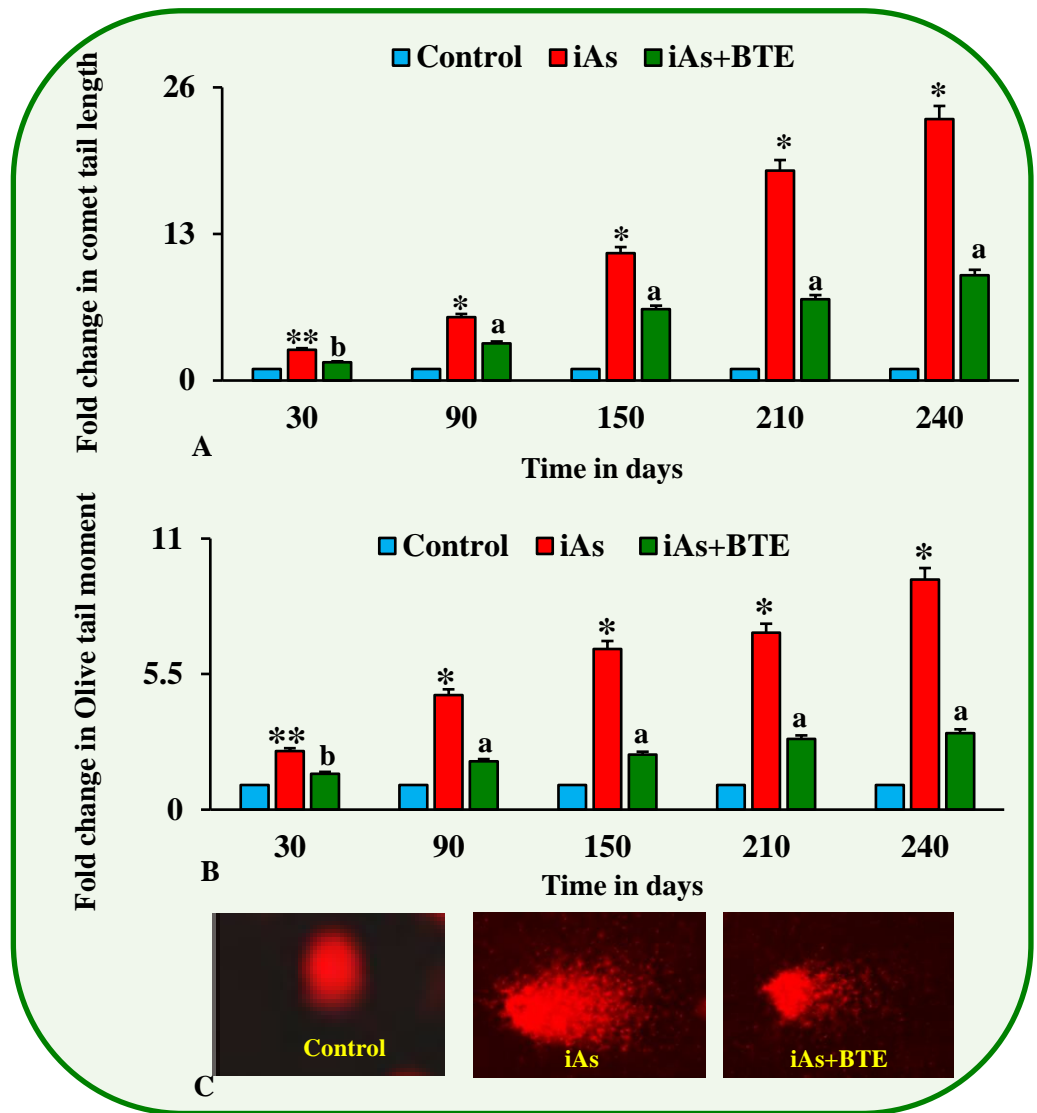


**Figure 4.57:** Determination of DNA damage using Single Cell Gel Electrophoresis (SCGE) or comet assay.

**Figure 4.57A** displays a bar graph representing mean comet tail length, in HaCaT cells, at 30, 90, 150, 210 and 240 days of treatment. Comet tail length is measured in  $\mu\text{m}$ . In iAs treated cells, it increases greatly with increase in treatment time while it is effectively decreased in the iAs+BTE treatment group.

**Figure 4.57B** displays a bar graph representing mean olive tail moment, in HaCaT cells, at 30, 90, 150, 210 and 240 days of treatment. Olive tail moment in iAs treated cells, is significantly elevated with increase in treatment time while it is suppressed in the iAs+BTE group. Increase in comet tail length and olive tail moment in the iAs treatment group, is significant at  $**p < 0.001$  and  $*p < 0.0001$ , compared to the control cells. Decrease of comet tail length and olive tail moment in the iAs+BTE treated cells is significant at  $^b p < 0.001$  and  $^a p < 0.0001$ .

Values are mean of three independent experiments  $\pm$ S.D.

**Figure 4.57C** displays representative images of comet formation in the respective treatment groups. The cells were stained with Ethidium Bromide and observed under a fluorescent microscope. The images were captured at 400X.

concluded that BTE effectively inhibits iAs induced DNA damage in HaCaT cells. Representative comet assay images have been displayed in the Figure 4.57C.

#### **4.36. Estimation of lipid and protein damage.**

The bar graphs depicted in Figures 4.58A and 4.58B represent MDA generation and protein carbonyl formation in HaCaT cells respectively. According to the obtained results, with chronic treatment of iAs, MDA generation and protein carbonyl formation in HaCaT cells increases remarkably, whereas, in the iAs+BTE treated cells both MDA generation and protein carbonyl formation are efficiently reduced. This result suggests increased lipid peroxidation and protein damage due to chronic iAs treatment, while, intervention by BTE reduces these cellular damages.

#### **4.37. Estimation of antioxidative capacity of HaCaT cells.**

Total antioxidative capacity and the activity of specific antioxidant enzymes like Catalase, SOD, GPx, GR, and GST have been represented as bar graphs in the Figures 4.59, 4.60A, 4.60B, 4.60C, 4.61A and 4.61B respectively. The results of these colorimetric assays clearly show, appreciable downregulation of total antioxidative capacity as well as the activity of individual antioxidant enzymes in the chronically iAs treated cells. In the iAs+BTE treated cells, the activity of the antioxidative enzymes was considerably higher than the iAs group indicating that, BTE enhanced the activities of antioxidant enzymes, which were depleted by iAs in the HaCaT cells.

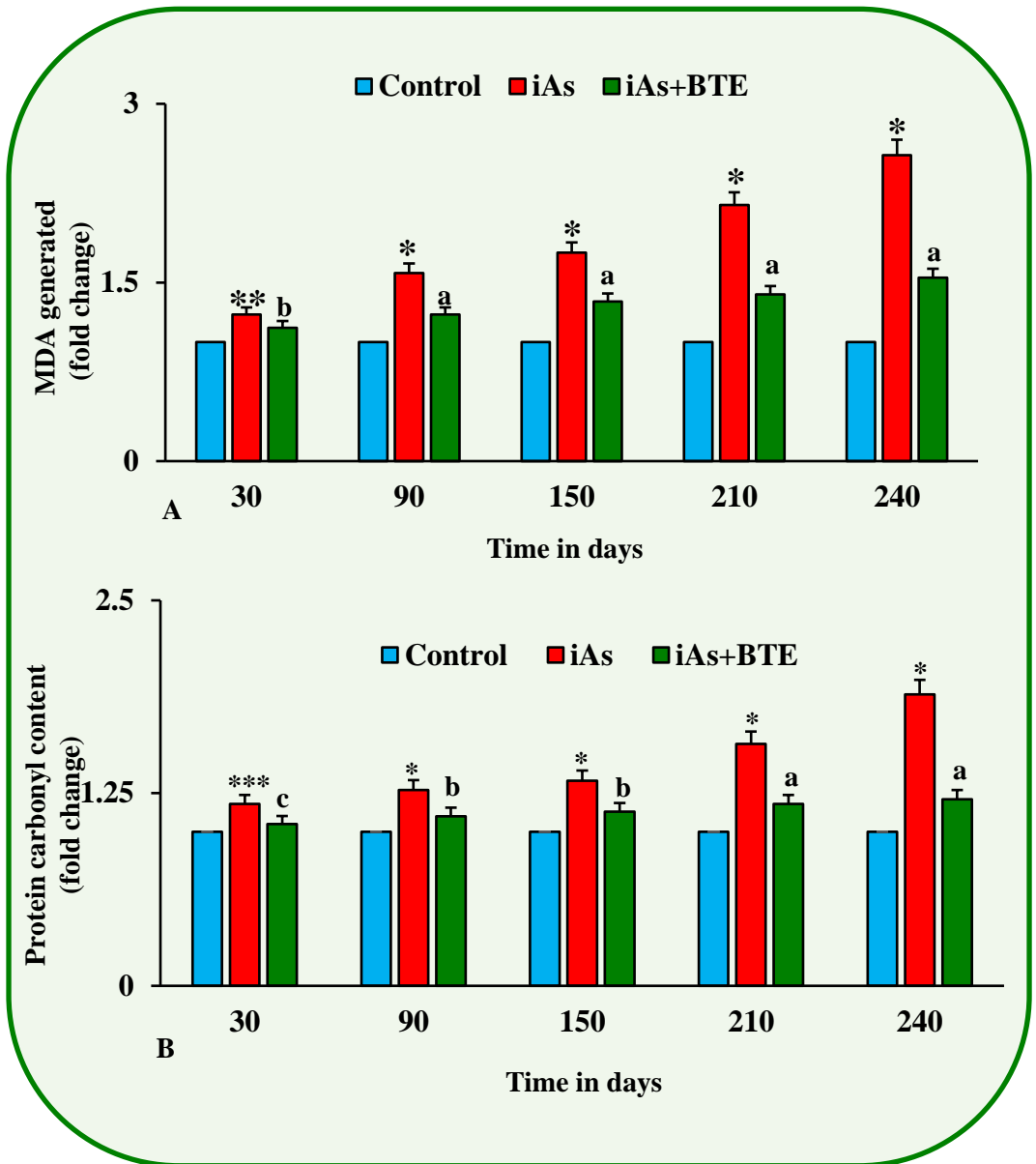


**Figure 4.58:** : Determination of lipid and protein damage.

**Figure 4.58A** displays a bar graph showing fold change in MDA generation, in HaCaT cells, at 30, 90, 150, 210 and 240 days of treatment. MDA generation increased with chronic iAs treatment, while in the iAs+BTE group, it is appreciably decreased.

**Figure 4.58B** displays a bar graph showing fold change in protein carbonyl content at 30, 90, 150, 210 and 240 days of treatment. Protein carbonyl formation showed an increasing trend with chronic iAs treatment, while intervention with BTE effectively reduced it.

Values are displayed as mean of three independent experiments  $\pm$ S.D.

Fold increase in MDA generation and protein carbonyl content, in the iAs transformed cells is significant at \*\*\* $p < 0.05$ , \*\* $p < 0.001$  and \* $p < 0.0001$ , with respect to the control group.

Fold decrease in MDA and protein carbonyl formation, in the iAs+BTE treated cells is significant at <sup>c</sup> $p < 0.05$ , <sup>b</sup> $p < 0.001$  and <sup>a</sup> $p < 0.0001$ , with respect to iAs group



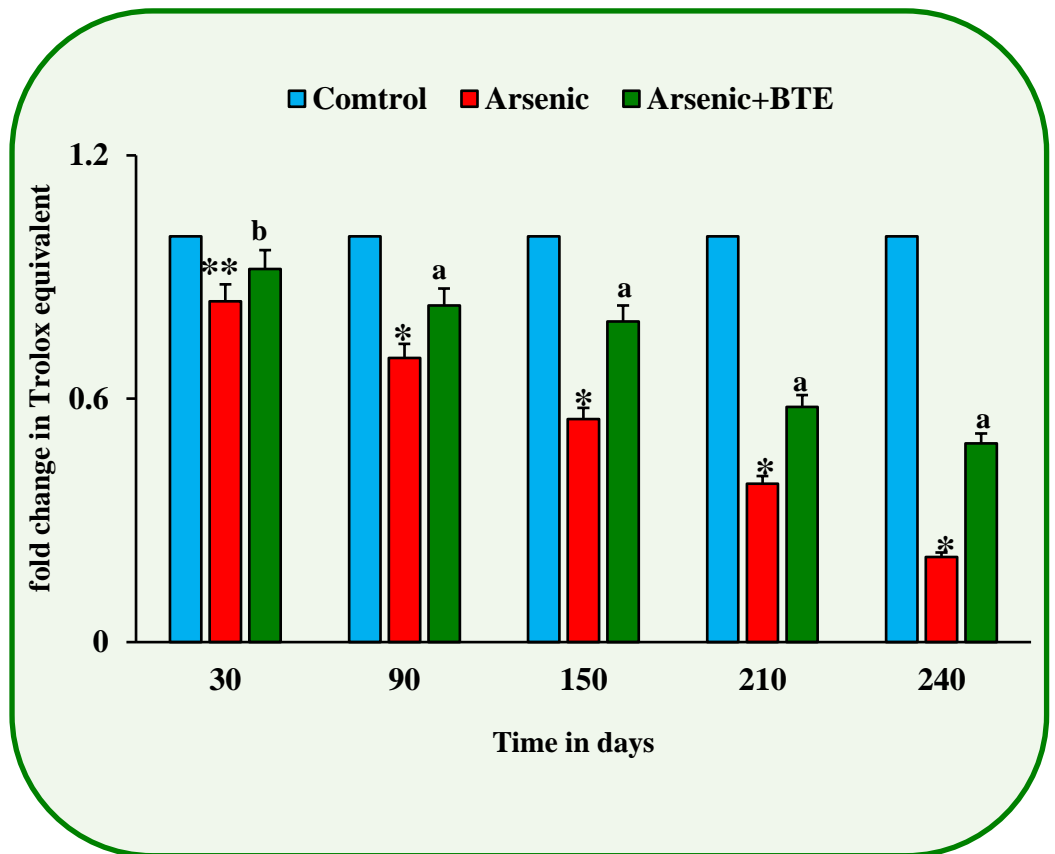


**Figure 4.59:** Determination of total antioxidant activity. Total antioxidant capacity was expressed as Trolox equivalent (Compared against the antioxidant capacity of Trolox, a tocopherol analogue). The bar graph displayed in the figure represents fold change of total antioxidative capacity, of HaCaT cell lysates, measured at 30, 90, 150, 210 and 240 days of treatment. Chronic iAs treatment results in prominent lowering of the total antioxidative capacity, while administration of BTE increased it effectively.

Values are calculated as mean of three independent experiments  $\pm$ S.D.

Fold decrease of Trolox equivalent, in iAs treatment group, is significant at \*\* $p < 0.001$  and \* $p < 0.0001$ , with respect to the control cells.

Fold increase of Trolox equivalent, in iAs+BTE treated cells, is significant at <sup>b</sup> $p < 0.001$  and <sup>a</sup> $p < 0.0001$ , with respect to the iAs treated cells.

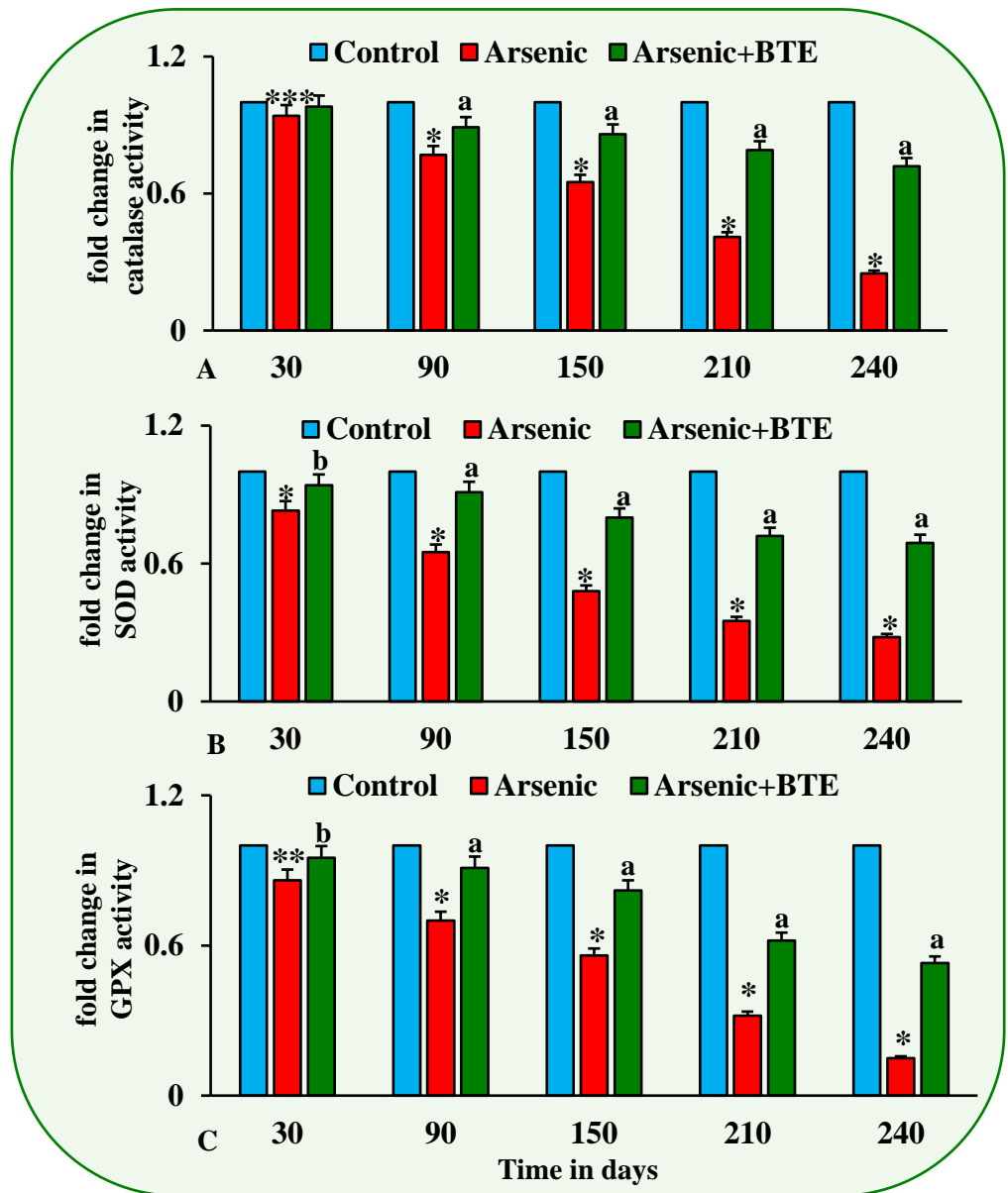


**Figure 4.60:** Determination of the activity of Catalase, SOD and GPx.

**Figure 4.60A** displays a bar graph showing fold change of Catalase activity, as measured in HaCaT cell lysates, at 30, 90, 150, 210 and 240 days of treatment. Catalase activity decreases remarkably in the iAs treated cells, while it is considerably high in the iAs+BTE treated cells.

**Figure 4.60B** displays fold change in SOD activity, in HaCaT cells, at 30, 90, 150, 210 and 240 days of treatment. Chronic iAs treatment results in effective suppression of SOD activity, while BTE treatment elevates its activity.

**Figure 4.60C** displays fold change of GPx activity, in HaCaT cells, measured at 30, 90, 150, 210 and 240 days of treatment. Chronic treatment with iAs results in prominent reduction in GPx activity, while in the iAs+BTE treatment group, it is increased. Values are calculated as mean of three independent experiments  $\pm$ S.D.

Reduction of activity in the iAs treated cells is significant at \*\*\* $p < 0.05$  \*\* $p < 0.001$  and \* $p < 0.0001$ , with respect to the control cells. Increase in activity in the iAs+BTE treated cells, is significant at <sup>b</sup> $p < 0.001$  and <sup>a</sup> $p < 0.0001$ , with respect to the iAs treatment group.

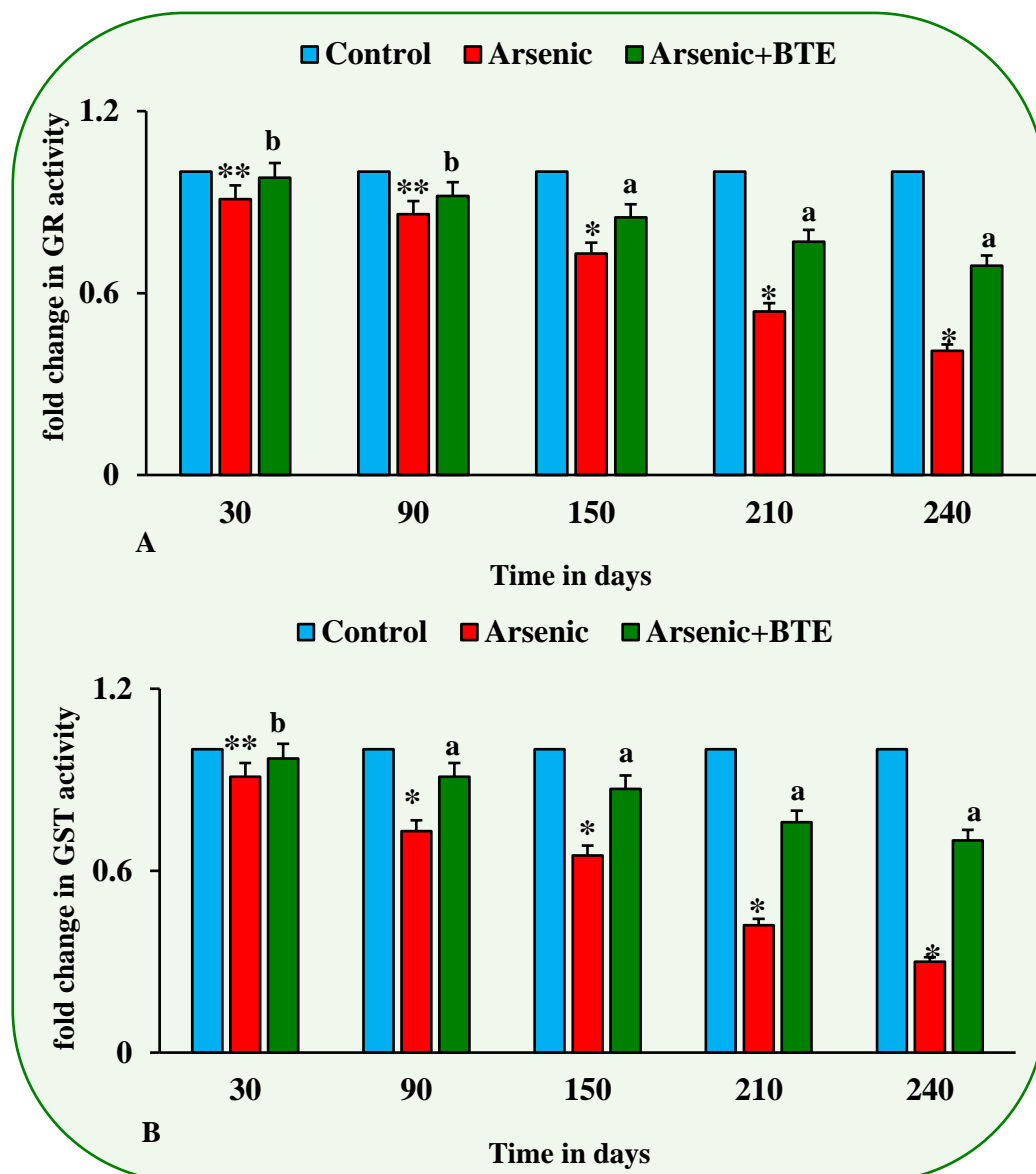


**Figure 4.61:** Determination of the activity of GR and GST.

**Figure 4.61A** displays a bar graph showing fold change in activity of GR, in HaCaT cells, at 30, 90, 150, 210 and 240 days of treatment. Appreciable reduction in activity of GR has been observed in the lysates of the HaCaT cells chronically treated with iAs, whereas the activity GR has been increased in the iAs+BTE treated cells.

**Figure 4.61B** displays a bar graph showing fold change in GST activity, in HaCaT cells, at 30, 90, 150, 210 and 240 days of treatment. iAs treated cells showed lowering of GST activity which is elevated in the iAs+BTE treatment group.

The values are calculated as mean of three independent experiments  $\pm$ S.D.

Decrease in activity of GR and GST in iAs treated cells is significant at  $**p < 0.001$  and  $*p < 0.0001$ , with respect to the control group.

Increase in activity of GR and GST in iAs+BTE treated cells is significant at  $^b p < 0.001$  and  $^a p < 0.0001$ , with respect to the iAs treated cells.

#### **4.38. Estimation of the activity of inflammatory cytokines and NF $\kappa$ B subunits in HaCaT cells**

The bar graphs depicted in Figures 4.62A and 4.62B represent fold change in activity of pro-inflammatory cytokines (TNF- $\alpha$ , IL2, IL6, IL8, IL13, IL17a and IL22) and anti-inflammatory cytokine (IL10). The results of the colorimetric activity assays reveal that, chronically iAs treated HaCaT cells showed remarkably higher activity of pro-inflammatory cytokines and lower activity of anti-inflammatory cytokine, while in the iAs+BTE treated cells, these findings are reversed. Therefore, according to the obtained results, iAs induces a chronic pro-inflammatory condition within the HaCaT cells by promoting the activity of pro-inflammatory cytokines and suppressing the activity of anti-inflammatory cytokine, whereas BTE inhibits this phenomenon.

Figures 4.63A and 4.63B depict bar graphs representing fold change in activity of p50 and p65 (NF $\kappa$ B subunits) respectively. P50 and p65 transcription factors act as downstream regulators of many inflammatory cytokines. According to the obtained results, the activities of both p50 and p65 are appreciably increased upon chronic iAs treatment, while in the iAs+BTE treatment group, they are remarkably suppressed. Thus, it appears that, BTE is able to effectively downregulate iAs induced elevated activity of p50 and p65.

#### **4.39. Modulation of the TGF- $\beta$ pathway in the HaCaT cells.**

Modulation of the TGF- $\beta$  pathway in the HaCaT cells has been investigated by immunoblotting assay, at 210 days of treatment. Representative immune blot image of TGF- $\beta$  and a bar graph showing fold change in its band intensity has been depicted in the Figures 4.64A and 4.64B respectively. The

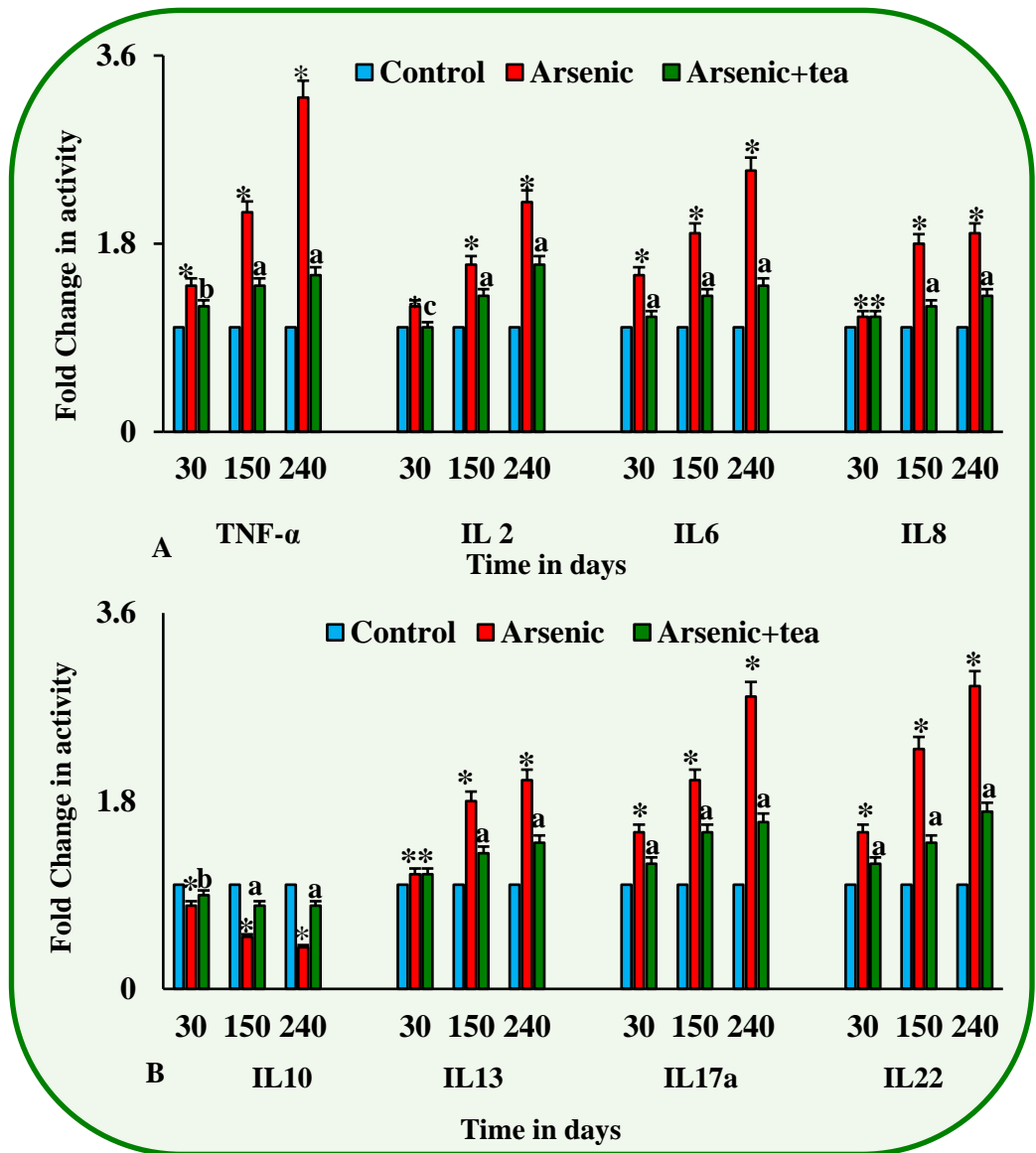


**Figure 4.62:** Determination of the activity of pro- and anti-inflammatory cytokines. **Figure 4.62A** displays a bar graph representing fold change, in mean band intensities of pro-inflammatory cytokine TNF- $\alpha$ , IL2, IL6 and IL8, in HaCaT cells, at 30, 150 and 240 days of treatment. Cells chronically treated with iAs showed prominent elevation of the activity of these pro-inflammatory cytokines, whereas, in the iAs+BTE treated cells, its was repressed.

**Figure 4.62B** displays a bar graph representing fold change in mean band intensities of anti-inflammatory cytokine IL10 and of pro-inflammatory cytokines IL13, IL17a and IL22. Chronic iAs treatment resulted in suppression of IL10 and elevation of IL13, IL17a and IL22, which was reversed in the BTE treatment group.

Values are mean of three independent experiments  $\pm$ S.D.

Modulation of activity of cytokines, in the iAs treated HaCaT cells is significant at \*\* $p < 0.001$  and \* $p < 0.0001$ , with respect to the control cells.

Modulation of activity of cytokines, in the iAs+BTE treated cells is significant at <sup>c</sup> $p < 0.05$ , <sup>b</sup> $p < 0.001$  and <sup>a</sup> $p < 0.0001$ , with respect to the iAs treatment group.

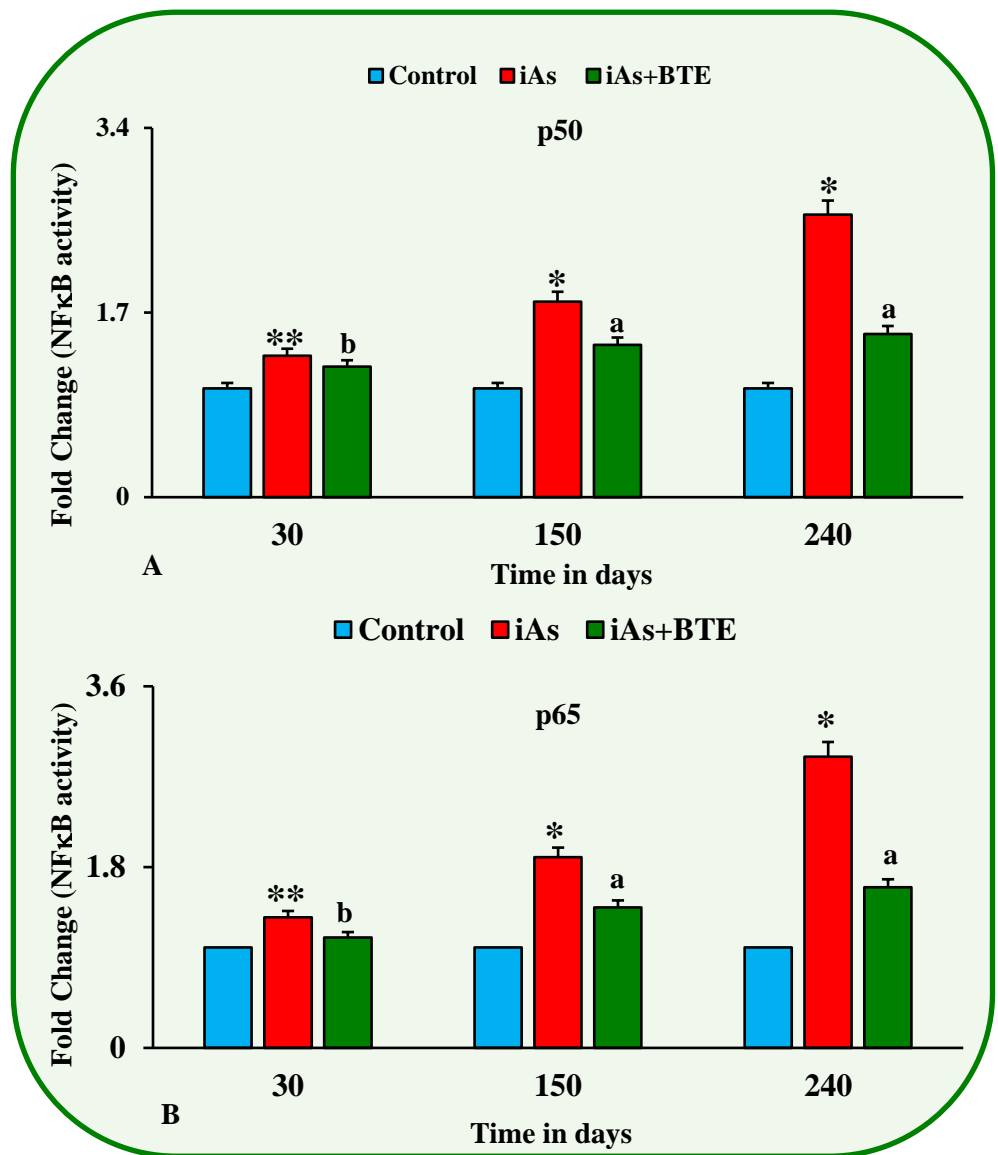


**Figure 4.63:** Fold change in activity of p50 and p65.

**Figure 4.63A** displays a bar graph which represents fold change in activity of p50, a subunit of NFκB, in normal human keratinocytes HaCaT cells, at 30, 150 and 240 days of treatment.

**Figure 4.63B** displays a bar graph representing fold change in activity of p65, another subunit of NFκB, at 30, 150 and 240 days of treatment.

The activity of p50 and p65 increased upon chronic treatment with iAs, which decreased in the iAs+BTE treated cells.

The values are mean of three independent experiments  $\pm$ S.D.

Fold change (increase) in activity, in the iAs treated cells is significant at \* $p < 0.0001$  and \*\* $p < 0.001$ , with respect to the control group.

Fold change (decrease) in activity in the iAs+BTE treated cells is significant at <sup>a</sup> $p < 0.0001$  and <sup>b</sup> $p < 0.001$ , with respect to the iAs treated cells.

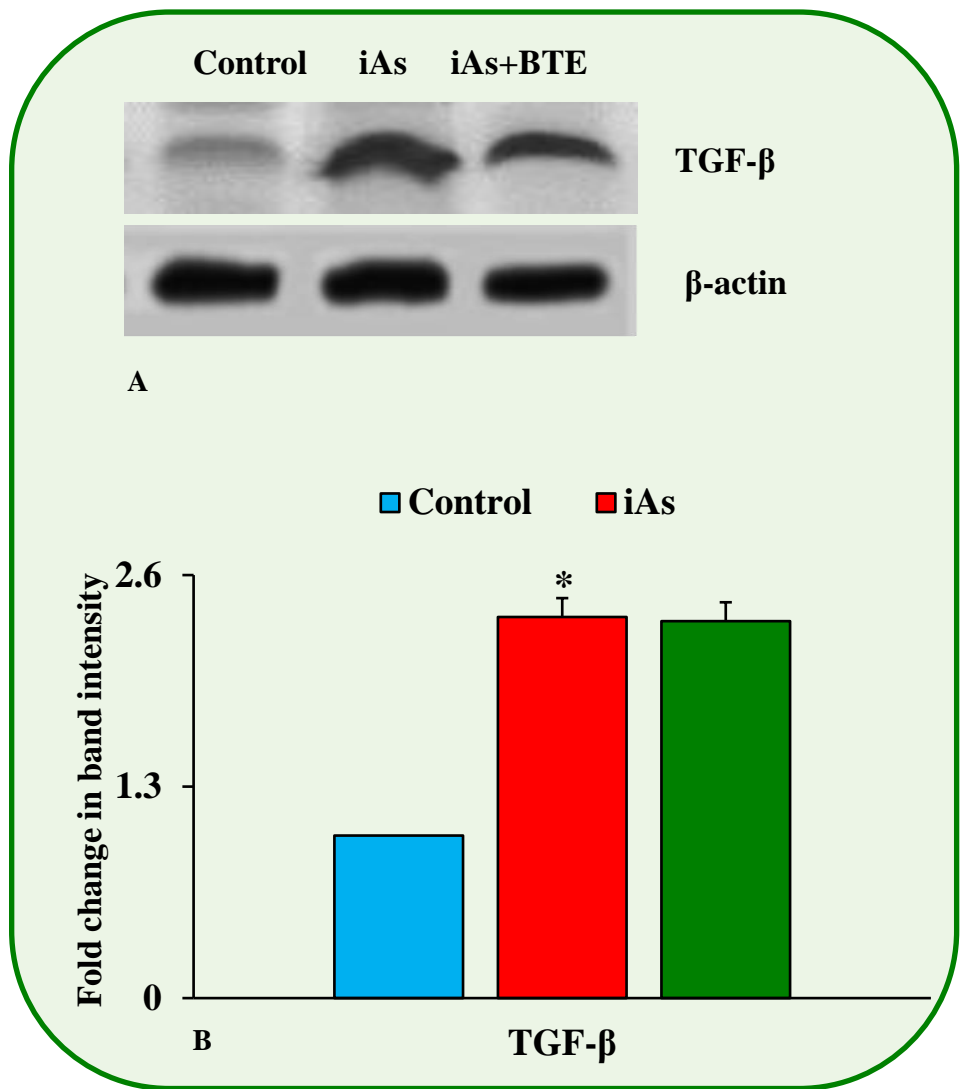


**Figure 4.64:** Estimation of the expression of TGF-β in HaCaT cells.

**Figure 4.64A** displays the representative immunoblot images of TGF-β in control, iAs and iAs+BTE treated HaCaT cells, at 210 days of treatment. β-actin was used as a loading control.

**Figure 4.64B** displays a bar graph representing the fold change in mean band intensity, of TGF-β, in control, iAs and iAs+BTE treated cells. Expression of TGF-β is elevated in the iAs treatment group, which also remains high in the iAs+BTE treated cells. Values are mean of three independent experiments ±S.D.

Fold change (increase) in band intensity, in the iAs treated cells, is significant at \*p<0.0001, with respect to the control group.

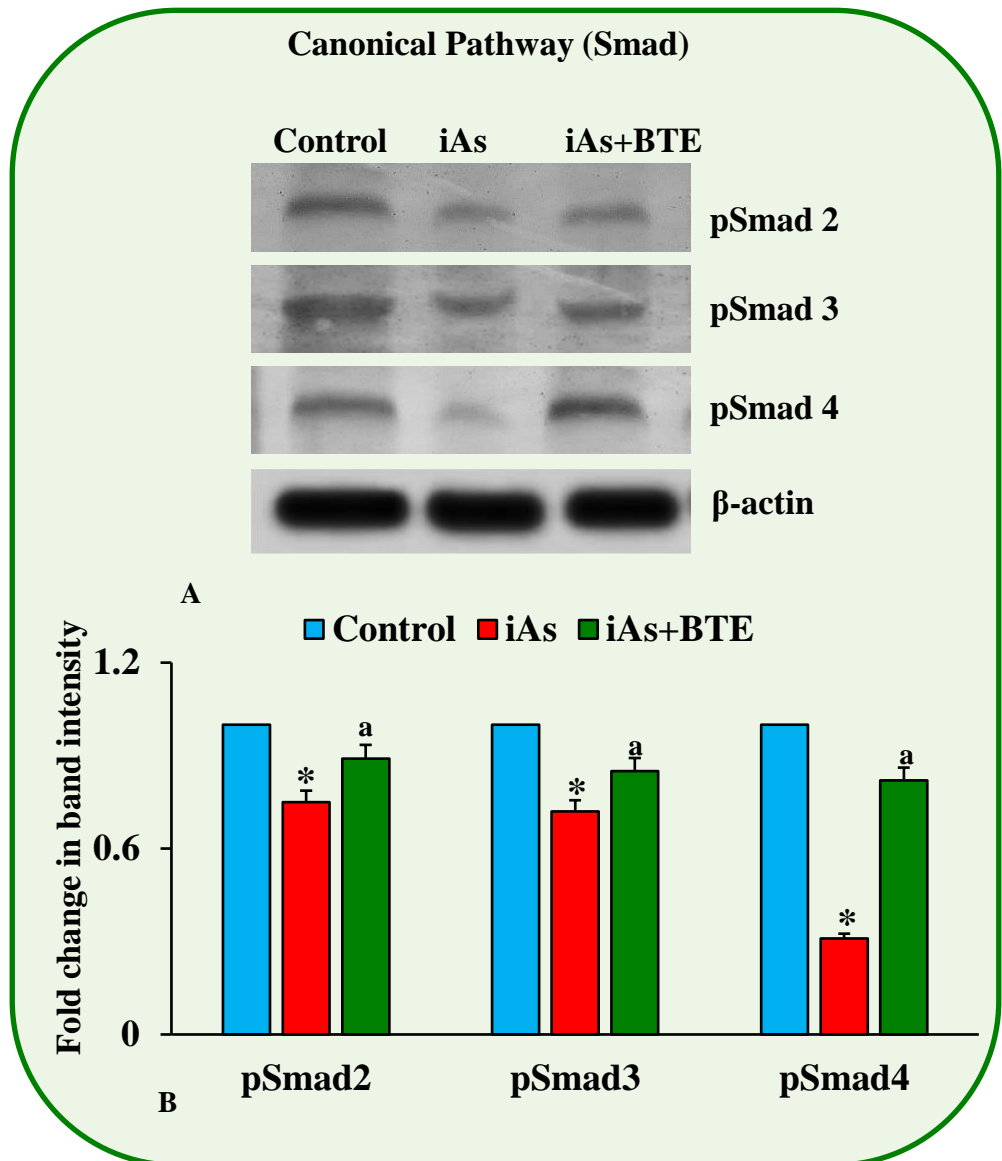
result indicates significant upregulation of TGF- $\beta$  upon chronic iAs treatment, which remains almost unchanged in the iAs+BTE treated cells.

Figure 4.65A displays representative immunoblot images of pSmad2, pSmad3 and pSmad4 and the respective band intensities have been displayed as a bar graph in Figure 4.65B. Chronic treatment with iAs shows significant ( $p < 0.0001$ ) downregulation of pSmad2, pSmad3 and pSmad4, while they are significantly ( $p < 0.0001$ ) upregulated in the iAs+BTE treated cells. This result indicates downregulation of the canonical Smad pathway in the iAs treated mice which appears to be reversed upon BTE treatment.

Figure 4.66A displays the representative immunoblot images of PTEN, PI3K, pAKT, p-mTOR, S6K and NF- $\kappa$ Bp65, while their respective band intensities have been displayed as a bar graph in the Figure 4.66B. The obtained results indicate that, upon iAs treatment, the expression of PI3K, pAKT, p-mTOR, S6K and NF- $\kappa$ Bp65 is significantly ( $p < 0.0001$ ) upregulated while that of PTEN is significantly ( $p < 0.0001$ ) downregulated. In the iAs+BTE treated HaCaT cells, the expression of PTEN appears to be significantly ( $p < 0.0001$ ) upregulated while that of PI3K, pAKT, p-mTOR, S6K and NF- $\kappa$ Bp65 is downregulated.

Representative immunoblot images of pTAK1, pMKK3, pMKK4, p38 and JNK1/2 have been depicted in the Figure 4.67A and the bar graph in the Figure 4.67B displays their respective band intensities. According to the obtained results, the expression of pTAK1, pMKK3, pMKK4, p38 and JNK1/2 increases remarkably in the iAs treated cells, while in the iAs+BTE treated cells, they are appreciably downregulated. Therefore, the results of the immunoblot assays suggest that, upon chronic iAs exposure, elevated TGF- $\beta$  relays its





**Figure 4.65:** Estimating the expression of signalling intermediates of the Smad pathway (canonical pathway of TGF- $\beta$ ) in HaCaT cells.

**Figure 4.65A** displays the representative immunoblot images of phospho-Smad2, phospho-Smad3 and phospho-Smad4, in control, iAs and iAs+BTE treated cells, at 210 days of treatment.  $\beta$ -actin was used as a loading control.

**Figure 4.65B** displays a bar graph showing fold change in mean band intensities of phospho-Smad2, phospho-Smad3 and phospho-Smad4. iAs treatment resulted in downregulation of phospho-Smad2, phospho-Smad3 and phospho-Smad4, while intervention with BTE reversed it. Values are mean of three independent experiments  $\pm$ S.D.

Fold change (decrease) in band intensity, in the iAs treated cells, is significant at \* $p < 0.0001$ , with respect to the control group.

Fold change (increase) in band intensity, in the iAs+BTE treated cells, is significant at <sup>a</sup> $p < 0.0001$ , in comparison to the iAs treated cells.

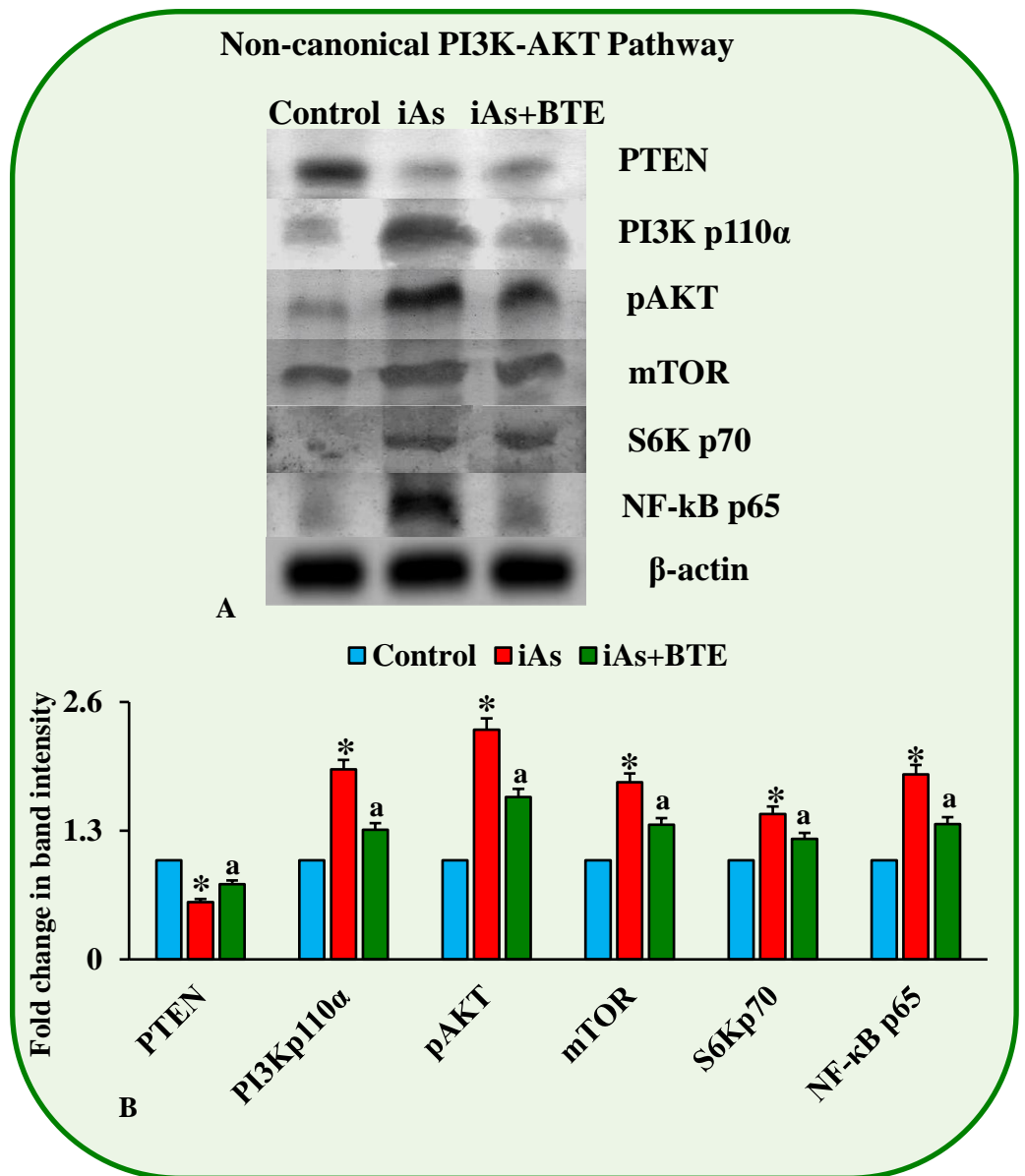


**Figure 4.66:** Estimating the expression of signalling intermediates of the PI3K-AKT pathway (non-canonical pathway of TGF- $\beta$ ), in normal human keratinocytes, HaCaT cells.

**Figure 4.66A** displays the representative immunoblot images of PTEN, PI3K, phospho-AKT, mTOR, S6K, and p65, in control, iAs and iAs+BTE treated HaCaT cells, at 210 days of treatment.  $\beta$ -actin was used as a loading control.

**Figure 4.66B** displays a bar graph showing fold change in mean band intensities of PTEN, PI3K, phospho-AKT, mTOR, S6K, and p65. iAs treatment results in downregulation of PTEN with simultaneous upregulation of PI3K, phospho-AKT, mTOR, S6K and p65. In the iAs+BTE treated cells, this expression pattern is reversed. Values are mean of three independent experiments.

Modulation of band intensity, in the iAs treated cells, is significant at  $*p < 0.0001$ , with respect to the control group.

Modulation of band intensity, in the iAs+BTE treated cells, is significant at  $^ap < 0.0001$ , in comparison to the iAs treatment group.

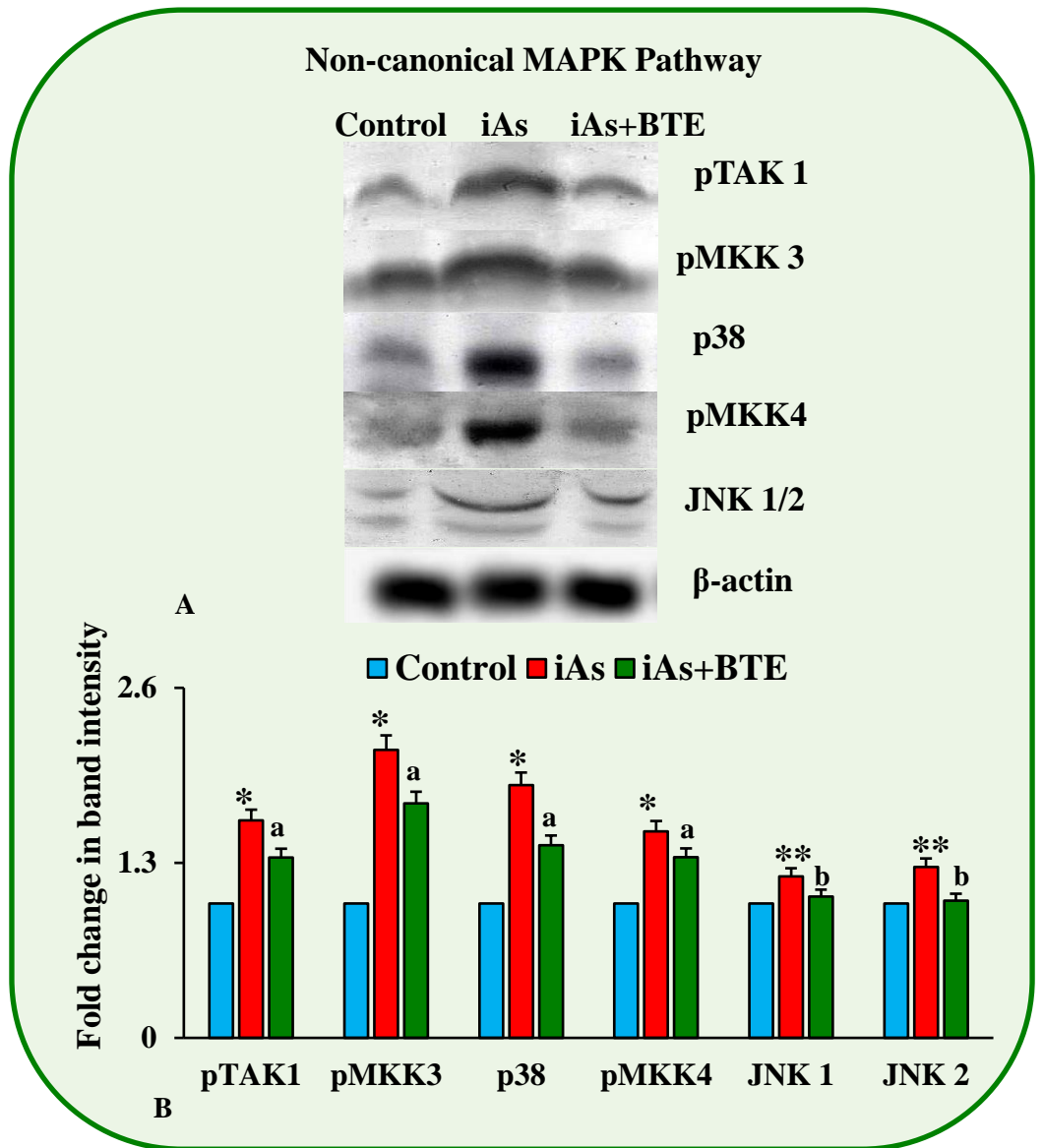


**Figure 4.67:** Estimating the expression of signalling intermediates of the MAPK pathway (non-canonical pathway of TGF- $\beta$ ), in normal human keratinocytes, HaCaT cells.

**Figure 4.67A** displays the representative immunoblot images of phospho-TAK1, phospho-MKK3, phospho-p38, phospho-MKK4, JNK1 and JNK2, in the control, iAs and iAs+BTE treated HaCaT cells, at 210 days of treatment.  $\beta$ -actin was used as a loading control.

**Figure 4.67B** displays a bar graph showing fold change in mean band intensities of phospho-TAK1, phospho-MKK3, phospho-p38, phospho-MKK4, JNK1 and JNK2. Expression of phospho-TAK1, phospho-MKK3, phospho-p38, phospho-MKK4, JNK1 and JNK2 is upregulated in the iAs treated cells, which is reversed in the iAs+BTE treated cells. Values are mean of three independent experiments  $\pm$ S.D.

Fold change (increase) of band intensities, in the iAs treated cells, is significant at \* $p < 0.0001$  and \*\* $p < 0.001$ , with respect to the control group.

Fold change (decrease) of band intensities, in the iAs+BTE treated cells, is significant at <sup>a</sup> $p < 0.0001$  and <sup>b</sup> $p < 0.001$ , in comparison to the iAs treated cells.

downstream signalling mainly via the non-canonical PI3K-AKT and MAPK pathways as the canonical Smad pathway remains suppressed. Upon BTE intervention, signalling intermediates of the Smad pathway, the PI3K-AKT and MAPK pathways get altered.

#### **4.40. Estimation of EMT induction in HaCaT cells.**

Expression of EMT markers in HaCaT cells have been analysed by flowcytometric, immunoblotting and immunofluorescent assays. The dot plot graphs of the respective epithelial (E-cadherin, Desmoplakin) and mesenchymal (Vimentin, N-cadherin, Snail, Slug, Twist and Zeb) markers, analysed at 210 days of treatment, have been depicted in the Figures 4.68A, 4.69A, 4.70A and 4.71A. The bar graphs displayed in the Figures 4.68B, 4.69B, 4.70B and 4.71B represent the percentage of positively stained cells of the respective epithelial and mesenchymal markers. The bar graphs depicted in the Figure 4.68C, 4.69C, 4.70C and 4.71C represent the fold change in the mean fluorescent intensities of the respective EMT markers. Results of the flow cytometric analysis suggests that, after 210 days of iAs treatment, there is induction of EMT, leading to significant ( $p < 0.0001$ ) suppression of epithelial markers with subsequent elevation of mesenchymal markers. In the iAs+BTE treated cells, the phenomenon of EMT appears to be reversed, where expression of epithelial markers are significantly ( $p < 0.0001$ ) high and mesenchymal markers are significantly ( $p < 0.0001$ ) low, indicating inhibition of EMT.

The images displayed in the Figures 4.72A, 4.73A, 4.74A and 4.75A depict the representative immunoblot images of the respective EMT markers, as assessed in the HaCaT cells, after 210 days of treatment. Band intensities of immunoblot assay, of the respective EMT markers, have been displayed as a bar

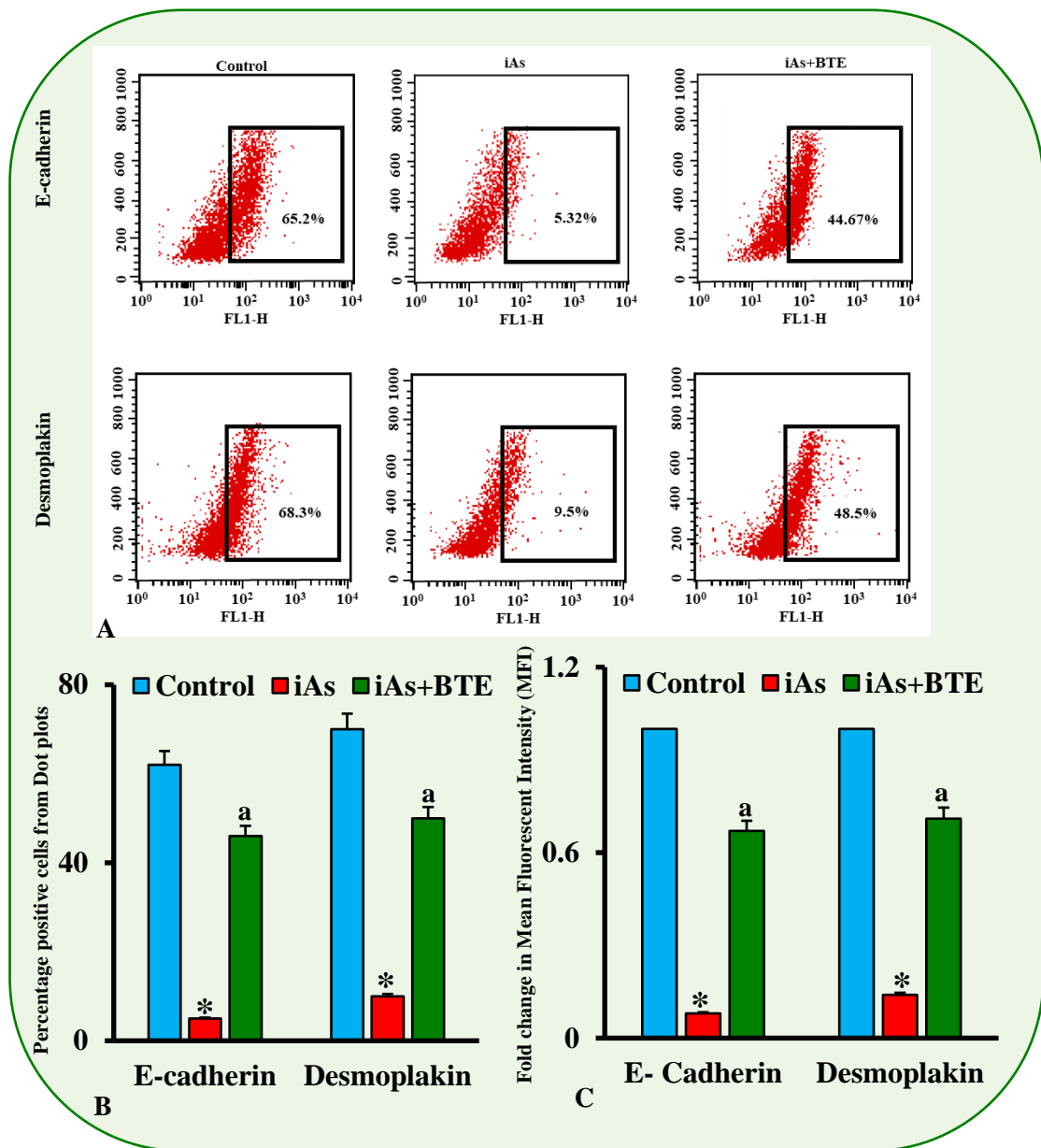


**Figure 4.68:** Flowcytometric analysis of EMT in HaCaT cells. Epithelial markers were assessed at 210 days of treatment.

**Figure 4.68A** shows representative dot plots for epithelial markers E-cadherin and Desmoplakin. The percentage of positively stained cells for each epithelial marker, in the control, iAs and iAs+BTE treatment groups, have been mentioned in the respective dot plots.

**Figure 4.68B** represents a bar graph displaying the mean percentages of the positively stained cells obtained from the dots plots of the respective Epithelial markers (E-cadherin and Desmoplakin)

**Figure 4.68C** represents the fold change in mean fluorescent intensities of the respective epithelial markers.

Values are the mean of three independent experiments  $\pm$  SD. Modulation of epithelial markers in the iAs treated cells are significant at  $*p < 0.0001$ , with respect to the control group. Modulation of the epithelial markers in the iAs+BTE treated cells are significant at  $^ap < 0.0001$ , with respect to the iAs treated cells.

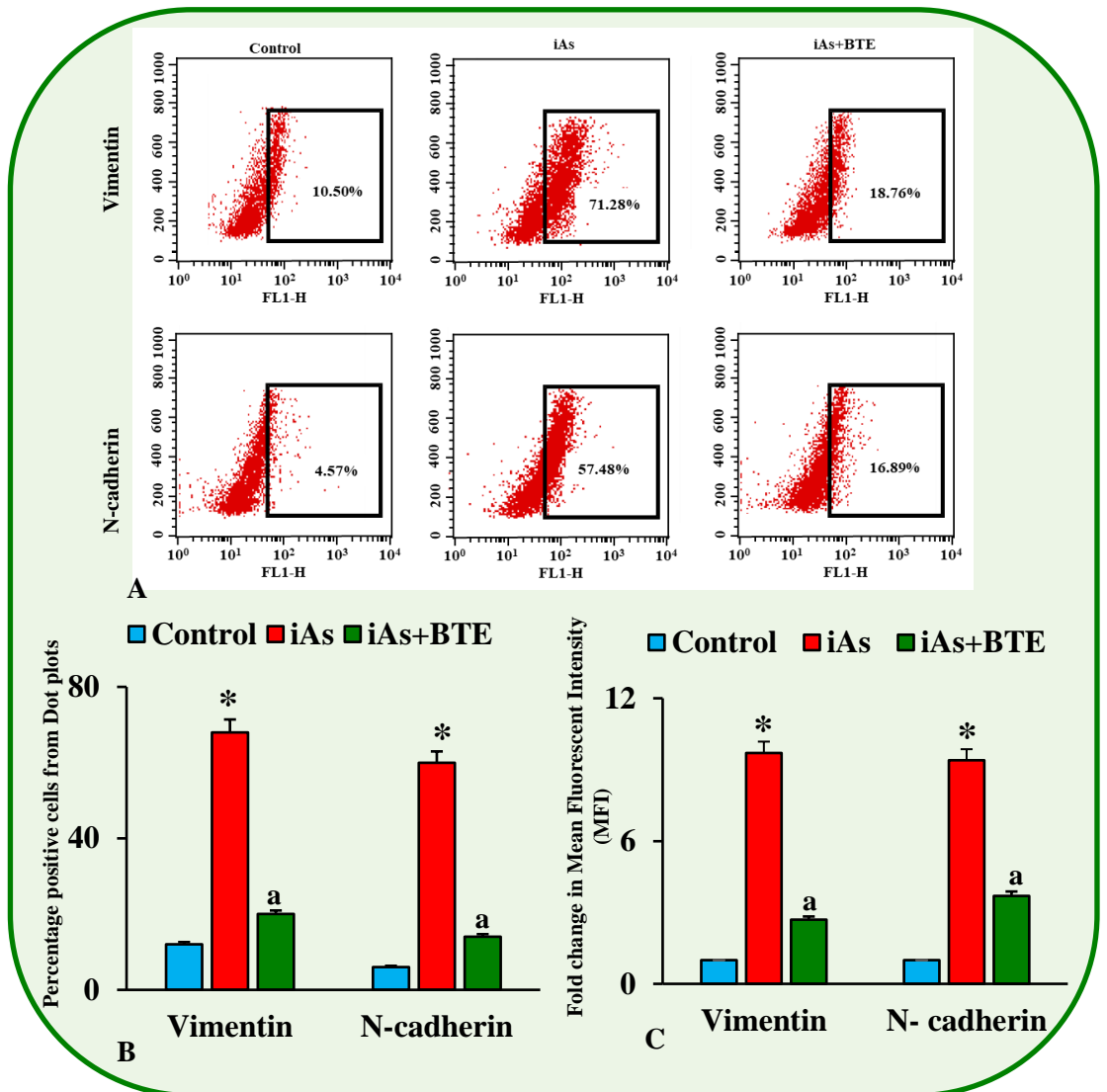


**Figure 4.69:** Flowcytometric analysis of EMT in HaCaT cells. Mesenchymal markers were assessed at 210 days of treatment.

**Figure 4.69A** shows representative dot plots for mesenchymal markers Vimentin and N-cadherin. The percentage of positively stained cells for each mesenchymal marker, in the control, iAs and iAs+BTE treatment groups, have been mentioned in the respective dot plots.

**Figure 4.69B** represents a bar graph displaying the mean percentages of the positively stained cells obtained from the dots plots of the respective mesenchymal markers (Vimentin and N-cadherin)

**Figure 4.69C** represents the fold change in mean fluorescent intensities of the respective mesenchymal markers.

Values are the mean of three independent experiments  $\pm$  SD.

Modulation of mesenchymal markers in the iAs treated cells are significant at  $*p < 0.0001$ , with respect to the control group.

Modulation of the mesenchymal markers in the iAs+BTE treated cells are significant at  $^ap < 0.0001$ , with respect to the iAs treated cells.

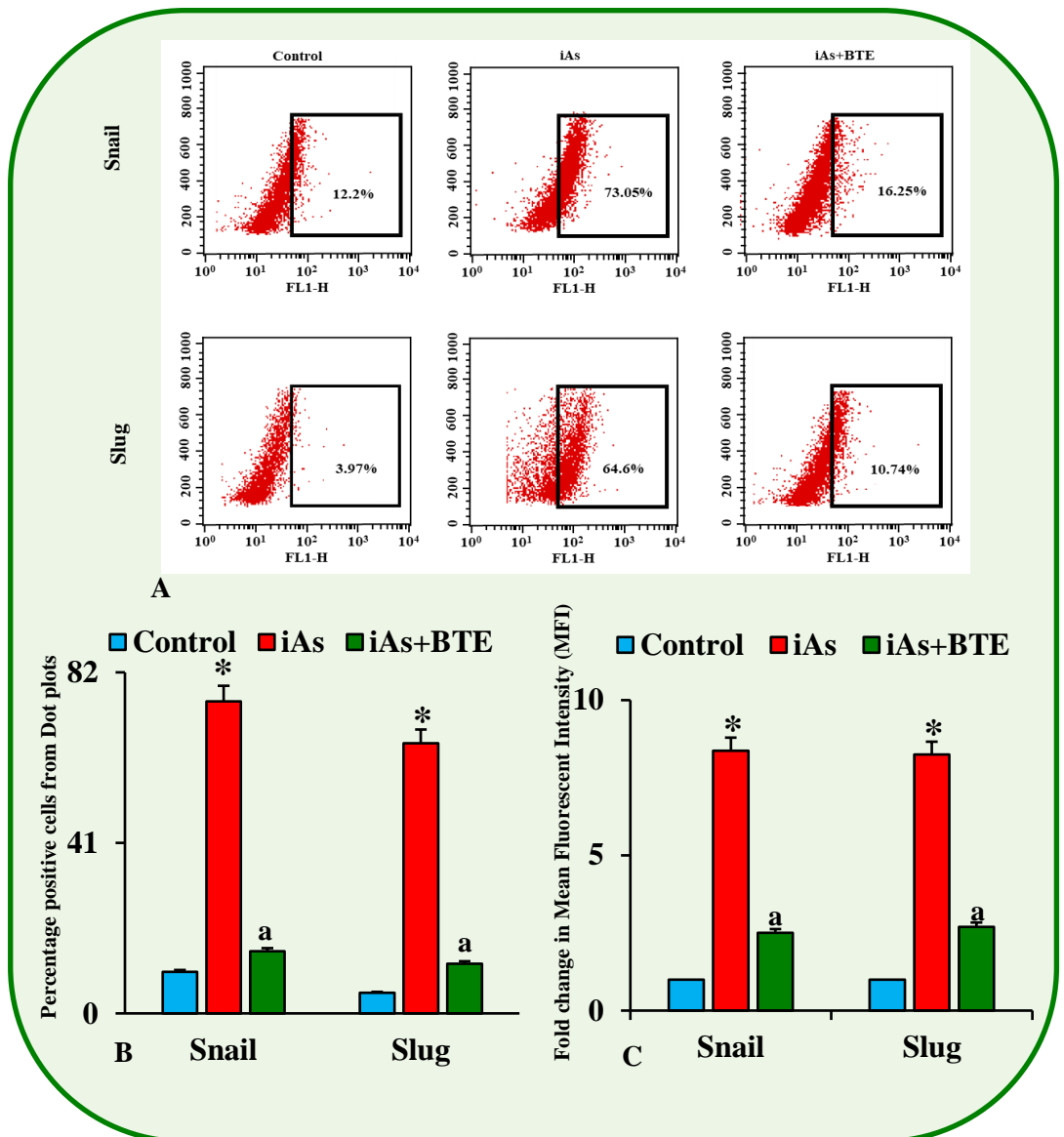


**Figure 4.70:** Flowcytometric analysis of EMT in HaCaT cells. Mesenchymal markers were assessed at 210 days of treatment.

**Figure 4.70A** shows representative dot plots for mesenchymal markers Snail and Slug. The percentage of positively stained cells for each mesenchymal marker, in the control, iAs and iAs+BTE treatment groups, have been mentioned in the respective dot plots.

**Figure 4.70B** represents a bar graph displaying the mean percentages of the positively stained cells obtained from the dots plots of the respective mesenchymal markers (Snail and Slug)

**Figure 4.70C** represents the fold change in mean fluorescent intensities of the respective mesenchymal markers.

Values are the mean of three independent experiments  $\pm$  SD.

Modulation of mesenchymal markers in the iAs treated cells are significant at  $*p < 0.0001$ , with respect to the control group.

Modulation of the mesenchymal markers in the iAs+BTE treated cells are significant at  $^ap < 0.0001$ , with respect to the iAs treated cells.

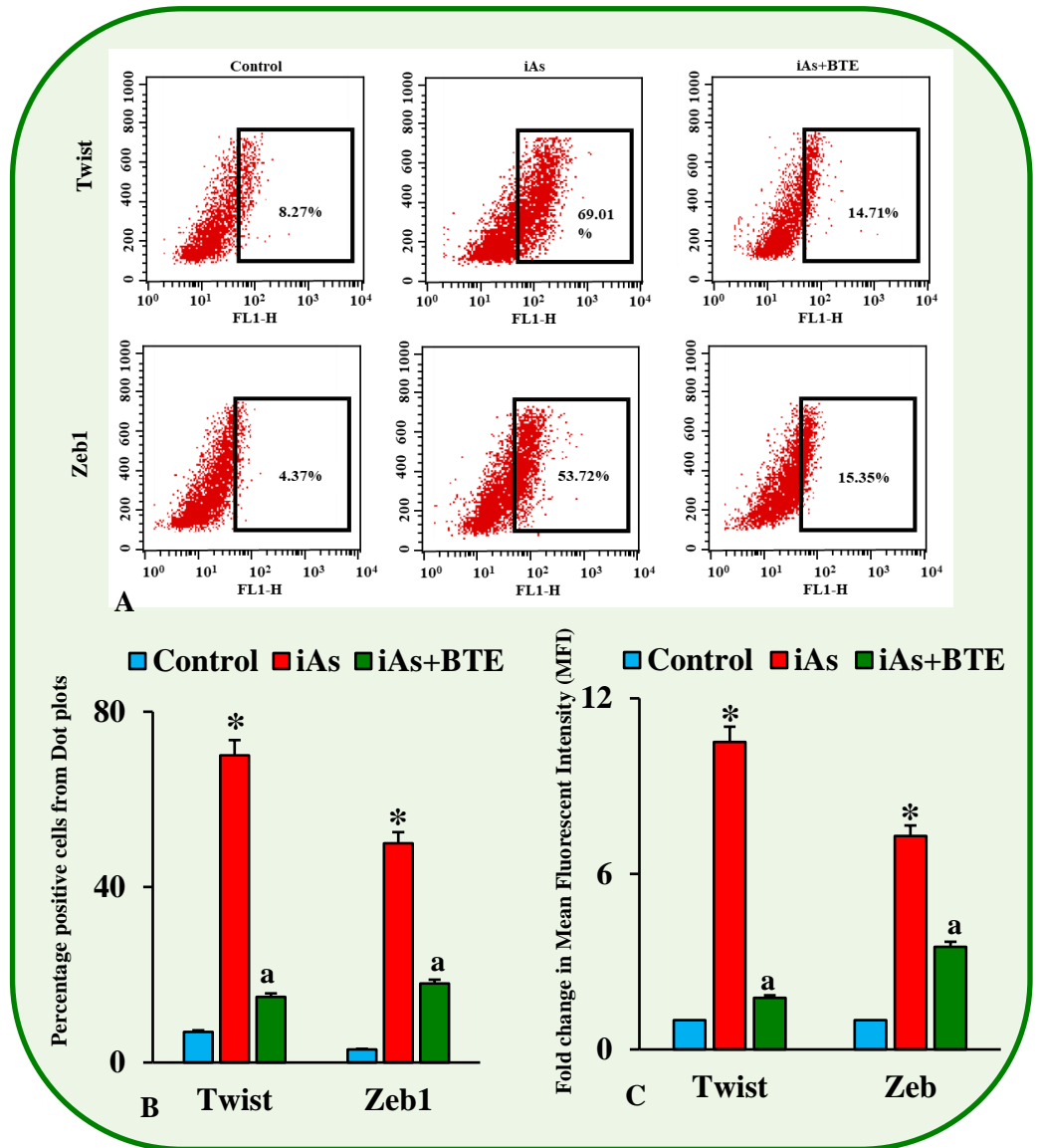


**Figure 4.71:** Flowcytometric analysis of EMT in HaCaT cells. Mesenchymal markers were assessed at 210 days of treatment.

**Figure 4.71A** shows representative dot plots for mesenchymal markers Twist and Zeb1. The percentage of positively stained cells for each mesenchymal marker, in the control, iAs and iAs+BTE treatment groups, have been mentioned in the respective dot plots.

**Figure 4.71B** represents a bar graph displaying the mean percentages of the positively stained cells obtained from the dots plots of the respective mesenchymal markers (Twist and Zeb)

**Figure 4.71C** represents the fold change in mean fluorescent intensities of the respective mesenchymal markers.

Values are the mean of three independent experiments  $\pm$  SD. Modulation of mesenchymal markers in the iAs treated cells are significant at  $*p < 0.0001$ , with respect to the control group. Modulation of the mesenchymal markers in the iAs+BTE treated cells are significant at  $^ap < 0.0001$ , with respect to the iAs treated cells.



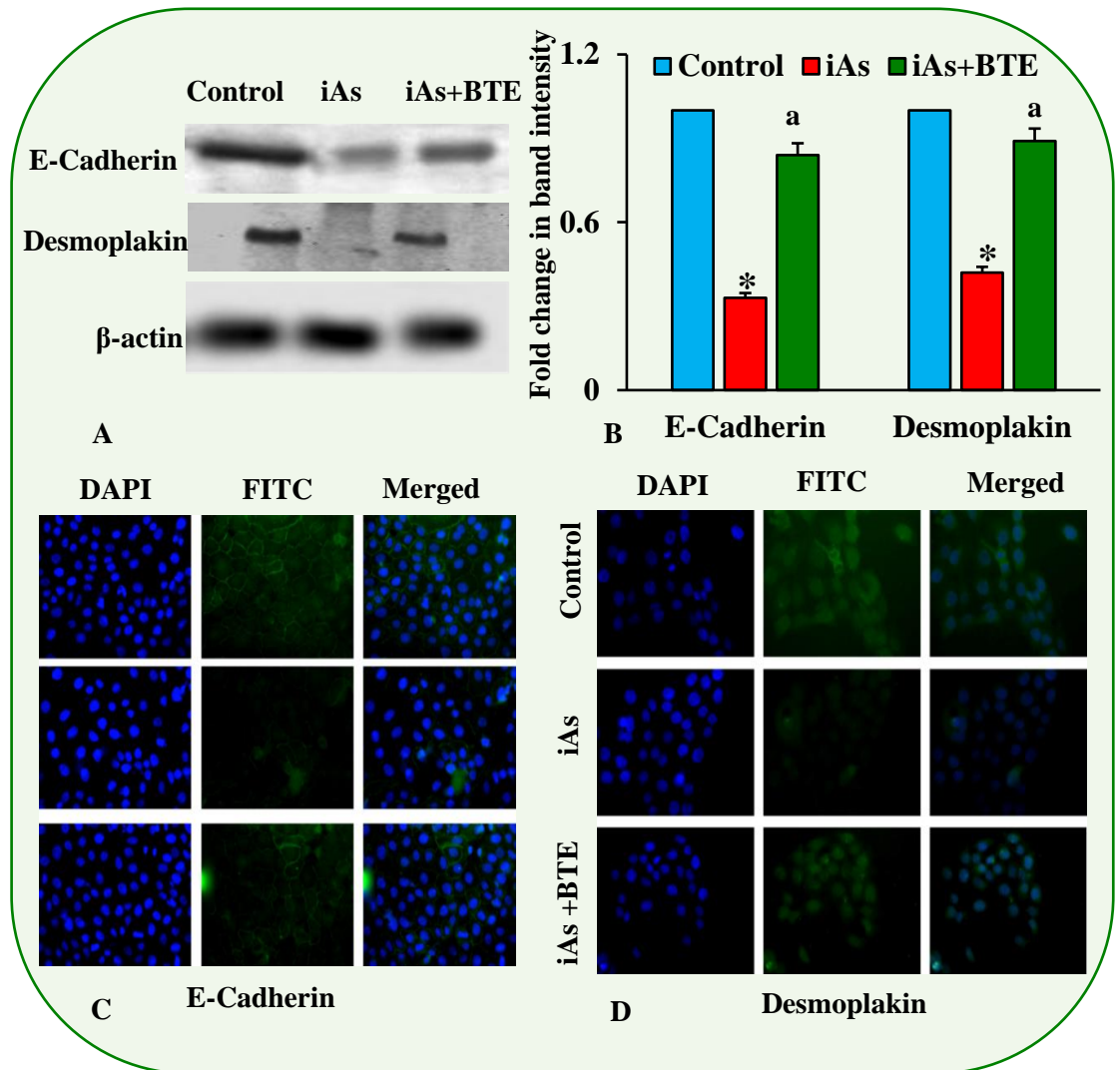


**Figure 4.72:** Assessment of EMT markers by Immunoblotting and Immunofluorescence assay in HaCaT cells, at 210 days treatment.

**Figure 4.72A** displays representative immunoblot images of epithelial markers, E-cadherin and Desmoplakin in the control, iAs and iAs+BTE treated HaCaT cells, at 210 days of treatment.  $\beta$ -actin was used as a loading control.

**Figure 4.72B** displays a bar graph representing fold change in mean band intensities of epithelial markers E-cadherin and Desmoplakin. Chronic treatment with iAs led to downregulation of the epithelial markers, which were upregulated in the iAs+BTE treated cells. Values are the mean of three independent experiments  $\pm$  SD.

Fold decrease in band intensity in the iAs treated cells is significant at  $^*p < 0.0001$ , with respect to the control group. Fold increase in band intensity in the iAs+BTE treated cells is significant at  $^ap < 0.0001$ , with respect to the iAs treated cells.

**Figure 4.72C and 4.72D** displays the immunofluorescence images of the epithelial markers, E-cadherin and Desmoplakin respectively, in the control, iAs and iAs+BTE treated cells. The epithelial markers were stained by FITC tagged secondary antibodies, while the nucleus was counterstained with DAPI. Images were captured by a fluorescent microscope at 400x and 50 fields were compared for each marker.

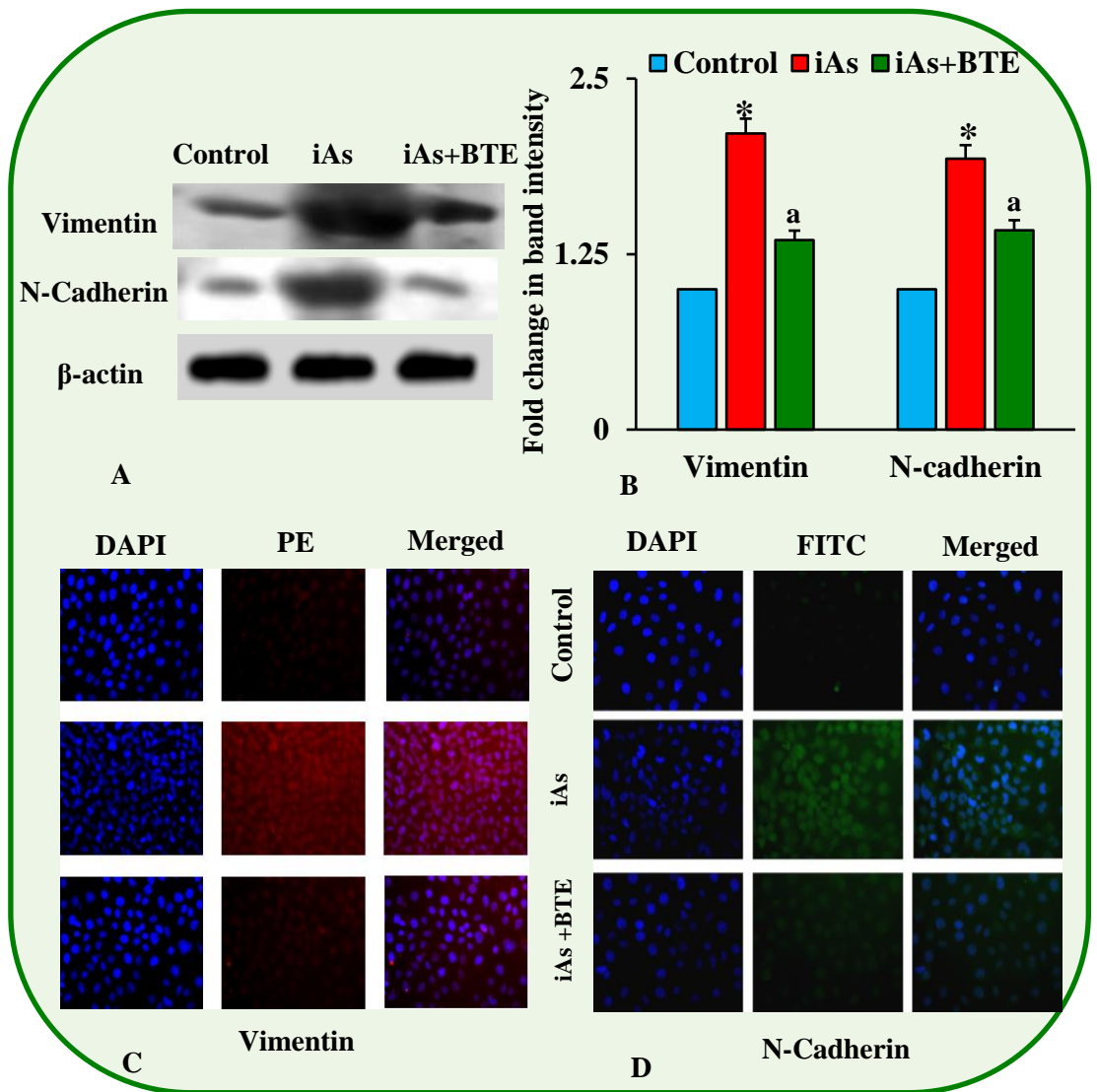


**Figure 4.73:** Assessment of EMT markers by Immunoblotting and Immunofluorescence assay in HaCaT cells, at 210 days treatment.

**Figure 4.73A** displays representative immunoblot images of mesenchymal markers, Vimentin and N-cadherin in the control, iAs and iAs+BTE treated HaCaT cells, at 210 days of treatment.  $\beta$ -actin was used as a loading control.

**Figure 4.73B** displays a bar graph representing fold change in mean band intensities of mesenchymal markers Vimentin and N-cadherin. Chronic treatment with iAs led to upregulation of the mesenchymal markers, which were downregulated in the iAs+BTE treated cells. Values are the mean of three independent experiments  $\pm$  SD.

Fold increase in band intensity in the iAs treated cells is significant at  $*p < 0.0001$ , with respect to the control group. Fold decrease in band intensity in the iAs+BTE treated cells is significant at  $^ap < 0.0001$ , with respect to the iAs treated cells.

**Figure 4.73C and 4.73D** displays the immunofluorescence images of the mesenchymal markers, Vimentin and N-cadherin respectively, in the control, iAs and iAs+BTE treated cells. Vimentin was stained by PE tagged, whereas, N-cadherin was stained by FITC tagged secondary antibodies. They were then counterstained with nuclear stain DAPI. Images were captured by a fluorescent microscope at 400x and 50 fields were compared for each marker.

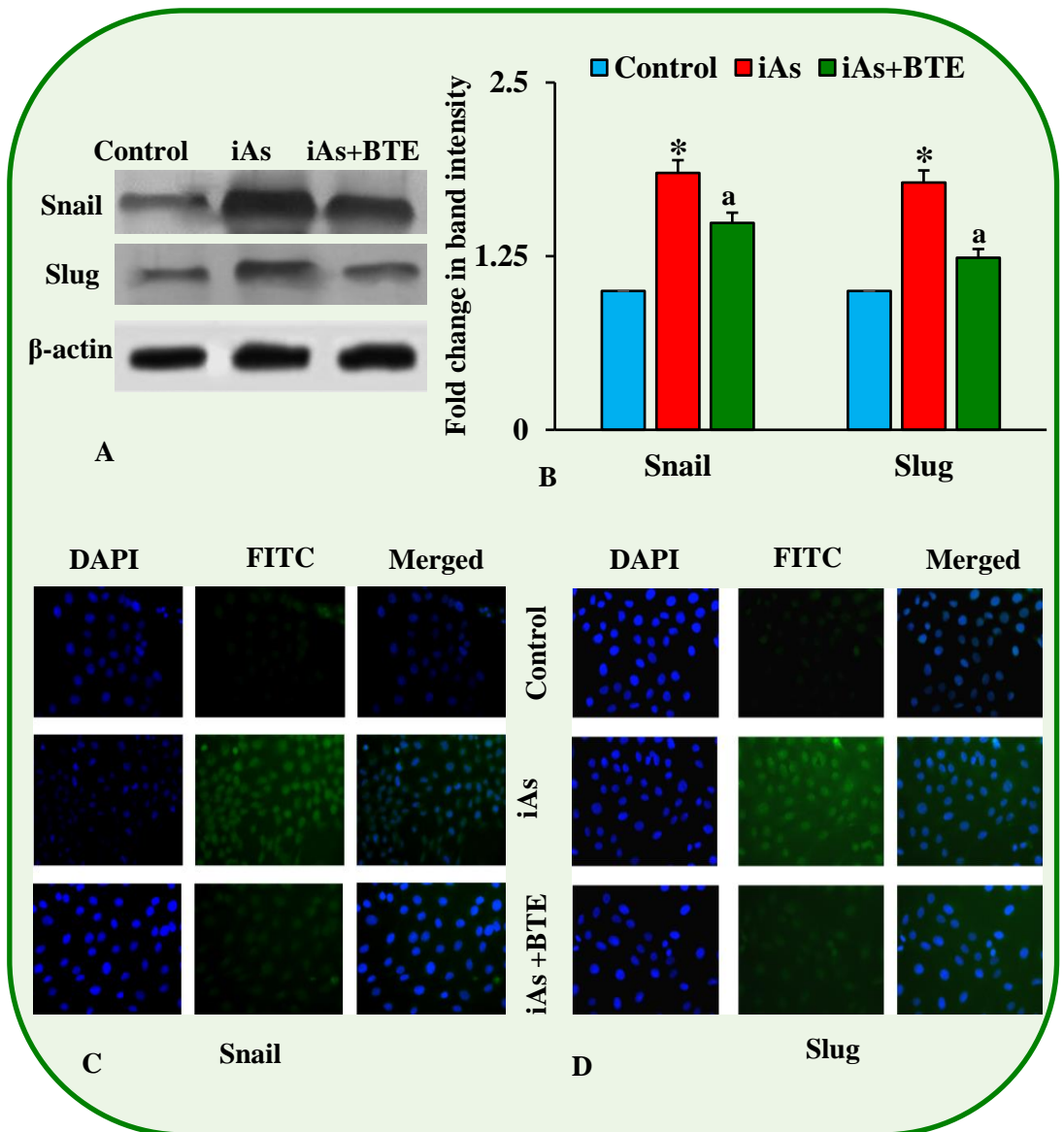


**Figure 4.74:** Assessment of EMT markers by Immunoblotting and Immunofluorescence assay in HaCaT cells, at 210 days treatment.

**Figure 4.74A** displays representative immunoblot images of mesenchymal markers, Snail and Slug in the control, iAs and iAs+BTE treated HaCaT cells, at 210 days of treatment.  $\beta$ -actin was used as a loading control.

**Figure 4.74B** displays a bar graph representing fold change in mean band intensities of mesenchymal markers Snail and Slug. Chronic treatment with iAs led to upregulation of these mesenchymal markers, which were downregulated in the iAs+BTE treated cells. Values are the mean of three independent experiments  $\pm$  SD.

Fold increase in band intensity in the iAs treated cells is significant at  $*p < 0.0001$ , with respect to the control group. Fold decrease in band intensity in the iAs+BTE treated cells is significant at  $^ap < 0.0001$ , with respect to the iAs treated cells.

**Figure 4.74C and 4.74D** displays the immunofluorescence images of the mesenchymal markers, Snail and Slug respectively, in the control, iAs and iAs+BTE treated cells. The mesenchymal markers were stained by FITC tagged secondary antibody and were then counterstained with nuclear stain DAPI. Images were captured by a fluorescent microscope at 400x and 50 fields were compared for each marker.

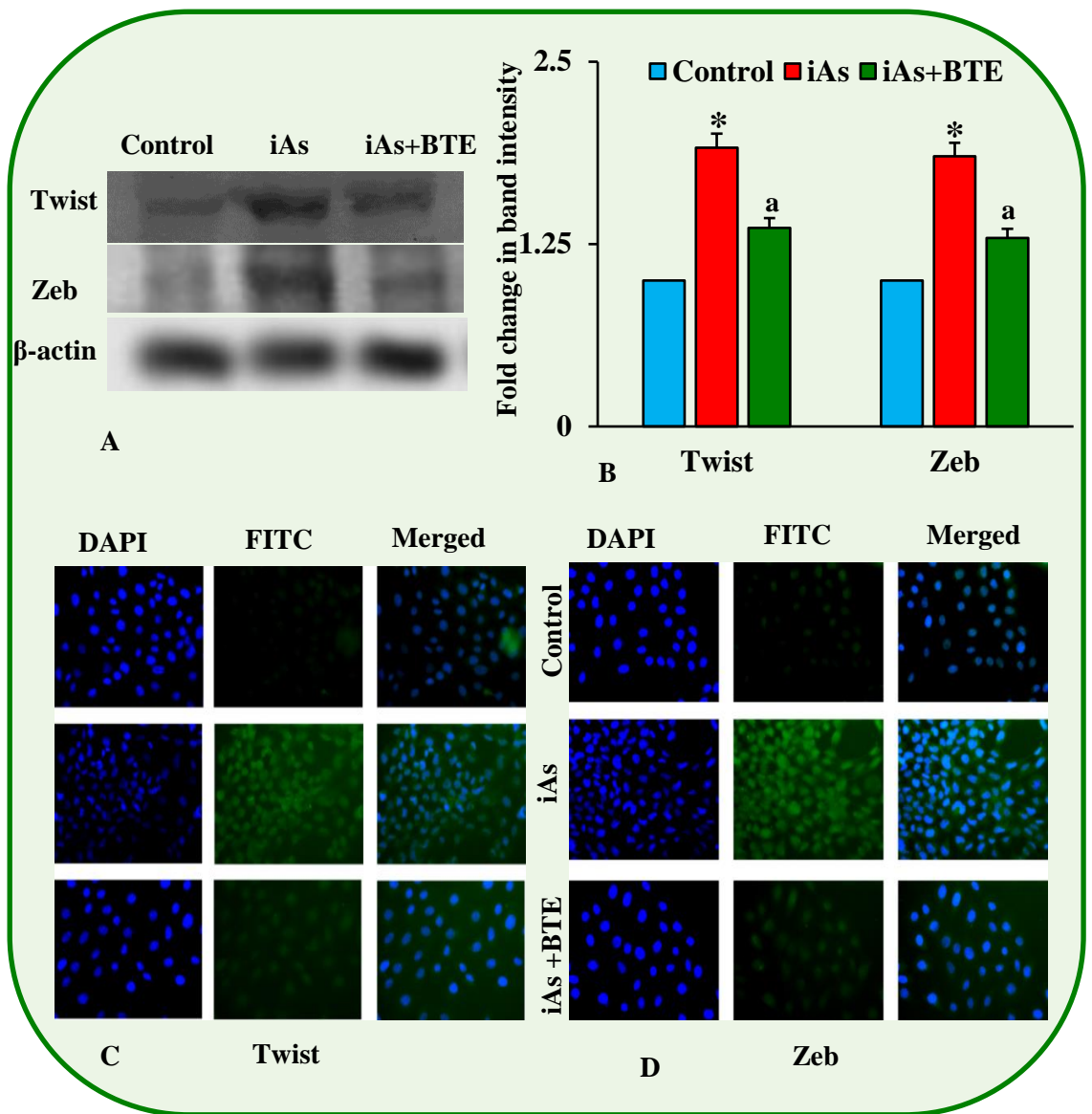


**Figure 4.75:** Assessment of EMT markers by Immunoblotting and Immunofluorescence assay in HaCaT cells, at 210 days treatment.

**Figure 4.75A** displays representative immunoblot images of mesenchymal markers, Twist and Zeb in the control, iAs and iAs+BTE treated HaCaT cells, at 210 days of treatment.  $\beta$ -actin was used as a loading control.

**Figure 4.75B** displays a bar graph representing fold change in mean band intensities of mesenchymal markers Twist and Zeb. Chronic treatment with iAs led to upregulation of these mesenchymal markers, which were downregulated in the iAs+BTE treated cells. Values are the mean of three independent experiments  $\pm$  SD.

Fold increase in band intensity in the iAs treated cells is significant at  $*p < 0.0001$ , with respect to the control group. Fold decrease in band intensity in the iAs+BTE treated cells is significant at  $^ap < 0.0001$ , with respect to the iAs treated cells.

**Figure 4.75C and 4.75D** displays the immunofluorescence images of the mesenchymal markers, Twist and Zeb respectively, in the control, iAs and iAs+BTE treated cells. The mesenchymal markers were stained by FITC tagged secondary antibody and were then counterstained with nuclear stain DAPI. Images were captured by a fluorescent microscope at 400x and 50 fields were compared for each marker.

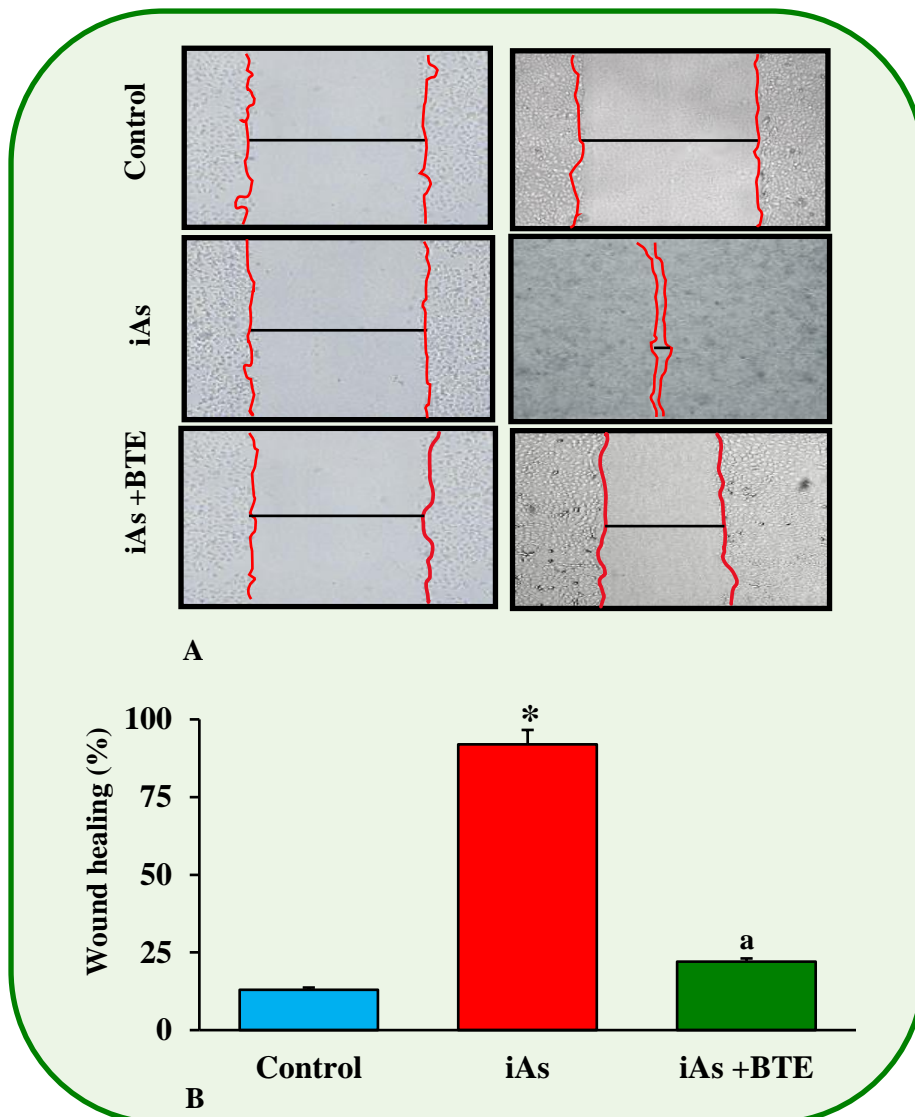
graph in the Figures 4.72B, 4.73B, 4.74B and 4.75B. Immunoblot assay results suggest, suppression of epithelial markers and elevation of mesenchymal markers, upon chronic iAs treatment in the HaCaT cells. In the iAs+BTE treated cells, epithelial markers are elevated and mesenchymal markers are suppressed, suggesting that BTE inhibits iAs induced EMT in the HaCaT cells.

Figure 4.72C and 4.72D represent the representative IF images of epithelial markers E-cadherin and Desmoplakin respectively. The representative IF images of the mesenchymal markers Vimentin, N-cadherin, Snail, Slug, Twist and Zeb have depicted in the Figures 4.73C, 4.73D, 4.74C, 4.74D, 4.75C and 4.75D respectively. The IF results reiterate our findings of flowcytometric and immunoblot assays, suggesting that, chronic iAs treatment in the HaCaT cells lead to induction of EMT which is inhibited by BTE intervention.

#### **4.41. Assessment of the migratory and invasive properties of the transformed HaCaT cells.**

Figure 4.76A depicts the representative images of the wound healing assay performed on the HaCaT cells, at 240 days of treatment. The percentage of wound healing has been represented as a bar graph in the Figure 4.76B. iAs transformed HaCaT cells showed significantly ( $p < 0.0001$ ) high capability of wound closure than the iAs+BTE treated cells, indicating that the iAs transformed HaCaT cells had very high migratory properties than the control or iAs+BTE treated cells.

Transwell migration and invasion assay were performed to investigate the migratory and invasive properties of the HaCaT cells. Both the assays were performed in a similar way except for the invasion assay, where the upper chamber was coated with extracellular matrix (ECM) gel.



**Figure 4.76:** Assessment of migratory property of HaCaT cell by wound healing assay, at 240 days of treatment.

**Figure 4.76A** shows representative images of wound healing assay (captured at 100x) using an inverted microscope. Wound was inflicted using a sterile pipette tip on a monolayer of HaCaT cells. Immediately and after 24 h of incubation, the width of the wound was photographed and measured.

**Figure 4.76 B** displays a bar graph representing the mean wound healing percentage, in the control, iAs and iAs+BTE treated cells, at 240 days of treatment. Values are the mean of three independent experiments  $\pm$  SD. Increase in mean wound closure percentage, in the iAs treated cells, is significant at  $^*p < 0.0001$ , with respect to control cells.

Decrease in mean wound closure percentage, in the iAs+BTE treated cells, is significant at  $^ap < 0.0001$ , with respect to the iAs group.



From Figures 4.77A and 4.78A, it can be easily estimated that, the population of the iAs treated cells in the lower chamber was much greater than the control cells, showing increased invasion and migration potential respectively, which are well controlled by BTE. Mean number of cells per field had been counted for invasion and migration assay and are depicted in Figures 4.77B and 4.78B respectively. De-staining of crystal violet, followed by OD measurement at 570 nm, gives a quantitative estimation of invasion and migration potential, which have been shown in Figure 4.77C and Figure 4.78C respectively. The results of the transwell invasion and migration assay show that, the iAs transformed cells have prominently high invasive and migratory capacity, which is not observed in the iAs+BTE treated cells.

The activity of matrix metalloproteinases (MMP) 2 and 9 have been studied by gelatin zymography, at 240 days of treatment and the results have been depicted in the Figure 4.79A. Representative immunoblot images of MMP2, MMP9, VEGF and EGFR, at 240 days of treatment, have been displayed in the Figures 4.79B, 4.79C and 4.79D respectively. Fold change in relative band intensities of Immunoblotting assay has been depicted as a bar graph in the Figure 4.79E. The results of the gelatin zymography assay and the immunoblotting assay indicate that the activity and expression of MMP2 and MMP9 in the iAs transformed cells is remarkably high, while in the iAs+BTE treated cells, it is significantly lower than the iAs transformed cells. The expression of angiogenic factors like VEGF and EGFR was upregulated in the iAs transformed cells, whereas in the iAs and BTE treated cells, it was prominently suppressed. These results indicate that the iAs transformed cells have very high migratory and invasive potential compared to the control cells,

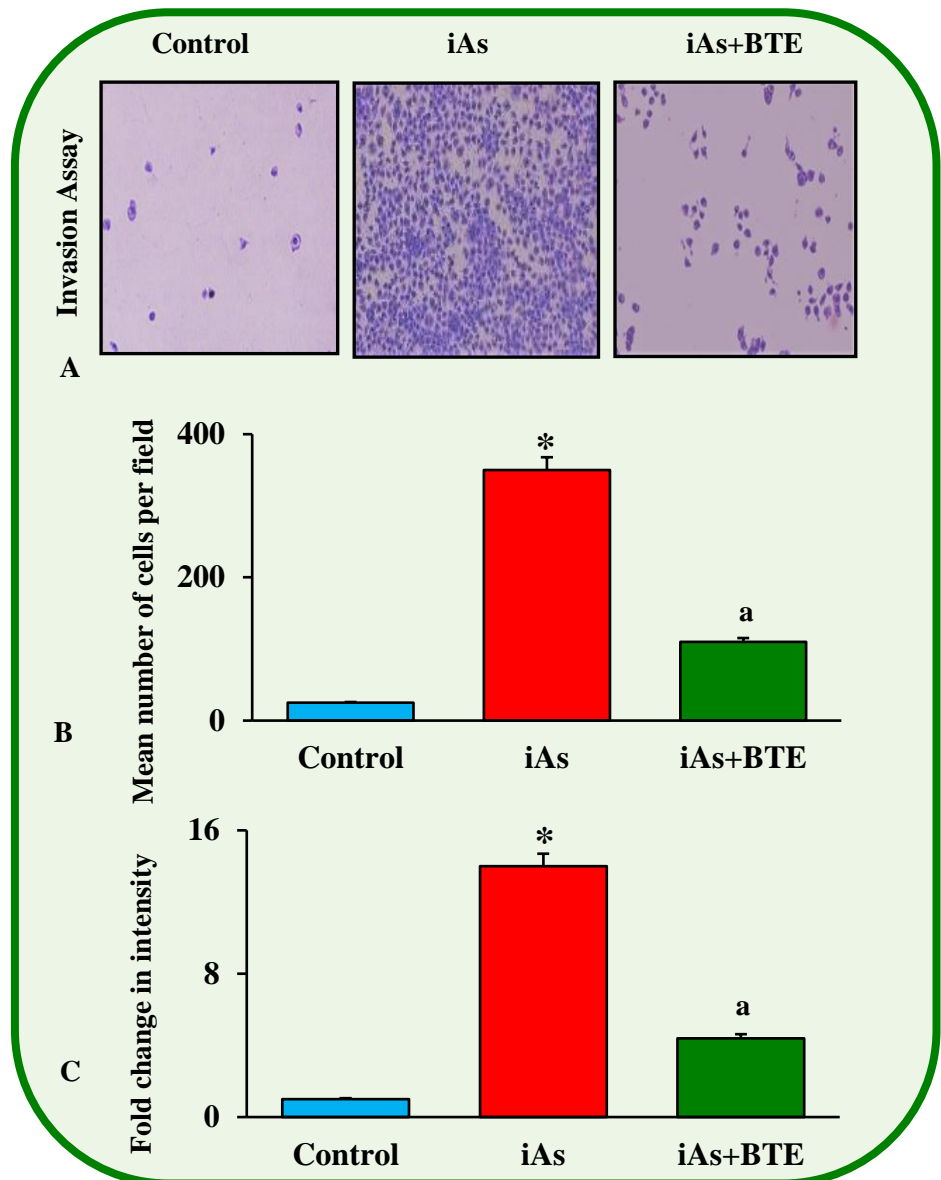


**Figure 4.77:** Assessment of the invasive property of the HaCaT cells by Transwell invasion assay at 240 days of treatment.

**Figure 4.77A** displays the representative images of Transwell Matrigel invasion assay, captured at 100x magnification, in the control, iAs and iAs+BTE treated HaCaT cells.

**Figure 4.77B** displays a bar graph representing mean number of invasive cells observed per field, in the control, iAs and iAs+BTE treatment groups, indicating invasive capacity of the cells.

**Figure 4.77C** displays a bar graph representing fold change in intensity of the eluted crystal violet stain, of the invasive cells, in the control, iAs and iAs+BTE treatment groups.

Values are the mean of three independent experiments  $\pm$  SD. Values of the iAs treated cells are significant at  $*p < 0.0001$ , with respect to the control group. Values of the iAs + BTE treated cells are significant at  $^ap < 0.0001$ , with respect to the iAs treatment group.



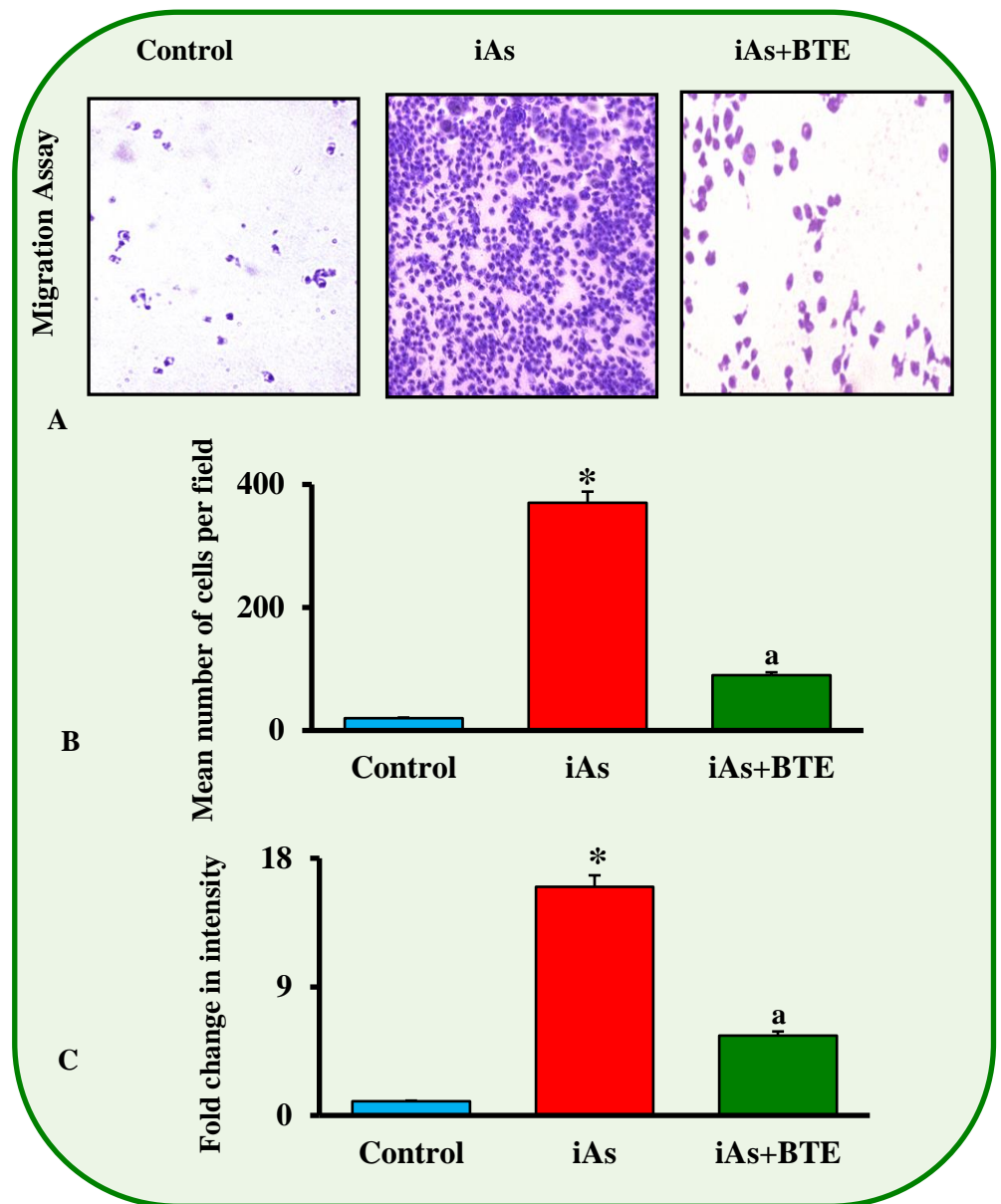


**Figure 4.78:** Assessment of the migratory property of the HaCaT cells by Transwell migration assay at 240 days of treatment.

**Figure 4.78A** displays the representative images of Transwell Matrigel migration assay, captured at 100x magnification, in the control, iAs and iAs+BTE treated HaCaT cells.

**Figure 4.78B** displays a bar graph representing mean number of migratory cells observed per field, in the control, iAs and iAs+BTE treatment groups, indicating migrative capacity of the cells.

**Figure 4.78C** displays a bar graph representing fold change in intensity of the eluted crystal violet stain, of the migratory cells, in the control, iAs and iAs+BTE treatment groups.

Values are the mean of three independent experiments  $\pm$  SD. Values of the iAs treated cells are significant at  $*p < 0.0001$ , with respect to the control group. Values of the iAs + BTE treated cells are significant at  $^ap < 0.0001$ , with respect to the iAs treatment group.

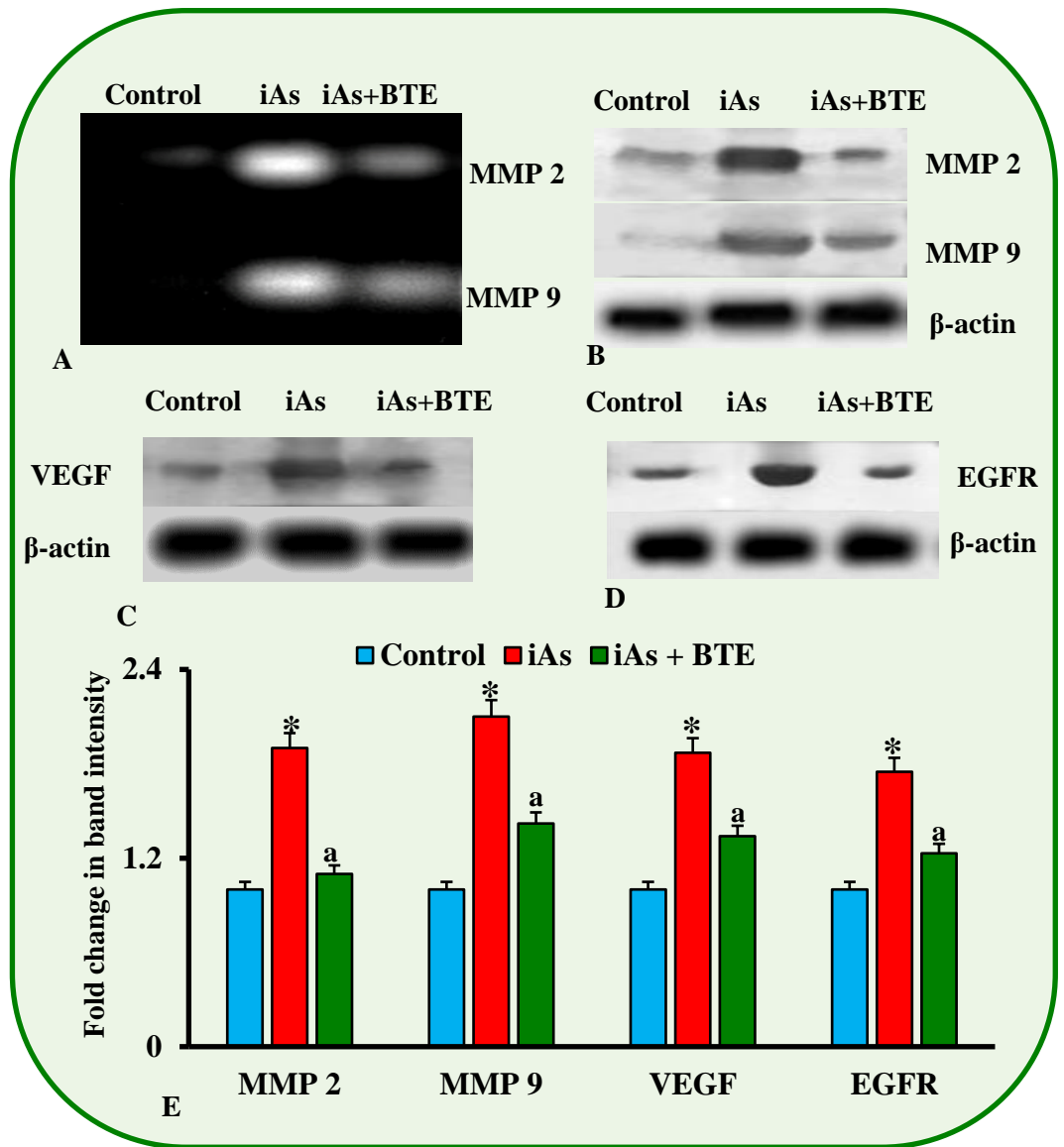


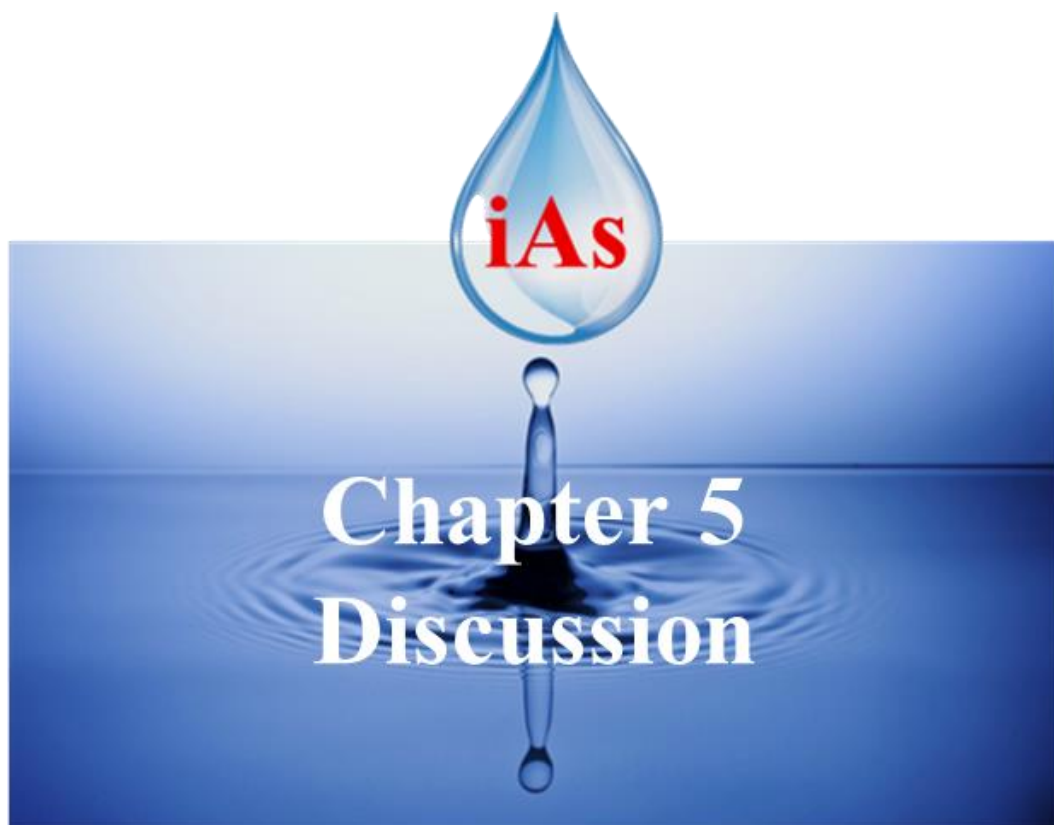
**Figure 4.79:** Assessment of gelatinolytic and angiogenic property of HaCaT cells at 240 days of treatment.

**Figure 4.79A** displays representative images of Gelatin Zymography Assay in the control, iAs and iAs + BTE treated HaCaT cells. The gelatinolytic activity of MMP2 and MMP9 have been depicted here.

**Figures 4.79B, 4.79C and 4.79D** display the representative immune blot images of MMP2, MMP9, VEGF and EGFR, in control, iAs and iAs + BTE treated HaCaT cells respectively.  $\beta$ -actin was used as a loading control.

**Figure 4.79E** displays a bar graph representing fold change in mean band intensities of the respective matrix metalloproteases (MMP2 & MMP9) and angiogenic factors (VEGF and EGFR) in the control, iAs and iAs+BTE treated HaCaT cells, at 240 days of treatment. Fold change in band intensities have been represented as mean of three independent experiments  $\pm$  SD. Fold increase in band intensity in the iAs treated cells is significant at  $*p < 0.0001$ , with respect to the control group. Fold decrease in band intensity in the iAs+BTE treated cells is significant at  $^ap < 0.0001$ , with respect to the iAs treated cells.

whereas intervention by BTE prevents development of migratory and invasive characteristics.



## 5. Discussion

Exposure to inorganic Arsenic (iAs) for a prolonged time leads to numerous diseases, rendering iAs to be a major health concern around the globe. Though not listed as a classical mutagen, iAs has been marked as a class 1 carcinogen by International Agency for Research on Cancer (IARC) [Klein et al., 2007]. Contamination of groundwater appears to be the most common source of iAs amongst humans. There are a number of strategies employed for remediation of groundwater iAs contamination [Azubuike et al., 2016]; but these are laborious and expensive, hence may not be a feasible option to be employed on large scale. It has been seen that, preliminary manifestations of chronic iAs exposure appears on the skin, which may eventually develop into invasive Squamous Cell Carcinoma (SCC). iAs mediates its carcinogenicity mainly through excess generation of ROS [Xian et al., 2019]. Therefore, to address the problem, quenching of free radical generation by iAs may be a better solution. Antioxidants may be a remedy to the problem. There are some synthetic compounds which may act as antioxidants; however, they are not free from demerits [Deepmala et al., 2015]. Naturally available plant derived molecules, with known mechanism of action may be a respite to the problem. These naturally available phytochemicals are cheap, may be taken orally and have minimum or no side effects, hence they appear to be an accepted solution. Most popular beverage tea with a plethora of medicinal attributes may come to the rescue. Green tea has already established its role in cancer prevention for its anti-oxidative, anti-inflammatory and anti-cancer potential [Maiti et al., 2019]; however, black tea is globally preferred over green tea. Hence, elucidation of the role of black tea to control the deleterious effects of iAs may be an important area. Present study investigates the probable mechanism of SCC of skin in Swiss albino mice (*in vivo* model) and normal human skin keratinocytes, HaCaT cells (*in vitro* model), by chronic exposure to iAs and its amelioration by Black Tea Extract (BTE). After 330 days of

continuous treatment with iAs (500 µg/l), most of the mice developed invasive SCC, as revealed by histological analysis [Ghosh et al., 2021a; Ghosh et al, 2022a]. Loss of epidermal structure along with prominent infiltration of the deeply stained, aggressive nuclei, covering more than 2/3rd of the dermal layer was evident from the findings. Co-administration of BTE along with iAs prevented the development of both in-situ and invasive SCC in mice skin. In BTE administered mice, hyperplastic as well as dysplastic changes were noted, and the epidermal architecture of the tissue remained almost unaltered. Major invasive structures within the dermal layer were found to be absent [Ghosh et al., 2021a; Ghosh et al, 2022a]. Similar findings were observed in *in vitro* studies. HaCaT cells continuously exposed to iAs resulted in transformation of the keratinocytes into spindle shaped elongated cells, which represent mesenchymal cells. Besides the morphological transformation, these cells are highly proliferative with much reduced doubling time, compared to that of the parental HaCaT cells. HaCaT cells receiving BTE (1 µM), along with iAs (100 nM), did not show any such changes even after 240 days of treatment [Ghosh et al., 2022b]. Therefore, BTE appears to hinder development of SCC in Swiss albino mice and inhibit carcinogenic transformations in HaCaT cells.

Present study reveals that chronic exposure of iAs leads to excess generation of free radicals, in both the *in vivo* as well as in the *in vitro* model. A strong link between chronic induction of free radicals and development of cancer, including skin cancer has been reported [Narendhirakannan and Hannah, 2013]. Excess ROS generated in iAs treated mice and HaCaT cells led to damage of DNA, protein and lipid [Ghosh et al., 2021a; Ghosh and Roy, 2023a]. DNA damage is a prerequisite for carcinogenesis. DNA damage in tumour suppressor genes; oncogenes with faulty or compromised DNA repair mechanisms fail to repair this damage. Presence of error in DNA, if not repaired efficiently causes mutation. Chromosomal damage may also result. Accumulation of mutation due to DNA damage may

lead to malignant transformations within the cells promoting cancer growth [Torgovnick and Schumacher, 2015]. Excess generation of ROS leads to post-translational modifications in proteins by adding carbonyl moieties like aldehydes, ketones or lactam; protein backbone gets cleaved and amino acid side chains get oxidised [Fedorova et al., 2014]. Carbonyl-stress occurs due to accumulation of carbonylated species; as a consequence of which redundancy of enzymes and increased toxicity is observed. A link between carbonyl-stress and various other degenerative disorders including inflammation has been reported [Fedorova et al., 2014]. Active ingredients of the phytochemical in BTE dampened the carbonyl-stress, generated due to iAs. Oxidation of PUFA (poly-unsaturated fatty-acids) in the phospholipids of the cell membranes causes lipid peroxidation and generates malondialdehyde, which is an electrophilic secondary species [Fedorova et al., 2014]. ROS, converts PUFA into a reactive radical; which sets up a chain reaction with other PUFA molecules converting them and generating more free radicals and lipid-peroxidation products (LPP) [Su et al., 2019]. Strong electrophilic LPPs have the tendency to interact with nucleophilic amino-acids in the side chains of the proteins, thereby altering their function [Fedorova et al., 2014]. The LPPs modify signalling pathways implicated in cell death, cell growth etc., leading to promotion of inflammation [Su et al., 2019]. Elevated Lipid peroxidation and protein carbonyl content is directly associated with ROS generation and carcinogenesis [Ma et al., 2013]. Present study highlights the chemopreventive role of BTE through repression of Lipid-peroxidation in iAs treated mice.

For maintenance of normal physiological steady state, reduction-oxidation homeostasis is vital. Antioxidant enzymes like SOD, catalase, GPx, GR, GST etc. maintain homeostasis by quenching free radicals. Exposure to iAs negatively influences the activity of antioxidant enzymes [Yu et al., 2017], enhancing the damage caused by ROS. This leads to delay in DNA-repair. Expression many of the repair enzymes involved in DNA repair

(BER, NER and NHEJ) get down-regulated due to chronic exposure to iAs. This is in agreement with the findings of other research groups [Martinez et al., 2011; Tong et al., 2015; Holcomb et al., 2017]. Present study reveals that chronic treatment with iAs resulted in reduction of total antioxidant activity and activity of specific antioxidant enzymes like Catalase, SOD, GPx, GR, and GST. Administration of BTE resulted in elevation of total antioxidant activity as well as the activity of individual antioxidant enzymes [Ghosh et al., 2021a; Ghosh and Roy, 2023a]. The repair machinery is activated upon detection of damage in DNA; if the damage is left unrepaired, or erroneously repaired, mutation occurs, and its accumulation may lead to cancer. In the present study, iAs was found to inhibit DNA repair potential as well as downregulate the expression of repair enzymes belonging to Base excision repair (BER), Nucleotide excision repair (NER) and Non-homologous end-joining (NHEJ). Exception is 8-Oxoguanine glycosylase (OGG1), which was upregulated upon chronic iAs treatment. In the BTE administered mice, DNA repair potential was upregulated along with the expression of repair enzymes belonging to the BER, NER and NHEJ pathway, except OGG1. Expression of OGG1 was reduced in BTE treatment group [Ghosh et al., 2021a; Ghosh and Roy, 2023a]. Thus, DNA damage may be reversed and impaired repair function due to iAs may be restored by BTE, rendering its preventive role in carcinogenesis. Formation of 8-oxoguanine (8-oxoG), a modified base within DNA, pairing with adenine is triggered by oxidative stress. Stable transversion mutation is resulted when 8-Oxoguanine glycosylase (OGG1) fails to repair 8-oxoG through BER pathway. Oxidative DNA damage is implicated in the development of skin cancers [Kunisada et al., 2005]. Owing to persistent oxidative stress, increased levels of 8-oxoG and OGG1 have been reported in ulcerative condition, along with prolonged inflammation [Kumagai et al., 2018]. The present study reveals increased expression of OGG1 in skin tissues of mice having cancer due to chronic exposure to iAs. It was reported from our



laboratory that 8-oxoguanine formation is induced by iAs, which resulted in increased OGG1 production [Roy et al., 2011]. BTE has shown significant reduction in OGG1 expression, indicating a role in restoration of repair machinery.

Chronic inflammation is linked with cancer [Coussens and Werb, 2002]. In *in vivo* models of skin cancer caused due to UV and chemical exposure, it was reported that deregulated and prolonged inflammation had a vital role in its causation [Kim et al., 2013]. Inflammation gets triggered by free radicals acting as signalling molecules; these active radicals aid in translocation of NF $\kappa$ B into the nucleus causing an alteration of cell growth and proliferation. Inflammation results in orchestration of numerous cytokines, both pro- and anti-inflammatory, which via the transcriptional activity of NF $\kappa$ B alter cellular homeostasis. NF $\kappa$ B is activated by TNF- $\alpha$  and this molecule eventually alters the apoptotic pathway involving ROS and c-Jun N-terminal kinase (JNK) signalling.

Lowering of ROS generation leads to deactivation of NF $\kappa$ B and reduction of IL6. Therefore, ROS generation and inflammation appear to be intertwined and both can control each other. According to this study, iAs induces chronic inflammatory condition by increasing the expression and activity of pro-inflammatory cytokines like TNF- $\alpha$ , IL 2, IL6, IL8, IL13, IL17a and IL22. The transcription factor nuclear factor- $\kappa$ B (NF $\kappa$ B) plays a crucial role in cell proliferation, apoptosis, cytokine production, and oncogenesis. Particularly the two subunits, p50 and p65, play important role in this regard. iAs reduced the expression of anti-inflammatory cytokine IL10. BTE, effectively hindered inflammatory responses by upregulating the anti-inflammatory cytokine and downregulating pro-inflammatory cytokines.

One of the major ways by which iAs can induce carcinogenesis is by epigenetic modulations. Epigenetic mechanisms regulate gene expression under normal

circumstances, but, atypical regulation may cause many human diseases including cancer. In the present study, we investigated the global methylation pattern of H3K4 and the results showed remarkable reduction of global methylation of H3K4 in the iAs treated mice, which appeared to be significantly reversed upon BTE administration [Ghosh et al., 2022a]. To further explain the findings, investigation into post translational modifications (PTM) of few histone loci were performed. PTMs of histones are considered to be prognostic markers of cancer [Khan et al., 2015] and the present investigation has been concentrated upon the PTM's of three histone loci, namely H4K16, H3K27 and H3K4, along with their respective histone methylases, demethylases and acetyltransferases.

H4K16ac and its acetyltransferase MYST1, is linked to the promoters of actively transcribed genes. Silencing of MYST1 by iAs reduces H4K16ac, which is implicated in DNA damage response [Miller and Jackson, 2012]. Loss of H4K16ac and MYST1 might be the reason for development of SCC in iAs treated mice, as observed in the present study. Downregulation of H4K16ac has been observed in many cancers like breast cancer, colorectal cancer, medulloblastoma, renal cell carcinoma, [Wu et al., 2020], as well as in ovarian cancer [Liu et al., 2013]. However, its upregulation has been reported in non-small cell lung carcinoma [Wu et al., 2020]. In glioblastoma a marked upregulation of MYST1 has been reported. [Dong et al., 2019]. Prevention of invasive SCC by intervention with BTE may be partly due to the upregulation of H4K16ac and MYST1. H3K27me3 is a transcriptional silencing mark [Sanulli et al., 2015], which has been found to be upregulated in several cancers. A negative correlation with patient survival rate and prognostic marker H3K27me3 has been reported [Tzao et al., 2009]. H3K27me3 plays a lead role in modulation of oncogenes, tumour suppressor genes, cell cycle regulatory and cell adhesion genes in gastric cancer [Zhang et al., 2009]. Methyl transferase EZH2 promotes methylation of H3K27me3 via the PRC2 complex [Sanulli et al., 2015]. This

methyl transferase is highly overexpressed in prostate cancer as a consequence of excessive methylation of H3K27me3 and silencing of several important tumour suppressor genes [Varambally et al., 2002; Ngollo et al., 2017]. EZH2 has been found to be upregulated in breast and ovarian carcinoma; inhibition of which promote apoptosis via H3K27me3 suppression [Gan et al., 2018]. JARID2 is an important part of the PRC2 complex and have been reported to play a key role in methylation and gene silencing [Sanulli et al., 2015]. The tumour suppressive role of KDM6A, which is a H3K27me3 demethylase, has been reported in pancreatic cancer [Andricovich et al., 2018].

Upregulation of H3K27me3 along with EZH2 and JARID2 has been observed in the present study, which indicates active participation of the PRC2 complex. Chronic exposure to iAs has been found to suppress KDM6A and may promote SCC of skin. This event has been found to be reversed by BTE [Ghosh et al., 2022a]. Contrastingly, in human lung carcinoma cell line A459 a repression of H3K27me3 upon iAs exposure was reported [Zhou et al., 2008]. Overexpression of H3K27me3 is promoted by excess ROS generation [Niu et al., 2015].

H3K4 loci has three methylation states, namely H3K4me1, H3K4me2 and H3K4me3, which are linked with promoters of the active genes and temporarily stalled genes [Dhar et al., 2018]. Higher expressions of H3K4me1 and MLL3 (the methyltransferase for H3K4me1) have been observed in mice having invasive SCC due to chronic exposure to iAs; the reason may be due to the formation of oncogenic super-enhancers, aggregation of 700–1300 bases of H3K4me1 and H3K27ac at the promoter regions of genes [Dhar et al., 2018]. Mono-methylation of H3K4 is promoted by MLL3, inducing oncogenic super-enhancer formation in an indirect way [Jia et al., 2020]. Suppression of MLL3 expression due to a mutation has been found in growth of colorectal cancer cells [Larsson et al., 2020]. MLL1, a methyl transferase plays an important role in

trimethylation of H3K4 loci [Fang et al., 2019]. In breast and prostate cancer inhibition of LSD1 (H3K4me1/2 demethylase) upregulates tumour suppressor activity [Lim et al., 2010]. Our findings reveal downregulation of H3K4me3 and MLL1 in the iAs treated Swiss albino mice. However, BTE in the present study showed no modulatory role in the expression of LSD1 [Ghosh et al., 2022a]. Silencing of tumour suppressor genes and promotion of carcinogenesis may be due to loss of both H3K4me3 and MLL1 [Dhar et al., 2018]. BTE elevates the expression of both H3K4me3 and MLL1, exhibiting its tumour suppressive activity. Abnormally high H3K4me3 (500–3500 bps), an epigenetic signature ‘Broad H3K4me3’ is present in the promoters of tumour suppressor genes or cell identity genes, lowering of which has been reported in cancer cells [Dhar et al., 2018]. However, in lung cancer cell line overexpression of H3K4me3 has been observed upon iAs exposure [Zhou et al., 2008]. iAs exposure alters global expression of H3K4me3 via modulation of histone methyl transferases and demethylases [Tu et al., 2018].

Literature reveals ROS generation and overexpression of H3K4me3 has a correlation [Niu et al., 2015]. H3K4Me2 and H3K4Me3, when repressed have a correlation with low grade carcinoma and chances of recurrence of breast, pancreatic, prostate, renal and non-small cell carcinoma [Barlesi et al., 2007, Elsheikh et al., 2009; Ellinger et al., 2010; Manuyakorn et al., 2010]. JARID1B, a demethylase of H3K4me3, has been found to be upregulated by chronic iAs exposure, with a simultaneous downregulation of H3K4me3, displaying its demethylating activity [Ghosh et al., 2022a]. Elevated expression of JARID1B has also been reported in prostate cancer, lung cancer, ER positive breast cancer, osteosarcoma, melanoma, glioma, oral cancers, gastric cancer, hepatocellular carcinoma and pancreatic cancer [Taylor-Papadimitriou and Burchell, 2017; Kristensen et al., 2012], metastatic triple negative breast cancer [Bamodu et al., 2016], colorectal cancer [Huang et al., 2020] and human hypopharyngeal squamous cell carcinoma [Zhang et al., 2016].

Suppression of JARID1B may retard epithelial to mesenchymal transition through upregulation of epithelial marker E-cadherin, thereby preventing carcinogenesis [Tang et al., 2015]. Our findings show that intervention with BTE failed to downregulate the iAs induced elevated level of JARID1B. However, significant upregulation of H3K4me3 was observed due to the administration of BTE. High concentration of JARID1B in cancer stem cells (CSC) expressed oral CSC markers including CD44 and ALDH1 and showed increased PI3K pathway activation [N.D. Facompre et al., 2016]. According to a report, in over 87% of head and neck squamous cell carcinoma elevated levels of JARID1B were observed [Cui et al., 2015]. It may be hypothesized that elevation of H3K4me3 by BTE may be due to inhibition of JARID1B, without leaving an impact on its expression level. In order to understand this finding, in-silico studies (docking) with JARID1B and the active molecules in black tea extract were undertaken. Theaflavin and theaflavin-3,3'-digallate are important components of BTE, among many others. Docking results reveal that both theaflavin and theaflavin-3,3'-digallate dock with JARID1B with high affinity [Ghosh et al., 2022a]. It is known that the Fe(II) ion is crucial for the demethylation activity of the JmjC domain. It is quite likely that theaflavin may have inhibitory effects on the Fe(II) ion, as according our docking study it docked very close to the Mn(II) that replaced Fe(II) in the crystal structure. The exact role of the JmjC domain in substrate recognition and binding is still not properly understood. However, as per our in-silico analysis, both theaflavin and theaflavin-3,3'-digallate docked with high affinity in the JmjC domain. Reports have confirmed the transportation of both these molecules to the nucleus, where they probably interact extensively with histone proteins [Mikutis et al., 2013]. Therefore, it is quite likely that BTE inhibits JARID1B from its demethylation activity due to theaflavin compounds docking at the JmjC domain. High affinity in docking results may not always prove good protein ligand docking [Chen, 2015]. To analyse the stability of docking, molecular

dynamical (MD) simulation needs to be performed. It is also used to analyse whether there are significant differences in the docked poses when MD simulations are run for tens of nanoseconds [Chen, 2015]. MM-PBSA analysis on Gromacs trajectories were performed to verify the stability of docking. The trajectories of both theaflavin and theaflavin-3,3'-digallate show that the initial poses are maintained even after 30 ns of simulation time. Therefore, we may infer that, chronic exposure to iAs altered repressive and activating histone marks like H3K27me3, H3K4me1, H3K4me3 and H4K16ac, through modulation of certain histone methyl transferases (HMTs), histone demethylases (HDMs) and histone acetyltransferases (HATs). BTE, on the other hand, showed its efficacy in modulating these markers, eliciting a promising chemopreventive role [Ghosh et al., 2022a].

The present study shows that excess generation of ROS is a direct consequence of chronic iAs exposure, which may also act as signalling intermediates engaged in cell proliferation, angiogenesis, EMT and metastasis [Aggarwal et al., 2019]. Transforming growth factor beta (TGF- $\beta$ ) is a multifunctional cytokine belonging to the transforming growth factor superfamily. Higher expression of TGF- $\beta$ , has been found in iAs treated Swiss albino mice and HaCaT cells, compared to the control groups. A correlation between high ROS generation and elevated expression of TGF- $\beta$  was evident from the present findings. ROS, through modulation of the TGF- $\beta$  pathway may lead to promotion of EMT, finally culminating in cancer [Lu et al., 2019]. TGF- $\beta$  controls many pathways involved in cell growth and proliferation [Kubiczkova et al., 2012]. In breast, colorectal, gastric, oesophageal, lung, and pancreatic cancers high expression of TGF- $\beta$  has been observed [Huang and Blobel, 2016]. Upregulation of TGF- $\beta$  is associated with greater invasive and metastatic property, as well as poor prognosis [Seoane et al., 2017]. TGF- $\beta$  is known to be secreted by both the tumour cells and the surrounding stromal cells which aids in maintenance of the tumour microenvironment [Wever et al., 2008]. TGF- $\beta$  also promotes

degradation of the extracellular matrix by inducing secretion of matrix metalloproteases, leading to tumour cell invasion. This molecule has a pivotal role in induction of angiogenesis, EMT, alteration of extracellular matrix and downregulation of immune surveillance [Huang and Blobe, 2016]. Present study exhibits that in the iAs + BTE treatment group, ROS generation was quenched efficiently, BTE being a strong antioxidant. However, BTE was unable to modulate the expression of TGF- $\beta$ . Prominent downregulation of pSmad2, pSmad3 and pSmad4 was observed in the iAs treated mice, hinting at suppression of canonical TGF- $\beta$  signalling cascade. Intervention with BTE keeps the canonical pathway active as evident by upregulation of pSmad2, pSmad3 and pSmad4 [Ghosh and Roy, 2023b]. Smad4 is a tumour suppressor, loss of which is associated with SCC of skin, head and neck cancer [Hernandez et al., 2019]. Based on the findings of other researchers, it may be said that development of SCC of skin in Swiss albino mice may be linked to downregulation of Smad4 by iAs. This may be prevented by presence of BTE, which upregulates Smad4.

TGF- $\beta$  in iAs treated Swiss albino mice may have transmitted its downstream signalling via the PI3K-AKT cascade, as evident from the suppression of PTEN, with corresponding elevation of PI3K, AKT, mTOR, S6K and NF $\kappa$ B/p65 expressions [Ghosh and Roy, 2023b]. PTEN, a tumour suppressor protein has been found to inhibit AKT. Due to this mTOR gets downregulated along with other downstream molecular mediators of AKT [Georgescu, 2010]. Results show that the downregulation of PTEN, in iAs treated mice, may be responsible for the development of SCC. It is known that mTOR gets activated by phosphorylated AKT, which further forms mTORC1 and acts along with S6K to promote cell motility and invasion [Lamouille and Derynck, 2007]. It has been reported that activation of mTOR results in formation of mTORC2, leading to cytoskeletal rearrangement, promoting invasive movement of the cells

[Lamouille et al., 2012]. Phosphorylation of AKT is reported to stabilize NF $\kappa$ B/p65 and aids in its translocation to the nucleus, thus facilitating cell proliferation and evasion of apoptosis [Akca et al., 2011]. Phosphorylated AKT stabilizes and activates transcription factors like Snail and Twist that cause EMT [Xue et al., 2012; Julien et al., 2007]. Elevation of PI3K-AKT pathway has been reported in SCC; therefore, downregulation of AKT together with its downstream signalling molecules may aid in skin cancer treatment [Mercurio et al., 2021; Hwang et al., 2020]. According to a study conducted with human breast epithelial cells, it was observed that activation of mTOR by TGF- $\beta$  resulted in their transformation and induction of EMT, stemness and drug resistance [Harvey et al., 2019]. Therefore, it may be presumed from our findings that TGF- $\beta$  guided activation of the PI3K-AKT pathway may promote EMT and induction of SCC of skin by chronic iAs treatment. From our immunoblot results, it was observed that the MAPK pathway also gets activated by chronic iAs exposure. Once TAK1 (MAPKKK) gets activated, it further activates MAPKK3 and MAPKK4, which is followed by upregulation of p38MAPK and JNK1/2 [Ghosh and Roy, 2023b]. Upregulation of TAK1 has been reported in different carcinomas e.g. gastric, oesophageal, thyroid, ovarian origin and osteosarcoma [Mukhopadhyay and Lee, 2020]. TAK1 promotes the nuclear localisation of NF $\kappa$ B/p65, which in turn promotes activation of Cyclin D1 and alters cell proliferation [Mukhopadhyay and Lee, 2020]. Therefore, upregulation of TAK1 boosts cell proliferation. Upregulation of p38 MAPK has a role in tumour promotion. Application of mechanical stress in pancreatic cancer cells resulted in activation of p38 MAPK leading to promotion of EMT and cell migration [Kalli et al., 2022]. An association between high level of p38 MAPK and EMT had been documented in mammary epithelial cells, exhibiting cancer stem cell characteristics and metastatic properties. p38 MAPK $\alpha$  when knocked down caused inhibition of EMT even when expression of transcription factors like Snail and Twist were high; suggesting a



relevance of p38 MAPK in tumorigenesis [Kudaravalli et al., 2022]. Higher expression of p38 MAPK $\gamma$  augmented the ability of breast cancer cells to form spheroid, hinting at onset of stem cell like characteristics [Xu et al., 2018]. Enhanced expression of JNK1/2 promotes EMT by the activation of mesenchymal factors like Snail and Twist in KB epithelial carcinoma cell line; downregulation of JNK1/2 suppresses EMT and migration of cancer cells [Zhan et al., 2013]. Inhibition of JNK in gastric cancer cells impedes EMT, as well as migration. Therefore, both p38 MAPK and JNK play a lead role in induction of EMT [Choi et al., 2016]. Activation of these two proteins has been reported in UV-induced SCC of skin and consequently inhibition of p38 MAPK and JNK may repress cancer progression [Zhang et al., 2012]

In the present study, it has been observed that iAs activated TGF- $\beta$  transmits its downstream signalling via the MAPK pathway along with the PI3K-AKT signalling cascade. Signalling intermediates of both the pathways studied can promote and regulate transcription factors which induce mesenchymal traits, culminating in EMT, in both Swiss albino mice and HaCaT cells. No such activation of signalling intermediates, of both PI3K-AKT and MAPK pathways, has been found after BTE intervention [Ghosh and Roy, 2022a; Ghosh and Roy, 2022b]; this is suggestive of the fact that downregulation of the non-canonical TGF- $\beta$  pathway is being facilitated by BTE. The signalling cascade downstream of TGF- $\beta$  follows the canonical Smad pathway in presence of BTE. Therefore, we may infer that BTE is quite efficient in suppressing the signalling molecular intermediates of the PI3K-AKT and MAPK pathways.

The epithelial and mesenchymal cells have a distinct variation in their appearance and arrangement. Typical characteristics of the epithelial cells are their columnar or cuboidal shape; they are arranged in single or multiple sheets like layers. Maintenance of the shape and structure of epithelial cells are attributed to the adherent

cadherin junctions, tight junctions, gap junctions, desmosomes, and interactions with the extra cellular matrix [Huang et al., 2012]. These epithelial cells lose their morphology and adopt spindle shape during transition and their apical and basal polarity as well as other cell junctions are also lost. Due to these modifications, mesenchymal cells get entry to invade the surrounding tissues and undergo metastasis [Serrano-Gomez et al., 2016]. Thus, EMT happens to be a quintessential phenomenon for carcinogenesis. Literature survey reveals that ROS generation plays a vital role in promotion of EMT via suppression of E-cadherin and increased expression of  $\alpha$ -SMA (Smooth muscle actin). Activation of the MAPK and TGF- $\beta$  pathway results in induction of EMT and ROS plays a lead role in this regard [Fukawa et al., 2012]. Therefore, excess generation of ROS owing to chronic exposure to iAs may promote carcinogenesis via induction of EMT. EMT is facilitated by subduing of key epithelial markers like E-cadherin, Desmoplakin etc. with concomitant upregulation or activation of several mesenchymal markers like Vimentin, N-cadherin etc. Transcription factors like Snail, Slug, Zeb and Twist are also notably upregulated during EMT. E-cadherin, a tumour suppressor maintains cell polarity and construction of epithelial barriers by formation of intracellular complex with adjacent cells. [Na et al., 2020]. The extracellular portion of E-cadherins of the adjacent cells attach with each other to form a bridge and by this way they connect to the cytoskeletons of the neighbouring cells [Tian et al., 2011]. Desmoplakin, another epithelial marker forms important components of the desmosomes that aid in the formation of intercellular adhesive junctions, which play vital role in cell-to-cell communication and maintain epithelial characteristics [Johnson et al., 2014]. The transcription factors Snail, Slug and Zeb1 which are mesenchymal markers subjugate the expression of E-cadherin by binding to the E-boxes located on the promoter region of E-cadherin gene (CDH1), culminating into the transcriptional silencing [Puisieux et al., 2014]. Twist is reported to suppress the expression of E-cadherin indirectly, but

according to some research findings it can also bind to the 2nd and 3rd E-boxes of the CDH1 gene [Serrano-Gomez et al., 2016]. Therefore, repression of E-cadherin by these transcription factors, be it direct, or indirect leads to loss of epithelial traits, with concomitant promotion of mesenchymal features. This cumulative action paves a way for progression of cancer. In the present study, immunoblotting, IHC, flowcytometric and immunofluorescent studies have confirmed the loss of epithelial markers (E-cadherin and Desmoplakin) and gain of mesenchymal markers (Vimentin, N-cadherin, Snail, Slug, Twist and Zeb) [Ghosh et al., 2022b; Ghosh and Roy, 2023b]. Results of the semi-quantitative RT-PCR revealed that suppression of epithelial markers and elevation of mesenchymal markers, upon iAs treatment, occurred not only at the protein level but also at the mRNA level. In the iAs+BTE treatment group, epithelial markers were upregulated and mesenchymal markers were downregulated, both at the translational and transcriptional level, indicating inhibition of EMT by BTE [Ghosh and Roy, 2023b]. Similar observations have been reported in *in vitro* studies, where the potential of BTE to revert EMT and repression of cell migration have been highlighted in human oral carcinoma cells (SCC4) [Chang et al., 2012]. Potential of BTE to prevent the progression of EMT even after being chronically exposed to iAs has been emphasized in the present study. As inhibition of EMT and cessation of cancer progression are highly correlated, therefore, an inference may be drawn that BTE prevents iAs induced carcinogenesis by halting EMT.

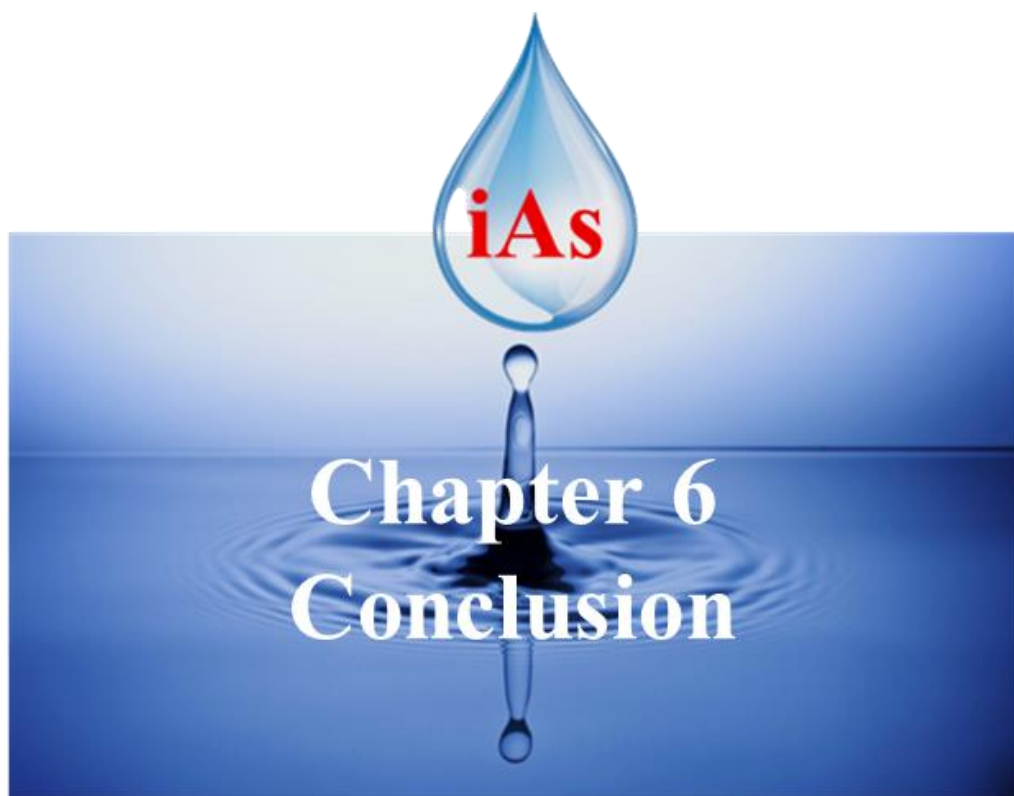
Metastasis is the detrimental part of cancer, which is a consequence of EMT. iAs treated cells which have undergone EMT display carcinogenic traits, like increased cell motility, enhanced invasive and migratory abilities as well as high propensity to digest the extracellular matrix and perform angiogenesis [Son and Moon, 2010]. Invasion of the surrounding tissue, leading to blood vessel formation (angiogenesis) as well as metastasis is a hallmark of cancer [Hanahan and Weinberg, 2011]. Present study unveils that due to

continuous exposure to low dose iAs, the normal human keratinocyte HaCaT cells are transformed into aggressive cancer cells. These transformed cells develop the ability to invade and migrate, as evident from transwell migration/invasion assay findings. Upregulation of angiogenic factors like VEGF, EGFR along with enhanced gelatinolytic capability due to over expression of MMP2 and MMP9 have been observed in these transformed HaCaT cells [Ghosh et al., 2022b]. It is the need of the hour to overcome the deleterious effects of iAs on human health. Presence of BTE along with iAs, may control the evil effect of the deadly metalloids. Hence, it may be assumed that BTE may be a promising chemopreventive agent which is capable to inhibit the carcinogenic insult due to iAs, by hindering EMT, preventing metastasis and thereby impeding the progression towards cancer. Therefore, we may say that BTE is able to counter the carcinogenicity of iAs both in *in-vivo* and *in-vitro* models.

Carcinogenicity of iAs has been discussed, which has been found to be efficiently ameliorated by BTE. This deadly metalloid is not only a carcinogen, but also a co-carcinogen, enhancing the carcinogenicity of other carcinogens. To study co-carcinogenicity of iAs, a two-step model of skin carcinogenesis using DMBA and TPA, was followed, which is a standard mouse skin cancer model [Abel et al., 2009]. Histological analysis exhibits that the groups of mice receiving co-treatment of DMBA and iAs, along with TPA, developed *in-situ* and invasive carcinoma much faster than those which received only DMBA. Early onset of cancer upon combined treatment of DMBA and iAs may be due to the co-carcinogenicity of iAs [Ghosh et al., 2021b]. In the present study, DMBA+iAs treated mice showed higher ROS generation; elevated levels of DNA, protein and lipid damage; compromised total antioxidant activity; higher activity of pro-inflammatory cytokines like TNF- $\alpha$ , IL6, IL17A, IL22 and of two subunits of NF $\kappa$ B, p50 and p65, in comparison to the DMBA treated mice. Present investigation indicates that iAs in presence

of DMBA is able to accelerate the process of SCC by inducing much higher ROS generation, which is the root cause of many adverse effects implicated in carcinogenesis. As a consequence, DMBA induced DNA damage, LPO and protein carbonyl content were much higher in presence of iAs. Besides, activation of pro-inflammatory cytokines and transcription factors are much escalated by the presence of iAs in comparison to DMBA treatment alone. Similarly, suppression of antioxidative capacity by DMBA is more pronounced when the animals are subjected to DMBA and iAs treatment simultaneously [Ghosh et al., 2021b]. All these findings suggest that presence of iAs may result in early appearance of carcinogenesis by DMBA, hinting at its co-carcinogenic nature.

Therefore, from the results obtained in this study, it may be inferred that, iAs is a potent inducer of SCC in *in vivo* and *in vitro* model; the globally popular beverage black tea has the potential to remediate the adverse effect on health, particularly in relation to development of squamous cell carcinoma of the skin.



## 6. Conclusion

Groundwater contamination appears to be one of the major sources of iAs exposure amongst humans. High concentrations of iAs in groundwater has been recorded in various places around the globe, including India. Chronic exposure to iAs, greater than the safe limit of 10µg/l, results in development of numerous health hazards, deadliest amongst them being cancer. Besides its carcinogenicity, iAs is a co-carcinogen, which has been found to enhance the carcinogenicity of DMBA in Swiss albino mice. Preliminary manifestations of chronic iAs exposure appears on the skin, which may develop into Squamous Cell Carcinoma (SCC). One of the primary mechanisms by which iAs induces its carcinogenicity, is by the generation of free radicals. At cellular level excess free radicals can cause DNA, protein, and lipid damage; inhibit DNA repair capacity; suppress the activity of antioxidant enzymes along with total antioxidant capacity and can also promote inflammatory conditions. Excess generation of free radicals may also act as signalling intermediates, modulating many pathways which control cell survival, growth, and proliferation, like TGF- $\beta$  pathway; induce epithelial to mesenchymal transition, metastasis; aberrant epigenetic modulations may be another manifestation. Drugs which are used to treat skin carcinoma are expensive and toxic with numerous side effects, therefore non-toxic phytochemicals may be a respite to the problem. Black tea, a popular beverage is a good antioxidant. Exploring this antioxidative property of black tea to quench free radicals and counter the associated adverse effects due to chronic iAs exposure may be a good strategy to combat the problem. The present study elucidates the effect of chronic iAs exposure, on Swiss albino mice and normal human skin keratinocytes (HaCaT cells), as well as investigates the ameliorative property of Black tea extract in the same.

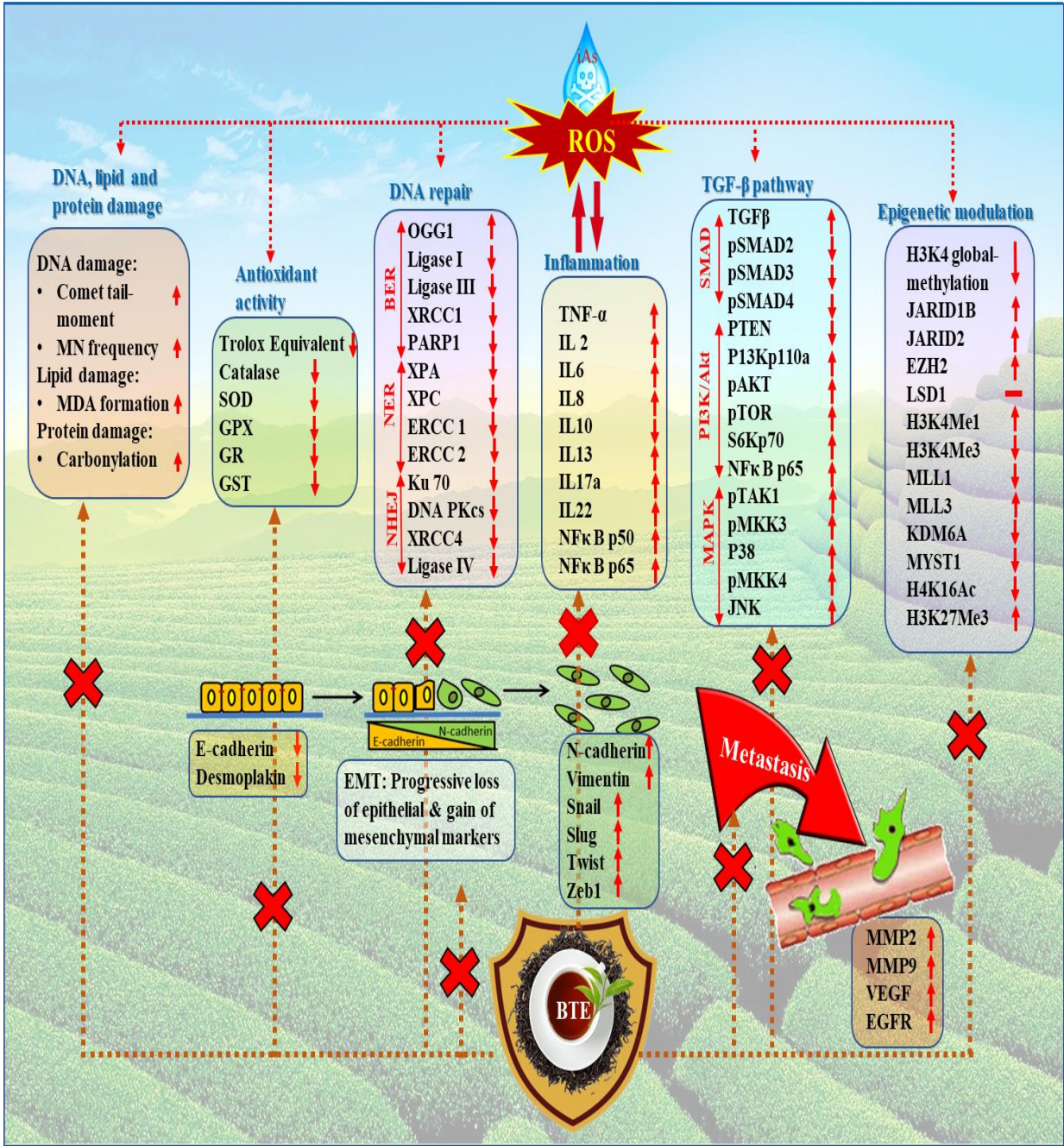
Chronic treatment with iAs (500 µg/l) for a period of 330 days resulted in the development of large, ulcerative tumours on the skin of Swiss albino mice which were histologically confirmed to be invasive SCC. Carcinogenic transformations were also observed in HaCaT cells. These cells when chronically treated with iAs (100 nM) for 240 days, showed morphological transformation, loss of contact inhibition, reduced doubling time and high proliferative index. The lesions developed in the iAs+BTE treated mice, after 330 days, were much smaller in size and histologically only hyperplastic and dysplastic changes were visible. The iAs+BTE treated HaCaT cells did not show any carcinogenic transformation, after 240 days of treatment. This indicates that, BTE may have mitigated the deleterious effect of iAs, both in Swiss albino mice and HaCaT cells leading to prevention of tumour development. Generation of free radicals was high in the iAs treated *in-vivo* and *in-vitro* models, which might have led to increased DNA, protein and lipid damage in them. Chronic iAs treatment resulted in suppression of activity of antioxidant enzymes, impairment of DNA repair capacity, downregulation of DNA repair enzymes implicated in BER, NER and NHEJ pathway. Induction of inflammatory conditions by elevating the activity and expression of pro-inflammatory cytokines (TNF- $\alpha$ , IL2, IL6, IL8, IL13, IL17a and IL22), with simultaneous lowering of activity and expression of anti-inflammatory cytokine (IL10) was another consequence of iAs exposure. BTE intervention resulted in quenching of excess free radicals generated due to iAs treatment, which eventually led to reduction of DNA, lipid, and protein damage. BTE was also found to elevate the activity of antioxidant enzymes, increase DNA repair capacity, upregulate the expression of DNA repair enzymes, suppress the activity and expression of pro-inflammatory cytokines with simultaneous enhancement of the activity and expression of anti-inflammatory cytokine. These findings indicate that, BTE might be able to counter the ill effects of chronic iAs exposure.

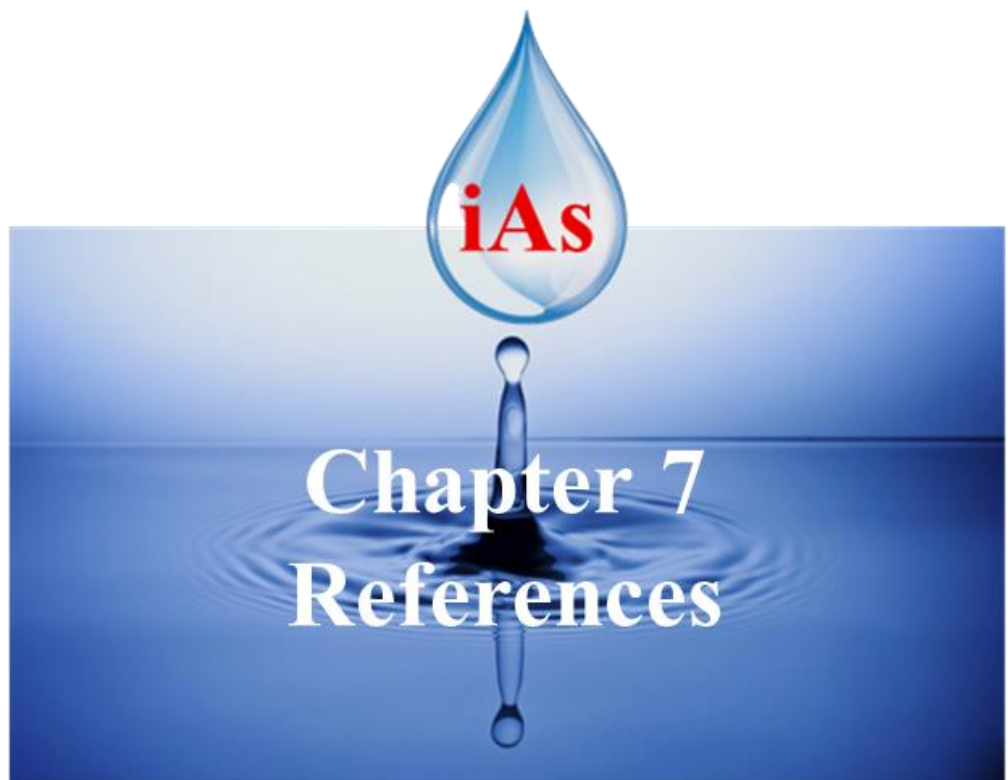


A global hypomethylation of the H3K4 locus in iAs administered mice was observed, which was found to be reversed in the BTE treatment group. Post translational modifications of three histone loci H4K16, H3K27, H3K4 and their respective acetyltransferases, histone methylases and demethylases were analysed in our study. Chronic treatment with iAs resulted in downregulation of H4K16ac and its acetyltransferase MYST1, loss of which has been reported in numerous cancers. In iAs+BTE treated mice, both H4K16ac and MYST1 was found to be upregulated. Upregulation of H3K27me3, its methyl transferase EZH2 and JARID2 (part of the PRC2 complex, involved in methylation of H3K27 locus), with simultaneous downregulation of demethylase KDM6A has been observed in the iAs treated mice. Upregulation of H3K27me3, EZH2 and downregulation of KDM6A has been implicated in various cancers. In the BTE administered mice, the expression of H3K27me3, its methyl transferase and demethylase were found to be reversed. Chronic iAs treatment also resulted in upregulation of H3K4me1 and its methyl transferase MLL3. Upregulation of H3K4me1 is associated with increased expression of oncogenes. In the BTE administered mice, the expression of H3K4me1 and MLL3 was downregulated. In the iAs treated mice, downregulation of H3K4me3, its methyltransferase MLL1 with concomitant upregulation of demethylase JARID1B was observed. H3K4me3 is associated with expression of tumour suppressor genes and its downregulation may promote cancer, whereas elevated expression of JARID1B has been reported in numerous cancers. BTE upregulates the expression of H3K4me3 and its methyl transferase MLL1, while it fails to suppress the expression of JARID1B. in-silico docking studies revealed high affinity docking of theaflavin and theaflavin-3,3'-digallate (major components of BTE) in the proposed demethylating (JmjC) domain of JARID1B, which resulted in its inhibition. Molecular simulation studies confirmed the stability of this docking, as these molecules maintained their initial docking

poses for more than 30 nano seconds. These findings gave an indication that intervention with BTE alters iAs induced aberrant epigenetic modulations.

Chronic iAs exposure also led to modulation of TGF- $\beta$  pathway. Upon chronic iAs treatment, upregulated TGF- $\beta$  transmitted its downstream signalling by the non-canonical PI3K-AKT and MAPK pathways. Contrarily, BTE administration, resulted in downregulation of the signalling intermediates of PI3K-AKT and MAPK pathways. These signalling intermediates are known to induce EMT and aid in cancer progression. Therefore, lowering of these signalling factors by BTE, highlights its role in cancer prevention. EMT is prerequisite for tumorigenesis and results of the present study suggest that, chronic iAs exposure induces EMT in both *in vivo* and *in vitro* models. Presence of BTE inhibits EMT by promoting upregulation of epithelial factors (E-cadherin and Desmoplakin) and downregulation of mesenchymal factors (Vimentin, N-cadherin, Snail, Slug, Twist and Zeb), both at the protein and at the mRNA level. Chronic iAs treatment promoted invasive, migratory and angiogenic transformations in HaCaT cells which may lead to metastasis. BTE treated cells showed reduction of invasive and migratory properties, suppression of gelatinolytic activity, downregulation of MMP2, MMP9 and lowering of angiogenic factors like VEGF and EGFR. Therefore, BTE can also inhibit metastatic and angiogenic transformations. The results of the present study reveal that BTE quenches free radical generation; reduces DNA, lipid and protein damage; promotes antioxidative enzyme activity; upregulates DNA repair enzymes and suppresses inflammation. It also reverses iAs induced aberrant epigenetic modulations; downregulates EMT promoting signalling intermediates of TGF- $\beta$  pathway; hinders EMT as well as inhibits metastasis and angiogenesis. Therefore, BTE appears to be an effective chemopreventive phytochemical which can mitigate iAs induced SCC of the skin.





## 7. References

1. Abel EL, Angel JM, Kiguchi K, DiGiovanni J. Multi-stage chemical carcinogenesis in mouse skin: fundamentals and applications. *Nat Protoc.* 2009;4(9):1350-62.
2. Abraham MJ, Murtola T, Schulz R, Páll S, Smith JC, Hess B, Lindahl E. GROMACS: high performance molecular simulations through multi-level parallelism from laptops to supercomputers. *SoftwareX.* 2015;1:19–25.
3. Acuner-Ozbabacan ES, Engin BH, Guven-Maiorov E, Kuzu G, Muratcioglu S, Baspinar A, Chen Z, Van Waes C, Gursoy A, Keskin O, Nussinov R. The structural network of Interleukin-10 and its implications in inflammation and cancer. *BMC Genomics.* 2014;15:S2.
4. Adams LS, Phung S, Yee N, Seeram NP, Li L, Chen S. Blueberry phytochemicals inhibit growth and metastatic potential of MDA-MB-231 breast cancer cells through modulation of the phosphatidylinositol 3-kinase pathway. *Cancer Res.* 2010;70(9):3594-605.
5. Aggarwal BB, Shishodia S, Takada Y, Jackson-Bernitsas D, Ahn KS, Sethi G, Ichikawa H. TNF blockade: an inflammatory issue. *Ernst Schering Res Found Workshop.* 2006;(56):161-86.
6. Aggarwal V, Tuli HS, Varol A, Thakral F, Yerer MB, Sak K, Varol M, Jain A, Khan MA, Sethi G. Role of Reactive Oxygen Species in Cancer Progression: Molecular Mechanisms and Recent Advancements. *Biomolecules.* 2019;9(11):735.
7. Akca H, Demiray A, Tokgun O, Yokota J. Invasiveness and anchorage independent growth ability augmented by PTEN inactivation through the PI3K/AKT/NFκB pathway in lung cancer cells. *Lung Cancer* 2011;73:302-9.
8. Alam R, Gorska M. 3. Lymphocytes. *J Allergy Clin Immunol.* 2003;111:S476-85.

9. Alarcón-Herrera MT, Martín-Alarcon DA, Gutiérrez M, Reynoso-Cuevas L, Martín-Domínguez A, Olmos-Márquez MA, Bundschuh J. Co-occurrence, possible origin, and health-risk assessment of arsenic and fluoride in drinking water sources in Mexico: Geographical data visualization. *Sci Total Environ.* 2020 1;698:134168.
10. Allred DC, Harvey JM, Berardo M, Clark GM. Prognostic and predictive factors in breast cancer by immunohistochemical analysis. *Mod Pathol.* 1998;11(2):155-68.
11. Andrew AS, Karagas MR, Hamilton JW. Decreased DNA repair gene expression among individuals exposed to arsenic in United States drinking water. *Int J Cancer.* 2003a;104(3):263-8.
12. Andrew AS, Warren AJ, Barchowsky A, Temple KA, Klei L, Soucy NV, O'Hara KA, Hamilton JW. Genomic and Proteomic Profiling of Responses to Toxic Metals in Human Lung Cells. *Environ Health Perspect.* 2003b;111:825–838.
13. Andricovich J, Perkail S, Kai Y, Casasanta N, Peng W, Tzatsos A. Loss of KDM6A Activates Super-Enhancers to Induce Gender-Specific Squamous-like Pancreatic Cancer and Confers Sensitivity to BET Inhibitors. *Cancer Cell.* 2018;33(3):512-526.e8.
14. Antman KH. Introduction: the history of arsenic trioxide in cancer therapy. *Oncologist.* 2001;6(2):1-2.
15. Azubuike CC, Chikere CB, Okpokwasili GC. Bioremediation techniques-classification based on site of application: principles, advantages, limitations and prospects. *World J Microbiol Biotechnol.* 2016;32:180.
16. Ba X, Boldogh I. 8-Oxoguanine DNA glycosylase 1: Beyond repair of the oxidatively modified base lesions. *Redox Biol.* 2018;14:669-678.

17. Baba AB, Rah B, Bhat GR, Mushtaq I, Parveen S, Hassan R, Hameed Zargar M, Afroze D. Transforming Growth Factor-Beta (TGF- $\beta$ ) Signalling in Cancer-A Betrayal Within. *Front Pharmacol.* 2022;13:791272.
18. Bag A, Bag N. Tea Polyphenols and Prevention of Epigenetic Aberrations in Cancer. *J Nat Sci Biol Med.* 2018;9(1):2-5.
19. Bamodu OA, Huang WC, Lee WH, Wu A, Wang LS, Hsiao M, Yeh CT, Chao TY. Aberrant KDM5B expression promotes aggressive breast cancer through MALAT1 overexpression and downregulation of hsa-miR-448. *BMC Cancer.* 2016;16:160.
20. Banerjee M, Banerjee N, Bhattacharjee P, Mondal D, Lythgoe PR, Martínez M, Pan J, Polya DA, Giri AK. High arsenic in rice is associated with elevated genotoxic effects in humans. *Sci Rep.* 2013;3:2195.
21. Banerjee S, Bueso-Ramos C, Aggarwal BB. Suppression of 7,12-dimethylbenz(a)anthracene-induced mammary carcinogenesis in rats by resveratrol: role of nuclear factor-kappaB, cyclooxygenase 2, and matrix metalloprotease 9. *Cancer Res.* 2002;62(17):4945-54.
22. Barlési F, Giaccone G, Gallegos-Ruiz MI, Loundou A, Span SW, Lefesvre P, Kruyt FA, Rodriguez JA. Global histone modifications predict prognosis of resected non small-cell lung cancer. *J Clin Oncol.* 2007;25(28):4358-64.
23. Bartolome RA, Garcia-Palmero I, Torres S, Lopez-Lucendo M, Balyasnikova IV, Casal JI. IL13 Receptor alpha2 Signaling Requires a Scaffold Protein, FAM120A, to Activate the FAK and PI3K Pathways in Colon Cancer Metastasis. *Cancer Res.* 2015;75:2434-44.
24. Bau DT, Gurr JR, Jan KY. Nitric oxide is involved in arsenite inhibition of pyrimidine dimer excision. *Carcinogenesis.* 2001;22:709-716.



25. Beck R, Styblo M, Sethupathy P. Arsenic Exposure and Type 2 Diabetes: MicroRNAs as Mechanistic Links? *Curr Diab Rep.* 2017;17(3):18.
26. Bhattacharya P, Mukherjee A, Mukherjee AB. Arsenic contaminated groundwater in India. In: Nriagu J (ed). *Encyclopaedia of environmental health.* Elsevier B.V, Amsterdam, pp 150–164; 2011.
27. Boukamp P, Petrussevska RT, Breitkreutz D, Hornung J, Markham A, Fusenig NE. Normal keratinization in a spontaneously immortalized aneuploid human keratinocyte cell line. *J Cell Biol.* 1988;106(3):761-71.
28. Boyce BF, Li P, Yao Z, Zhang Q, Badell IR, Schwarz EM, O'Keefe RJ, Xing L. TNF-alpha and pathologic bone resorption. *Keio J Med.* 2005;54(3):127-31.
29. Caldon CE. Estrogen signaling and the DNA damage response in hormone dependent breast cancers. *Front Oncol.* 2014;4:106.
30. Cannan WJ, Rashid I, Tomkinson AE, Wallace SS, Pederson DS. The Human Ligase III $\alpha$ -XRCC1 Protein Complex Performs DNA Nick Repair after Transient Unwrapping of Nucleosomal DNA. *J Biol Chem.* 2017;292(13):5227-5238.
31. Cantone L, Nordio F, Hou L, Apostoli P, Bonzini M, Tarantini L, Angelici L, Bollati V, Zanobetti A, Schwartz J, Bertazzi PA, Baccarelli A. Inhalable metal-rich air particles and histone H3K4 dimethylation and H3K9 acetylation in a cross-sectional study of steel workers. *Environ Health Perspect.* 2011;119(7):964-9.
32. Chakraborti D, Rahman MM, Das B, Chatterjee A, Das D, Nayak B, Pal A, Chowdhury UK, Ahmed S, Biswas BK. Groundwater arsenic contamination and its health effects in India. *Hydrogeol J.* 2017;25:1–17.
33. Chakraborti D, Singh SK, Rahman MM, Dutta RN, Mukherjee SC, Pati S, Kar PB. Groundwater Arsenic Contamination in the Ganga River Basin: A Future Health Danger. *Int J Environ Res Public Health.* 2018 Jan 23;15(2):180.



34. Chang YC, Chen PN, Chu SC, Lin CY, Kuo WH, Hsieh YS. Black tea polyphenols reverse epithelial-to-mesenchymal transition and suppress cancer invasion and proteases in human oral cancer cells. *J Agric Food Chem*. 2012;60(34):8395-403.
35. Chen H, Li S, Liu J, Diwan BA, Barrett JC, Waalkes MP. Chronic inorganic arsenic exposure induces hepatic global and individual gene hypomethylation: implications for arsenic hepatocarcinogenesis. *Carcinogenesis*. 2004;25(9):1779-86.
36. Chen H, Zhu B, Zhao L, Liu Y, Zhao F, Feng J, Jin Y, Sun J, Geng R, Wei Y. Allicin Inhibits Proliferation and Invasion in Vitro and in Vivo via SHP-1-Mediated STAT3 Signaling in Cholangiocarcinoma. *Cell Physiol Biochem*. 2018;47(2):641-653.
37. Chen L, Fan J, Chen H, Meng Z, Chen Z, Wang P, Liu L. The IL-8/CXCR1 axis is associated with cancer stem cell-like properties and correlates with clinical prognosis in human pancreatic cancer cases. *Sci Rep*. 2014;4:5911.
38. Chen WT, Hung WC, Kang WY, Huang YC, Chai CY. Urothelial carcinomas arising in arsenic contaminated areas are associated with hypermethylation of the gene promoter of the death-associated protein kinase. *Histopathology*. 2007;51:785–92.
39. Chen YC. Beware of docking. *Trends Pharmacol Sci*. 2015;36:78–95.
40. Choi Y, Ko YS, Park J, Choi Y, Kim Y, Pyo JS, Jang BG, Hwang DH, Kim WH, Lee BL. HER2-induced metastasis is mediated by AKT/JNK/EMT signalling pathway in gastric cancer. *World J Gastroenterol*. 2016;22(41):9141-9153.
41. Choudhari AS, Mandave PC, Deshpande M, Ranjekar P, Prakash O. Phytochemicals in Cancer Treatment: From Preclinical Studies to Clinical Practice. *Front Pharmacol*. 2020;10:1614.

42. Chung J, Huda MN, Shin Y, Han S, Akter S, Kang I, Ha J, Choe W, Choi TG, Kim SS. Correlation between Oxidative Stress and Transforming Growth Factor-Beta in Cancers. *Int J Mol Sci.* 2021;22(24):13181.
43. Chung JY, Yu SD, Hong YS. Environmental source of arsenic exposure. *J Prev Med Public Health.* 2014;47(5):253-7.
44. Cipolla BG, Mandron E, Lefort JM, Coadou Y, Della Negra E, Corbel L, Le Scodan R, Azzouzi AR, Mottet N. Effect of Sulforaphane in Men with Biochemical Recurrence after Radical Prostatectomy. *Cancer Prev Res (Phila).* 2015;8(8):712-9.
45. Cojocneanu Petric R, Braicu C, Raduly L, Zanoaga O, Dragos N, Monroig P, Dumitrascu D, Berindan-Neagoe I. Phytochemicals modulate carcinogenic signalling pathways in breast and hormone-related cancers. *Onco Targets Ther.* 2015;8:2053-66.
46. Coppin JF, Qu W, Waalkes MP. Interplay between cellular methyl metabolism and adaptive efflux during oncogenic transformation from chronic arsenic exposure in human cells. *J Biol Chem.* 2008;283(28):19342-50.
47. Coussens LM, Werb Z. Inflammation and cancer. *Nature.* 2002.;420:860-7.
48. Cui Z, Song L, Hou Z, Han Y, Hu Y, Wu Y, Chen W, Mao L. PLU-1/JARID1B overexpression predicts proliferation properties in head and neck squamous cell carcinoma. *Oncol Rep.* 2015;33(5):2454-60.
49. Cullen WR. Chemical mechanism of arsenic biomethylation. *Chem Res Toxicol.* 2014;27: 457-61.
50. Cullen WR. *Is Arsenic an Aphrodisiac? The Sociochemistry of an Element,* Cambridge, UK, RSC Publishing. 2008.
51. Cullen WR. The toxicity of trimethylarsine: an urban myth. *J Environ Monit.* 2005;7(1):11-5.

52. Cunha LL, Morari EC, Nonogaki S, Marcello MA, Soares FA, Vassallo J, Ward LS. Interleukin 10 expression is related to aggressiveness and poor prognosis of patients with thyroid cancer. *Cancer Immunol Immunother.* 2017;66(2):141-148.
53. Darvesh AS, Aggarwal BB, Bishayee A. Curcumin and liver cancer: a review. *Curr Pharm Biotechnol.* 2012;13(1):218-28.
54. Das D, Bindhani B, Mukherjee B, Saha H, Biswas P, Dutta K, Prasad P, Sinha D, Ray MR. Chronic low-level arsenic exposure reduces lung function in male population without skin lesions. *Int J Public Health.* 2014;59(4):655-63.
55. Datta A, Deng S, Gopal V, Yap KC, Halim CE, Lye ML, Ong MS, Tan TZ, Sethi G, Hooi SC, Kumar AP, Yap CT. Cytoskeletal Dynamics in Epithelial-Mesenchymal Transition: Insights into Therapeutic Targets for Cancer Metastasis. *Cancers (Basel).* 2021;13(8):1882.
56. De Wever O, Demetter P, Mareel M, Bracke M. Stromal myofibroblasts are drivers of invasive cancer growth. *Int J Cancer.* 2008;123(10):2229-38.
57. Deepmala, Slattery J, Kumar N, Delhey L, Berk M, Dean O, Spielholz C, Frye R. Clinical trials of N-acetylcysteine in psychiatry and neurology: A systematic review. *Neurosci Biobehav Rev.* 2015 Aug;55:294-321.
58. DeNardo DG, Coussens LM. Inflammation and breast cancer. Balancing immune response: Crosstalk between adaptive and innate immune cells during breast cancer progression. *Breast Cancer Res.* 2007;9: 212.
59. Deng QP, Wang MJ, Zeng X, Chen GG, Huang RY. Effects of Glycyrrhizin in a Mouse Model of Lung Adenocarcinoma. *Cell Physiol Biochem.* 2017;41(4):1383-1392.
60. Dhar SS, Zhao D, Lin T, Gu B, Pal K, Wu SJ, Alam H, Lv J, Yun K, Gopalakrishnan V, Flores ER, Northcott PA, Rajaram V, Li W, Shilatifard A,

- Sillitoe RV, Chen K, Lee MG. MLL4 Is Required to Maintain Broad H3K4me3 Peaks and Super-Enhancers at Tumor Suppressor Genes. *Mol Cell*. 2018;70(5):825-841.
61. Dong Z, Zou J, Li J, Pang Y, Liu Y, Deng C, Chen F, Cui H. MYST1/KAT8 contributes to tumor progression by activating EGFR signalling in glioblastoma cells. *Cancer Med*. 2019;8(18):7793-7808.
62. Dou J, Wang Z, Ma L, Peng B, Mao K, Li C, Su M, Zhou C, Peng G. Baicalein and baicalin inhibit colon cancer using two distinct fashions of apoptosis and senescence. *Oncotarget*. 2018;9(28):20089-20102.
63. Dunn GP, Bruce AT, Ikeda H, Old LJ, Schreiber RD. Cancer immunoediting: from immunosurveillance to tumour escape. *Nat Immunol*. 2002; 3: 991–998.
64. Dutta K, Prasad P, Sinha D. Chronic low level arsenic exposure evokes inflammatory responses and DNA damage. *Int J Hyg Environ Health*. 2015;218(6):564-74.
65. Ebert F, Weiss A, Bültmeyer M, Hamann I, Hartwig A, Schwerdtle T. Arsenicals affect base excision repair by several mechanisms. *Mutat Res Fundam Mol Mech Mutagen*. 2011;715:32–41.
66. Ebrahimi B, Tucker SL, Li D, Abbruzzese JL, Kurzrock R. Cytokines in pancreatic carcinoma: correlation with phenotypic characteristics and prognosis. *Cancer*. 2004 Dec 15;101(12):2727-36.
67. Eckstein M, Eleazer R, Rea M, Fondufe-Mittendorf Y. Epigenomic reprogramming in inorganic arsenic-mediated gene expression patterns during carcinogenesis. *Rev Environ Health*. 2017;32:93-103.
68. Ellinger J, Kahl P, Mertens C, Rogenhofer S, Hauser S, Hartmann W, Bastian PJ, Büttner R, Müller SC, von Ruecker A. Prognostic relevance of global histone H3

- lysine 4 (H3K4) methylation in renal cell carcinoma. *Int J Cancer*. 2010;127(10):2360-6.
69. Ellinsworth DC. Arsenic, reactive oxygen, and endothelial dysfunction. *J Pharmacol Exp Ther*. 2015;353(3):458-64.
70. Elsheikh SE, Green AR, Rakha EA, Powe DG, Ahmed RA, Collins HM, Soria D, Garibaldi JM, Paish CE, Ammar AA, Grainge MJ, Ball GR, Abdelghany MK, Martinez-Pomares L, Heery DM, Ellis IO. Global histone modifications in breast cancer correlate with tumor phenotypes, prognostic factors, and patient outcome. *Cancer Res*. 2009;69(9):3802-9.
71. Facompre ND, Harmeyer KM, Sole X, Kabraji S, Belden Z, Sahu V, Whelan K, Tanaka K, Weinstein GS, Montone KT, Roesch A, Gimotty PA, Herlyn M, Rustgi AK, Nakagawa H, Ramaswamy S, Basu D. JARID1B Enables Transit between Distinct States of the Stem-like Cell Population in Oral Cancers. *Cancer Res*. 2016;76(18):5538-49.
72. Fang Y, Zhang D, Hu T, Zhao H, Zhao X, Lou Z, He Y, Qin W, Xia J, Zhang X, Ye LC. KMT2A histone methyltransferase contributes to colorectal cancer development by promoting cathepsin Z transcriptional activation. *Cancer Med*. 2019;8(7):3544-3552.
73. Fedorova M, Bollineni RC, Hoffmann R. Protein carbonylation as a major hallmark of oxidative damage: update of analytical strategies. *Mass Spectrom Rev*. 2014;33(2):79-97.
74. Feng L, Qi Q, Wang P, Chen H, Chen Z, Meng Z, Liu L. Serum levels of IL-6, IL-8, and IL-10 are indicators of prognosis in pancreatic cancer. *J Int Med Res*. 2018;46(12):5228-5236.

75. Flora SJ, Bhadauria S, Kannan GM, Singh N. Arsenic induced oxidative stress and the role of antioxidant supplementation during chelation: a review. *J Environ Biol.* 2007;28(2):333-47.
76. Fouad YA, Aanei C. Revisiting the hallmarks of cancer. *Am J Cancer Res.* 2017;7(5):1016–1036.
77. Fujiki H, Sueoka E, Watanabe T, Suganuma M. Primary cancer prevention by green tea, and tertiary cancer prevention by the combination of green tea catechins and anticancer compounds. *J Cancer Prev.* 2015;20(1):1-4.
78. Fukawa T, Kajiya H, Ozeki S, Ikebe T, Okabe K. Reactive oxygen species stimulates epithelial mesenchymal transition in normal human epidermal keratinocytes via TGF-beta secretion. *Exp Cell Res.* 2012;318(15):1926-32.
79. Gabitass RF, Annels NE, Stocken DD, Pandha HA, Middleton GW. Elevated myeloid-derived suppressor cells in pancreatic, esophageal and gastric cancer are an independent prognostic factor and are associated with significant elevation of the Th2 cytokine interleukin-13. *Cancer Immunol Immunother.* 2011;60:1419–30.
80. Gan L, Yang Y, Li Q, Feng Y, Liu T, Guo W. Epigenetic regulation of cancer progression by EZH2: from biological insights to therapeutic potential. *Biomark Res.* 2018;6:10.
81. Gandhi, N.A.; Pirozzi, G.; Graham, N.M.H. Commonality of the IL-4/IL-13 pathway in atopic diseases. *Expert Rev Clin Immunol* 2017;13:425–437.
82. Garland T. Arsenic. In: Gupta RC (ed). *Veterinary Toxicology*. 3<sup>rd</sup> edition. Elsevier, London, pp. 411–415; 2018.
83. Gee JR, Saltzstein DR, Kim K, Kolesar J, Huang W, Havighurst TC, Wollmer BW, Stublaski J, Downs T, Mukhtar H, House MG, Parnes HL, Bailey HH. A Phase II Randomized, Double-blind, Presurgical Trial of Polyphenon E in Bladder Cancer

- Patients to Evaluate Pharmacodynamics and Bladder Tissue Biomarkers. *Cancer Prev Res (Phila)*. 2017;10(5):298-307.
84. Georgescu MM. PTEN tumor suppressor network in PI3K-Akt pathway control. *Genes Cancer* 2010;1:1170-7.
85. Ghosh A, Lahiri A, Mukherjee S, Roy M, Datta A. Prevention of inorganic arsenic induced squamous cell carcinoma of the skin in Swiss albino mice by black tea through epigenetic modulation. *Heliyon*. 2022a;8(8):e10341.
86. Ghosh A, Mukherjee S, Roy M. Co-Carcinogenicity of Arsenic: Probable Mechanisms. *Int J Curr Microbiol App Sci*. 2021b;10(11): 294-305.
87. Ghosh A, Mukherjee S, Roy M. Black tea extract prevents inorganic arsenic induced uncontrolled proliferation, epithelial to mesenchymal transition and induction of metastatic properties in HaCaT keratinocytes - an in vitro study. *Toxicol In Vitro*. 2022b;85:105478.
88. Ghosh A, Mukherjee S, Roy M. Chemopreventive Role of Black Tea Extract in Swiss Albino Mice Exposed to Inorganic Arsenic. *Asian Pac J Cancer Prev*. 2021a;22(11):3647-3661.
89. Ghosh A, Roy M. Black Tea Extract Prevents iAs Induced Transformation of HaCaT Cells via Modulation of Cellular Damage, Inflammation and TGF- $\beta$  Signalling Cascade. *Int J Curr Microbiol App Sci*. 2023a;12(1): 171-189.
90. Ghosh A, Roy M. Black Tea Extract, via Modulation of TGF- $\beta$  Pathway, Prevents Inorganic Arsenic-induced Development of Squamous Cell Carcinoma of the Skin in Swiss Albino Mice. *J Cancer Prev*. 2023b;28(1):12-23.
91. Glasauer A, Chandel NS. Targeting antioxidants for cancer therapy. *Biochem Pharmacol*. 2014;92(1):90-101.

92. Glick AB. The Role of TGF $\beta$  Signalling in Squamous Cell Cancer: Lessons from Mouse Models. *J Skin Cancer*. 2012;2012:249063.
93. Gosslau A, En Jao DL, Huang MT, Ho CT, Evans D, Rawson NE, Chen KY. Effects of the black tea polyphenol theaflavin-2 on apoptotic and inflammatory pathways in vitro and in vivo. *Mol Nutr Food Res*. 2011;55(2):198-208.
94. Green LC, Wagner DA, Glogowski J, Skipper PL, Wishnok JS, Tannenbaum SR. Analysis of nitrate, nitrite, and [15N]nitrate in biological fluids. *Anal Biochem*. 1982;126(1):131-8.
95. Guan R, Van Le Q, Yang H, Zhang D, Gu H, Yang Y, Sonne C, Lam SS, Zhong J, Jianguang Z, Liu R, Peng W. A review of dietary phytochemicals and their relation to oxidative stress and human diseases. *Chemosphere*. 2021;271:129499.
96. Ha TY. The role of regulatory T cells in cancer. *Immune Netw*. 2009;9(6):209-35.
97. Hamadeh HK, Trouba KJ, Amin RP, Afshari CA, and Germolec D. Coordination of altered DNA repair and damage pathways in arsenite-exposed keratinocytes. *Toxicol Sci*. 2002;69:306–316.
98. Hamidi A, von Bulow V, Hamidi R, Winssinger N, Barluenga S, Heldin CH, Landström M. Polyubiquitination of transforming growth factor  $\beta$  (TGF $\beta$ )-associated kinase 1 mediates nuclear factor- $\kappa$ B activation in response to different inflammatory stimuli. *J Biol Chem*. 2012;287(1):123-133.
99. Hanahan D, Weinberg RA. *Cell*. The hallmarks of cancer. 2000;100(1):57-70.
100. Hanahan D, Weinberg RA. Hallmarks of cancer: the next generation. *Cell*. 2011;144(5):646-74.
101. Haque S, Morris JC. Transforming growth factor- $\beta$ : A therapeutic target for cancer. *Hum Vaccin Immunother*. 2017;13(8):1741-50.



102. Harvey RF, Pöyry TAA, Stoneley M, Willis AE. Signalling from mTOR to eIF2 $\alpha$  mediates cell migration in response to the chemotherapeutic doxorubicin. *Sci Signal*. 2019;12:eaaw6763.
103. Hayakawa S, Ohishi T, Miyoshi N, Oishi Y, Nakamura Y, Isemura M. Anti-Cancer Effects of Green Tea Epigallocatechin-3-Gallate and Coffee Chlorogenic Acid. *Molecules*. 2020;25(19):4553.
104. Hayakawa T, Kobayashi Y, Cui X, Hirano S. A new metabolic pathway of arsenite: arsenic glutathione complexes are substrates for human arsenic methyltransferase Cyt19. *Arch Toxicol*. 2005;79:183-91.
105. Healy SM, Casarez EA, Ayala-Fierro F, Aposhian HV. Enzymatic methylation of arsenic compounds. V. arsenite methyltransferase activity in tissues of mice. *Toxicol Appl Pharmacol*. 1998;148:65–70.
106. Heber D, Zhang Y, Yang J, Ma JE, Henning SM, Li Z. Green tea, black tea, and oolong tea polyphenols reduce visceral fat and inflammation in mice fed high-fat, high-sucrose obesogenic diets. *J Nutr*. 2014;144(9):1385-93.
107. Helm CW, States JC. Sodium arsenite and hyperthermia modulate cisplatin-DNA damage responses and enhance platinum accumulation in murine metastatic ovarian cancer xenograft after hyperthermic intraperitoneal chemotherapy (HIPEC). *J Ovarian Res*. 2011;4:9.
108. Hernandez AL, Young CD, Wang JH, Wang XJ. Lessons learned from SMAD4 loss in squamous cell carcinomas. *Mol Carcinog* 2019;58:1648-55.
109. Holcomb N, Goswami M, Han SG, Scott T, D'Orazio J, Orren DK, Gairola CG, Mellon I. Inorganic arsenic inhibits the nucleotide excision repair pathway and reduces the expression of XPC. *DNA Repair (Amst)*. 2017;52:70-80.

110. Hon GC, Hawkins RD, Caballero OL, Lo C, Lister R, Pelizzola M, Valsesia A, Ye Z, Kuan S, Edsall LE, Camargo AA, Stevenson BJ, Ecker JR, Bafna V, Strausberg RL, Simpson AJ, Ren B. Global DNA hypomethylation coupled to repressive chromatin domain formation and gene silencing in breast cancer. *Genome Res.* 2012;22(2):246-58.
111. Hossain MB, Vahter M, Concha G, Broberg K. Environmental arsenic exposure and DNA methylation of the tumor suppressor gene p16 and the DNA repair gene MLH1: effect of arsenic metabolism and genotype. *Metallomics.* 2012;4(11):1167-75.
112. Howe CG, Gamble MV. Influence of Arsenic on Global Levels of Histone Posttranslational Modifications: a Review of the Literature and Challenges in the Field. *Curr Environ Health Rep.* 2016;3(3):225-37.
113. Howells LM, Berry DP, Elliott PJ, Jacobson EW, Hoffmann E, Hegarty B, Brown K, Steward WP, Gescher AJ. Phase I randomized, double-blind pilot study of micronized resveratrol (SRT501) in patients with hepatic metastases--safety, pharmacokinetics, and pharmacodynamics. *Cancer Prev Res (Phila).* 2011;4(9):1419-25.
114. Hsu LI, Chen GS, Lee CH, Yang TY, Chen YH, Wang YH, Hsueh YM, Chiou HY, Wu MM, Chen CJ. Use of arsenic-induced palmoplantar hyperkeratosis and skin cancers to predict risk of subsequent internal malignancy. *Am J Epidemiol.* 2013;177(3):202-12.
115. Hu Y, Li J, Lou B, Wu R, Wang G, Lu C, Wang H, Pi J, Xu Y. The Role of Reactive Oxygen Species in Arsenic Toxicity. *Biomolecules.* 2020;10(2):240.
116. Huang D, Xiao F, Hao H, Hua F, Luo Z, Huang Z, Li Q, Chen S, Cheng X, Zhang X, Fang W, Hu X, Liu F. JARID1B promotes colorectal cancer proliferation

- and Wnt/ $\beta$ -catenin signaling via decreasing CDX2 level. *Cell Commun Signal*. 2020;18(1):169.
117. Huang JJ, Blobe GC. Dichotomous roles of TGF- $\beta$  in human cancer. *Biochem Soc Trans*. 2016;44(5):1441-1454.
118. Huang L, Song Y, Lian J, Wang Z. Allicin inhibits the invasion of lung adenocarcinoma cells by altering tissue inhibitor of metalloproteinase/matrix metalloproteinase balance via reducing the activity of phosphoinositide 3-kinase/AKT signalling. *Oncol Lett*. 2017;14(1):468-474.
119. Huang RY, Guilford P, Thiery JP. Early events in cell adhesion and polarity during epithelial-mesenchymal transition. *J Cell Sci*. 2012;125:4417-22.
120. Huang Z, Zhang Z, Zhou C, Liu L, Huang C. Epithelial-mesenchymal transition: The history, regulatory mechanism, and cancer therapeutic opportunities. *MedComm (2020)*. 2022;3(2):e144.
121. Hughes MF, Beck BD, Chen Y, Lewis AS, Thomas DJ. Arsenic exposure and toxicology: a historical perspective. *Toxicol Sci*. 2011;123(2):305-32.
122. Hunt KM, Srivastava RK, Elmets CA, Athar M. The mechanistic basis of arsenicosis: pathogenesis of skin cancer. *Cancer Lett*. 2014 28;354(2):211-9.
123. Hunter CA, Jones SA. IL-6 as a keystone cytokine in health and disease. *Nat Immunol* 2015;16:448–457.
124. Hwang SY, Chae JI, Kwak AW, Lee MH, Shim JH. Alternative options for skin cancer therapy via regulation of AKT and related signaling pathways. *Int J Mol Sci*. 2020;21:6869.
125. Idriss HT, Al-Assar O, Wilson SH. DNA polymerase  $\beta$ . *Int J Biochem Cell Biol* 2002;34:321–324.

126. Ishikawa F, Kaneko E, Sugimoto T, Ishijima T, Wakamatsu M, Yuasa A, Sampei R, Mori K, Nose K, Shibamura M. A mitochondrial thioredoxin-sensitive mechanism regulates TGF- $\beta$ -mediated gene expression associated with epithelial-mesenchymal transition. *Biochem Biophys Res Commun*. 2014;443(3):821-7.
127. Jia Q, Chen S, Tan Y, Li Y, Tang F. Oncogenic super-enhancer formation in tumorigenesis and its molecular mechanisms. *Exp Mol Med*. 2020;52(5):713-723.
128. Jiang J, Wang K, Chen Y, Chen H, Nice EC, Huang C. Redox regulation in tumor cell epithelial-mesenchymal transition: molecular basis and therapeutic strategy. *Signal Transduct Target Ther*. 2017;2:17036.
129. Jiang T, Zhou C, Ren S. Role of IL-2 in cancer immunotherapy. *Oncoimmunology*. 2016;5(6):e1163462.
130. Jjingo D, Conley AB, Yi SV, Lunyak VV, Jordan IK. On the presence and role of human gene-body DNA methylation. *Oncotarget*. 2012;3(4):462-74.
131. Jo WJ, Ren X, Chu F, Aleshin M, Wintz H, Burlingame A, Smith MT, Vulpe CD, Zhang L. Acetylated H4K16 by MYST1 protects UROtsa cells from arsenic toxicity and is decreased following chronic arsenic exposure. *Toxicol Appl Pharmacol*. 2009;241(3):294-02.
132. Johansson C, Velupillai S, Tumber A, Szykowska A, Hookway ES, Nowak RP, Strain-Damerell C, Gileadi C, Philpott M, Burgess-Brown N, Wu N, Kopec J, Nuzzi A, Steuber H, Egner U, Badock V, Munro S, LaThangue NB, Westaway S, Brown J, Athanasou N, Prinjha R, Brennan PE, Oppermann U. Structural analysis of human KDM5B guides histone demethylase inhibitor development. *Nat Chem Biol*. 2016;12(7):539-45.

133. Johnson JL, Najor NA, Green KJ. Desmosomes: regulators of cellular signaling and adhesion in epidermal health and disease. *Cold Spring Harb Perspect Med.* 2014;4(11):a015297.
134. Joseph MJ, Dangi-Garimella S, Shields MA, Diamond ME, Sun L, Koblinski JE, Munshi HG. Slug is a downstream mediator of transforming growth factor-beta1-induced matrix metalloproteinase-9 expression and invasion of oral cancer cells. *J Cell Biochem.* 2009;108:726-36.
135. Julien S, Puig I, Caretti E, Bonaventure J, Nelles L, van Roy F, Dargemont C, de Herreros AG, Bellacosa A, Larue L. Activation of NF-kappa B by Akt upregulates Snail expression and induces epithelium mesenchyme transition. *Oncogene.* 2007;26(53):7445-56.
136. Junttila, I.S. Tuning the Cytokine Responses: An Update on Interleukin (IL)-4 and IL-13 Receptor Complexes. *Front Immunol* 2018;9:888.
137. Kalli M, Li R, Mills GB, Stylianopoulos T, Zervantonakis IK. Mechanical stress signalling in pancreatic cancer cells triggers p38 MAPK- and JNK-dependent cytoskeleton remodelling and promotes cell migration via Rac1/cdc42/Myosin II. *Mol Cancer Res.* 2022;20:485-97.
138. Kallio J, Hämäläinen M, Luukkaala T, Moilanen E, Tammela TL, Kellokumpu-Lehtinen PL. Resistin and interleukin 6 as predictive factors for recurrence and long-term prognosis in renal cell cancer. *Urol Oncol.* 2017;35(9):544.e25-544.e31.
139. Kawabata A, Yanaihara N, Nagata C, Saito M, Noguchi D, Takenaka M, Iida Y, Takano H, Yamada K, Iwamoto M, Kiyokawa T, Okamoto A. Prognostic impact of interleukin-6 expression in stage I ovarian clear cell carcinoma. *Gynecol Oncol.* 2017;146(3):609-14.

140. Khan H, Changkija B, Konwar R. Role of Interleukin-10 in Breast Cancer. *Breast Cancer Res Treat.* 2012; 133(1): 11-21.
141. Khan MYA, Gani KM, Chakrapani GJ. Assessment of surface water quality and its spatial variation. A case study of Ramganga River, Ganga Basin, India. *Arab J Geosci* 2016;9(1):28.
142. Khan N, Mukhtar H. Multitargeted therapy of cancer by green tea polyphenols. *Cancer Lett.* 2008;269(2):269-80.
143. Khan SA, Reddy D, Gupta S. Global histone post-translational modifications and cancer: Biomarkers for diagnosis, prognosis and treatment? *World J Biol Chem.* 2015;6(4):333-45.
144. Kim HG, Kim DJ, Li S, Lee KY, Li X, Bode AM, Dong Z. Polycomb (PcG) proteins, BMI1 and SUZ12, regulate arsenic-induced cell transformation. *J Biol Chem.* 2012;287(38):31920-28.
145. Kim Y, Lee SK, Bae S, Kim H, Park Y, Chu NK, Kim SG, Kim HR, Hwang YI, Kang JS, Lee WJ. The anti-inflammatory effect of alloferon on UVB-induced skin inflammation through the down-regulation of pro-inflammatory cytokines. *Immunol Lett.* 2013;149(1-2):110-18.
146. Kimura Y, Okuda H. Resveratrol isolated from *Polygonum cuspidatum* root prevents tumor growth and metastasis to lung and tumor-induced neovascularization in Lewis lung carcinoma-bearing mice. *J Nutr.* 2001;131(6):1844-49.
147. Klein CB, Leszczynska J, Hickey C, Rossman TG. Further evidence against a direct genotoxic mode of action for arsenic-induced cancer. *Toxicol Appl Pharmacol.* 2007;222:289–97.

148. Kochnev Y, Hellemann E, Cassidy KC, Durrant JD. Webina: an open-source library and web app that runs AutoDock Vina entirely in the web browser. *Bioinformatics*. 2020;36(16):4513-15.
149. Korc M, Smad4. Gatekeeper gene in head and neck squamous cell carcinoma. *J Clin Invest*. 2009;119: 3208-11.
150. Krieg C, Letourneau S, Pantaleo G, Boyman O. Improved IL-2 immunotherapy by selective stimulation of IL-2 receptors on lymphocytes and endothelial cells. *Proc Natl Acad Sci* 2010;107:11906-11.
151. Kristensen LH, Nielsen AL, Helgstrand C, Lees M, Cloos P, Kastrup JS, Helin K, Olsen L, Gajhede M. Studies of H3K4me3 demethylation by KDM5B/Jarid1B/PLU1 reveals strong substrate recognition in vitro and identifies 2,4-pyridine-dicarboxylic acid as an in vitro and in cell inhibitor. *FEBS J*. 2012;279(11):1905-14.
152. Krstić J, Trivanović D, Mojsilović S, Santibanez JF. Transforming Growth Factor-Beta and Oxidative Stress Interplay: Implications in Tumorigenesis and Cancer Progression. *Oxid Med Cell Longev*. 2015;2015:654594.
153. Kubiczikova L, Sedlarikova L, Hajek R, Sevcikova S. TGF- $\beta$  - an excellent servant but a bad master. *J Transl Med*. 2012;10:183.
154. Kudaravalli S, den Hollander P, Mani SA. Role of p38 MAP kinase in cancer stem cells and metastasis. *Oncogene*. 2022;41:3177-85.
155. Kumagai Y, Hirahashi M, Takizawa K, Yamamoto H, Gushima M, Esaki M, Matsumoto T, Nakamura M, Kitazono T, Oda Y. Overexpression of MTH1 and OGG1 proteins in ulcerative colitis-associated carcinogenesis. *Oncol Lett*. 2018;16(2):1765-76.

156. Kumar NB, Pow-Sang J, Spiess PE, Park J, Salup R, Williams CR, Parnes H, Schell MJ. Randomized, placebo-controlled trial evaluating the safety of one-year administration of green tea catechins. *Oncotarget*. 2016;7(43):70794-02.
157. Kumari A, Shonibare Z, Monavarian M, Arend RC, Lee NY, Inman GJ, Mythreye K. TGF $\beta$  signalling networks in ovarian cancer progression and plasticity. *Clin Exp Metastasis*. 2021;38(2):139-61.
158. Kumari R, Kumar R, Lynn A. g\_mmpbsa- A GROMACS tool for high-throughput MM-PBSA calculations, *J Chem Inf Model*. 2014;54:1951–62.
159. Kunisada M, Sakumi K, Tominaga Y, Budiyanto A, Ueda M, Ichihashi M, Nakabeppu Y, Nishigori C. 8-Oxoguanine formation induced by chronic UVB exposure makes Ogg1 knockout mice susceptible to skin carcinogenesis. *Cancer Res*. 2005;65(14):6006-10.
160. Kunnumakkara AB, Bordoloi D, Harsha C, Banik K, Gupta SC, Aggarwal BB. Curcumin mediates anticancer effects by modulating multiple cells signalling pathways. *Clin Sci (Lond)*. 2017;131(15):1781-99.
161. Lamouille S, Connolly E, Smyth JW, Akhurst RJ, Derynck R. TGF- $\beta$ -induced activation of mTOR complex 2 drives epithelial mesenchymal transition and cell invasion. *J Cell Sci*. 2012;125:1259-73.
162. Lamouille S, Derynck R. Cell size and invasion in TGF-beta induced epithelial to mesenchymal transition is regulated by activation of the mTOR pathway. *J Cell Biol*. 2007;178:437-51.
163. Lamouille S, Xu J, Derynck R. Molecular mechanisms of epithelial-mesenchymal transition. *Nat Rev Mol Cell Biol*. 2014;15:178-96
164. Larsson C, Cordeddu L, Siggens L, Pandzic T, Kundu S, He L, Ali MA, Pristovšek N, Hartman K, Ekwall K, Sjöblom T. Restoration of KMT2C/MLL3 in



- human colorectal cancer cells reinforces genome-wide H3K4me1 profiles and influences cell growth and gene expression. *Clin Epigenetics*. 2020;12(1):74.
165. Lee SY, Ju MK, Jeon HM, Lee YJ, Kim CH, Park HG, Han SI, Kang HS. Reactive oxygen species induce epithelial-mesenchymal transition, glycolytic switch, and mitochondrial repression through the Dlx-2/Snail signalling pathways in MCF-7 cells. *Mol Med Rep*. 2019;20(3):2339-2346.
166. Lee WL, Huang JY, Shyur LF. Phytoagents for cancer management: regulation of nucleic acid oxidation, ROS, and related mechanisms. *Oxid Med Cell Longev*. 2013;2013:925804.
167. Li J, Poi MJ, Tsai MD. Regulatory mechanisms of tumor suppressor P16(INK4A) and their relevance to cancer. *Biochemistry*. 2011;50(25):5566-82.
168. Li Y, Yu H, Jiao S, Yang J. Prognostic value of IL-10 expression in tumor tissues of breast cancer patients. *Xi Bao Yu Fen Zi Mian Yi Xue Za Zhi*. 2014;30(5):517-20.
169. Libbey RB, Williams-Jones AE, Melosh BL, Backeberg NR. Characterization of geothermal activity along the North American–Caribbean Plate boundary in Guatemala: The Joaquina geothermal field. *Geothermics* 2015;56:17–34.
170. Lim S, Janzer A, Becker A, Zimmer A, Schüle R, Buettner R, Kirfel J. Lysine-specific demethylase 1 (LSD1) is highly expressed in ER-negative breast cancers and a biomarker predicting aggressive biology. *Carcinogenesis*. 2010;31(3):512-20.
171. Lin C, Liu H, Zhang H, He H, Li H, Shen Z, Qin J, Qin X, Xu J, Sun Y. Interleukin-13 receptor  $\alpha 2$  is associated with poor prognosis in patients with gastric cancer after gastrectomy. *Oncotarget*. 2016;7(31):49281-88.

172. Littman DR, Rudensky AY. Th17 and regulatory T cells in mediating and restraining inflammation. *Cell* 2010;140:845-58;
173. Liu D, Wu D, Zhao L, Yang Y, Ding J, Dong L, Hu L, Wang F, Zhao X, Cai Y, Jin J. Arsenic Trioxide Reduces Global Histone H4 Acetylation at Lysine 16 through Direct Binding to Histone Acetyltransferase hMOF in Human Cells. *PLoS One*. 2015;10(10):e0141014.
174. Liu J, Benbrahim-Tallaa L, Qian X, Yu L, Xie Y, Boos J, Qu W, Waalkes MP. Further studies on aberrant gene expression associated with arsenic-induced malignant transformation in rat liver TRL1215 cells. *Toxicol Appl Pharmacol*. 2006;216(3):407-15.
175. Liu N, Zhang R, Zhao X, Su J, Bian X, Ni J, Yue Y, Cai Y, Jin J. A potential diagnostic marker for ovarian cancer: Involvement of the histone acetyltransferase, human males absent on the first. *Oncol Lett*. 2013;6(2):393-00.
176. Liu S, Sun Q, Wang F, Zhang L, Song Y, Xi S, Sun G. Arsenic induced overexpression of inflammatory cytokines based on the human urothelial cell model in vitro and urinary secretion of individuals chronically exposed to arsenic. *Chem Res Toxicol*. 2014;27(11):1934-42.
177. Liu W, Lu X, Shi P, Yang G, Zhou Z, Li W, Mao X, Jiang D, Chen C. TNF- $\alpha$  increases breast cancer stem-like cells through up-regulating TAZ expression via the non-canonical NF- $\kappa$ B pathway. *Sci Rep*. 2020;10(1):1804.
178. Lo MC, Yip TC, Ngan KC, Cheng WW, Law CK, Chan PS, Chan KC, Wong CK, Wong RN, Lo KW, Ng WT, Lee WM, Tsao SW, Kwong LW, Lung ML, Mak NK. Role of MIF/CXCL8/CXCR2 signalling in the growth of nasopharyngeal carcinoma tumor spheres. *Cancer Lett*. 2013 Jul 10;335(1):81-92.

179. Lu L, Zhang M, Wang X, Zhang Y, Chai Z, Ying M, Guan J, Gong W, Zhao Z, Liu L, Hu Y, Lu W, Dong J. Baicalein enhances the antitumor efficacy of docetaxel on non-small cell lung cancer in a  $\beta$ -catenin-dependent manner. *Phytother Res.* 2020;34(1):104-17.
180. Lu Q, Wang WW, Zhang MZ, Ma ZX, Qiu XR, Shen M, Yin XX. ROS induces epithelial-mesenchymal transition via the TGF- $\beta$ 1/PI3K/Akt/mTOR pathway in diabetic nephropathy. *Exp Ther Med.* 2019;17(1):835-46.
181. Maiti S, Nazmeen A, Medda N, Patra R, Ghosh TK. Flavonoids green tea against oxidant stress and inflammation with related human diseases. *Clin Nutr Exp.* 2019;24:1-14.
182. Malek TR. The biology of interleukin-2. *Annu Rev Immunol* 2008; 26:453-79.
183. Malladi S, Macalinao DG, Jin X, He L, Basnet H, Zou Y, de Stanchina E, Massagué J. Metastatic latency and immune evasion through autocrine inhibition of WNT. *Cell.* 2016;165:45–60.
184. Manuyakorn A, Paulus R, Farrell J, Dawson NA, Tze S, Cheung-Lau G, Hines OJ, Reber H, Seligson DB, Horvath S, Kurdistani SK, Guha C, Dawson DW. Cellular histone modification patterns predict prognosis and treatment response in resectable pancreatic adenocarcinoma: results from RTOG 9704. *J Clin Oncol.* 2010;28(8):1358-65.
185. Marsh J. Separation of arsenic. In: Carson J, editor. *The American Journal of Pharmacy.* Vol. II. Philadelphia, PA: Merriew and Gunn; 1837;2:307–14.
186. Martinez VD, Vucic EA, Becker-Santos DD, Gil L, Lam WL. Arsenic exposure and the induction of human cancers. *J Toxicol.* 2011;2011:431287.

187. Maru G, Gandhi K, Ramchandani A, Kumar G. Inflammation and Cancer (Advances in Experimental Medicine and Biology Book 816). In: Aggarwal BB, Sung B, Gupta C (eds). The role of inflammation in skin cancer. Springer, Basel, pp 437-69; 2014.
188. Mass MJ, Tennant A, Roop BC, Cullen WR, Styblo M, Thomas DJ, Kligerman AD. Methylated trivalent arsenic species are genotoxic. *Chem Res Toxicol.* 2001;14:355–61
189. McArthur J.M. Arsenic in groundwater. In: Sikdar PK (ed). Groundwater Development and Management. Springer, Cham, pp 279–308; 2019.
190. Mercurio L, Albanesi C, Madonna S. Recent updates on the involvement of PI3K/AKT/mTOR molecular cascade in the pathogenesis of hyperproliferative skin disorders. *Front Med (Lausanne).* 2021;8:665647.
191. Miao Z, Wu L, Lu M, Meng X, Gao B, Qiao X, Zhang W, Xue D. Analysis of the transcriptional regulation of cancer-related genes by aberrant DNA methylation of the cis-regulation sites in the promoter region during hepatocyte carcinogenesis caused by arsenic. *Oncotarget.* 2015;6(25):21493-06.
192. Mikutis G, Karaköse H, Jaiswal R, LeGresley A, Islam T, Fernandez-Lahore M, Kuhnert N. Phenolic promiscuity in the cell nucleus--epigallocatechingallate (EGCG) and theaflavin-3,3'-digallate from green and black tea bind to model cell nuclear structures including histone proteins, double stranded DNA and telomeric quadruplex DNA. *Food Funct.* 2013;4(2):328-37.
193. Miller KM, Jackson SP. Histone marks: repairing DNA breaks within the context of chromatin. *Biochem Soc Trans.* 2012;40(2):370-76.
194. Mitsunaga S, Ikeda M, Shimizu S, Ohno I, Furuse J, Inagaki M, Higashi S, Kato H, Terao K, Ochiai A. Serum levels of IL-6 and IL-1 $\beta$  can predict the efficacy

- of gemcitabine in patients with advanced pancreatic cancer. *Br J Cancer*. 2013;108(10):2063-69.
195. Miyata Y, Shida Y, Hakariya T, Sakai H. Anti-Cancer Effects of Green Tea Polyphenols Against Prostate Cancer. *Molecules*. 2019;24(1):193.
196. Mo J, Xia Y, Wade TJ, DeMarini DM, Davidson M, and Mumford J. Altered gene expression by low-dose arsenic exposure in humans and cultured cardiomyocytes: Assessment by real-time PCR arrays. *Int J Environ Res Public Health*. 2011;8:2090–2108.
197. Mock CD, Jordan BC, Selvam C. Recent Advances of Curcumin and its Analogues in Breast Cancer Prevention and Treatment. *RSC Adv*. 2015;5(92):75575-88.
198. Moore RJ, Owens DM, Stamp G, Arnott C, Burke F, East N, Holdsworth H, Turner L, Rollins B, Pasparakis M, Kollias G, Balkwill F. Mice deficient in tumour necrosis factor-alpha are resistant to skin carcinogenesis. *Nat Med*. 1999;5(7):828-31.
199. Mukhopadhyay H, Lee NY. Multifaceted roles of TAK1 signaling in cancer. *Oncogene*. 2020;39:1402-13.
200. Na TY, Schecterson L, Mendonsa AM, Gumbiner BM. The functional activity of E-cadherin controls tumor cell metastasis at multiple steps. *Proc Natl Acad Sci U S A*. 2020;117(11):5931-37.
201. Naranmandura H, Xu S, Koike S, Pan LQ, Chen B, Wang YW, Rehman K, Wu B, Chen Z, Suzuki N. The endoplasmic reticulum is a target organelle for trivalent dimethylarsinic acid (DMAIII)-induced cytotoxicity. *Toxicol Appl Pharmacol*. 2012;260(3):241-49.

202. Nardinocchi L, Sonogo G, Passarelli F, Avitabile S, Scarponi C, Failla CM, Simoni S, Albanesi C, Cavani A. Interleukin-17 and interleukin-22 promote tumor progression in human nonmelanoma skin cancer. *Eur J Immunol.* 2015;45:922-31.
203. Narendhirakannan RT, Hannah MA. Oxidative stress and skin cancer: an overview. *Indian J Clin Biochem.* 2013;28(2):110-15.
204. Neagu M, Constantin C, Caruntu C, Dumitru C, Surcel M, Zurac S. Inflammation: A key process in skin tumorigenesis. *Oncol Lett.* 2019;17(5):4068-84.
205. Neagu M, Constantin C, Manda G, Margaritescu I. Biomarkers of metastatic melanoma. *Biomarkers Med.* 2009;3:71-89.
206. Neagu M, Constantin C, Tanase C. Immune-related biomarkers for diagnosis/prognosis and therapy monitoring of cutaneous melanoma. *Expert Rev Mol Diagn.* 2010;10:897-919.
207. Nelson WC, Lykins MH, Mackey J, Newill VA, Finklea JF, Hammer DI. Mortality among orchard workers exposed to lead arsenate spray: a cohort study. *J Chronic Dis.* 1973;26(2):105-18.
208. Ngollo M, Lebert A, Daures M, Judes G, Rifai K, Dubois L, Kemeny JL, Penault-Llorca F, Bignon YJ, Guy L, Bernard-Gallon D. Global analysis of H3K27me3 as an epigenetic marker in prostate cancer progression. *BMC Cancer.* 2017;17(1):261.
209. Ning Y, Lenz HJ. Targeting IL-8 in colorectal cancer. *Expert Opin Ther Targets* 2012;16:491–97.
210. Niu Y, DesMarais TL, Tong Z, Yao Y, Costa M. Oxidative stress alters global histone modification and DNA methylation. *Free Radic Biol Med.* 2015;82:22-28.

211. Nollen M, Ebert F, Moser J, Mullenders LHF, Hartwig A, Schwerdtle T. Impact of arsenic on nucleotide excision repair: XPC function, protein level, and gene expression. *Mol. Nutr. Food Res.* 2009;53:572–82.
212. Oba S, Nagata C, Nakamura K, Fujii K, Kawachi T, Takatsuka N, Shimizu H. Consumption of coffee, green tea, oolong tea, black tea, chocolate snacks and the caffeine content in relation to risk of diabetes in Japanese men and women. *Br J Nutr.* 2010;103(3):453-59.
213. Ohkawa H, Ohishi N, Yagi K. Assay for lipid peroxides in animal tissues by thiobarbituric acid reaction. *Anal Biochem.* 1979;95(2):351-58.
214. Osmond MJ, Kunz BA, Snow ET. Age and exposure to arsenic alter base excision repair transcript levels in mice. *Mutagenesis* 2010;25:517–22.
215. Pal P, Sen M, Manna A, Pal J, Pal P, Roy S, Roy P. Contamination of groundwater by arsenic: a review of occurrence, causes, impacts, remedies and membrane-based purification. *J Integr Environ Sci.* 2009;6(4):295-16
216. Pang X, Tang YL, Liang XH. Transforming growth factor- $\beta$  signalling in head and neck squamous cell carcinoma: Insights into cellular responses. *Oncol Lett.* 2018;16(4):4799-06.
217. Paul WE, Zhu J. How are T(H)2-type immune responses initiated and amplified? *Nat Rev Immunol* 2010;10:225-35.
218. Pavlova NN, Thompson CB. The emerging hallmarks of cancer metabolism. *Cell Metab.* 2016; 23:27–47.
219. Peryea FJ. Historical use of lead arsenate insecticides, resulting soil contamination and implications for soil remediation. In *Proceedings, 16<sup>th</sup> World Congress of Soil Science, 20–26 August 1998, Montpellier, France*, pp. 7.

220. Pfeifer GP. Defining Driver DNA Methylation Changes in Human Cancer. *Int J Mol Sci.* 2018;19(4):1166.
221. Pilsner JR, Liu X, Ahsan H, Ilievski V, Slavkovich V, Levy D, Factor-Litvak P, Graziano JH, Gamble MV. Folate deficiency, hyperhomocysteinemia, low urinary creatinine, and hypomethylation of leukocyte DNA are risk factors for arsenic-induced skin lesions. *Environ Health Perspect.* 2009;117(2):254-60.
222. Pop S, Enciu AM, Tarcomnicu I, Gille E, Tanase C. Phytochemicals in cancer prevention: modulating epigenetic alterations of DNA methylation. *Phytochem Rev.* 2019;18:1005–24.
223. Principe DR, Timbers KE, Atia LG, Koch RM, Rana A. TGF $\beta$  Signalling in the Pancreatic Tumor Microenvironment. *Cancers (Basel).* 2021;13(20):5086.
224. Prso IB, Kocjan W, Simić H, Brumini G, Pezelj-Ribarić S, Borčić J, Ferreri S, Karlović IM. Tumor necrosis factor-alpha and interleukin 6 in human periapical lesions. *Mediators Inflamm.* 2007;2007:38210.
225. Puisieux A, Brabletz T, Caramel J. Oncogenic roles of EMT-inducing transcription factors. *Nat Cell Biol.* 2014;16(6):488-94.
226. Qazi A, Pal J, Maitah M, Fulciniti M, Pelluru D, Nanjappa P, Lee S, Batchu RB, Prasad M, Bryant CS, Rajput S, Gryaznov S, Beer DG, Weaver DW, Munshi NC, Goyal RK, Shamma MA. Anticancer activity of a broccoli derivative, sulforaphane, in barrett adenocarcinoma: potential use in chemoprevention and as adjuvant in chemotherapy. *Transl Oncol.* 2010;3(6):389-99.
227. Qiao B, Johnson NW, Gao J. Epithelial-mesenchymal transition in oral squamous cell carcinoma triggered by transforming growth factor-beta1 is Snail family-dependent and correlates with matrix metalloproteinase-2 and -9 expressions. *Int J Oncol.* 2010;37: 663-68.



228. Qiao J, Kong X, Kong A, Han M. Pharmacokinetics and biotransformation of tea polyphenols. *Curr Drug Metab.* 2014;15(1):30-36.
229. Rahaman MS, Rahman MM, Mise N, Sikder MT, Ichihara G, Uddin MK, Kurasaki M, Ichihara S. Environmental arsenic exposure and its contribution to human diseases, toxicity mechanism and management. *Environ Pollut.* 2021;289:117940.
230. Ranjan A. Spatial Analysis of Arsenic Contamination of Groundwater around the World and India. *Int J Innov Stud Sociol Humanities.* 2019;4(10):6-15.
231. Ratnaike RN. Acute and chronic arsenic toxicity. *Postgrad Med J.* 2003;79(933):391-96.
232. Ravenscroft P, Brammer H, Richards KS. *Arsenic Pollution: A Global Synthesis.* Wiley-Blackwell, London; 2009.
233. Rea IM, Gibson DS, McGilligan V, McNerlan SE, Alexander HD, Ross OA. Age and Age-Related Diseases: Role of Inflammation Triggers and Cytokines. *Front Immunol.* 2018;9:586.
234. Rehman K, Naranmandura H. Arsenic metabolism and thioarsenicals. *Metallomics.* 2012; 4: 881-92.
235. Reichard JF, Schnekenburger M, Puga A. Long term low-dose arsenic exposure induces loss of DNA methylation. *Biochem Biophys Res Commun.* 2007;352(1):188-92.
236. Ren X, McHale CM, Skibola CF, Smith AH, Smith MT, Zhang L. An emerging role for epigenetic dysregulation in arsenic toxicity and carcinogenesis. *Environ Health Perspect.* 2011;119(1):11-9.
237. Riethmiller S. From Atoxyl to Salvarsan: searching for the magic bullet. *Chemotherapy.* 2005;51(5):234-42.

238. Rose AM, Spender LC, Stephen C, Mitchell A, Rickaby W, Bray S, Evans AT, Dayal J, Purdie KJ, Harwood CA, Proby CM, Leigh IM, Coates PJ, Inman GJ. Reduced SMAD2/3 activation independently predicts increased depth of human cutaneous squamous cell carcinoma. *Oncotarget*. 2018;9(18):14552-66.
239. Roy M, Chakrabarty S, Sinha D, Bhattacharya RK, Siddiqi M. Anticlastogenic, antigenotoxic and apoptotic activity of epigallocatechin gallate: a green tea polyphenol. *Mutat Res*. 2003;523-524:33-41.
240. Roy M, Sinha D, Mukherjee S, Biswas J. Curcumin prevents DNA damage and enhances the repair potential in a chronically arsenic-exposed human population in West Bengal, India. *Eur J Cancer Prev*. 2011;20(2):123-31.
241. Rubin E, Wu X, Zhu T, Cheung JCY, Chen H, Lorincz A, Pandita RK, Sharma GG, Ha HC, Gasson J, Hanakahi LA, Pandita TK, Sukumar S. A role for the HOXB7 homeodomain protein in DNA repair. *Cancer Res*. 2007;67:1527-35.
242. Rudensky AY. Regulatory T cells and Foxp3. *Immunol Rev* 2011;241:260-68.
243. Russo RC, Garcia CC, Teixeira MM, Amaral FA. The CXCL8/IL-8 chemokine family and its receptors in inflammatory diseases. *Expert Rev Clin Immunol*. 2014 May;10(5):593-19.
244. Sabat R, Grütz G, Warszawska K, Kirsch S, Witte E, Wolk K, Geginat J. Biology of interleukin-10. *Cytokine Growth Factor Rev*. 2010;21(5):331-44.
245. Saha D, Ray RK. Groundwater resources of India: potential, challenges and management. In: Sikdar PK (ed). *Groundwater Development and Management*. Springer, Cham, pp 19-42; 2019.
246. Sanner MF. Python: a programming language for software integration and development. *J Mol Graph Model*. 1999;17:57-61.

247. Sanulli S, Justin N, Teissandier A, Ancelin K, Portoso M, Caron M, Michaud A, Lombard B, da Rocha ST, Offer J, Loew D, Servant N, Wassef M, Burlina F, Gamblin SJ, Heard E, Margueron R. Jarid2 Methylation via the PRC2 Complex Regulates H3K27me3 Deposition during Cell Differentiation. *Mol Cell*. 2015;57(5):769-83.
248. Sarkar R, Mukherjee S, Biswas J, Roy M. Phenethyl isothiocyanate, by virtue of its antioxidant activity, inhibits invasiveness and metastatic potential of breast cancer cells: HIF-1 $\alpha$  as a putative target. *Free Radic Res*. 2016;50(1):84-00.
249. Scharer OD. Nucleotide Excision Repair in Eukaryotes. *Cold Spring Harbor Perspect Biol*. 2013;5:a012609.
250. Scheindlin S. The duplicitous nature of inorganic arsenic. *Mol Interv*. 2005;5(2):60-64.
251. Sekeres MA. New data with arsenic trioxide in leukemias and myelodysplastic syndromes. *Clin Lymphoma Myeloma*. 2007;8(1):S7-S12.
252. Seoane J, Gomis RR. TGF- $\beta$  Family Signalling in Tumor Suppression and Cancer Progression. *Cold Spring Harb Perspect Biol*. 2017;9(12):a022277.
253. Serrano-Gomez SJ, Maziveyi M, Alahari SK. Regulation of epithelial-mesenchymal transition through epigenetic and post-translational modifications. *Mol Cancer*. 2016;15:18.
254. Shaji E, Santosh M, Sarath KV, Prakash P, Deepchand V, Divya BV. Arsenic contamination of groundwater: A global synopsis with focus on the Indian Peninsula. *Geosci Front*. 2021;12(3):101079.
255. Shechter D, Dormann HL, Allis CD, Hake SB. Extraction, purification and analysis of histones. *Nat Protoc*. 2007;2(6):1445-57.

256. Sheikhpour E, Noorbakhsh P, Foroughi E, Farahnak S, Nasiri R, Neamatzadeh H. A Survey on the Role of Interleukin-10 in Breast Cancer: A Narrative. *Rep Biochem Mol Biol*. 2018;7(1):30-37.
257. Shi H, Shi X, Liu KJ. Oxidative mechanism of arsenic toxicity and carcinogenesis. *Mol Cell Biochem*. 2004 ;255(1-2):67-78.
258. Silva LB, dos Santos Neto AP, Maia SMAS, dos Santos Guimarães C, Quidute IL, Carvalho AAT, Júnior SA, Leão JC. The Role of TNF- $\alpha$  as a Proinflammatory Cytokine in Pathological Processes. *Open Dent J*. 2019;13:332-38.
259. Sim GC, Radvanyi L. The IL-2 cytokine family in cancer immunotherapy. *Cytokine Growth Factor Rev*. 2014; 25:377-90.
260. Sinha D, Roy M, Dey S, Siddiqi M, Bhattacharya RK. Modulation of arsenic induced cytotoxicity by tea. *Asian Pac J Cancer Prev*. 2003;4(3):233-37.
261. Sinha D, Roy S, Roy M. Antioxidant potential of tea reduces arsenite induced oxidative stress in Swiss albino mice. *Food Chem Toxicol*. 2010;48(4):1032-39.
262. Sinha P, Clements VK, Ostrand-Rosenberg S. Interleukin-13-regulated M2 macrophages in combination with myeloid suppressor cells block immune surveillance against metastasis. *Cancer Res*. 2005;65:11743–51.
263. Smith A, Teknos TN, Pan Q. Epithelial to mesenchymal transition in head and neck squamous cell carcinoma. *Oral Oncol*. 2013;49: 287-92.
264. Son H, Moon A. Epithelial-mesenchymal Transition and Cell Invasion. *Toxicol Res*. 2010;26(4):245-52.
265. Song X, Traub B, Shi J, Kornmann M. Possible Roles of Interleukin-4 and -13 and Their Receptors in Gastric and Colon Cancer. *Int J Mol Sci*. 2021;22(2):727.

266. Sorg TJ, Chen AS, Wang L. Arsenic species in drinking water wells in the USA with high arsenic concentrations. *Water Res.* 2014;48:156-69.
267. Srinivas US, Tan BWQ, Vellayappan BA, Jeyasekharan AD. ROS and the DNA damage response in cancer. *Redox Biol.* 2019;25:101084
268. Srivastava HM, Dey U, Ghosh A, Tripathi JP, Abbas S, Taraphder A, Roy M. Growth of tumor due to Arsenic and its mitigation by black tea in Swiss albino mice. *Alex Eng J.* 2020;59(3):1345-57.
269. Steinmaus C, Yuan Y, Bates MN, Smith AH. Case control study of bladder cancer and drinking water arsenic in the western United States. *Am J Epidemiol.* 2003;158:1193–01.
270. Steward WP, Brown K. Cancer chemoprevention: a rapidly evolving field. *Br J Cancer.* 2013;109(1):1-7.
271. Su LJ, Zhang JH, Gomez H, Murugan R, Hong X, Xu D, Jiang F, Peng ZY. Reactive Oxygen Species-Induced Lipid Peroxidation in Apoptosis, Autophagy, and Ferroptosis. *Oxid Med Cell Longev.* 2019;2019:5080843.
272. Su X, Jiang X, Meng L, Dong X, Shen Y, Xin Y. Anticancer Activity of Sulforaphane: The Epigenetic Mechanisms and the Nrf2 Signalling Pathway. *Oxid Med Cell Longev.* 2018;2018:5438179.
273. Suzuki A, Leland P, Joshi BH, Puri RK. Targeting of IL-4 and IL-13 receptors for cancer therapy. *Cytokine* 2015;75:79–88
274. Sykora P, Snow ET. Modulation of DNA polymerase beta-dependent base excision repair in cultured human cells after low dose exposure to arsenite. *Toxicol Appl Pharmacol.* 2008;228(3):385-94.
275. Tam LM, Price NE, Wang Y. Molecular Mechanisms of Arsenic-Induced Disruption of DNA Repair. *Chem Res Toxicol.* 2020;33(3):709-26.

276. Tandon SK, Sinha R. The Ganga River: A summary view of a large river system of the Indian sub-continent. In: Singh D (ed). *The Indian Rivers*. Springer Hydrogeology. Springer, Singapore, pp 61-73; 2018.
277. Tang B, Qi G, Tang F, Yuan S, Wang Z, Liang X, Li B, Yu S, Liu J, Huang Q, Wei Y, Zhai R, Lei B, Yu H, Jiao X, He S. JARID1B promotes metastasis and epithelial-mesenchymal transition via PTEN/AKT signalling in hepatocellular carcinoma cells. *Oncotarget*. 2015;6(14):12723-39.
278. Taverna S, Giallombardo M, Pucci M, Flugy A, Manno M, Raccosta S, Rolfo C, De Leo G, Alessandro R. Curcumin inhibits in vitro and in vivo chronic myelogenous leukemia cells growth: a possible role for exosomal disposal of miR-21. *Oncotarget*. 2015;6(26):21918-33.
279. Taylor V, Goodale B, Raab A, Schwerdtle T, Reimer K, Conklin S, Karagas MR, Francesconi KA. Human exposure to organic arsenic species from seafood. *Sci Total Environ*. 2017;580:266-82.
280. Taylor-Papadimitriou J, Burchell J. JARID1/KDM5 demethylases as cancer targets? *Expert Opin Ther Targets*. 2017;21(1):5-7.
281. Thangapazham RL, Singh AK, Sharma A, Warren J, Gaddipati JP, Maheshwari RK. Green tea polyphenols and its constituent epigallocatechin gallate inhibits proliferation of human breast cancer cells in vitro and in vivo. *Cancer Lett*. 2007;245(1-2):232-41.
282. Tian X, Liu Z, Niu B, Zhang J, Tan TK, Lee SR, Zhao Y, Harris DC, Zheng G. E-cadherin/ $\beta$ -catenin complex and the epithelial barrier. *J Biomed Biotechnol*. 2011;2011:567305.

283. Tong D, Ortega J, Kim C, Huang J, Gu L, Li GM. Arsenic Inhibits DNA Mismatch Repair by Promoting EGFR Expression and PCNA Phosphorylation. *J Biol Chem*. 2015;290(23):14536-41.
284. Torgovnick A, Schumacher B. DNA repair mechanisms in cancer development and therapy. *Front Genet*. 2015;6:157.
285. Trott O, Olson AJ. AutoDock Vina: improving the speed and accuracy of docking with a new scoring function, efficient optimization, and multithreading. *J Comput Chem*. 2010;31(2):455-61.
286. Tu W, Liu Y, Xie C, Zhou X. Arsenite downregulates H3K4 trimethylation and H3K9 dimethylation during transformation of human bronchial epithelial cells. *J Appl Toxicol*. 2018;38(4):480-88.
287. Tzao C, Tung HJ, Jin JS, Sun GH, Hsu HS, Chen BH, Yu CP, Lee SC. Prognostic significance of global histone modifications in resected squamous cell carcinoma of the esophagus. *Mod Pathol*. 2009;22(2):252-60.
288. Tzavlaki K, Moustakas A. TGF- $\beta$  Signaling. *Biomolecules*. 2020;10(3):487.
289. U.S. EPA. (2008). Reregistration Eligibility Decision for Chromated Arsenicals. EPA 739-R-08-1006, p. 90. Available at: [http://www.epa.gov/oppsrrd1/REDs/cca\\_red.pdf](http://www.epa.gov/oppsrrd1/REDs/cca_red.pdf).
290. Vahidnia A, van der Voet GB, de Wolff FA. Arsenic neurotoxicity--a review. *Hum Exp Toxicol*. 2007;26(10):823-32.
291. Varambally S, Dhanasekaran SM, Zhou M, Barrette TR, Kumar-Sinha C, Sanda MG, Ghosh D, Pienta KJ, Sewalt RG, Otte AP, Rubin MA, Chinnaiyan AM. The polycomb group protein EZH2 is involved in progression of prostate cancer. *Nature*. 2002;419(6907):624-29.

292. Vincent T, Neve EP, Johnson JR, Kukalev A, Rojo F, Albanell J, Pietras K, Virtanen I, Philipson L, Leopold PL, Crystal RG, de Herreros AG, Moustakas A, Pettersson RF, Fuxe J. A SNAIL1-SMAD3/4 transcriptional repressor complex promotes TGF-beta mediated epithelial-mesenchymal transition. *Nat Cell Biol.* 2009;11(8):943-50.
293. Wang H, Wang L, Chi PD, Wang WD, Chen XQ, Geng QR, Xia ZJ, Lu Y. High level of interleukin-10 in serum predicts poor prognosis in multiple myeloma. *Br J Cancer.* 2016;114(4):463-8.
294. Wang YC, Bachrach U. The specific anti-cancer activity of green tea (-)-epigallocatechin-3-gallate (EGCG). *Amino Acids.* 2002;22(2):131-43.
295. Watanabe T, Hirano S. Metabolism of arsenic and its toxicological relevance. *Arch Toxicol.* 2013;87(6):969-79.
296. Waxman S, Anderson KC. History of the development of arsenic derivatives in cancer therapy. *Oncologist.* 2001;6(2):3-10.
297. Weston A, Harris CC. Multistage Carcinogenesis. In: Kufe DW, Pollock RE, Weichselbaum RR, (eds). *Holland-Frei Cancer Medicine.* 6<sup>th</sup> edition. Hamilton.
298. Williamson LM, Lees-Miller SP. Estrogen receptor  $\alpha$ -mediated transcription induces cell cycle-dependent DNA double-strand breaks. *Carcinogenesis.* 2011;32(3):279-85.
299. Wu D, Qiu Y, Jiao Y, Qiu Z, Liu D. Small Molecules Targeting HATs, HDACs, and BRDs in Cancer Therapy. *Front Oncol.* 2020;10:560487.
300. Wu MM, Chiou HY, Ho IC, Chen CJ, Lee TC. Gene expression of inflammatory molecules in circulating lymphocytes from arsenic-exposed human subjects. *Environ. Health Perspect.* 2003;111:1429-38.



301. Wu YY, Li W, Xu Y, Jin EH, Tu YY. Evaluation of the antioxidant effects of four main theaflavin derivatives through chemiluminescence and DNA damage analyses. *J Zhejiang Univ Sci B*. 2011;12(9):744-51.
302. Xian D, Lai R, Song J, Xiong X, Zhong J. Emerging Perspective: Role of Increased ROS and Redox Imbalance in Skin Carcinogenesis. *Oxid Med Cell Longev*. 2019;2019:8127362.
303. Xu M, Wang S, Wang Y, Wu H, Frank JA, Zhang Z, et al. Role of p38 $\gamma$  MAPK in regulation of EMT and cancer stem cells. *Biochim Biophys Acta Mol Basis Dis*. 2018;1864:3605-17.
304. Xue G, Restuccia DF, Lan Q, Hynx D, Dirnhofer S, Hess D, Rüegg C, Hemmings BA. Akt/PKB-mediated phosphorylation of Twist1 promotes tumour metastasis via mediating cross-talk between PI3K/Akt and TGF- $\beta$  signalling axes. *Cancer Discov*. 2012;2(3):248-59.
305. Yan XB, Xie T, Wang SD, Wang Z, Li HY, Ye ZM. Apigenin inhibits proliferation of human chondrosarcoma cells via cell cycle arrest and mitochondrial apoptosis induced by ROS generation-an in vitro and in vivo study. *Int. J. Clin. Exp. Med*. 2018;11(3):1615-31.
306. Yanofsky VR, Mercer SE, Phelps RG. Histopathological variants of cutaneous squamous cell carcinoma: a review. *J Skin Cancer*. 2011;2011:210813.
307. Yu JH, Kim H. Oxidative stress and cytokines in the pathogenesis of pancreatic cancer. *J Cancer Prev*. 2014;19(2):97-02.
308. Yu NH, Pei H, Huang YP, Li YF. (-)-Epigallocatechin-3-Gallate Inhibits Arsenic-Induced Inflammation and Apoptosis through Suppression of Oxidative Stress in Mice. *Cell Physiol Biochem*. 2017;41(5):1788-00.

309. Zehnder M, Delaleu N, Du Y, Bickel M. Cytokine gene expression: Part of host defence in pulpitis. *Cytokine*. 2003;22(3-4):84-88.
310. Zhan X, Feng X, Kong Y, Chen Y, Tan W. JNK signalling maintains the mesenchymal properties of multi-drug resistant human epidermoid carcinoma KB cells through snail and twist1. *BMC Cancer*. 2013;13:180.
311. Zhang A, Li H, Xiao Y, Chen L, Zhu X, Li J, Ma L, Pan X, Chen W, He Z. Aberrant methylation of nucleotide excision repair genes is associated with chronic arsenic poisoning. *Biomarkers*. 2017;22:429–38.
312. Zhang J, An X, Han Y, Ma R, Yang K, Zhang L, Chi J, Li W, Llobet-Navas D, Xu Y, Jiang Y. Overexpression of JARID1B promotes differentiation via SHIP1/AKT signaling in human hypopharyngeal squamous cell carcinoma. *Cell Death Dis*. 2016;7(9):e2358.
313. Zhang J, Bowden GT. Activation of p38 MAP kinase and JNK pathways by UVA irradiation. *Photochem Photobiol Sci*. 2012;11:54-61.
314. Zhang L, Zhong K, Dai Y, Zhou H. Genome-wide analysis of histone H3 lysine 27 trimethylation by ChIP-chip in gastric cancer patients. *J Gastroenterol*. 2009;44(4):305-12.
315. Zhang W, Su J, Xu H, Yu S, Liu Y, Zhang Y, Sun L, Yue Y, Zhou X. Dicumarol inhibits PDK1 and targets multiple malignant behaviors of ovarian cancer cells. *PLoS One*. 2017;12(6):e0179672.
316. Zhang Y, Alexander PB, Wang XF. TGF- $\beta$  Family Signalling in the Control of Cell Proliferation and Survival. *Cold Spring Harb Perspect Biol*. 2017;9(4):a022145.
317. Zhang YE. Non-smad signaling pathways of the TGF- $\beta$  family. *Cold Spring Harb Perspect Biol*. 2017;9:a022129.

318. Zhang YJ, Gan RY, Li S, Zhou Y, Li AN, Xu DP, Li HB. Antioxidant Phytochemicals for the Prevention and Treatment of Chronic Diseases. *Molecules*. 2015;20(12):21138-56.
319. Zhang Z, Pi R, Luo J, Liu J, Zhang A, Sun B. Association between arsenic exposure and inflammatory cytokines and C-reaction protein: A systematic review and meta-analysis. *Medicine (Baltimore)*. 2022;101(50):e32352.
320. Zhao CQ, Young MR, Diwan BA, Coogan TP, Waalkes MP. Association of arsenic-induced malignant transformation with DNA hypomethylation and aberrant gene expression. *Proc Natl Acad Sci U S A*. 1997;94(20):10907-12.
321. Zhao G, Han X, Zheng S, Li Z, Sha Y, Ni J, Sun Z, Qiao S, Song Z. Curcumin induces autophagy, inhibits proliferation and invasion by downregulating AKT/mTOR signalling pathway in human melanoma cells. *Oncol Rep*. 2016;35(2):1065-74.
322. Zhou Q, Xi S. A review on arsenic carcinogenesis: Epidemiology, metabolism, genotoxicity and epigenetic changes. *Regul Toxicol Pharmacol*. 2018;99:78–88.
323. Zhou X, Cooper KL, Huestis J, Xu H, Burchiel SW, Hudson LG, and Liu KJ. S-nitrosation on zinc finger motif of PARP-1 as a mechanism of DNA repair inhibition by arsenite. *Oncotarget*. 2016;7:80482–92.
324. Zhou X, Li Q, Arita A, Sun H, Costa M. Effects of nickel, chromate, and arsenite on histone 3 lysine methylation. *Toxicol Appl Pharmacol*. 2009;236(1):78-84.
325. Zhou X, Sun H, Ellen TP, Chen H, Costa M. Arsenite alters global histone H3 methylation. *Carcinogenesis*. 2008;29(9):1831-36.

326. Zhu W, Qin W, Zhang K, Rottinghaus GE, Chen YC, Kliethermes B, Sauter ER. Trans-resveratrol alters mammary promoter hypermethylation in women at increased risk for breast cancer. *Nutr Cancer*. 2012;64(3):393-00.

## List of publications

### *Original articles*

1. **Archismaan Ghosh** and Madhumita Roy (2023). Black Tea Extract, via Modulation of TGF- $\beta$  Pathway, Prevents Inorganic Arsenic-induced Development of Squamous Cell Carcinoma of the Skin in Swiss Albino Mice. *Journal of cancer prevention*, 28(1):12-23. <https://doi.org/10.15430/JCP.2023.28.1.12>
2. **Archismaan Ghosh** and Madhumita Roy (2023). Black Tea Extract Prevents iAs Induced Transformation of HaCaT Cells via Modulation of Cellular Damage, Inflammation and TGF- $\beta$  Signalling Cascade. *Int.J.Curr.Microbiol.App.Sci.*, 12(01): 171-189. <https://doi.org/10.20546/ijcmas.2023.1201.020>
3. **Archismaan Ghosh**, Sutapa Mukherjee and Madhumita Roy (2022). Black tea extract prevents inorganic arsenic induced uncontrolled proliferation, epithelial to mesenchymal transition and induction of metastatic properties in HaCaT keratinocytes - an in vitro study. *Toxicology in vitro*, 85: 105478. <https://doi.org/10.1016/j.tiv.2022.105478>.
4. **Archismaan Ghosh**, Ansuman Lahiri, Sutapa Mukherjee, Madhumita Roy, and Amitava Datta (2022). Prevention of inorganic arsenic induced squamous cell carcinoma of the skin in Swiss albino mice by black tea through epigenetic modulation. *Heliyon*, 8(8): e10341. <https://doi.org/10.1016/j.heliyon.2022.e10341>
5. **Archismaan Ghosh**, Sutapa Mukherjee and Madhumita Roy (2021). Chemopreventive Role of Black Tea Extract in Swiss Albino Mice Exposed to Inorganic Arsenic. *Asian Pacific journal of Cancer Prevention*, 22(11): 3647–3661. <https://doi.org/10.31557/APJCP.2021.22.11.3647>

6. **Archismaan Ghosh**, Sutapa Mukherjee and Madhumita Roy (2021). Co-Carcinogenicity of Arsenic: Probable Mechanisms. *Int. J. Curr. Microbiol. App. Sci.*, 10(11): 294-305. <https://doi.org/10.20546/ijcmas.2021.1011.03>
7. **Archismaan Ghosh**, Apurba Mukherjee, Sutapa Mukherjee and Madhumita Roy (2020). Assessment of Susceptibility towards iAs Induced Carcinogenesis in West Bengal, India. *Int. J. Curr. Microbiol. App. Sci.*, 9(3): 1998-2011. <https://doi.org/10.20546/ijcmas.2020.903.232>
8. HM Srivastava, Urmimala Dey, **Archismaan Ghosh**, Jai Prakash Tripathi, Syed Abbas, A Taraphder, and Madhumita Roy (2020). Growth of tumour due to arsenic and its mitigation by black tea in Swiss albino mice. *Alexandria Engineering Journal*, 59(3): 1345-1357. <https://doi.org/10.1016/j.aej.2020.03.001>
9. Souvick Biswas, Elizabeth Mahapatra, **Archismaan Ghosh**, Salini Das, Madhumita Roy, and Sutapa Mukherjee (2021). Curcumin Rescues Doxorubicin Responsiveness via Regulating Aurora a Signaling Network in Breast Cancer Cells. *Asian Pacific journal of Cancer Prevention*, 22(3): 957–970. <https://doi.org/10.31557/APJCP.2021.22.3.95>

#### ***Review articles and book chapters***

1. **Archismaan Ghosh**, Sutapa Mukherjee, Amitava Datta and Madhumita Roy (2021). Modulatory role of tea in arsenic induced epigenetic alterations in carcinogenesis. *Nucleus*, 64: 143–156. <https://doi.org/10.1007/s13237-020-00346-9>
2. **Archismaan Ghosh** and Madhumita Roy. Prevalence of Gallbladder Cancer in Arsenic Endemic Areas (2020). *Nov Appro in Can Study*, 4(4). NACS.000593. <https://doi.org/10.31031/NACS.2020.04.000593>

3. **Archismaan Ghosh**, Apurba Mukherjee, Sutapa Mukherjee and Madhumita Roy (2019). Role of Black Tea in prevention of Skin Carcinogenesis, *LAP LAMBERT Academic Publishing*.
4. Elizabeth Mahapatra, Salini Das, Souvick Biswas, **Archismaan Ghosh**, Debomita Sengupta, Madhumita Roy, and Sutapa Mukherjee (2021). Insights of Cisplatin Resistance in Cervical Cancer: A Decision Making for Cellular Survival. In (Ed.), *Cervical Cancer - A Global Public Health Treatise*. *IntechOpen*. <https://doi.org/10.5772/intechopen.98489>
5. Madhumita Roy, **Archismaan Ghosh** and Amitava Dutta (2023). The potential of black tea in combating arsenic toxicity. In (Ed.), *Tea in Health and Disease Prevention-2nd Edition*. *Elsevier*. [In press].

# Black Tea Extract, via Modulation of TGF- $\beta$ Pathway, Prevents Inorganic Arsenic-induced Development of Squamous Cell Carcinoma of the Skin in Swiss Albino Mice

Archismaan Ghosh, Madhumita Roy

Department of Environmental Carcinogenesis & Toxicology, Chittaranjan National Cancer Institute, Kolkata, India

Chronic exposure to inorganic arsenic (iAs) elevates reactive oxygen species (ROS) generation and up-regulates TGF- $\beta$  signalling. This promotes induction of epithelial to mesenchymal transition (EMT) and causes the development of squamous cell carcinoma (SCC) of skin. Black tea is a popular beverage worldwide and an effective antioxidant. Chemopreventive potential of black tea extract (BTE) against iAs induced carcinogenicity has been explored here. The study aims to investigate the role of BTE in prevention of iAs-induced SCC of skin in Swiss albino mice via the modulation of TGF- $\beta$  signalling and EMT. Mice were divided into (1) control, (2) iAs, (3) iAs+BTE, and (4) BTE groups and were administered iAs and BTE alone, or in combination for 330 days. Histological studies were performed to assess development of SCC. ROS generation was estimated by flowcytometry. Expression of TGF- $\beta$  and downstream proteins belonging to suppressor of mothers against decapentaplegic (Smad), phosphoinositide-3-kinase (PI3K)-protein kinase B (AKT) and mitogen-activated protein kinase (MAPK) pathways was assessed by immunoblotting. Expression of EMT markers was evaluated by immunoblotting, immunohistochemistry and semi-quantitative reverse transcriptase-PCR. After 330 days of iAs treatment, development of invasive SCC of skin probably due to excess ROS generation, elevation of TGF- $\beta$ , downregulation of the Smad pathway, upregulation of PI3K-AKT and MAPK signalling molecules and induction of EMT was observed. All these modulations were found to be reversed by BTE, which inhibits iAs induced SCC of skin by quenching excess ROS, promoting Smad mediated TGF- $\beta$  signalling, downregulating signalling intermediates of PI3K-AKT and MAPK pathways and inhibiting EMT.

**Key Words** Tea, Arsenic, Transforming growth factor beta, Epithelial-mesenchymal transition, Chemoprevention

## INTRODUCTION

Chronic exposure to inorganic arsenic (iAs), classified as a class 1 carcinogen by International Agency for Research on Cancer [1], causes numerous health problems [2]. Epidemiological evidence implicates chronic iAs exposure causes carcinogenesis of various organs like skin, lungs, kidney, bladder, etc. [3,4]. Drinking of iAs contaminated water is a common route of exposure to this environmental pollutant [5]. Primary symptoms of chronic iAs exposure include hyperpigmentation, hypopigmentation, keratosis, Bowen's disease, etc. These skin disorders often develop into malignancies like squamous cell carcinoma (SCC) and basal cell carcinoma [6].

Swiss albino mice chronically exposed to iAs encountered

excess generation of reactive oxygen species (ROS), resulting in DNA, lipid and protein damage, induction of inflammatory cytokine production, and impairment of repair enzymes [7], as well as aberrant epigenetic modulations [8]. Excess ROS generation is linked to induction of cancer and its progression. ROS can also modulate signalling pathways by acting as secondary messengers, facilitating cell proliferation and survival [9]. One of the signalling mechanisms altered by excess ROS generation involves the pathway, where the downstream molecules like suppressor of mothers against decapentaplegic (Smad), mitogen-activated protein kinase (MAPK), and NF- $\kappa$ B are modulated, leading to increased cell motility [10]. TGF- $\beta$  on the other hand can induce excess ROS generation, as well as help maintain high levels of ROS within the system by impairing the activity of antioxidants [11].

Received January 18, 2023, Revised February 2, 2023, Accepted February 4, 2023

Correspondence to Madhumita Roy, E-mail: mitacnci@yahoo.co.in, https://orcid.org/0000-0002-3551-8534



This is an Open Access article distributed under the terms of the Creative Commons Attribution Non-Commercial License, which permits unrestricted non-commercial use, distribution, and reproduction in any medium, provided the original work is properly cited.

Copyright © 2023 Korean Society of Cancer Prevention



Original Research Article

<https://doi.org/10.20546/ijcmas.2023.1201.020>

## Black Tea Extract Prevents iAs Induced Transformation of HaCaT Cells via Modulation of Cellular Damage, Inflammation and TGF- $\beta$ Signalling Cascade

Archismaan Ghosh  and Madhumita Roy 

Department of Environmental Carcinogenesis and Toxicology, Chittaranjan National Cancer Institute,  
37, S P Mukherjee Road, Kolkata – 700026, India

\*Corresponding author

### ABSTRACT

#### Keywords

Inorganic Arsenic (iAs), Black tea Extract (BTE), ROS, RNS, TGF- $\beta$

#### Article Info

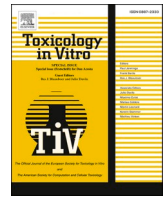
**Received:**  
10 December 2022  
**Accepted:**  
28 December 2022  
**Available Online:**  
10 January 2023

Chronic exposure to inorganic arsenic (iAs) leads to development of cancer of various organs, most prevalent being skin cancer. iAs induces its carcinogenic potential by excess generation of free radicals, which induces DNA, protein, lipid damage; suppresses activity of antioxidant enzymes; enhances prolonged inflammatory conditions and modulates TGF- $\beta$  signalling cascade, all of which promote carcinogenesis. Black tea extract (BTE), a popular beverage and an established antioxidant, has been used in present study to combat the ill effects of iAs exposure. Present study has been conducted on normal human skin keratinocytes, HaCaT cells. Estimation of Reactive Oxygen Species (ROS) and Reactive Nitrogen Species (RNS) generation was done using 2',7'-dichlorodihydrofluorescein diacetate (DCFH-DA) and Greiss reagent. Damage to DNA (by Micronuclei and Comet assay), protein (by protein carbonyl assay kit) and lipid (by lipid peroxidation) were assessed. Activity of antioxidant enzymes, inflammatory cytokines, p50 and p65 subunits of NF- $\kappa$ B were assessed using respective kits. Immunoblotting assay was performed to assess expression of TGF- $\beta$  and modulation of its downstream signalling molecules. Results indicate that BTE quenches iAs induced free radicals; inhibits DNA, protein and lipid damage; prevents deactivation of antioxidant enzymes; suppresses inflammation and prevents EMT inducing modulation of TGF- $\beta$  pathway, thus thwarting iAs induced carcinogenesis in HaCaT cells.

### Introduction

Colourless, odourless, tasteless metalloid Arsenic, 33<sup>rd</sup> element in the periodic table, is omnipresent in our surroundings (Roy *et al.*, 2014). In nature, it is found in both inorganic and organic forms, inorganic form of arsenic is considered to be more toxic than the organic form (Rahaman *et al.*, 2021). Arsenic is a major environmental pollutant and it

may contaminate air, water and soil due to both natural and anthropogenic causes. Groundwater is one of the major sources of drinking water in the world and contamination of it by inorganic Arsenic (iAs) is a serious health hazard worldwide (Chung *et al.*, 2014). Humans chronically exposed to iAs develop numerous dermatological, cardiovascular, gastrointestinal as well as neurological diseases but most serious amongst them being cancer of different



# Black tea extract prevents inorganic arsenic induced uncontrolled proliferation, epithelial to mesenchymal transition and induction of metastatic properties in HaCaT keratinocytes - an in vitro study

Archismaan Ghosh, Sutapa Mukherjee, Madhumita Roy\*

<sup>a</sup> Dept. Environmental Carcinogenesis & Toxicology, Chittaranjan National Cancer Institute, 37, S P Mukherjee Road, Kolkata 700019, India

## ARTICLE INFO

Editor: Dr. P Jennings

### Keywords:

Inorganic arsenic  
Black tea extract  
EMT  
Metastasis  
Chemoprevention

## ABSTRACT

A major global problem is chronic exposure to inorganic arsenic (iAs) which causes various health hazards including cancer. Escalation of reactive oxygen species (ROS) generation by chronic iAs exposure promotes Epithelial to Mesenchymal transition (EMT) which is followed by metastatic progression. In the present study, skin keratinocyte cells (HaCaT) were divided into three groups: (i) untreated, (ii) chronically iAs exposed, (iii) black tea extract (BTE) along with iAs treated. ROS was estimated by flowcytometry, expression of EMT markers were assessed by flowcytometry, western-blotting and Immunofluorescence. For metastatic studies, wound-healing assay, gelatin zymography, western-blot, transwell migration/invasion assay had been performed. Long term exposure of HaCaT cells to iAs causes excess generation of ROS. Morphological transformation and EMT were apparent at 210 days of exposure. Development of metastatic characteristics were observed at 240 days. Alterations in the parameters induced by iAs were found to be ameliorated by BTE. BTE was found to quench excess generation of ROS by iAs, subsequently inhibiting the chain of events like EMT and metastasis. Therefore, BTE may be considered as a potential phytochemical to prevent the deleterious effect of iAs. Skin carcinogenesis induced by iAs may thus be prevented by BTE via inhibition of EMT.

## 1. Introduction

The omnipresent metalloid arsenic, is one of the major environmental pollutants (Riedmann et al., 2015). Pollution of drinking water by inorganic arsenic (iAs) has become a major global problem. Concentration of iAs in groundwater, in many regions of the world, is many folds higher than 10 µg/L safe limit, as recommended by World Health Organisation (WHO) (Chakraborti et al., 2018). High concentration of iAs present in drinking water, when chronically exposed to individuals, induces the development of innumerable diseases such as cardiovascular disease, peripheral vascular disease, hypertension, arteriosclerosis as well as cancer of various organs like bladder, lungs, prostate, skin etc. (Chakraborti et al., 2018). The preliminary manifestation of chronic arsenic exposure is generally observed in the skin where exposed individuals develop hyper-pigmentation, hypo-pigmentation, Bowens' disease and arsenic keratosis. Many of these conditions may further aggravate and result in development of Squamous cell carcinoma (SCC) or Basal cell carcinoma (BCC), two of the most predominant forms of

non-melanoma skin cancer (NMSC) (Huang et al., 2019).

The basal layer of epidermis harbours the stem cells which differentiate into cornified squamous cells and form the outermost layer of the skin. There exists a balance between the differentiation and keratinocyte proliferation which maintains the architecture of the epidermis of the skin (Bangert et al., 2011). Chronic exposure to arsenic greatly hampers this balance which ultimately promotes the various diseased conditions (arsenic keratosis, hyper/hypo-pigmentation etc.) of the skin ultimately culminating into carcinogenesis (Udensi et al., 2011). An important phenomenon which has been observed to occur during carcinogenesis is Epithelial to Mesenchymal transition (EMT). EMT was known to occur during embryogenesis and wound healing but now it has also been widely observed during carcinogenesis, where it promotes tumorigenesis and metastasis (Hodorogea et al., 2019). During EMT, the epithelial cells lose their differentiated properties and express mesenchymal phenotype which enhances the invasiveness and aggressiveness of the cancer cells, ultimately leading to metastasis. This phenomenon involves overexpression of the mesenchymal markers (N-cadherin, Vimentin etc.)

\* Corresponding author at: Dept. Environmental Carcinogenesis & Toxicology, Chittaranjan National Cancer Institute, 37, S P Mukherjee Road, Kolkata 700029, India.

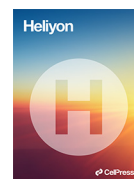
E-mail address: [mitacnci@yahoo.co.in](mailto:mitacnci@yahoo.co.in) (M. Roy).

<https://doi.org/10.1016/j.tiv.2022.105478>

Received 11 July 2022; Received in revised form 7 September 2022; Accepted 13 September 2022

Available online 16 September 2022

0887-2333/© 2022 Elsevier Ltd. All rights reserved.



## Research article

## Prevention of inorganic arsenic induced squamous cell carcinoma of the skin in Swiss albino mice by black tea through epigenetic modulation

Archismaan Ghosh<sup>a</sup>, Ansuman Lahiri<sup>b</sup>, Sutapa Mukherjee<sup>a</sup>, Madhumita Roy<sup>a</sup>, Amitava Datta<sup>c,\*</sup><sup>a</sup> Department of Environmental Carcinogenesis & Toxicology, Chittaranjan National Cancer Institute, 37, S P Mukherjee Road, Kolkata 700026, India<sup>b</sup> Department of Biophysics, Molecular Biology & Bioinformatics, University of Calcutta, 92, APC Road, Kolkata 700009, India<sup>c</sup> Department of Computer Science and Software Engineering, University of Western Australia, Perth, WA 6009, Australia

## ARTICLE INFO

## Keywords:

Inorganic arsenic  
Squamous cell carcinoma  
Methyltransferases  
Demethylases  
Acetyltransferases  
Black tea extract  
JARID1B

## ABSTRACT

Consumption of inorganic Arsenic (iAs) above the safe level may lead to many diseases including cancers of skin. It is known that carcinogenicity of iAs is mediated through generation of excessive reactive oxygen species and polyphenols present in black tea extract (BTE) ameliorate the deleterious effect. Epigenetics also plays vital roles in carcinogenesis. The aim of this paper is to study the influence of iAs on epigenetics and the modulatory effect of BTE.

Male Swiss albino mice were divided into three groups, (i) control, (ii) iAs-administered and (iii) iAs + BTE administered. Group (ii) developed invasive squamous cell carcinoma (SCC) of the skin after 330 days, while only hyperplastic and dysplastic changes were observed in group (iii). Expression levels of histone methylation, acetylation marks and several histone methylases, demethylases and acetylases due to iAs were studied; most aberrant expression levels due to iAs were modulated by BTE. JARID1B, a histone demethylase implicated as one of the markers in SCC and a therapeutic target gets upregulated by iAs, but is not influenced by BTE. However, SCC is prevented by BTE. Upregulation of JARID1B by iAs represses H3K4me3; BTE upregulates H3K4me3 without influencing JARID1B expression level. It is known that theaflavin compounds in BTE are transported to the nucleus and interact with histone proteins. *in-silico* findings in this paper hint that theaflavin compounds present in BTE are very good inhibitors of JARID1B and BTE inhibits its demethylating activity. BTE reverses the epigenetic alterations caused by iAs, thus aids in prevention of SCC.

## 1. Introduction

Genetic mutation, epigenetic modulation and environmental factors contribute to carcinogenesis. Chronic exposure to inorganic arsenic (iAs), a class I carcinogen declared by IARC [1] beyond the safe level (10 µg/L, as set by WHO) [1], leads to numerous diseases including cancers of the skin, bladder, kidney and liver [2]. Globally iAs contaminated drinking water is a major health hazard. Air borne particulate matter released from several industries also adds to the risk [3]. Arsenic mediates its carcinogenicity by excessive generation of reactive oxygen species (ROS) [2]. Metabolism of inorganic arsenic (iAs) utilises S-adenosyl methionine (SAM), whose depletion occurs due to chronic exposure to iAs, altering global methylation pattern of DNA and gene expression [4]. iAs is also known to induce different types of epigenetic modulations, and the present study focuses on post-translational histone modifications (PTM) including histone methylation, demethylation and acetylation. The main

contributions of this study are two-fold. The carcinogenic effect of iAs on squamous cell carcinoma (SCC) due to PTM and the alleviation of these effects by black tea extract (BTE) have been studied extensively *in vivo* in the mouse model. The effects of iAs on several of these methylases and demethylases have not been reported before to the best of our knowledge. This paper also establishes the potential of theaflavin compounds (present in BTE) as inhibitors of JARID1B, a di- and tri-demethylase of H3K4 through extensive *in silico* studies.

Antioxidants mitigate the carcinogenicity of iAs due to ROS, as generation of ROS drives epigenetic alterations [5]. The genetic and epigenetic modulation by phytochemicals have been reviewed extensively in the context of carcinogenesis [6]. Tea contains polyphenols and is a good source of antioxidants [7]. Major constituents of black tea are theaflavins (TF) and thearubigins (TR). TF, a seven-member benzotropolone ring is formed due to co-oxidation of pairs of epimerized catechins. This molecule is capable of chelating transition metals, thereby countering free

\* Corresponding author.

E-mail address: [amitava.datta@uwa.edu.au](mailto:amitava.datta@uwa.edu.au) (A. Datta).<https://doi.org/10.1016/j.heliyon.2022.e10341>

Received 22 January 2022; Received in revised form 16 March 2022; Accepted 1 August 2022

2405-8440/© 2022 The Author(s). Published by Elsevier Ltd. This is an open access article under the CC BY-NC-ND license (<http://creativecommons.org/licenses/by-nc-nd/4.0/>).

# Chemopreventive Role of Black Tea Extract in Swiss Albino Mice Exposed to Inorganic Arsenic

Archismaan Ghosh, Sutapa Mukherjee, Madhumita Roy\*

## Abstract

**Objective:** Chronic exposure to inorganic arsenic (iAs) may cause a number of health problems including skin cancer. Present study is aimed to look into the potential of black tea extract (BTE) to prevent the development of skin carcinoma in Swiss albino mice. **Methods:** The study was done on Swiss albino mice, chronically exposed to inorganic arsenic. 150 mice were housed in different cages, 5 in each cage. The control mice did not receive any treatment. Mice were sacrificed at 30, 90, 180, 270 and 330 days. Development of carcinogenesis was assessed by histological studies. Generation of Reactive Oxygen Species (ROS) and Reactive Oxygen Species (RNS) were estimated using 2',7'-dichlorodihydrofluorescein diacetate (DCFH-DA) and Greiss reagent respectively, and their consequences on DNA (by Micronuclei and Comet assay), protein (by protein carbonyl assay kit) and lipid (by lipid peroxidation) were estimated. Activity of antioxidant enzymes, along with total antioxidant capacity were measured by respective kits. Repair percentage was obtained by Comet assay. Western blotting was employed to study the expression of repair enzymes and expression of cytokines. Sandwich Enzyme-linked Immunosorbent Assay (ELISA) technique was employed to study the activity of various cytokines. **Results:** At 330 days, invasive squamous cell carcinoma of the skin developed. With increasing time generation of ROS and RNS increased, causing damage to DNA, protein and lipid. Antioxidant defence system gets repressed with time. Capacity to repair the DNA damage is inhibited by iAs, due to alteration in repair enzymes - XRCC I, DNA Ligase I, PARP I, ERCC1, ERCC2, XPA, DNA Ligase IV, DNA PKc and Ku-70. Another consequence of iAs exposure is chronic inflammation due to disrupted cytokine level. Intervention with BTE reverses these deleterious effects, preventing development of skin carcinogenesis.

**Keywords:** Inorganic arsenic- skin carcinogenesis- black tea extract- ROS

*Asian Pac J Cancer Prev*, 22 (11), 3647-3661

## Introduction

Chronic exposure to the metalloid arsenic, which exists in both organic and inorganic forms, may cause numerous health hazards (Tchounwou et al., 2012), and the inorganic form is more toxic (Hughes et al., 2011). Chronic exposure to inorganic arsenic (iAs) may result in a plethora of diseases, both non-malignant, as well as malignant (Martinez et al., 2011) and cancer of skin, kidney, bladder, lung etc. are endemic.

Excess generation of reactive oxygen species (ROS) due to iAs is an important contributory factor to its carcinogenicity (Zhang et al., 2015). Higher level of ROS mediates its damage at the cellular level, affecting nucleic acids, lipids and proteins (Pizzino et al., 2017). Higher fluxes of ROS generation lead to formation of protein carbonyl due to oxidation of amino acid residues (Sinha et al., 2010). High level of ROS also leads to lipid peroxidation of polyunsaturated fatty acids, generating malondialdehyde, which elicits cytotoxic effects and damage to cell membrane. Defragmentation

of lipid chains, resulting in excess fluidity and enhanced permeability of the cell membrane may occur due to ROS (Yusupov et al., 2010). Antioxidants are important for reducing damage due to ROS.

Antioxidant enzymes act in defence of the cells against excess ROS induced DNA, lipid and protein damage, maintaining homeostasis by reducing the damage. Some of these antioxidant enzymes are superoxide dismutase (SOD), catalase, Glutathione peroxidase (GPX), Glutathione reductase (GR), Glutathione transferase (GT) etc. (Caverzan et al., 2016). Normally a balance between ROS and antioxidant defence is maintained, preventing permanent damage, either by removal or by efficient repair of the damaged parts. There are certain repair mechanisms: (i) base excision repair (BER), which repairs single-strand breaks due to oxidative DNA damage; (ii) nucleotide excision repair (NER) that repairs DNA cross links and bulky adducts due to insult by environmental challenges; (iii) nonhomologous end joining (NHEJ) which is implicated in DNA repair in eukaryotic systems (Rowe et al., 2008). All these act to counter DNA damage. Chronic

Original Research Article

<https://doi.org/10.20546/ijcmas.2021.1011.033>

## Co-Carcinogenicity of Arsenic: Probable Mechanisms

Archismaan Ghosh, Sutapa Mukherjee and Madhumita Roy\*

Department of Environmental Carcinogenesis & Toxicology, Chittaranjan National Cancer  
Institute, 37, S P Mukherjee Road, Kolkata 700026, India

\*Corresponding author

### ABSTRACT

Presence of carcinogens, like Polycyclic Aromatic Hydrocarbons (PAH), in the form of cigarette smoke, vehicular emission and industrial emissions in our immediate surroundings is a potent health hazard. Arsenic, a carcinogenic metalloid, omnipresent in the environment, can act as co-carcinogen, where it enhances the carcinogenicity of other carcinogens. In the present study, the co-carcinogenic effect of Arsenic has been investigated, upon the 7,12-dimethylbenz[a]-anthracene (DMBA), a PAH, induced skin cancer model, in Swiss albino mice. Histological analysis revealed earlier development of invasive carcinoma in the DMBA and arsenic treated group in comparison to the DMBA treated mice alone. To understand this phenomena, ROS generation, DNA damage, lipid peroxidation, protein carbonyl content, total antioxidant capacity and activity of pro-inflammatory cytokines (TNF- $\alpha$ , IL6, IL17a, IL22) and their downstream modulators (NF- $\kappa$ B) was assessed. The results suggested that arsenic in the presence of DMBA induced higher ROS generation, greater DNA damage, elevated lipid peroxidation, increased protein carbonyl content, upregulated activity of pro-inflammatory cytokines and their downstream regulators as well as down regulated the total antioxidant capacity in comparison to DMBA alone. These findings hint at the co-carcinogenic potential of arsenic, as it significantly enhances the carcinogenicity of DMBA and hastens carcinogenesis.

#### Keywords

Arsenic, co-carcinogenicity, DMBA, ROS, inflammation

#### Article Info

**Received:**

12 October 2021

**Accepted:**

05 November 2021

**Available Online:**

10 November 2021

### Introduction

The present external condition of an individual which influences its development and growth, is generally referred to as its environment (Belpomme *et al.*, 2007). Research has shown that environmental factors play an important role in development of cancers (Rushton *et al.*, 2003). There are numerous cancer-causing environmental factors to which we are

exposed. Amongst these factors, Polycyclic Aromatic Hydrocarbons (PAH) are notable, which are often present in our immediate surroundings (Lawal, 2017). These are a group of very potent carcinogens, as evident from epidemiological and animal studies. PAHs, can attach to fine carbon particles and remain suspended in air. They are produced due to combustion of organic substances and are found in factory and cigarette smoke, waste



Original Research Article

<https://doi.org/10.20546/ijcmas.2020.903.232>

## Assessment of Susceptibility towards iAs Induced Carcinogenesis in West Bengal, India

Archismaan Ghosh, Apurba Mukherjee, Sutapa Mukherjee and Madhumita Roy\*

Department Environmental Carcinogenesis & Toxicology, Chittaranjan National Cancer Institute, 37, S P Mukherjee Road, Kolkata, India

\*Corresponding author

### ABSTRACT

#### Keywords

Arsenic, ROS, carcinogenesis, cytokines, telomerase, DNA repair, NF- $\kappa$ B

#### Article Info

##### Accepted:

15 February 2020

##### Available Online:

10 March 2020

Inorganic Arsenic (iAs) contamination of groundwater had been a major health hazard. In West-Bengal, many areas had been found to have high level of iAs in groundwater. Chronic exposure to iAs may lead to the generation of Reactive Oxygen Species (ROS) and Reactive Nitrogen Species (RNS). This results in DNA damage, inflammation, impairment of repair activity, thereby culminating in carcinogenesis. Higher telomerase activity may be another manifestation of iAs exposure. This is a pilot study involving 15 subjects residing in an arsenic endemic area of West-Bengal. Accumulation of iAs was tested in the nail, hair and blood samples of these individuals. Extent of ROS, RNS, DNA damage, expression of repair enzymes and status of pro-inflammatory cytokines had been studied. Telomerase activity and NF- $\kappa$ B were also studied. 15 samples were collected from subjects residing in an area having iAs within safe limits. It was observed that in samples from iAs endemic region, ROS and RNS generation was high, followed by DNA damage. These individuals showed higher telomerase activity compared to the control. Status of NF- $\kappa$ B and pro-inflammatory cytokines had been found to be elevated in comparison to the control. Therefore, these parameters could assess the susceptibility of these individuals towards carcinogenesis.

### Introduction

The metalloid arsenic is commonly found in the earth's crust, ranking 20<sup>th</sup> in the abundance amongst other elements and existing in both +5 and +3 oxidation states. It exists both in organic and inorganic state (Roy *et al.*, 2014). Inorganic arsenic (iAs) is

more harmful in the biological system, than their organic counterpart. They are released from the rocks into groundwater naturally as well as anthropogenically (Martinez *et al.*, 2011), contaminating the groundwater water.

Groundwater arsenic contamination is a major health hazard worldwide. Chronic exposure to



Alexandria University  
**Alexandria Engineering Journal**

[www.elsevier.com/locate/aej](http://www.elsevier.com/locate/aej)  
[www.sciencedirect.com](http://www.sciencedirect.com)



ORIGINAL ARTICLE

# Growth of tumor due to Arsenic and its mitigation by black tea in Swiss albino mice



H.M. Srivastava<sup>a,b,h</sup>, Urmimala Dey<sup>c</sup>, Archismaan Ghosh<sup>d</sup>, Jai Prakash Tripathi<sup>e</sup>, Syed Abbas<sup>f,\*</sup>, A. Taraphder<sup>g,c,f</sup>, Madhumita Roy<sup>d</sup>

<sup>a</sup> Department of Mathematics and Statistics, University of Victoria, Victoria, British Columbia V8W 3R4, Canada

<sup>b</sup> Department of Medical Research, China Medical University Hospital, China Medical University, Taichung 40402, Taiwan, Republic of China

<sup>c</sup> Centre for Theoretical Studies, Indian Institute of Technology Kharagpur, Kharagpur 721302, India

<sup>d</sup> Department of Environmental Carcinogenesis and Toxicology, Chittaranjan National Cancer Institute, 37 S. P. Mukherjee Road, Kolkata 700026, India

<sup>e</sup> Department of Mathematics, Central University of Rajasthan, Bandersindri, Kishangarh, Ajmer, 305817 Rajasthan, India

<sup>f</sup> School of Basic Sciences, Indian Institute of Technology, Mandi 175005, India

<sup>g</sup> Department of Physics, Indian Institute of Technology Kharagpur, Kharagpur 721302, India

<sup>h</sup> Department of Mathematics and Informatics, Azerbaijan University, AZ1007 Baku, Azerbaijan

Received 15 January 2020; revised 28 February 2020; accepted 2 March 2020

Available online 20 March 2020

## KEYWORDS

Tumor growth dynamics;  
 Immune response;  
 Stability theory

**Abstract** Inorganic arsenic causes carcinogenesis in a large part of the world. Its potential is elicited by the generation of ROS, which leads to damages to DNA, lipid and protein. Black tea, an antioxidant, can mitigate such deleterious effects by quenching ROS. We study Arsenic-toxicity and its amelioration by black tea in a colony of albino mice: a homology exists between the protein coding regions of mice and human. We observe that black tea has salutary effects on tumor-growth: it arrests damaged cell growth and produces early saturation of the damage. The experimental data obtained by us are modelled with dynamical equations. This is followed by a search for steady states and their stability analysis.

© 2020 The Authors. Published by Elsevier B.V. on behalf of Faculty of Engineering, Alexandria University. This is an open access article under the CC BY-NC-ND license (<http://creativecommons.org/licenses/by-nc-nd/4.0/>).

## 1. Introduction

Arsenic, plentifully available in earth's crust [12] is a metalloid, found in both organic and inorganic forms with two oxidation

\* Corresponding author.

E-mail addresses: [abbas@iitmandi.ac.in](mailto:abbas@iitmandi.ac.in), [sabbas.iitk@gmail.com](mailto:sabbas.iitk@gmail.com) (S. Abbas).

Peer review under responsibility of Faculty of Engineering, Alexandria University.

<https://doi.org/10.1016/j.aej.2020.03.001>

1110-0168 © 2020 The Authors. Published by Elsevier B.V. on behalf of Faculty of Engineering, Alexandria University.

This is an open access article under the CC BY-NC-ND license (<http://creativecommons.org/licenses/by-nc-nd/4.0/>).

states, +3 (arsenite) and +5 (arsenate). It leaches into the ground water from copper or lead containing rocks. Anthropogenic activities like mining also release it to ground water [14]. Exposure to arsenic happens primarily from drinking water, air and food [4]. A lot of health hazards are indeed correlated to chronic inorganic arsenic (iAs) exposure and the current estimate is about 200 million people in 40 countries have been exposed to high degree of iAs (much higher than permissible limit, 10 µg/l [16]) from ground water alone. Arsenic

# Curcumin Rescues Doxorubicin Responsiveness via Regulating Aurora a Signaling Network in Breast Cancer Cells

Souvick Biswas, Elizabeth Mahapatra, Archismaan Ghosh, Salini Das, Madhumita Roy, Sutapa Mukherjee\*

## Abstract

**Background:** Insensitivity towards anthracycline drugs like doxorubicin poses a significant challenge in the treatment of breast cancer. Among several factors, Aurora A (a mitotic serine threonine kinase) plays crucial roles in acquiring non-responsiveness towards doxorubicin. However, the mechanisms underlying need to be elucidated. The present study was therefore designed to evaluate the underlying mechanisms of Aurora A mediated doxorubicin insensitivity in MCF-7Dox/R, an isolated resistant-subline of MCF-7 (breast adenocarcinoma cell line). Effect of curcumin, a natural phytochemical in restoring doxorubicin sensitivity by targeting Aurora A was assessed furthermore. **Methods:** A doxorubicin resistant subline (MCF-7Dox/R) was isolated from the parental MCF-7 cells by treating the cell with gradual step-wise increasing concentration of the drug. Expressions of Aurora A and its target proteins (Akt, I $\kappa$ B $\alpha$  and NF $\kappa$ B) were assessed in both parental and MCF-7Dox/R cells. Both the cell lines were pretreated with curcumin prior to doxorubicin treatment. Cellular proliferation rate was measured using BrdU (5-bromo-2'-deoxyuridine) assay kit. Intracellular doxorubicin accumulation was estimated spectrofluorimetrically. Cellular uptake of curcumin (spectrophotometric and spectrofluorimetric method) and its nuclear localization was confirmed by confocal microscopic study. Protein expressions were determined by western blot analysis. Localization of Aurora A was ascertained by immunofluorescence assay. To explore the possible outcome of impact of curcumin on Aurora A, cell-cycle distribution and apoptosis were performed subsequently. **Results:** Higher expressions of Aurora A in MCF-7Dox/R cells led to phosphorylation of Akt as well as I $\kappa$ B $\alpha$ . Phosphorylated I $\kappa$ B $\alpha$  preceded release of NF $\kappa$ B. Phospho-Akt, NF $\kappa$ B consequentially decreased doxorubicin accumulation by enhancing the expressions of ABCG2 and Pgp1 respectively. Curcumin by regulating Aurora A and its target molecules sensitized resistant subline towards doxorubicin mediated G2/M-arrest and apoptosis. **Conclusion:** Molecular targeting of Aurora A by curcumin restores chemosensitivity by increasing the efficacy of doxorubicin in breast cancer.

**Keywords:** Aurora A- doxorubicin insensitivity- breast cancer- curcumin

*Asian Pac J Cancer Prev*, **22** (3), 957-970

## Introduction

Doxorubicin, conventionally used as chemotherapeutic agent against breast cancer limits its therapeutic benefits due to development of acquired insensitivity following long-term therapy (Christowitz et al., 2019). Therefore, understanding the molecular factors hindering the responsiveness of breast cancer cells towards doxorubicin is crucial to unravel and prevent therapeutic insensitivity.

Human Aurora A protein belonging to the family of serine/threonine kinases is expressed within the centrosome during the early S phase and helps in centrosome duplication and maturation. During G2/M transition Aurora A facilitates mitotic entry by triggering duplicated centrosomes to be separated (Tang et al., 2017). Aurora A undergoes autophosphorylation at Threonine 288

residue to become functionally active. In a wide variety of cancers including breast cancer, aberrant expressions or gene amplification of Aurora A has been documented; indicating its involvement in prosurvival activity and tumorigenesis (D'Assoro et al., 2013; Ferchichi et al., 2013; Zardavas et al., 2014; Cirak et al., 2015). Emerging evidences have documented an association between Aurora A overexpression and decreased chemosensitivity in cancer (He et al., 2014; Kuang et al., 2017; Wang et al., 2017). In triple negative breast cancer cells, response towards doxorubicin was reported to be restored by administration of Aurora A inhibitor (Romanelli et al., 2012). Apart from mitotic involvement, aberrant activation of the non-canonical Aurora A/SMAD5 oncogenic axis in breast cancer has been documented, which eventually led to chemoinsensitivity (Opyrchal et al., 2017). However,





# Modulatory role of tea in arsenic induced epigenetic alterations in carcinogenesis

Archismaan Ghosh<sup>1</sup> · Sutapa Mukherjee<sup>1</sup> · Madhumita Roy<sup>1</sup> · Amitava Datta<sup>2</sup>

Received: 3 September 2020 / Accepted: 8 December 2020  
© Archana Sharma Foundation of Calcutta 2021

## Abstract

Epigenetic alterations, broadly divided into DNA methylation, Histone modifications and interference by non-coding RNAs can often lead to carcinogenesis. Alterations in epigenetic machinery may be due to numerous factors, including exposure to toxic chemicals. These toxicants include heavy metals as well. The metalloid arsenic is an environmental pollutant and its chronic exposure causes cancer. Etiology of arsenic induced cancer includes epigenetic alterations, among others. Inorganic-arsenic is the lead cause of hypermethylation of tumor-suppressor genes and hypomethylation of genes involved in cell proliferation, growth and invasion. It can induce histone methylations and acetylations along with modulation of miRNAs, promoting cancer. Therefore, control of epigenetic alterations is vital. Chemoprevention using phytochemicals is an effective strategy to mitigate the deleterious effect of chronic arsenic exposure. Flavonoids, a group of phytochemicals have shown numerous evidences of epigenetic modulations halting carcinogenesis. Catechins represent one of the most active groups of flavonoids. Tea, a popular beverage, is one of the richest sources of catechins. Green tea contains highly active catechins like epigallocatechin-3-gallate (EGCG), epigallocatechin (EGC), epicatechingallate (ECG) etc. while black tea contains oxidized polymeric catechins like theaflavin and thearubigin. Green tea catechins have elicited their potential as an epigenetic modulator, establishing their chemopreventive attributes. Therefore, administration of tea may be an effective strategy to mitigate the epigenetic alterations, induced by chronic exposure to arsenic, in individuals of endemic areas.

**Keywords** Epigenetic · Arsenic · Cancer · Chemoprevention · Tea

## Epigenetic regulation

The term, “epigenetics” is used to refer to heritable modifications that occur without alterations in the DNA sequence. Epigenetic changes refer to modification of the structure of the chromatin and accessibility of the DNA via histone modifications and DNA methylation, thereby controlling the

pattern of gene expression. Epigenetics play an important role in the normal development and differentiation of individual organisms. Environmental alterations or pathological conditions may also alter the epigenetic regulation within organisms, thus altering the phenotype of the organism [39]. The occurrence and maintenance of varied cellular processes utilizing the same genetic information requires efficient epigenetic regulations. Epigenetic regulation occurs commonly through DNA methylation, post translational modifications of histones or chromatin and through the regulation of non-coding RNA's. Discrepancies in epigenetic tags result in aberrant initiation and inhibition of genetic expressions culminating into numerous pathological conditions including cancer [30, 37]. Epigenetic modifications within the cells can be broadly categorized into the following categories, namely, DNA modifications, histone modifications and non-coding RNA's.

---

Corresponding Editor: Somnath Paul.

---

Reviewers: Udayan Bhattacharya, Debapriya Mondal, Debmita Chatterjee.

---

✉ Madhumita Roy  
mitacnci@yahoo.co.in

<sup>1</sup> Department of Environmental Carcinogenesis & Toxicology, Chittaranjan National Cancer Institute, 37, S P Mukherjee Road, Kolkata 700026, India

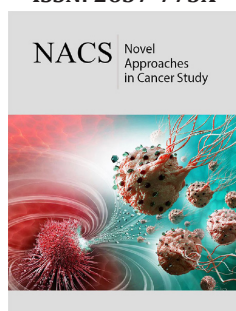
<sup>2</sup> Department of Computer Science & Software Engineering, University of Western Australia, 35 Stirling Highway, Perth, WA 6009, Australia

# Prevalence of Gallbladder Cancer in Arsenic Endemic Areas

Archismaan Ghosh and Madhumita Roy\*

Department of Environmental Carcinogenesis & Toxicology, Chittaranjan National Cancer Institute, 37, S P Mukherjee Road, Kolkata, India

ISSN: 2637-773X



**\*Corresponding author:** Madhumita Roy, Department of Environmental Carcinogenesis & Toxicology, Chittaranjan National Cancer Institute, 37, S P Mukherjee Road, Kolkata, India, Email: mitacnci@yahoo.co.in

**Submission:**  March 13, 2020

**Published:**  May 04, 2020

Volume 4 - Issue 4

**How to cite this article:** Archismaan Ghosh, Madhumita Roy. Prevalence of Gallbladder Cancer in Arsenic Endemic Areas. *Nov Appro in Can Study*. 4(4). NACS.000593. 2020. DOI: [10.31031/NACS.2020.04.000593](https://doi.org/10.31031/NACS.2020.04.000593)

**Copyright@** Madhumita Roy. This article is distributed under the terms of the Creative Commons Attribution 4.0 International License, which permits unrestricted use and redistribution provided that the original author and source are credited.

## Abstract

Association between exposure to high arsenic content and gallbladder cancer is scanty. Few reports suggest that the incidence of gallbladder cancer is high along the Indo-Gangetic belt. Inflammation, which is a causative factor for gallbladder carcinoma can be induced by arsenic. Prognosis of gallbladder cancer is poor. Therefore, it is worthwhile to find a correlation between arsenic exposure and its incidence to identify a population who are at high risk category.

**Keywords:** Arsenic; Gallbladder cancer; inflammation; Indo Gangetic belt

## Introduction

Groundwater is one the most important source of drinking water in the world. Contamination of groundwater by arsenic is a major health issue which is escalating day by day. More and more areas are being reported with arsenic content much higher than the safe limit of 10µg/L set by WHO [1]. Apart from a plethora of health hazards, chronic exposure to arsenic is known to cause cancer of the skin, lung, bladder, liver, kidney and prostate [2]. Association between presence of arsenic and cancer of the gallbladder has not been reported as much. But, epidemiological evidence indicates a link between incidences of gallbladder cancer in arsenic endemic areas. World wide geographic distribution of arsenic contaminated areas share remarkable similarity with regions reporting high prevalence of gallbladder cancer, especially in Chile, India and Bangladesh [3]. In India, the Indo-Gangetic belt has the highest number of recorded cases of gallbladder cancer, maximum amongst them being reported from the Kamrup district in Assam [4]. This region of Eastern India also harbors areas with the highest groundwater arsenic contamination [5].

Gall bladder cancer is a rare malignancy but has very high mortality rate with less than 5 years of survivability [6,7]. Apart from known risk factors like age, sex, presence of gall stones, ethnic origin [8], and environment may be a key player in the etiology of gallbladder cancer. Environmental risk factors include water contamination by heavy metals like lead, cobalt, mercury, arsenic, chromium, and cadmium. Of these, exposure to elevated amount of cadmium, cobalt, lead, mercury is marked as causative factors for gallbladder carcinogenesis [9]. Prognosis of gallbladder cancer is poor and that may be attributed to its late diagnosis, when the disease has advanced and metastasis has already taken place [8].

Arsenic has been declared as a Group 1 carcinogen by the International Agency for Research on Cancer, based on the substantial evidence for their carcinogenicity in humans [2]. The Majority of the ingested arsenic undergoes biotransformation in the liver and the metabolites are excreted mainly in the urine, causing renal cancer [10]. These metabolites often are excreted into the bile [11,12]. Arsenic may be responsible for carcinogenesis of the biliary tract cancer, the most common of which being gallbladder cancer [13]. Statistical analysis investigating the ecological correlation between the arsenic concentrations and incidences of gall bladder cancer have shown positive trends both in Indian and Taiwanese populations [2].



Madhumita Roy  
Archismaan Ghosh  
Apurba Mukherjee

# Role of Black Tea in Prevention of Skin Carcinogenesis

 **LAMBERT**  
Academic Publishing

# Insights of Cisplatin Resistance in Cervical Cancer: A Decision Making for Cellular Survival

*Elizabeth Mahapatra, Salini Das, Souvick Biswas, Archismaan Ghosh, Debomita Sengupta, Madhumita Roy and Sutapa Mukherjee*

## Abstract

The clinical scenario of acquired cisplatin resistance is considered as a major impediment in cervical cancer treatment. Bulky drug-DNA adducts formed by cisplatin elicits *DNA damage response (DDR)* which either subsequently induces apoptosis in the cervical cancer cells or enables them to adapt with drug assault by invigorating pro-survival molecular cascades. When HPV infected cervical cancer cells encounter cisplatin, a complex molecular interaction between *deregulated tumor suppressors, DNA damage-repair enzymes, and prosurvival molecules* get initiated. Ambiguous molecular triggers allow cancer cells to cull apoptosis by opting for a survival fate. Overriding of the apoptotic cues by the pro-survival cues renders a *cisplatin resistant phenotype* in the tumor microenvironment. The present review undrapes the impact of deregulated signaling nexus formed due to crosstalk of the key molecules related to cell survival and apoptosis in orchestrating platinum resistance in cervical cancer.

**Keywords:** HPV, Cervical cancer, Cisplatin resistance, tumor suppressors, DNA-damage repair, prosurvival signaling

## 1. Introduction

Cervical cancer, one of the widespread gynecological cancers, accounts for the maximum deaths amongst women across the globe. As per GLOBOCAN 2018, cervical cancer is helmed as the fourth leading cause of mortality and morbidity in women after breast and ovarian cancers [1]. As revealed from the data collated by World Health Organization (WHO) in 2013, over 85% of the cervical cancer cases had surfaced mostly from developing countries with a poor socio-economic backdrop [2]. Women, owing to lack of awareness, often arrive for seeking medical help when the malignant growth of cervix has attained advancement [3].

Infections with a special class of oncogenic DNA viruses called *Human Papilloma Viruses (HPVs)*, hailing from the viral family *Papillomaviridae*, are highly accredited for the malignant transformation of cervix. Principally, HPVs are sexually transmitted [4]. On the basis of its carcinogenic potentials, HPVs can be categorized as –(i) *low-risk HPVs (lr-HPVs)* like HPV 6, 11, 42, 43 and 44, and (ii) *high-risk*

## Conferences Attended

1. **Archismaan Ghosh** and Madhumita Roy. Prevention Of Inorganic Arsenic Induced Squamous Cell Carcinoma of The Skin in Swiss Albino Mice by Black Tea Through Post-translational Epigenetic Modulations. Oral presentation at *2nd International colloquium RMBPD-2022* organized by Department of Zoology, University of Delhi, held on 24 and 25th February 2022.
2. **Archismaan Ghosh** attended an international Webinar on *The Relevance of Omics and Regenerative Medicine in the Pandemic Situation (5<sup>th</sup> Edition)* Organized by Dept. of Zoology, University of Kerala from March 27<sup>th</sup> to March 29<sup>th</sup>, 2021.
3. **Archismaan Ghosh** attended 40TH Annual Conference of *Indian Association for Cancer Research* Organized By: Institute of Life Sciences, Bhubaneswar held on 1<sup>st</sup> March 2021.
4. **Archismaan Ghosh** attended a webinar entitled “*The Concept of Cancer Stem Cells: Progress and Promises*” under the series “Webinar-The Biomics” organized by National Institute of Biomedical Genomics, Kalyani on 8.11.2020.
5. **Archismaan Ghosh** attended a webinar entitled “*Controlling Stem Cell Fate through Intracellular Trafficking*” under the series “Webinar-The Biomics” organized by National Institute of Biomedical Genomics, Kalyani on 8.11.2020.
6. **Archismaan Ghosh** attended a webinar entitled “*Effective RNA Extraction for COVID-19 testing*” organized by Confederation of Indian Industry on 13.04.2020.
7. **Archismaan Ghosh**, Sutapa Mukherjee and Madhumita Roy. EMT driven Skin Carcinogenesis by iAs: Modulation by Black Tea. Poster presentation at *One-day symposium and IACR – WB chapter on Cancer Research: Bench to Bedside* held at CNCI, Kolkata on 11th January 2020.

8. **Archismaan Ghosh**, Sutapa Mukherjee and Madhumita Roy. EMT driven skin carcinogenesis by iAs: Modulation by Black Tea. Oral Presentation at *International Conference on Sustainable Environment and Healthcare (ICSEH- 2019)* held on 21st and 22nd December 2019 at Jadavpur University, Kolkata.
9. **Archismaan Ghosh**, Sutapa Mukherjee and Madhumita Roy. Black tea Prevents EMT driven carcinogenesis induced by iAs. Poster presentation at *19th All India Congress of Genetics and Genomics & International Symposium on “Air pollution and its Impact on human health”* held at CSIR-IICB Kolkata, Jadavpur from 2-4th December 2019.
10. **Archismaan Ghosh**, Sutapa Mukherjee and Madhumita Roy. EMT driven skin carcinogenesis by iAs: Modulation by black Tea. Poster presentation at *International Conference on “Neutraceuticals and Chronic Diseases- 2019”* held at IIT Guwahati, Assam from 23 rd – 25 th September, 2019.
11. **Archismaan Ghosh**, Sutapa Mukherjee and Madhumita Roy. Prevention of arsenic induced skin carcinogenesis by black tea. Oral presentation at *2nd Annual Conference on “Recent Trends in Cancer Research, Early Diagonistics, Prevention and Therapy”* organized by the Chittaranjan National Cancer Institute (CNCI), Kolkata held from 04.02.2019 to 05. 02. 2019.
12. **Archismaan Ghosh** attended one day mini symposium organized by the *IACR-West Bengal Chapter & Chittaranjan National Cancer Institute (CNCI)* at CNCI, Kolkata held on 14. 09. 2018.
13. **Archismaan Ghosh** attended one day symposium on “Recent Trends in Biological Research” organized by the *Society of Biological Chemists (I)* at Amity University, Kolkata held on 08. 09. 2018.

14. **Archismaan Ghosh** attended one day symposium on “Recent Trends in Immunology” organized by the *Department of Immunoregulation and Immunodiagnostics (IRID), Chittaranjan National Cancer Institute (CNCI), Kolkata* held on 01. 05. 2018.
15. **Archismaan Ghosh**, Sutapa Mukherjee and Madhumita Roy. Role of Black Tea in prevention of Skin carcinogenesis. Poster presentation in an international conference on “*Trends in Biochemical and Biomedical Research Advances and Challenges (TBBR-2018)*”, organised by Department of Biochemistry, Institute of Science, Banaras Hindu University from 13th -15th February, 2018.

## Achievements/Awards

1. Qualified 19<sup>th</sup> State Eligibility Test-2015 held on 6.12.2015.
2. Qualified GATE 2016 with an all-India Rank of 919 in Life science.
3. Qualified for Lectureship- NET June 2016 with a rank of 38.
4. Qualified for JRF -CSIR-UGC NET December 2017 with a rank of 74 under CSIR fellowship scheme.
5. Received best poster presentation award at International Conference on “Nutraceuticals and Chronic Diseases” INCD 2019, held at IIT Guwahati, Assam from 23rd – 25th September 2019.
6. Received best paper presentation award for an oral presentation at International Conference on Sustainable Environment and Healthcare (ICSEH- 2019), held on 21st and 22nd December 2019, at Jadavpur University.
7. Received best paper for poster presentation at one day symposium and IACR – WB chapter on Cancer Research: Bench to Bedside held at CNCI, Kolkata, held on 11th January 2020.
8. Received certificate of Appreciation for outstanding performance in oral presentation at 2nd International colloquium RMBPD-2022 organised by Department of Zoology, University of Delhi, held on 24 and 25th February 2022.



